The Dissertation Committee for Ji-Hoon Lee certifies that this is the approved version of the following dissertation:

The role of *liquid facets-Related* in *Drosophila* development

Committee:

Janice Fischer, Supervisor

Paul Macdonald

Theresa O'Halloran

Philip Tucker

Steven Vokes

The role of *liquid facets-Related* in *Drosophila* development

by

Ji-Hoon Lee, B.S.; M.S.

Dissertation

Presented to the Faculty of the Graduate School of

The University of Texas at Austin

in Partial Fulfillment

of the Requirements

for the Degree of

Doctor of Philosophy

The University of Texas at Austin

December 2011

Dedication

To my parents, my wife, and my two daughters

Acknowledgements

Many thanks to my mentor Janice Fischer. Her insightful intelligence as a geneticist heavily influenced on me from my first day of rotation in her lab and throughout my entire graduate research. Also, I will never forget her encouragement, which made me try harder to learn and overcome difficulties I experienced during my graduate study. I am also very grateful to the members of my dissertation committee, Paul Macdonald, Phil Tucker, Terry O'Halloran, Steve Vokes, and the late John Sisson for their help and support. I would like to thank past and current Fischer lab members, Erin Overstreet, Susie Banks, Kristin Patterson, Bomsoo Cho, Xuanhua Xie, Sheila Bal, Gerrit van der Ende, Suk Ho Eun, Martin Kracklauer, and Yaning Wu. Especially, I would thank Stephen Fleenor, who was my colleague and friend for almost 3 years as an undergraduate student and technician after graduation. I would like to acknowledge rotation students who worked with me: Yoni Bibliowicz, Sukyoung Kim, Audra Hoffman, Kate Johnson, and Seung Hee Cho. I would also like to thank all of the UT Fly Club members: Paul Macdonald, David Stein, and Ophelia Papoulas and people in their labs. I acknowledge monetary support of Lindsey Bruce Endowed Fellowship and Dorthea Bennett Summer Fellowship from UT Austin. I have been very lucky to have many great friends in Austin, especially Bum-Kyu Lee, Hyung Cheol Kim, Young Sam Lee, Dae-Seok Eom, Yonghwan Kim, and Hae Ryung Chang, who shared daily life with me. I would also thank Dong-Hwan Kim and his family. I would like to thank my parents and all of my family in Korea for their love. Lastly, I would like to express my deep appreciation to my wife Ji Hyun and my two daughters Sabine and Celine.

The role of *liquid facets-Related* in *Drosophila* development

Publication No._____

Ji-Hoon Lee, Ph.D.

The University of Texas at Austin, 2011

Supervisor: Janice Fischer

The goal of my graduate research is to find the role of a *Drosophila* gene, *liquid facets-Related*, encoding an ENTH (Epsin N-term homology) domain protein using developing *Drosophila* eye as a model system. The ENTH domain is a well-conserved globular domain with affinity to phosphoinositides, and found in endocytic Epsins and Golgi Epsins. With the ENTH domain and peptide motifs, such as clathrin binding motifs and other protein binding motifs, endocytic Epsins and Golgi Epsins are localized to the plasma membrane and the Golgi membrane, respectively. The main function of Epsins is to facilitate clathrin-dependent vesicle formation. An interesting finding from endocytic Epsin research using *Drosophila* is that this seemingly generic factor has in fact a specific role in the Notch signaling pathway by mediating ligand endocytosis which is crucial for receptor activation in the adjacent cell. The role of Golgi Epsin, on the other hand, has not been understood in a multi-cellular context. A former graduate student in our lab, Erin Overstreet, generated loss-of-function mutants of *liquid facets-Related* and found that this gene is essential for viability and important for cell growth and patterning in *Drosophila eye* development. Her finding suggests that *liquid facets-Related* has a

specific role in development. She also found that the ENTH domain is dispensable for the function of *liquid facets-Related*. This is an interesting result because studies using other model organisms show that ENTH domain directly recognizes the cargos, suggestive of essential function it in Golgi Epsin. Therefore, I aimed to figure out what is the function of *liquid facets-Related* in a multi-cellular context using the *Drosophila* eye as a model system. To address this, I further characterized the mutant phenotype, screened for dominant modifiers of the hypomorphic eye phenotype, and performed structure/function assays that helped me to generate specific hypotheses and then I tested them.

My graduate research contributed to understanding the role of *liquid facets-Related* by providing the *in vivo* function, identifying genetic interactions, and specifying the domain necessary and sufficient for its function. First of all, characterization of the mutant phenotype indicated that *liquid facets-Related* is crucial for proliferation, suppression of apoptosis, insulin receptor-independent cell growth, and progression of the morphogenetic furrow at the D/V midline in the developing *Drosophila* eye. Secondly, from a forward genetic screen, I found *Delta, neuralized, polychaetoid (ZO-1), string (cdc25)*, and *altered disjunction (Mps1)* as dominant enhancers of the hypomorphic eye phenotype, suggestive of the role of *liquid facets-Related* in the Notch signaling pathway and cell cycle regulation. I also found that *wingless* and *armadillo* dominantly enhance the hypomorphic phenotype of *liquid facets-Related*, which suggests that *liquid facets-Related* has a role in the Wingless signaling pathway. Indeed, the expression of a transcriptional target of the Wingless signal, *dachsous*, is reduced in *liquid facets-Related* null cells. Baso-lateral levels of E-cadherin and Armadillo are increased in the *liquid facets-Related* null cells, which is consistent with the fact that E-cadherin antagonizes the Wingless signal activity. Finally, an unexpected result from structure/function analysis is that *exon 6* of the *liquid facet-Related* gene is necessary and sufficient to rescue all

visible morphological defects of null mutants. This is interesting because *exon 6* is conserved in Golgi Epsin gene only in several insects but not in most other species including yeast, nematode, mouse, and human. In fact, *exon 6* is a homolog of a recently studied gene known as *tel2*. Evidence suggests that *liquid facets-Related* is *Drosophila tel2*. As the function of Tel2 is not clearly understood, this study may contribute to better understand the essential role of Tel2 in *Drosophila* and other model systems.

Table of Contents

List of Tables

List of Figures

Chapter 1: Introduction

1.1 THE *DROSOPHILA* EYE AS A POWERFUL TOOL FOR GENETIC STUDY

The *Drosophila* adult compound eye as a model system

The *Drosophila* eye was first recognized as a place to find a mutant phenotype in 1910 when T. H. Morgan published his first paper. Using *Drosophila* as a model organism the mode of inheritance of a gene *white*, which affects the *Drosophila* eye color, was introduced (Morgan, 1910). For the last 100 years, geneticists have identified many mutants with mutant eye phenotypes. Although many of them did so wanting to understand how the *Drosophila* eye works, other researchers simply used the *Drosophila* eye as a model system to gain mechanistic understanding of gene function in cell-cell interactions during organogenesis, with the hope that their findings may also be applied to other tissues and other organisms like humans.

The *Drosophila* eye is a useful genetic tool because its simple structure makes it easy to identify mutant phenotypes. The *Drosophila* compound eye is composed of about 750 facets or ommatidia (Wolff and Ready, 1993). The shape and size of each ommatidium is the same, making the *Drosophila* eye smooth externally with regularly ordered facets (Fig. 1-1A). Each ommatidium has 19 cells including 8 photoreceptor cells and 11 accessory cells. Each photoreceptor cell has a specialized organelle called a rhabdomere, which is densely packed membrane, filled with specific rhodopsin molecules. Because the rhabdomere is so dense and each photoreceptor cell has its own specific position, tangential sections of a wild-type adult eye readily show arrays of trapezoids – each trapezoid indicating an ommatidium and each "dot" in the trapezoids indicating a rhabdomere of a specific photoreceptor cell (Fig. 1-1A', C). One important

merit of the *Drosophila* eye as a model for genetic study resides here. Ommatidia in the eye form simple and regular arrays, because each ommatidium has a fixed number of differentiated cells with a typical shape, size and location. To achieve this regularity, all developmental processes including proliferation, differentiation, patterning, and cell growth should happen properly as programmed. Any mishap in this genetic program causes irregularity or "roughness" and is readily detectable at the surface of the external eye (Fig. 1-1A, B). Those phenotypic changes make the detection of mutants easy, even in living flies, and thus makes the *Drosophila* eye a nice tool for genetic study. As each developmental stage of the *Drosophila* eye is well characterized (see below), it is possible to identify what happened to the tissue at any particular stage to find the function of the gene.

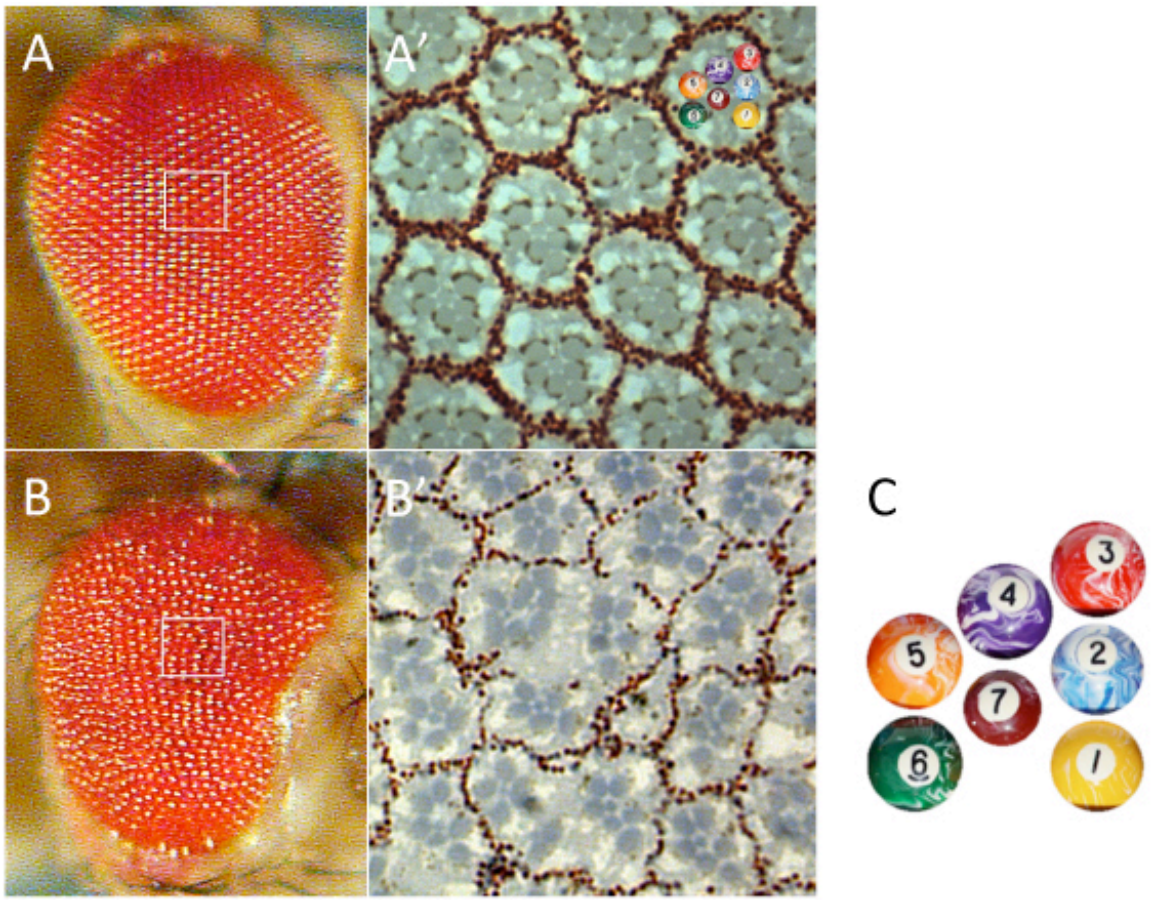

Figure 1-1. Wild-type and mutant *Drosophila* eye.

Images of a wild-type *Drosophila* eye (A, A') and a mutant eye (B, B'). (A) shows an external eye of a wild-type fly. (B) shows an external eye of a mutant fly, as an example of the rough eye phenotype. Compare the irregular surface of the mutant eye in (B) to the smooth regular wild-type eye in (A). (A') is a tangential section of a wild-type eye. (B') is a tangential section of a mutant eye. Compare the regular array of ommatidia each with the typical trapezoidal rhabdomere constellation in (A') to irregular array of ommatidia with various number and pattern of rhabdomere in (B'). Genotypes: (A, A') Oregon R, (B, B') $lqfR^{P}/lqfR^{P}$. Squares in (A) and (B) indicate area where (A') and (B') can be found when tangentially sectioned, respectively. (C) indicates the trapezoidal pattern of rhabdomere in each ommatidium labeled with R-cell numbers.

The eye imaginal disc, a developing *Drosophila* eye

The *Drosophila* adult eye is from a primordial tissue growing in the larva called the eye imaginal disc. The external surface cuticle and appendages of adult *Drosophila* form from imaginal discs except for the abdomen, which is from imaginal histoblasts. For example, the adult wings and thorax are formed from wing imaginal discs, adult legs are formed from leg imaginal discs, adult eyes and part of the head epidermis are from eye imaginal discs, etc.

An eye imaginal disc or simply the eye disc is composed of two sheets of epithelial cells with its edges sealed like a bag, except one edge is fused with the antenna disc. The top sheet is a thin squamous cell layer called the peripodial epithelium, which has important roles during eye development (Cho et al, 2000). The peripodial epithelium differentiates as epidermis covering the head capsule along with tissues differentiated from antenna discs after disc eversion during pupal stage. The bottom layer is retinal epithelium, which differentiates into an adult eye. For the remainder of my thesis, retinal epithelia will be called eye discs.

An eye disc is initiated as a group of ~6-23 founder cells during embryogenesis (Garcia-Bellido & Merriam, 1969; Wieschaus & Gehring, 1976). These undifferentiated progenitor cells undergo cell division continually until they exit the cell cycle and differentiate with the signal from the morphogenetic furrow (see below). The number of cells increases to about 130 at the late first instar larva stage and to ~1300-1600 at the early third instar stage (Becker, 1957). Cell division continues until the cell number reaches to about 9700, which is deduced from the fact that ~13 seed cells are required to

initiate one ommatidium in an eye with ~750 ommatidia. When differentiation begins (behind the morphogenetic furrow, see below), 5 cells out of 13 seed cells are first recruited as photoreceptors and the rest ~8 cells undergo one more synchronized cell cycle to replenish cells to be recruited later as photoreceptor cells or accessory cells. It is important to have the right number of cells at the right time and place in accordance with the developmental program of the organism to ultimately have normal *Drosophila* eyes. Therefore, it is crucial to properly regulate the cell proliferation in this tissue at each developmental stage.

The morphogenetic furrow plays a crucial role in *Drosophila* eye development to coordinate proliferation and differentiation. The morphogenetic furrow is the cue for differentiation. It is a single anatomical stripe on an eye disc in the third instar larva due to physical constriction at the apical region of cells in the row (Fig. 1-2A, C, D). The morphogenetic furrow initiates at the posterior end during the early third instar larva stage and moves anteriorly to cover the entire disc by the early pupal stage. Ahead of the furrow, dividing cells exit the cell cycle and are arrested at G1 phase (Baker, 2007) (Fig. 2-1A, B). In the furrow, clusters of cells begin to emerge. It starts as a rosette consisting of ~13 seed cells, as mentioned earlier, and transforms into an arc-shaped cluster, then into a 5-cell cluster. Accordingly, photoreceptors (R-cells) are recruited within the cluster beginning with R8 and then R2, R5, R3, and R4 to form the 5-cell cluster (Fig. 1-2C, E). Following this, all the rest of the cells not recruited yet undergo one more synchronized cell cycle, as described earlier, that can be visualized as the second mitotic wave with cell cycle markers such as bromodeoxyuridine (Fig. 2-1B). As clusters become more mature, they recruit R1, R6, and finally R7, and after that, differentiation of accessory cells

follows. Any mistake in the patterning process due to mutations in required genes may lead to an eye phenotype such as a "rough" eye.

The adult eye and eye disc have anterior/posterior (A/P) and dorsal/ventral (D/V) axes. The anterior margin of an eye disc is fused with an antennal disc, whereas the posterior end forms a narrow cable-like tissue called the optic stalk where axons of R-cells pass through and connect to the larval brain. Since the morphogenetic furrow begins at the posterior end and moves anterior, mutations in genes required for furrow movement (e.g. rough) can lead to patterning problems in the anterior region resulting in such a phenotype. The D/V axis can be observed in tangentially sectioned adult eyes. Each ommatidium has a trapezoidal rhabdomere pattern due to asymmetry in R3 and R4. All ommatidia in the dorsal area have R3 facing toward the dorsal margin, while all ommatidia in the ventral area have R3 facing toward the ventral margin (Fig. 1-1A', C). All cells in an eye disc start with a ventral fate and cells with dorsal fate only arise when the dorsal selector gene pannier establishes dorsal lineage (Maurel-Zaffran & Treisman, 2000). A hallmark of ventral cells is the expression of *fringe*, which plays a crucial role in Notch signal activation at the D/V midline, and therefore establishing a D/V midline and eye growth (Cho & Choi, 1998; Dominguez & de Celis, 1998).

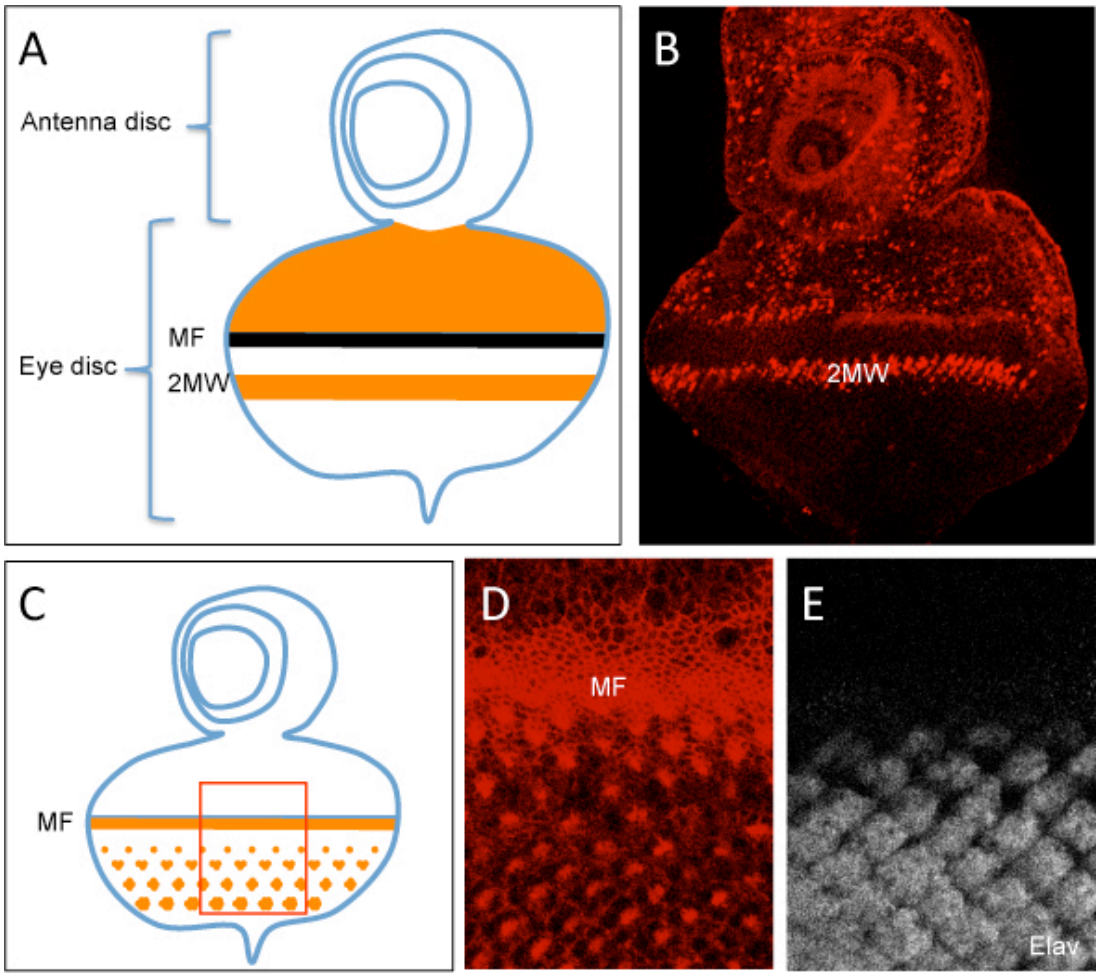

Figure 1-2. An eye disc is a developing *Drosophila* eye.

(A) A cartoon showing an eye-antenna disc with an emphasis on proliferation in the eye disc. In the eye disc, cells ahead of the morphogenetic furrow (MF) are progenitors that proliferate continuously. At the morphogenetic furrow, cell division is inhibited. After R8, R2, and R5 were recruited, the rest of cells undergo one synchronized cell cycle, which can be visualized with BrdU as the second mitotic wave (2MW). (B) An eye-antenna disc stained with BrdU (red). Cells undergoing cell cycle are shown ahead of the forrow and at the second mitotic wave. (C) A cartoon showing an eye-antenna disc with an emphasis on differentiation in the eye disc. Behind the furrow, photoreceptor recruitement initiates in each cluster. Beginning with R8, R2/5, R3/4, R1/6, and lastly R7 are sequentially recruited. Clusters just began differentiation are closest to the furrow. The morphogenetic furrow was visualized with one of the plasma membrane marker anti-Armadillo (D). R-cells were visualized with a neuronal cell marker anti-Elav (E).

Defects in proliferation can result in a "no disc" phenotype

Cell proliferation is very important during development. If a gene with an important function in proliferation is lost, it may cause embryonic lethality. However, mutants for genes important for proliferation frequently result in larval lethality with tiny or no imaginal discs. Genes with this mutant phenotype include *MCM2, dpa, Orc2, Egfr, InR, raf, Mad, Med, vn, Ser, and gbb-60A,* which encode proteins for proliferation with various molecular functions ranging from DNA replication to signaling (Chen et al, 1996; Clifford & Schupbach, 1989; Feger et al, 1995; Khalsa et al, 1998; Landis et al, 1997; Nishida et al, 1988; Raftery et al, 1995; Sekelsky et al, 1995; Speicher et al, 1994; Treisman et al, 1995). What is the basis of the larval lethality with tiny or no imaginal discs?

During the embryogenesis of *Drosophila*, the first 10 rounds of mitotic cell divisions occur with almost no transcription of the zygotic genome. Cell divisions for larval cells are finished by mid-embryogenesis. Larval growth after this happens with cell growth rather than cell division (Gatti & Baker, 1989). Therefore, cell divisions for larval cells can be accomplished in most cases with maternally provided materials. However, the cells in imaginal discs divide during larval and pupal stage and zygotic gene expression is required for cell division during the stages. Larvae without imaginal discs can survive up to the late third instar larval stage or early pupal stage because imaginal discs are dispensable for the larva (Shearn et al, 1971). However, such larvae or pupae cannot survive any longer without imaginal discs because imaginal discs are absolutely required at the pupal stage.

This logic has been applied to perform a genetic screen to find genes required for the cell cycle (Shearn et al, 1971). After mutagenesis, they screened for mutants that exhibited third instar larval or early pupal lethality, and dissected the larvae to see if they had abnormally small or no imaginal discs. This screen identified many complementation groups with various cell cycle defects and many of them are not yet mapped to genes (Gatti & Baker, 1989). I will show in Chapter 2 that I identified one of the mutants as allelic to *liquid facets-Related*.

Genetic tools of *Drosophila* to study gene function

During the last several decades, many useful methods for genetic study have been devised and become available to *Drosophila* researchers. I will explain three of them, which I depended on for my research.

First of all, specifically designed exogenous genes can be expressed in a tissue specific way using the *UAS/gal4* system (Brand & Perrimon, 1993) (Fig. 1-3). *UAS* is a yeast enhancer and Gal4 is a yeast transcription factor that recognizes the *UAS* sequence. If a transgene has a *UAS* and is inserted in the *Drosophila* genome, it can be expressed specifically where *gal4* is expressed (Fischer et al, 1988). As many enhancers that regulate tissue specific expression of genes are known, *gal4* cDNA can hijack such enhancers to express transgenes tissue specifically. For example, the enhancer for an eye specific gene *eyeless* can be used to express Gal4 specifically in the eye disc at a very early stage. The Gal4 protein now turns on the expression of transgenes with the *UAS* (Fig. 1-3). This is a useful method with many applications such as observing the gain-of-function phenotype of certain genes.

Next, mitotic clones in a developing fly tissue can be generated using the *flp*/*FRT* technique (Golic & Lindquist, 1989) (Fig. 1-4). FLP is a site-specific recombinase that recognizes a DNA sequence *FRT*. If one homologous chromosome has an *FRT* at a specific place and a specific mutation away from the centromere, and the other homolog has an *FRT* at the same spot and a marker such as *lacZ* controlled by a ubiquitous promoter away from the centromere, the two homologs can exchange whole chromosome arms under the control of *flp* expression when the cell undergo mitosis. *flp* can be expressed either using a tissue-specific promoter or the heat-shock promoter. Then, two cells produced at the same time can now have two different genotypes, neither of them the same as the original genotype: one cell has two copies of the mutant allele but no *lacZ*, and the other cell has two copies of *lacZ* but no mutant allele. The background cells that did not undergo the recombination have one copy of the mutant allele and one copy of the *lacZ*. With this method, homozygous mutant cells can be generated right next to wild-type cells. The cell population propagated from the homozygous mutant daughter cell is called a mutant clone and the cell population from the daughter with two *lacZ* or markers is called a twin spot (Fig. 1-4). The mutant clone and twin spot are from two cells "born" at the same time, so this method can also be used to test if a mutant has proliferation defect by comparing the sizes of clone and its twin.

Finally, a whole eye clone homozygous for a certain mutant gene can be produced in a heterozygous background genotype using the *GMR-hid* technique (Stowers & Schwarz, 1999) (Fig. 1-5). This is useful when the mutant is homozygous lethal. *GMR* is a strong late onset, eye-specific promoter expressed behind the morphogenetic furrow. *hid* is a potent apoptosis inducer. Therefore, *GMR-hid* kills cells that express it. If this method is combined with the *flp*/*FRT* technique, it is possible to make cells with two

copies of the mutant allele and without *GMR-hid* that thus survive (Fig. 1-5). I used this method to see the *liquid facets-Related* null phenotype in the eye and to screen for genes enhancing the *liquid facets-Related* hypomorphic phenotype (See Chapters 2 and 3).

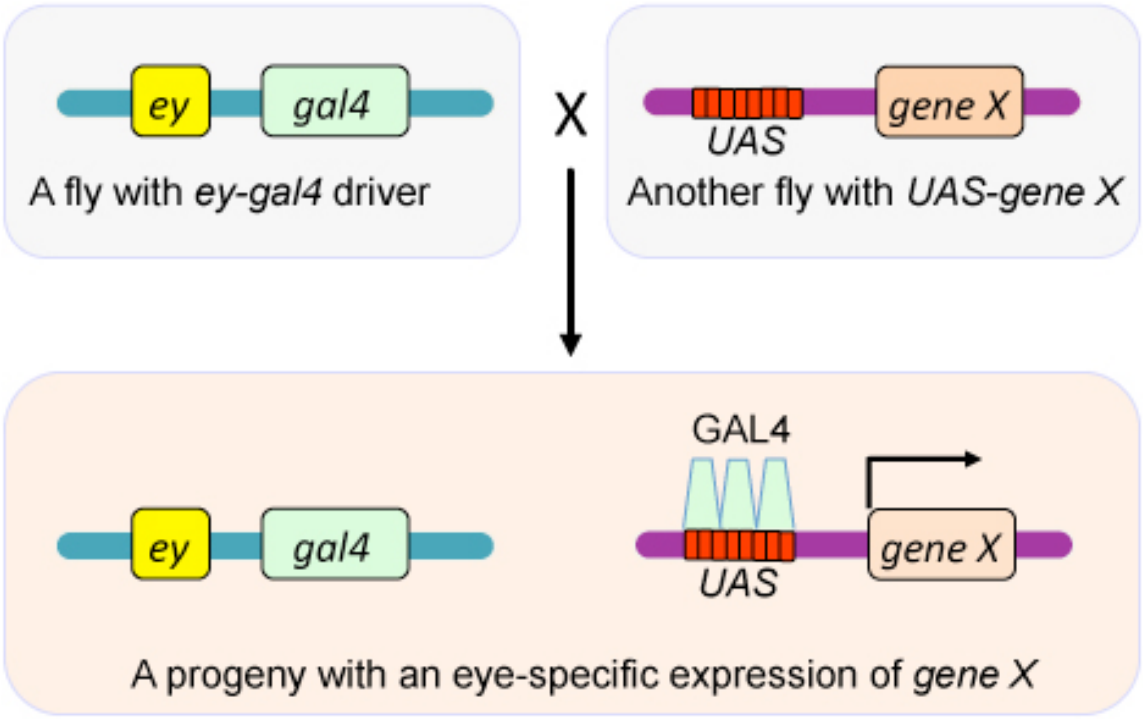

Figure 1-3. Eye-specific gene expression using the *UAS/gal4* system.

Shown is a cartoon to explain the *UAS/gal4* system. The upper left box represents a male or female fly expressing *gal4* under the control of the *eyeless (ey)* enhancer. The upper right box represents another fly of opposite sex with *UAS-gene X* transgene. The box shown at the bottom represents the progeny of them with both *ey-gal4* and *UAS-gene X*. Gal4 protein expressed in an eye-specific way drives the expression of *gene X* through *UAS* enhancer.

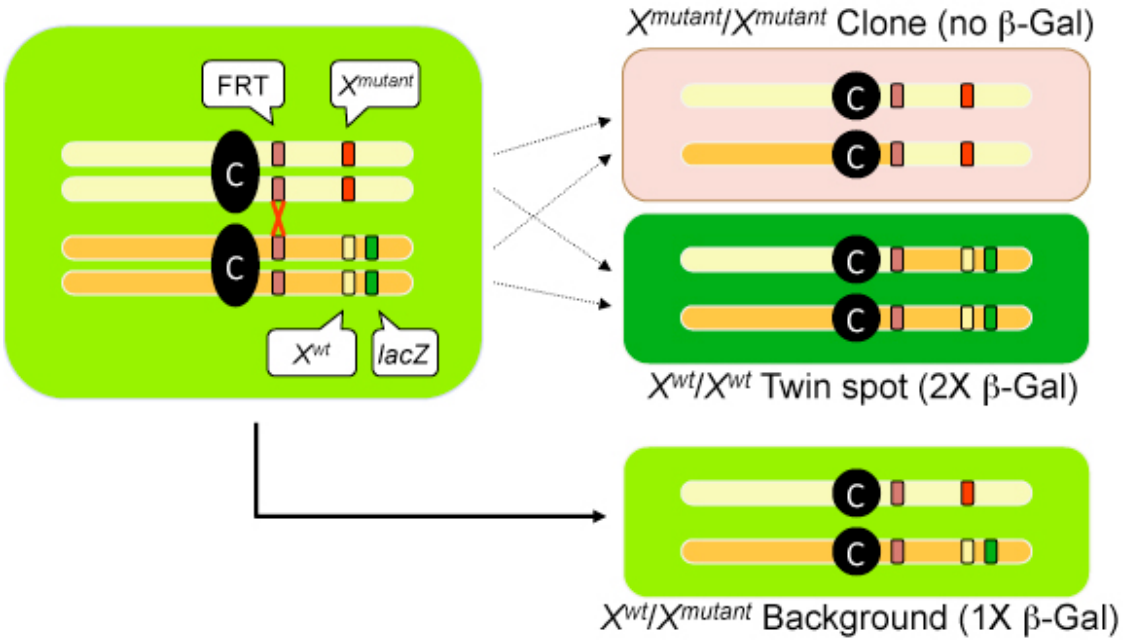

Figure 1-4. Generation of a mitotic clone using *flp/FRT*.

Shown is a cartoon to explain *flp/FRT* system. The box on the left indicates a cell undergoing mitosis. This cell is in a fly heterozygous at gene *X*. The homolog with X^{wt} is with *lacZ* whereas the other homolog with X^{mutant} is without *lacZ*. Site-specific recombination is induced at the *FRT* site where *flp* is expressed. Two daughter cells are generated with the completion of the mitosis. The upper right box indicates a daughter cell homozygous X^{mutant} marked with the absence of *lacZ* expression. The middle right box indicates the other daughter cell homozygous X^{wt} marked with 2x expression of *lacZ*. The bottom right box indicates a cell did not undergo recombination. Black circle with "C" indicates a centromere.

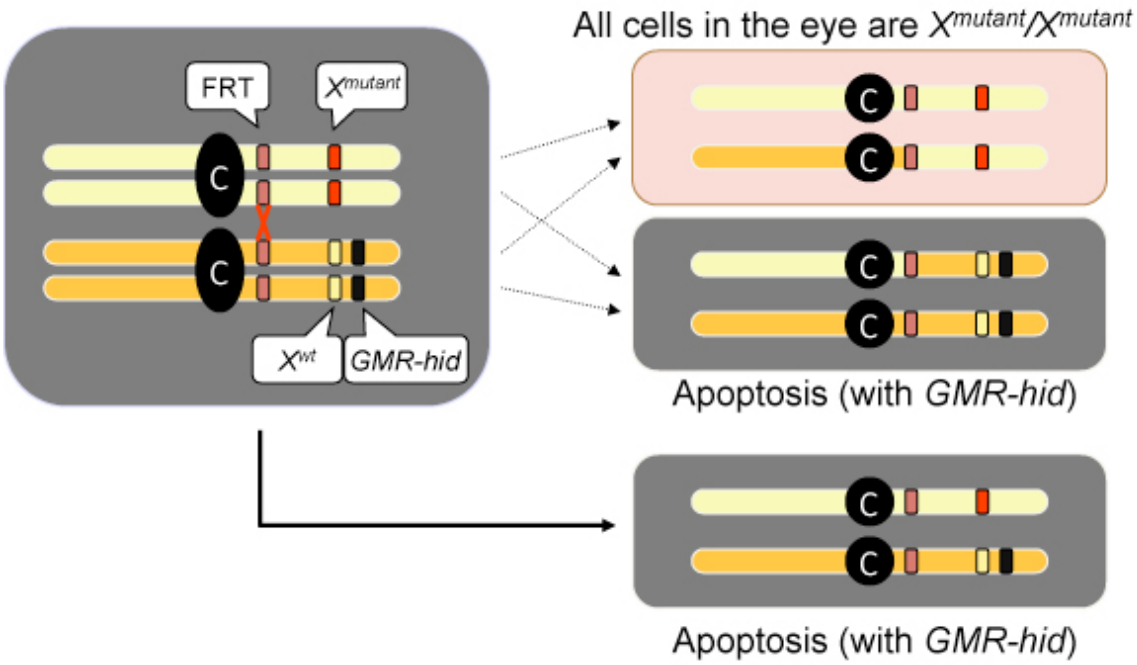

Figure 1-5. Generation of a whole eye clone using *flp*/*FRT GMR-hid* technique.

Shown is a cartoon to explain *flp*/*FRT GMR-hid* system. The box on the left indicates a cell undergoing mitosis. This cell is in a fly heterozygous at gene *X*. The homolog with X^{wt} is with *GMR-hid* whereas the other homolog with X^{mutant} is without *GMR-hid*. Site-specific recombination is induced at the *FRT* site where *flp* is expressed. Two daughter cells are generated with the completion of the mitosis. The upper right box indicates a daughter cell homozygous X^{mutant} marked with the absence of *GMR-hid* expression. The middle right box indicates the other daughter cell homozygous X^{wt} with 2x *GMR-hid*. The bottom right box indicates a cell did not undergo recombination with a *GMR-hid*. Cells with *GMR-hid* undergo apoptosis in an eye-spefic way. Ultimately, only X^{mutant} homozygotes will survive in the affected eye. Black circle with "C" indicates a centromere.

1.2 INTRACELLULAR VESICLE TRAFFICKING

Vesicle trafficking

Eukaryotic cells are enclosed with plasma membrane and compartmentalized with subcellular organelles in the plasma membrane. In living cells, these membranous compartments are not static. They continuously communicate with each other by means of sharing membranes, materials inside the membranes, and membrane proteins. For this communication between membranous organelles, vesicles or tubules are formed at the departing organelles and they are targeted to fuse with the destination organelles.

There are many kinds of vesicles and routes of trafficking and they can be classified depending on the type of coat proteins, such as clathrin, coat protein complex I and II (COPI and COPII), and the recently identified Exomer (Barlowe et al, 1994; Pearse, 1976; Wang et al, 2006a) (Fig. 1-6). Clathrin is required for clathrin-dependent endocytosis and trafficking between the endosomes and Golgi. COPI mediates retrograde trafficking from the Golgi to ER, and between Golgi cisternae to maintain their integrity. COPII mediates anterograde trafficking from the ER to Golgi to export newly synthesized proteins. Exomer was suggested relatively recently as a coat for TGN to plasma membrane trafficking (Wang et al, 2006a). Each kind of coat protein needs its own set of adapters that connect coats to the membrane and cargos. Clathrin-dependent trafficking is studied most extensively and a plays role in different routes. For this reason, intracellular trafficking can be simply sub-categorized as clathrin-dependent and clathrin-independent trafficking.

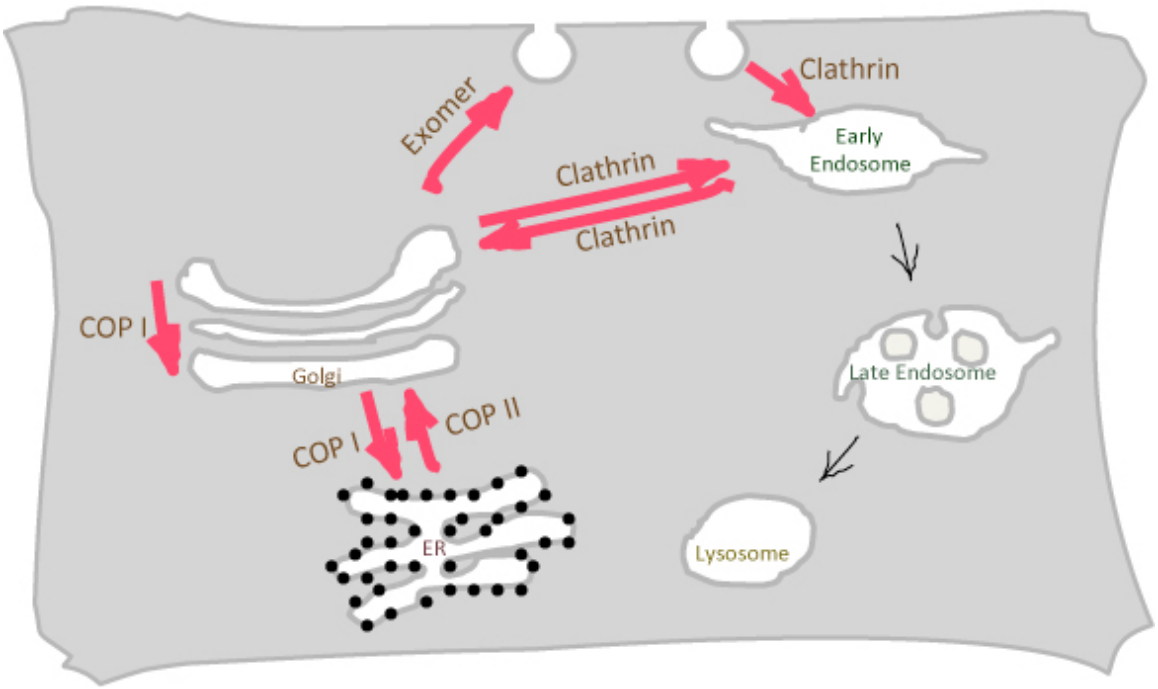

Figure 1-6. Routes of intracellular trafficking mediated by different coat proteins.

This cartoon shows the routes of intracellular trafficking mediated by known coat proteins. COP I mediates retrograde trafficking from the Golgi to ER and in between Golgi stacks. COP II mediates anterograde trafficking from the ER to Golgi. Clathrin mediates endocytosis and Golgi-endosome trafficking in both directions. Exomer is involved in secretion.

Clathrin-dependent vesicle trafficking

The outer layer of a clathrin-coated vesicle is covered with a polygonal basket composed of clathrin triskelions, which is a heterohexamer of 3 clathrin heavy chains and 3 clathrin light chains (Fig. 1-7A). Clathrin triskelions can self-assemble to form a clathrin basket (Crowther & Pearse, 1981), which is a driving force of vesicle organization. The N-terminus of clathrin heavy chain has a β-propeller structure, which is important in protein-protein interaction with clathrin adapters (ter Haar et al, 1998) (Fig. 1-7B).

Peptide motifs in clathrin adapters can bind to the β-propeller in between the blades. A peptide motif called the clathrin box with the sequence LΦxΦ[DE], where Φ is an amino acid with bulky hydrophobic residue like leucine, isoleucine, methionine, phenylalanine, and valine, is first found from a clathrin adapter AP3 with its ability to bind to the clathrin β-propeller (Dell'Angelica et al, 1998). The sequence [SD]LL is also found as a peptide motif for clathrin binding from AP180 and many other clathrin-binding proteins (Morgan et al, 2000). Yet another sequence PWDLW called W-box is identified from amphiphysins and Snx9 (Miele et al, 2004).

Clathrin cannot bind to membrane or cargo proteins by itself. Clathrin requires a subset of proteins called clathrin adapters to be connected to the membrane. For this reason, clathrin adapters play important roles in clathrin-coated vesicle formation. Because different membranes have somewhat different compositions, there are specific clathrin adapters for each route of clathrin-coated vesicle trafficking. Clathrin-coated

vesicles for endocytosis and for Golgi/endosome trafficking have completely different sets of adapters and accessory factors. With their domains and peptide motifs, clathrin adapters bind to clathrin, lipids, cargo proteins and other clathrin adapters, forming a rigid connection in between the coat and the membrane.

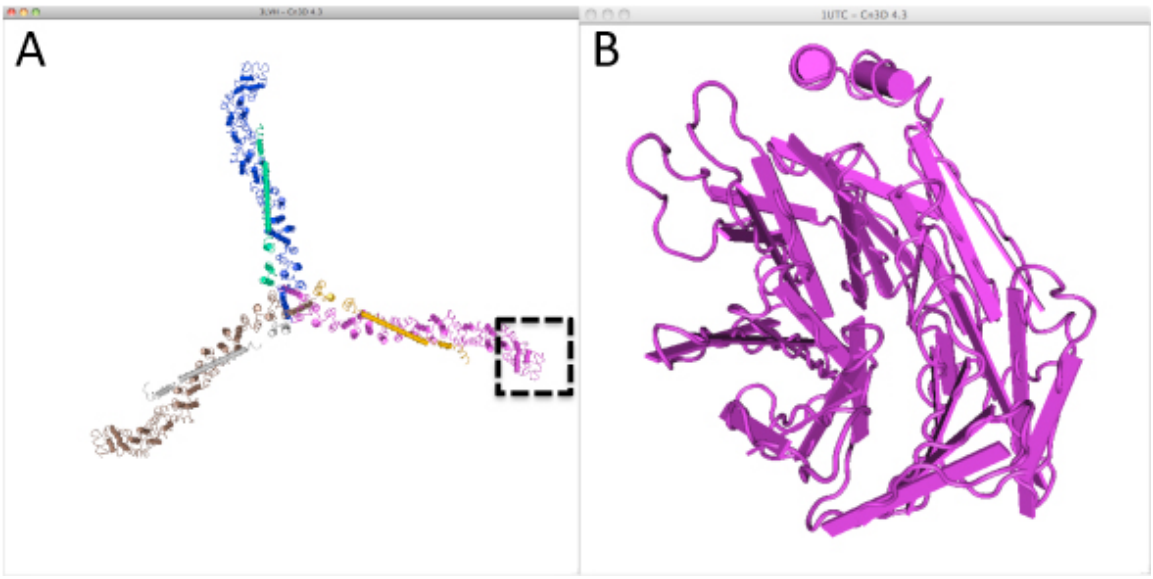

Figure 1-7. The crystal structure of clathrin tri-skeleon and N-terminal β-propeller.

(A) a heterohexamer of three clathrin heavy chains (purple, brown, and blue) and three clathrin light chains (yellow, grey, and green) (Wilbur et al, 2010). The square with broken line indicates the N-terminus of a clathrin heavy chain magnified in (B). (B) is to show a β-propeller structure of clarthrin heavy chain N-terminus (purple) (Miele et al, 2004). Cn3D program was used to generate these images. PDB ID: (A) 3LVH; (B) 1UTC. (Amphiphysin was erased from the original image generated by Cn3D in (B) to show just β-propeller structure.)

Clathrin adapters

Adapter protein complexes (APs) were first found as clathrin adapters with the observation that a clathrin cage could be generated in nonphysiological conditions *in vitro*, but not in physiological condition except in the presence of cytosol. APs were the major players in the cytosol (Kirchhausen, 1999; Owen et al, 2004). There are 4 types of APs (AP1, AP2, AP3, and AP4), each of which is required for specific routes of trafficking. Recently, the fifth AP, AP5, was identified (Hirst et al, 2011). Among them, AP1 plays a role in clathrin-dependent trafficking between Golgi and endosomes and AP2 functions in for clathrin-dependent endocytosis (Owen et al, 2004).

APs are heterotetramers with two large subunits (a β and one of α, γ, δ, or ε), a medium-sized subunit (μ), and a small subunit (σ) (Fig. 1-8A, B). The large subunits are composed with three structural units. The N-terminal trunk domain is the core region of the complex with the function of lipid binding. The C-terminal appendage domain is important in protein-protein interaction with other adapters or accessory factors in the vesicle. A flexible unstructured region links the N- and C-terms (Owen et al, 2004).

AP2, the adapter for endocytosis, is composed of β2, α, μ2, and σ2 subunits (Fig. 1-8A). Appendages of β2 and α are important for interaction with other clathrin adapters including Epsin (Owen et al, 2004). This interaction is mediated by peptide motifs such as DP[FW], FxDxF, or WXX[FW] in AP2. The trunk domain of the α subunit and the μ2 subunit in AP2 interact with phosphatidylinositols PI(4,5)P2 and PI(3,4,5)P3, which are

enriched at the plasma membrane. The μ2 subunit is also important in interaction of cargos with YxxΦ motif on the cytosolic side.

AP1, Like AP2, is also a tetramer, but is constituted with different subunits: β1, γ, μ1, and σ1 (Fig. 1-8B). AP1 has the strongest affinity to PI(4)P, which is enriched at the Golgi (Wang et al, 2003). This interaction plays an important role in localizing AP1 to the Golgi membrane. The γ-appendage of AP1 provides binding surfaces for its binding partners such as Golgi Epsin (Hirst et al, 2003; Kalthoff et al, 2002; Mills et al, 2003).

Golgi-localized, γ-ear-containing, Arf-binding proteins (GGAs) are another type of monomeric clathrin adapter (Fig. 1-8C). Structurally, GGAs have a VHS (Vps27, Hrs, STAM) domain to bind to cargos with DxxLL motifs, a GAT (GGA and TOM) domain to bind to proteins like ubiquitin, Arf1, and rabaptin5, and a GAE (γ-adaptin ear) domain, from the N-terminal to the C-terminal. The GAE domain is homologous to the AP1 γ-appendage and binds to the same proteins as γ-appendage does. A short proline-rich linker connects the VHS domain and the GAT domain, and a long flexible linker flanks GAT domain and GAE domain (Owen et al, 2004).

It seems to be a common strategy in clathrin adapters to have domain(s) and motifs connected with a long flexible unstructured loop. It may be an advantage for clathrin adapters to have a long flexible loop to maximize the chance of multiple dynamic interactions with molecules to form a vesicle. Another type of clathrin adapter, Epsin, also has this structure.

There are two types of Epsins, endocytic Epsin and Golgi Epsin (Fig. 1-8D, E). Each has a single globular ENTH (Epsin N-term homology) domain that has affinity for phosphoinositides. The ENTH domain in endocytic Epsin has higher affinity to PI(4,5)P2, while that of Golgi Epsin binds to PI(4)P preferentially. Other than the ENTH domain, the whole protein is unstructured with peptide motifs for protein-protein interactions dispersed in the flexible stretch. Endocytic Epsin has UIMs (ubiquitin interacting motifs), CBMs (clathrin binding motifs), NPF motifs for EH-binding, and Dx[FW] motifs for AP2 appendage binding. Golgi Epsin has clathrin binding motifs and AP1/GGA binding motifs but not UIM (Owen et al, 2004).

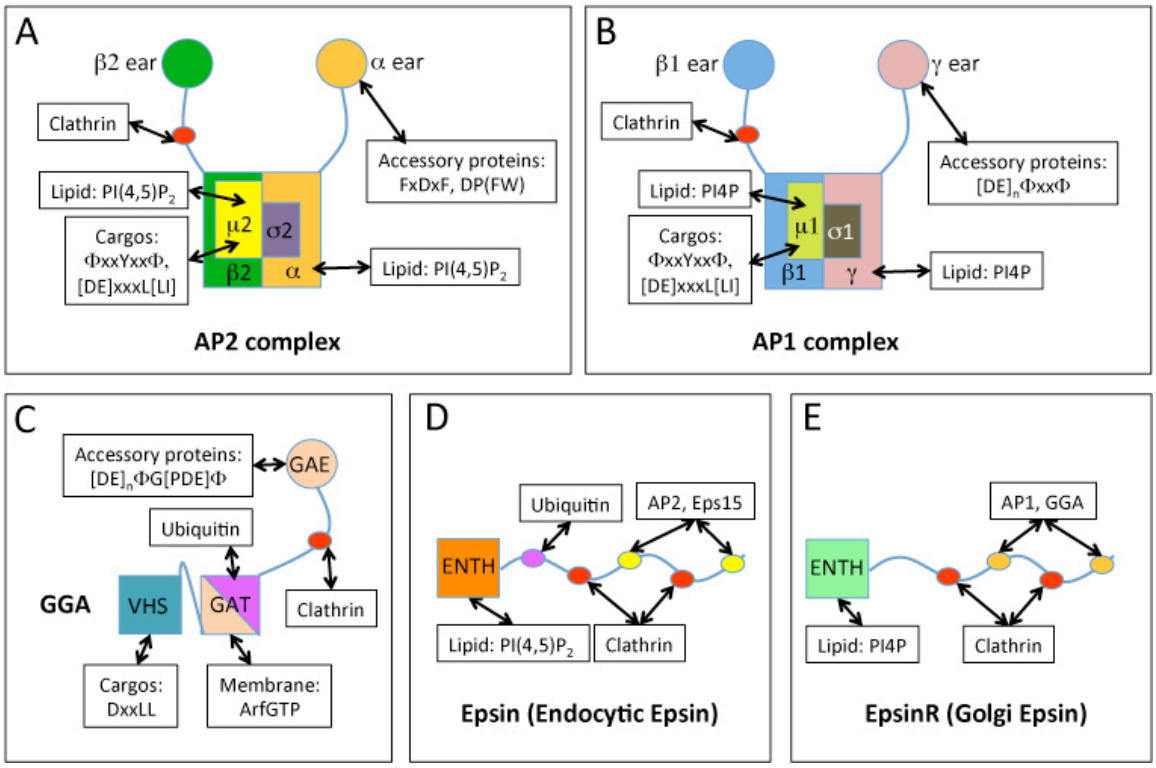

Figure 1-8. Clathrin adapters.

Cartoons to show clathrin adapters: (A) AP-2 complex; (B) AP-1 complex; (C) GGA; (D) Epsin (Endocytic Epsin); (E) EpsinR (Golgi Epsin). Binding partners for each domain and peptide motif were shown.

Some trafficking genes have specific roles in multi-cellular contexts

Trafficking components are probably required for trafficking of many cargos and thought to be generic. However, probably due to the redundancy, at least some of them have specific roles in multi-cellular contexts. One such example is the function of endocytic Epsin in the Notch signaling pathway.

Endocytic Epsin plays a specific role in the Notch signaling pathway (Overstreet et al, 2004; Wang & Struhl, 2004). The Notch signaling pathway is a cell-to-cell communication mechanism studied extensively in the context of developing tissues of animals such as *Drosophila*. Notch signaling is used in many developmental contexts with many different outcomes, including cell fate decisions between neuronal and non-neuronal cell differentiation in the *Drosophila* eye (Carthew, 2007). A membrane-attached ligand, Delta or Serrate, in the signal-sending cell signals the receptor, Notch, in a neighboring cell. Once the Notch receptor is activated, it undergoes a series of cleavages mediated by γ-secretase and other proteases to release the Notch intracellular domain, which turns on target gene expression in the nucleus (Fig. 1-9). With this pathway, signal-sending cells initiate neuronal differentiation and signal-receiving cells choose to be non-neuronal cells. To activate the Notch receptor, ligand has to make a protein-protein interaction with Notch, and undergo endocytosis into the signaling cell (Piddini & Vincent, 2003) (Fig. 1-9). There are several models explaining why Delta ligand has to undergo endocytosis to send signal, but one generally accepted model is that endocytosis generates a pulling force on the Notch protein and helps to expose the cleavage site of the receptor (Weinmaster & Fischer, 2011). The clathrin adapter Epsin is required for the endocytosis of ligand into the signal-sending cell. Mutants in the

Drosophila epsin gene, *liquid facets* (*lqf*), phenocopy *Notch* pathway mutants (Cadavid et al, 2000). Furthermore, Notch target genes are not expressed in *lqf* mutant cell clones in developing tissues, and ligand accumulates at the plasma membrane in the mutant cells (Overstreet et al, 2004). The finding that Epsin plays an essential role in Notch signaling highlights the importance of endocytosis to the core mechanism of Notch signaling and suggests that there might be more trafficking components that play important roles in other signaling pathways.

The essential function of the retromer complex in the Wingless signaling pathway presents another example of trafficking components in signaling pathways (Fig. 1-10). The retromer complex is a multi-protein complex with core components of Vps35, Vps29, and Vps26, with the function of forming tubules at early endosomes for the retrograde trafficking to Golgi (Seaman et al, 1998). Clathrin and Golgi Epsin are also known to function along with the retromer complex in this process (Popoff et al, 2007). In Wingless signaling, Wingless ligand is produced in a subset of cells and secreted to form a gradient in the developing tissue so each cell in the tissue reads the signal to determine its fate. For secretion of the ligand, secreting cells have a protein called Wntless that binds to ligand in the Golgi and guides the ligand to the plasma membrane where it is secreted. Probably due to the limiting amount of Wntless, Wntless has to be recycled back to the Golgi so that secretion can be continued. In the ligand secreting cells, retromer complex is shown to play an essential role in the recycling of Wntless (Belenkaya et al, 2008; Franch-Marro et al, 2008; Port et al, 2008). As there are other trafficking proteins that function in retrograde trafficking from early endosomes to Golgi, such as clathrin and Golgi Epsin, it would be interesting to test if Wntless recycling

requires all of these components or if the retromer complex is the only specific factor in the process (see Chapter 4) (Fig. 1-10).

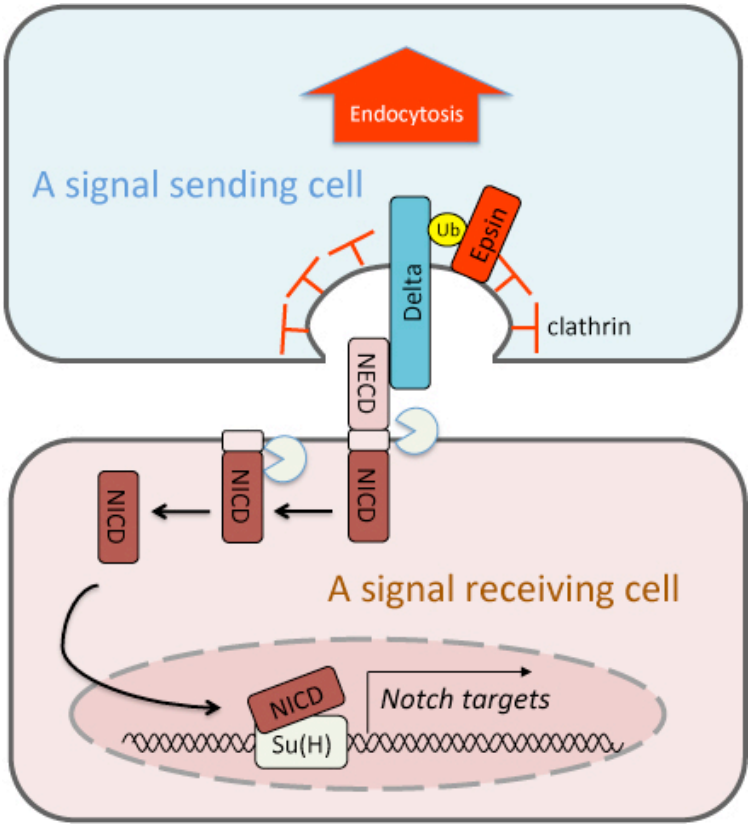

Figure 1-9. The Notch signaling pathway.

This cartoon shows essential events in the Notch signaling pathway. The upper box indicates a signal sending cell. Delta, bound with Notch, is endocytosed to send signal to the signal receiving cell. The lower box indicates the signal receiving cell. With the signal from Delta, Notch undergoes a serial cleavages. Notch intracellular domain (NICD) is translocated into the nucleus and turns on the target gene expression as a complex with Su(H).

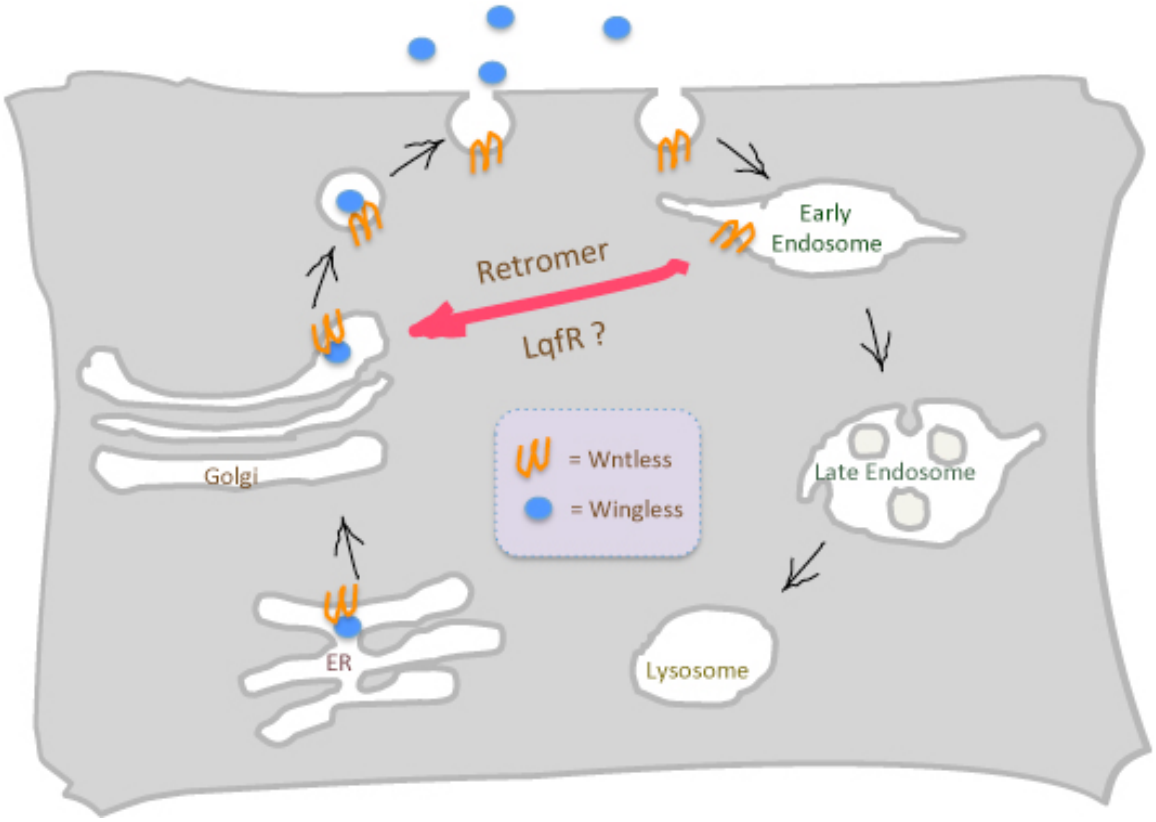

Figure 1-10. Routes of intracellular trafficking mediated by different coat proteins.

This cartoon shows the routes of intracellular trafficking mediated by known coat proteins. COP I mediates retrograde trafficking from the Golgi to ER and in between Golgi stacks. COP II mediates anterograde trafficking from the ER to Golgi. Clathrin mediates endocytosis and Golgi-endosome trafficking in both directions. Exomer is involved in secretion.

Golgi Epsin is conserved in all eukaryotes

Golgi Epsin is a clathrin adapter mediating clathrin vesicle formation for trafficking between Golgi and endosomes. Golgi Epsin has an ENTH domain, which has amino acid sequence similarity with that of endocytic Epsin. However, the ENTH domain in Golgi Epsin preferentially binds to phosphatidylinositol monophosphate enriched in Golgi and endosome membranes (Hirst et al, 2003). Its C-terminal side is an unstructured loop with peptide motifs for protein-protein interaction. While the ENTH domain is very well conserved in all eukaryotes studied so far, C-terminal sequences are overall poorly conserved. In the genome of *Saccharomyces cerevisiae, ent3* encodes an ENTH domain protein for protein sorting into the multi-vesicular body (Friant et al, 2003). *ent5* also encodes a functionally redundant protein with an ANTH domain, which is structurally similar to the ENTH domain (Eugster et al, 2004). In higher species like humans and other vertebrates, there is only one Golgi Epsin homolog encoding an ENTH domain protein, but it is known by various names including *epsin-Related*, *enthoprotin*, *clint1,* and *epsin4* (Hirst et al, 2003; Kalthoff et al, 2002; Pimm et al, 2005; Wasiak et al, 2002). *Drosophila* also has one Golgi Epsin gene that we call *liquid facets-Related*.

In *S. cerevisiae*, there are two functionally redundant Golgi Epsins, Ent3p and Ent5p. While deletion mutants in each of *ent3* and *ent5* did not show any phenotype, *ent3Δent5Δ* double deletion showed the phenotype of fragmented vacuoles due to a defect in trafficking to multi-vesicular bodies of biosynthetic or endocytic cargos that are ubiquitylated (Eugster et al, 2004). Golgi Epsin in mammals has not been studied at the organismal level, but established cell lines have been used to study the function of Golgi

Epsin from a cell biological perspective. From these studies, the routes and cargos that require Golgi Epsin function have been discovered.

Several cargo proteins of Golgi Epsin have been suggested. First, Vti1b, a SNARE (soluble NSF attachment protein [SNAP] receptors) protein required in a membrane fusion event for endosomal and lysosomal trafficking, has been found as a specific cargo that requires Golgi Epsin function. A yeast two-hybrid screen and subsequent binding assays identified that rat Vti1b and the yeast homolog Vti1p specifically binds to the ENTH domain in Golgi Epsin of respective species (Chidambaram et al, 2004). This interaction has been studied in more detail using the crystal structure of the complex from yeast homologs (Wang et al, 2011). The interaction is important for correct localization of Vti1b.

Based on sequence homology, there are 4 subtypes of SNARE proteins, Qa, Qb, Qc, and R, and QabcR complex forms a functional unit of SNARE. Since Vti1p, a Qb-SNARE, was found as a cargo of Golgi Epsin, Chidambaram and colleagues searched for other SNAREs that form complex with Vti1p to identify more cargos of Golgi Epsin. They suggested a Qa-SNARE Pep12p and a Qc-SNARE Syn8p were cargos of yeast Golgi Epsin using evidence of protein-protein interactions and genetic interactions, as well as localization defects of Pep12p (Chidambaram et al, 2008).

The yeast chitin synthase Chs3p is also suggested as a cargo of Golgi Epsin. Chs3p formed a complex with yeast Golgi Epsin and was retained in the *trans*-Golgi network (TGN) and intracellular compartments. In *ent3Δent5Δ* double knockouts, Chs3p was accumulated at the plasma membrane (Copic et al, 2007). This suggests that Golgi

Epsin may function in Golgi-to-endosome trafficking to keep cargo proteins away from the secretion pathway.

In mammalian cells, Golgi Epsin plays a role in retrograde trafficking from the early endosome to the TGN, which links endocytosis and the biosynthetic/secretory pathway (Saint-Pol et al, 2004). Shiga toxin B subunit (STxB) has been used as a marker for retrograde trafficking because Shiga toxin enters the cell, is trafficked to the Golgi through endocytosis and the endosome-to-Golgi route, and is not toxic. While STxB endocytosis was slightly affected by the inhibition of clathrin expression, early endosome-to-Golgi trafficking was strongly reduced. AP1 was not required for STxB retrograde trafficking, but Golgi Epsin was. Endogenous proteins, TGN38/46 and mannose 6-phosphate receptor, are recycled after secretion through this retrograde trafficking, and their retrograde trafficking was blocked without Golgi Epsin function (Saint-Pol et al, 2004). This finding suggests that Golgi Epsin may generally be required for the retrograde trafficking.

The function of Golgi Epsin in a multi-cellular context has not been reported until our first paper describing the function of *Drosophila* Golgi Epsin (Lee et al, 2009) was published. Right after our paper, Dodd and colleagues published their paper describing the function of Golgi Epsin in zebrafish (Dodd et al, 2009). They found Golgi Epsin from a screen for genes involved in inflammation regulation. Mutation in Golgi Epsin caused chronic inflammation in epidermal tissues, bidirectional trafficking of leukocytes between the epidermal tissues and vasculature, and increased phagocytosis of cellular debris in leukocytes (Dodd et al, 2009). They also found that their mutant fish had defects in hemidesmosome formation. The hemidesmosome is a structure composed of integrins and their associated proteins found at the basal surface of epithelia to attach to the basal

membrane. Golgi Epsin and Lethal giant larvae 2, which is important in formation and maintenance of the hemidesmosome, synergistically regulated epithelial homeostasis. They suggested that the phenotype resembles the human condition psoriasis (Dodd et al, 2009).

1.3 THE WINGLESS SIGNALING PATHWAY IS IMPORTANT FOR PROLIFERATION

I introduce the Wingless signaling pathway because *liquid facets-Related* is found to have a role in the canonical Wingless signaling pathway (Chapter 4).

Wingless signaling pathway: an overview

The Wingless (Wnt) signaling pathway is a well-conserved pathway iteratively used in a context-dependent manner in animal development ranging from *Drosophila* and *C. elegans* to mammals (Moon et al, 2002). Components in the pathway are also found as oncogenes. This pathway was studied in *Drosophila* and vertebrates independently until Rijsewijk and colleagues found that *Drosophila wingless* and the vertebrate oncogene *int-1* were homologous. They renamed vertebrate Int-1 as Wnt (Rijsewijk et al, 1987).

In the canonical Wingless signaling pathway, Armadillo (β-catenin) is a key downstream component that functions as a transcriptional co-activator to turn on target gene expression. This pathway is also called the β-catenin-dependent Wingless signaling pathway, which indicates that Wingless can also turn on the signal without activating the transcriptional activity of Armadillo. This pathway is called the β-catenin-independent pathway, which includes the Wnt planar cell polarity pathway and Wnt/Ca^{2+} pathway

(Chien et al, 2009; Kohn & Moon, 2005). In this section, I will focus on the canonical β-catenin-dependent Wingless signaling pathway.

Core components in the canonical Wingless signaling pathway

In the canonical Wingless signaling pathway (Moon et al, 2002), the cell turns on a signal cascade with the Wingless ligand that binds to its receptors, Frizzled and Arrow (LRP5/6), at the plasma membrane. This event sends signal into the cell ultimately to accumulate cytosolic Armadillo so it can enter in to the nucleus. Armadillo in the nucleus binds to DNA binding protein Pangolin (LEF/TCF) to turn on the target gene expression. Without the signal, the cell actively degrades Armadillo. Since Armadillo is a key component in the signaling cascade, anything that regulates cellular Armadillo levels is important in the signaling pathway. Furthermore, the level of Armadillo decides the strength of the signal that, in turn, decides the levels of the target gene expression.

There is a single gene encoding Wingless ligand in *Drosophila* (Bejsovec & Wieschaus, 1995). Wingless is a glycoprotein morphogen that forms a gradient in developing tissues. In an early *Drosophila* eye disc, *wingless* is expressed in a small group of cells at both margins distal to the D/V midline (Yang et al, 2002). The Wingless ligand is then secreted from the cells and forms a gradient highest at the margin and lowest at the D/V midline. This gradient is decoded as a transcriptional activation signal through Armadillo by each cell in the field (Tomlinson, 2003).

Mechanistically, Wingless signaling inhibits a protein complex called the "destruction complex" composed of the core proteins Axin, glycogen synthase kinase-3 (GSK3), and adenomatous polyposis coli (APC) (Benchabane et al, 2008) (Fig. 1-11). When the signal is off, the complex binds to cytosolic Armadillo and GSK3 directly

phosphorylates Armadillo. This phosphorylation serves to tag Armadillo to be ubiquitylated and degraded. Once the signal is on, the destruction complex is inhibited through Dishevelled and cytosolic Armadillo is stabilized and accumulates. Ultimately, Armadillo is translocated into the nucleus and turns on target gene expression along with the DNA binding protein Pangolin (Brunner et al, 1997). Armadillo does not have a known nuclear localization signal. In fact, it has been shown that purified β-catenin can be translocated into the nucleus by itself *in vitro* (Fagotto et al, 1998). However, it is also known that co-incubation with cytosolic extract inhibits nuclear translocation, suggesting that there are some inhibitory factors in the extract (Fagotto et al, 1998). One such factor is Axin that anchors β-catenin at the cytoplasm (Tolwinski & Wieschaus, 2001).

One of the transcriptional targets is the atypical cadherin gene *dachsous*. In an *armadillo* null clone in eye discs, *dachsous* expression is shut off, and cells in *armadillo* overexpressing clones express *dachsous* ectopically (Yang et al, 2002). In the developing *Drosophila* eye, Dachsous and its inter-cellular binding partner Fat play an important role in planar cell polarity (Yang et al, 2002). However, Dachsous and Fat are also upstream components of the Hippo pathway, which regulates proliferation in the epithelium (Willecke et al, 2008).

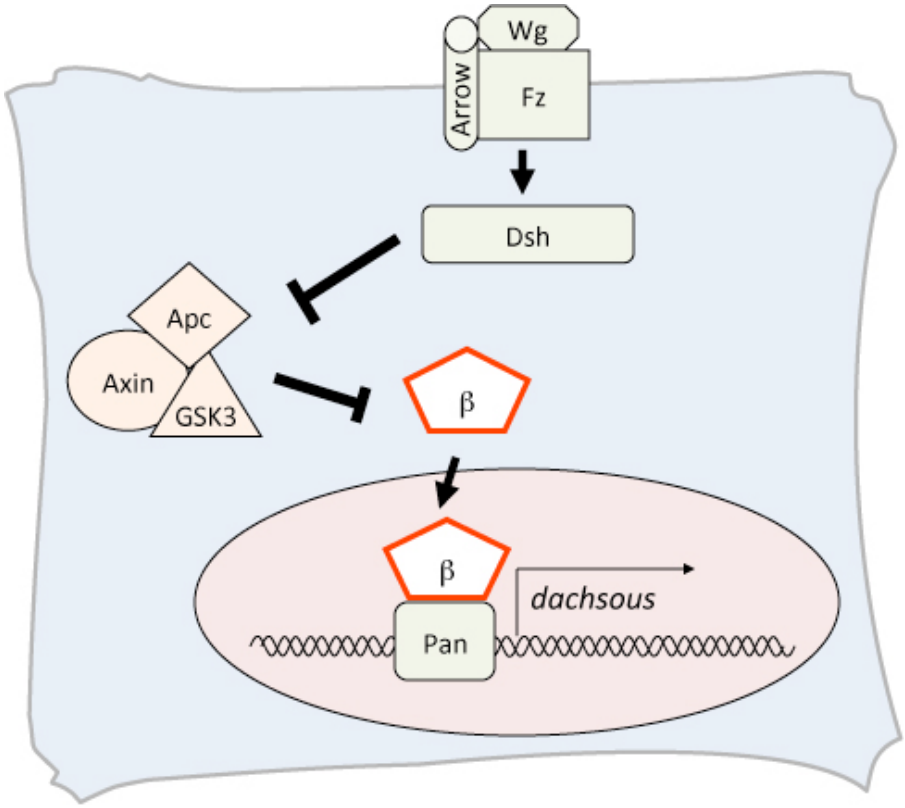

Figure 1-11. The canonical Wingless signaling pathway.

This cartoon shows regulators of the canonical Wingless signaling pathway. When the Wingless ligand binds on the receptors, Frizzled and Arrow, the activity of "destruction complex", composed of Axin, APC, and GSK3, is inhibited. As a result, β-catenin accumulates and turns on the target gene expression with Pangolin. One of the known target in developing *Drosophila* eye is dachsous.

Abbreviations: Wg=Wingless; Fz= Frizzled; β=β-catenin; Pan=Pangolin.

The role of E-cadherin and adherens junctions in the Wingless signaling

Cells in epithelia are tied together laterally with junctions and the adherens junction seals gaps between cells at the most apical area. The central component in an adherens junction is the transmembrane protein E-cadherin, which interacts homotypically via its extracellular domain with another E-cadherin in an opposing cell (Kemler, 1992). Therefore, the E-cadherin extracellular domain has a critical role in cell-cell interaction.

The intracellular part of E-cadherin is even more interesting. It plays two important roles in the cell (Heuberger & Birchmeier, 2010). First, by providing surfaces for protein-protein interaction, it builds up protein complex with other adherens junction proteins such as Armadillo and α-catenin. Protein complex formation is essential for E-cadherin function. Without β-catenin binding, E-cadherin is retained in ER and unable to be targeted to the plasma membrane (Chen et al, 1999). Also, newly synthesized E-cadherin is unstructured in the absence of β-catenin (Huber et al, 2001). The second role of the intracellular domain is in regulating Wnt signal activity through its binding partner β-catenin. β-catenin, the transcriptional activator in the Wingless signaling pathway, can be sub-divided into two pools based on its localization: E-cadherin-bound pool and "free" pool, most of which are bound to TCF/LEF (Cadigan & Nusse, 1997). While "free" pool of β-catenin functions as a transcriptional co-activator in signaling, E-cadherin-bound Armadillo functions as a component of the adherens junction and cannot activate gene expression.

Dual functions of Armadillo raise the interesting issue that the cellular level of E-cadherin can influence transcriptional activity of Armadillo. If a group of cells in an epithelium has too much E-cadherin, cytosolic Armadillo can be titrated out and the Wingless signal activity can be reduced. In *Drosophila*, when wild-type E-cadherin or a truncated mutant without the extracellular domain is overexpressed in the wing disc, adult flies have a notched wing phenotype. This phenotype is strongly suppressed with co-overexpression of Armadillo (Sanson et al, 1996). A similar phenomenon happens in mammalian cells. In SW480, a colorectal cancer cell line where β-catenin transcriptional activity is higher than normal cells, overexpressed E-cadherin caused reduced proliferation due to its β-catenin binding part (Gottardi et al, 2001). To summarize, due to the pleiotropic role of Armadillo, E-cadherin plays an inhibitory role in canonical Wingless signal activity in certain contexts.

1.4 *TEL2* IS AN ESSENTIAL AND PLEIOTROPIC GENE CONSERVED IN EUKARYOTES

Drosophila liquid facets-Related has exons for the ENTH domain and other peptide motifs for the function of Golgi Epsin. However, there is yet another huge *exon 6* at the end of one of the splice form of the *lqfR* mRNA (see Chapter 2). This exon is not found in Golgi Epsin genes from other species including yeast, nematode, and vertebrate, but is found as a separate gene, *tel2* (also known as *clk-2* or *rad-5*).

Various genetic screens identified *tel2*

A *tel2* homolog was first identified as *rad-5* as a result of a screen using *C. elegans* for genes hypersensitive to UV or X-ray irradiation (Hartman & Herman, 1982).

Later, *rad-5* turned out to be allelic to *clk-2* (Ahmed et al, 2001). *clk-2* was also found in a genetic screen using *C. elegans*, but for genes with altered developmental and behavioral timing, a so-called "clock" phenotype, instead of radiation sensitivity (Lakowski & Hekimi, 1996). From the screen, they identified three genes, *clk-1, clk-2, and clk-3*, which extended life span significantly when mutated. Among them, *clk-2* was later found to be orthologous to yeast *tel2* (Benard et al, 2001).

The name *tel2* first came from a yeast genetic screen for genes regulating telomere length (Lustig & Petes, 1986). 200 yeast strains with temperature sensitive mutations were screened for shorter or longer telomere lengths. From this screen, they found 3 strains with shorter telomeres that ended up in 2 complementation groups, named *tel1* and *tel2*, respectively (Lustig & Petes, 1986). However, unlike yeast *tel2*, *C. elegans clk-2* mutants had longer telomere and overexpression of *clk-2* caused it to be shorter (Lakowski & Hekimi, 1996).

tel1 is a well conserved gene in all eukaryotes. When the mammalian ortholog *ATM (ataxia-telangiectasia, mutated)* is mutated, it causes ataxia telangiectasia, a human genetic disorder largely due to chromosome instability (Derheimer & Kastan, 2010). *tel1* and *tel2* are functionally related. Tel1 requires Tel2 for its correct targeting on DNA break point where Tel1 functions (Anderson et al, 2008). However, how the molecular mechanism is unknown. Compared to *tel1* that has been studied extensively in various model organisms due to its homology to a human disease gene, *tel2* function is not clearly understood.

Tel2 is essential for mouse embryonic development. Targeted deletion of *tel2* in mouse caused embryonic lethality (Takai et al, 2007). However, there was not an obvious

telomere length defect. Further molecular studies from the group, using a cell line, revealed an interesting function of Tel2 (see below).

In summary, genetic studies of *tel2* using model systems show a variety of phenotypes including defects in telomere length, radiation sensitivity, duration of the lifetime, and protein targeting, some of which are not consistent between species.

Molecular studies of Tel2

Takai and colleagues further analyzed Tel2 using a MEF cell line, and revealed that Tel2 is important for proliferation and has a role in stabilizing phosphatidylinositol 3-kinase-related protein kinases (PIKKs), which includes 6 mammalian kinases mammalian target of rapamycin (mTOR), ATM, ATM and Rad3 related (ATR), DNA-dependent protein kinase catalytic subunit ataxia (DNA-PKcs), suppressor with morphological effect on genitalia 1 (SMG1), and transformation/transcription domain-associated protein (TRRAP) (Takai et al, 2007). In Tel2 conditional knocked out MEFs, the levels of PIKKs were each significantly reduced. Furthermore, co-immunoprecipitation followed by MALDI-TOF mass spectrometric analysis and follow up experiments identified that PIKKs interacts with Tel2, suggestive of Tel2 function as stabilizing PIKKs through protein-protein interactions (Takai et al, 2007). The Tel2 function in binding with and stabilizing PIKKs in the mammalian cell line is partially confirmed by yeast studies. Yeast Tel2 co-immunoprecipitated with yeast PIKKs, Tel1 and Mec1 (yeast homolog of ATR), but Tel2-1 with missense mutation S129N failed to precipitate either Tel1 or Mec1 (Anderson et al, 2008), suggesting S129 is important in the protein-protein interaction. This may not be due to an overall change in the structure, because the *tel2-1* mutant is viable while the *tel2* knockout is lethal, and Tel2-1 protein

level and size in the gel were equal to wild-type (Anderson et al, 2008). The levels of Tel1 and Mec1 were also decreased in Tel2-1 mutants. These results raise an interesting hypothesis that the Tel2 phenotype is due to collective loss-of-function of PIKKs due to their decreased protein levels.

Anderson and Blackburn tested the hypothesis, and showed that the effect of Tel2 on stabilizing PIKKs can be uncoupled from the effect on the function of PIKKs (Anderson & Blackburn, 2008; Anderson et al, 2008). The level of Mec1 was moderately decreased in *tel2-1* mutants, and Mec1 and Tel2-1 was not detected. However, Mec1 protein did not completely disappear and based on Mec1 activity during DNA damage response, the lower levels of Mec1 were enough to provide function (Anderson & Blackburn, 2008). In *tel2-1* mutant yeast, the Tel1 level is reduced to about 60-80% of wild type and Tel2 function on DNA damage is abrogated (Anderson et al, 2008). In the *tel2-1* mutant, Tel1 protein cannot be targeted to the site of DNA damage although *tel2-1* did not affect nuclear localization of Tel1. However, even when Tel1 was overexpressed in *tel2-1* cells, Tel2 function was not restored, which indicates that the reason Tel1 malfunctions in the *tel2-1* mutant is not due to the level of the protein (Anderson et al, 2008). Then, why are the levels of PIKKs are decreased in *tel2* mutants? Anderson et al. suggests that the levels of PIKKs are decreased because Tel2 is a binding partner of PIKKs, and it is common that protein stability and levels are dependent on the existence of its binding partner.

If the *tel2* phenotype is due to depleted PIKKs, the *tel2* phenotype should mimic known mutant phenotypes of PIKKs. However, functional analysis of *clk-2/tel2* using *C. elegans* shows that Tel2 depletion does not phenocopy PIKK depletion (Moser et al, 2009). They found that *clk-2* mutants have a delayed embryonic cell cycle due to

increased DNA damage. However, it has been shown that co-depletion of *atl-1* (*C. elegans ATR*) and *chk-1* fully inactivate the DNA replication checkpoint (Brauchle et al, 2003), and Moser et al. showed that *atl-1*/*chk-1* co-depletion expedites cell cycle timing. Furthermore, co-depletion of *atl-1*/*chk-1* rescued the cell cycle delay phenotype in *clk-2* mutants. These results indicate that *clk-2* triggers the *atl-1*/*chk-1* dependent DNA damage checkpoint, and *clk-2* and *atl-1* are antagonistic (Moser et al, 2009). Moser et al. further showed that *clk-2* is required for germ cell proliferation rather than differentiation. They also found abnormal spindle rotation in *clk-2* mutants and suggested that this might be somehow related to the Wnt signaling pathway, because the spindle rotation defect can be caused by a spindle polarization defect and *mom-2 (wnt)* and *mom-5 (frizzled)* mutants have spindle polarization defects (Bischoff & Schnabel, 2006; Walston et al, 2004).

The crystal structure of budding yeast Tel2 has been determined recently (Takai et al, 2010) (Fig. 1-12). Tel2 protein forms an overall helical repeat structure, in which pairs of α-helices form units to build up a superhelical assembly called α-solenoid (Takai et al, 2010). Two structural domains, N-terminal solenoid (NTD) and C-terminal solenoid (CTD), are connected with a loop. There is another protease sensitive loop within the CTD. The NTD has amino acid residues 1-354 and 21 α-helices. Residues 355-386 form a loop folding backward to the middle of NTD region, so that the CTD stems from NTD from the middle. CTD consists of 9 α-helices forming 4 pairs of repeats and one terminal helix (Takai et al, 2010). This results in an overall 'y'-shaped structure with NTD being the long arm, and CTD being the short arm (Fig. 1-12). The sequence conservation between yeast Tel2 and human Tel2 is 12.2% identity at the NTD and 19.8% identity at the CTD (Takai et al, 2010) (Fig. 1-13). Tel2 structure is homologous to HEAT repeat

family proteins (Andrade et al, 2001), and structurally closest to the VHS domain of STAM1 and a part of importin β (Takai et al, 2010).

Proteomic analysis identified two Tel2-interacting partners, Tti1 and Tti2 (Hayashi et al, 2007; Shevchenko et al, 2008). Tel2, Tti1, and Tti2 are also called TTT complex. Tti1 and Tti2 are also recently identified in screens for genes required for resistance to ionizing radiation in human cell line U2OS (Hurov et al, 2010) and chromosome stability in yeast (Stirling et al, 2011). TTT complex components require each other for their stability (Hurov et al, 2010).

Although tel2 has been identified from multiple independent genetic screens using various model organisms, the mechanistic basis of tel2 function is still unclear. Takai et al. first provided an intriguing hypothesis that Tel2 function might be explained as a collective loss-of-function of all PIKKs. However, experimental data from other groups using yeast and nematode argued against the hypothesis. Further genetic and molecular analyses would be required to better understand the mechanism of Tel2 function.

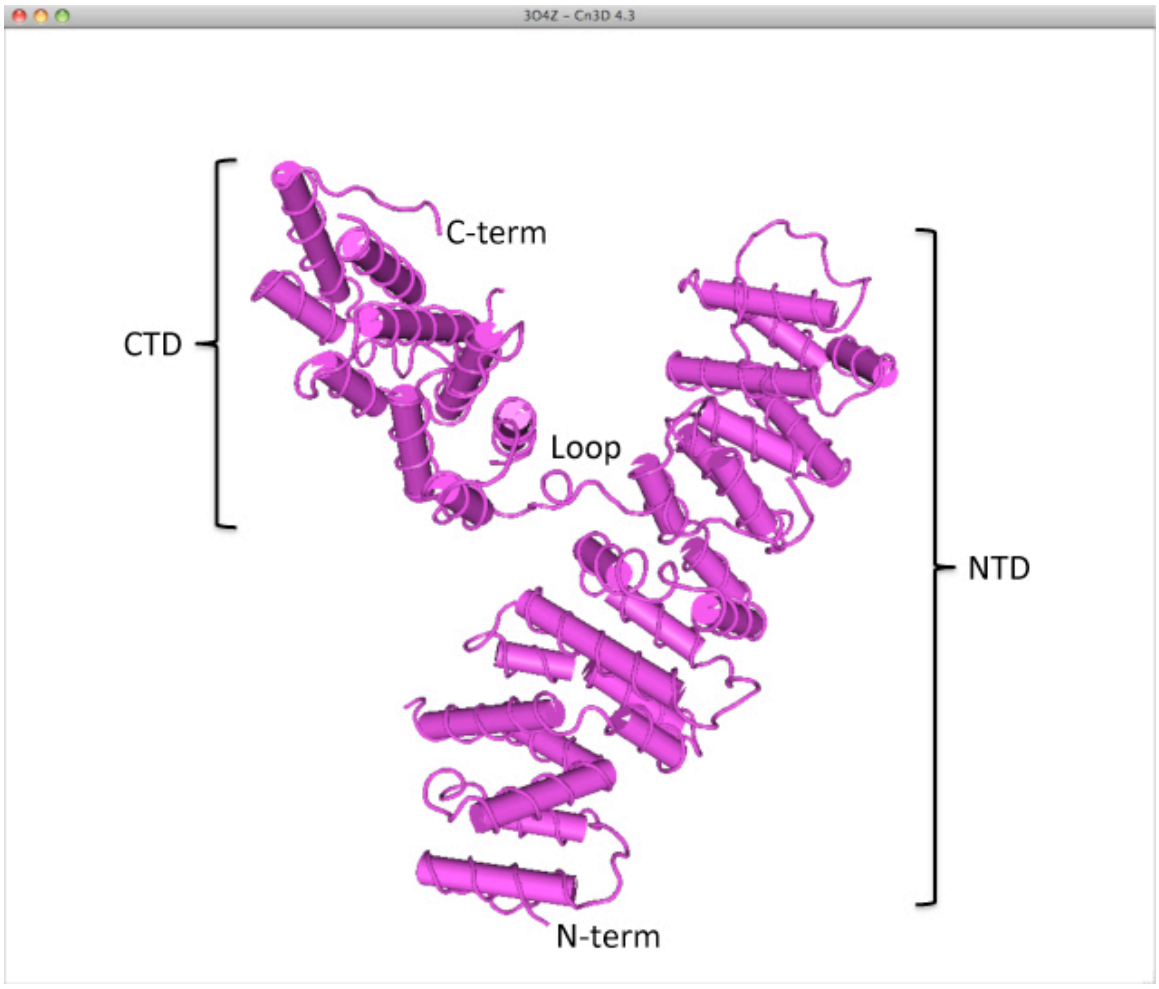

Figure 1-12. The crystal structure of yeast Tel2.

Shown is a α-solenoid structure of yeast Tel2 (purple). N-terminal solenoid (NTD), C-terminal solenoid (CTD) and a loop between them form overall “y”-shaped structure. Cn3D program was used for these images. PDB ID: 3O4Z.

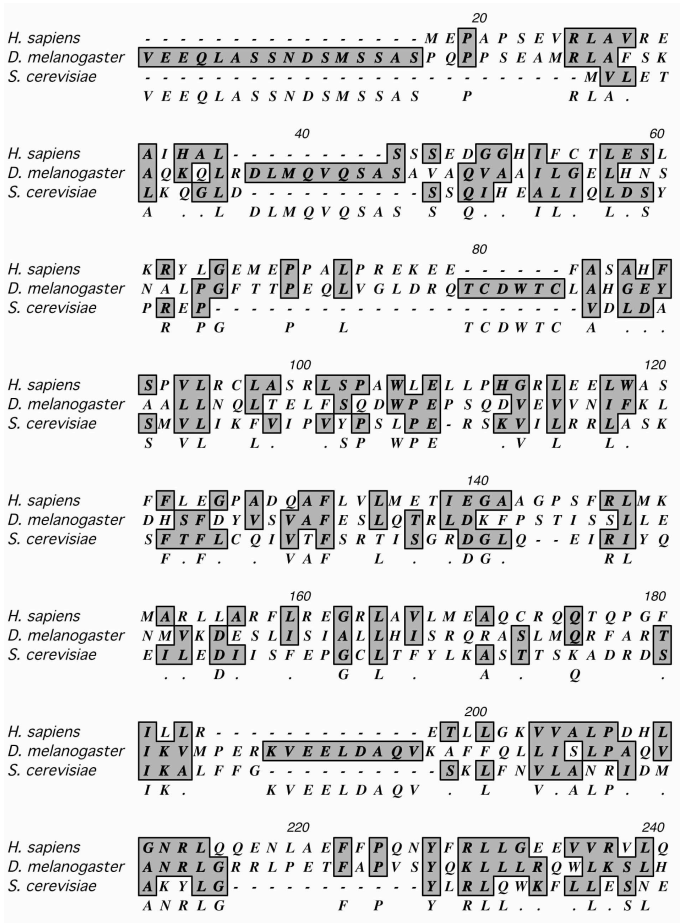

Figure 1-13. Sequence alignment of human and yeast Tel2 and *Drosophila* LqfR exon 6.

The amino acid sequences of *H. sapiens* Tel2, *D. melanogaster* LqfR exon 6, and *S. cerevisiae* Tel2 were aligned. *H. sapiens* versus *S. cerevisiae*: Aligned Length = 850; Gaps = 23; Identities = 116 (13%); Similarities = 102 (12%). *H. sapiens* versus *D. melanogaster*: Aligned Length = 929; Gaps = 15; Identities = 181 (19%); Similarities = 158 (17%). *D. melanogaster* versus *S. cerevisiae*: Aligned Length = 924; Gaps = 18; Identities = 110 (11%); Similarities = 121 (13%). MacVector program was used for the alignment.

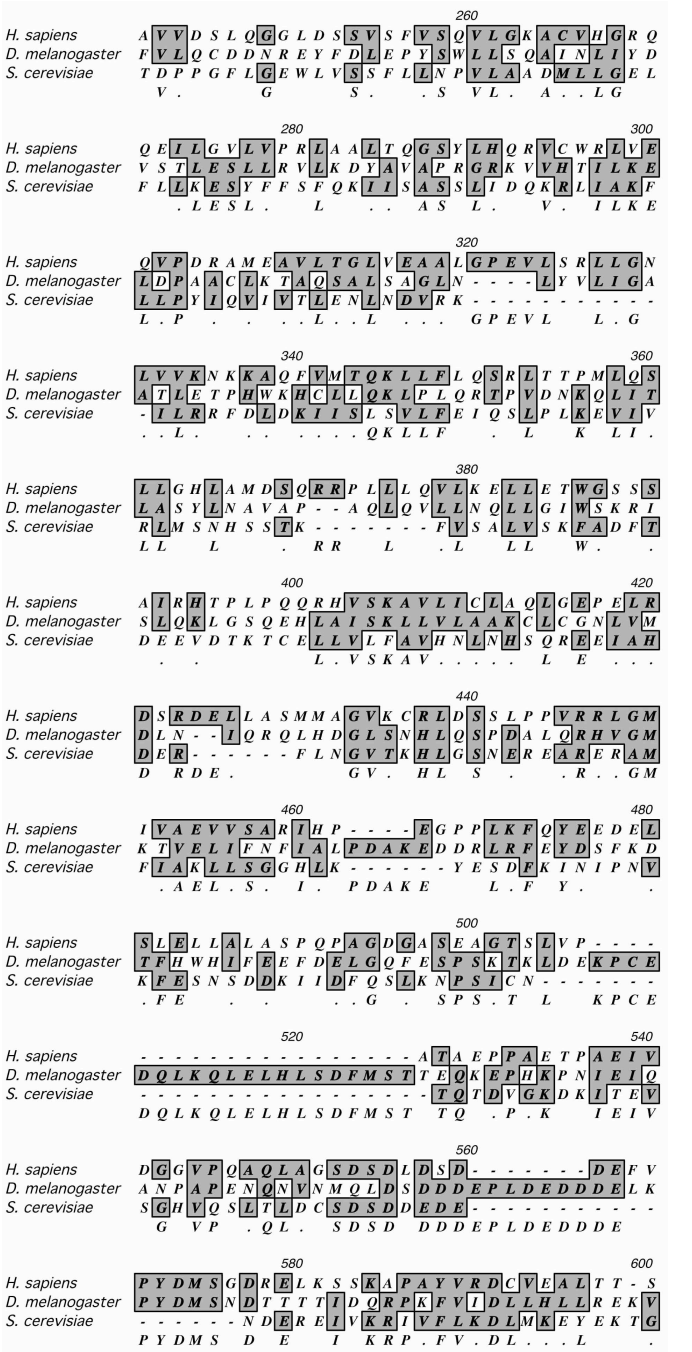

Figure 1-13. Sequence alignment of human and yeast Tel2 and *Drosophila* LqfR exon 6 (continued).

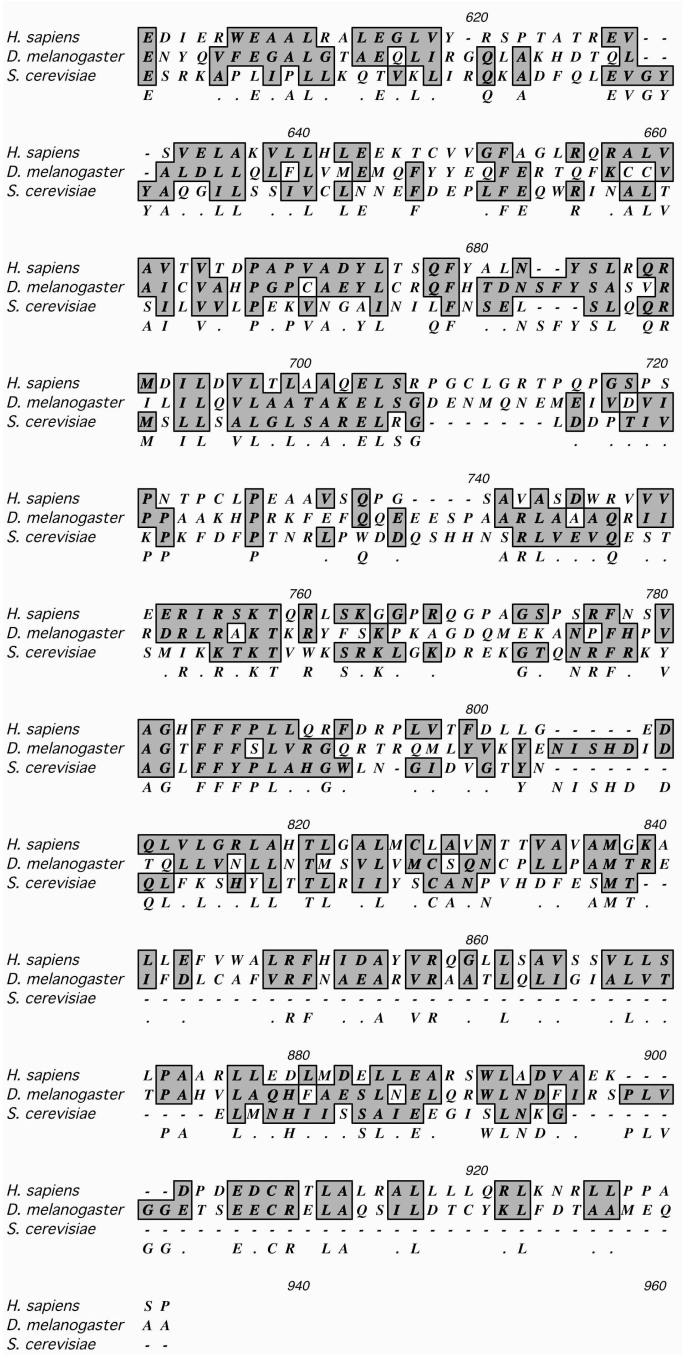

Figure 1-13. Sequence alignment of human and yeast Tel2 and *Drosophila* LqfR exon 6 (continued).

1.5 GOAL OF MY GRADUATE RESEARCH

The goal of my graduate research is to find the role of *Drosophila* Golgi Epsin gene *liquid facets-Related (lqfR)* in *Drosophila* development. I was initially interested in the possibility that *liquid facets-Related* was required for a specific signaling pathway by regulating the intracellular trafficking of a specific cargo protein that is essential for a signaling pathway. This idea stemmed from what our lab found with regard to *Drosophila* endocytic Epsin Liquid facets being specifically required for Notch signaling by mediating endocytosis of ubiquitylated ligand in signal sending cells (Overstreet et al, 2004). As the function of endocytic Epsin in the Notch signaling pathway was also confirmed in *C. elegans* and in the mouse, it is now considered a core mechanism of Notch activation (Chen et al, 2009; Tian et al, 2004).

When I started this project in 2005, Golgi Epsin function has begun to be published using yeast and mammalian cell lines, but its role in a multi-cellular context was unknown. A former graduate student in our lab Erin Overstreet initiated the project. Erin Overstreet found that the gene produces two transcripts from alternative splicing. She obtained a $lqfR^{P}$ hypomorphic allele with a P element inserted at the *5'-UTR* of the gene from Bloomington stock center and generated the $lqfR^{\Delta 117}$ null allele by imprecise excision of a mobilized P element. Initial phenotypic characterization determined that the hypomorph was semi-lethal with a kidney-shaped rough eye phenotype. The null allele was homozygous lethal at the third instar larval stage. The whole eye clone generated with the *FRT/GMR-hid* technique was tiny with few ommatidia. Sectioned adult eyes with *lqfR* null clones showed that the mutant cells were smaller compared to wild type neighbors. Erin also generated a specific LqfR antibody using a bacterially expressed

partial protein containing *exons 1-5*, and determined that LqfR co-localizes with known Golgi markers. Erin Overstreet also generated transgenic flies with a *lqfR* genomic DNA fragment and *lqfRa* cDNA in *pUASt* vector and showed that all mutant phenotypes were rescued by either the genomic DNA fragment or overexpressed *lqfRa* with an *Actin5C-gal4* driver.

Erin Overstreet set up the stage to study the role of *lqfR*. Her results indicated that *lqfR* encodes a *Drosophila* single homolog of Golgi Epsin, and the phenotype especially in cell growth and patterning suggests that it may be required for a specific signaling pathway(s).

To further understand the function of *lqfR*, I approached with three strategies. First of all, I further characterized the mutant phenotype of *lqfR* mutants to determine the basis of the morphological phenotype that I observed (Chapter 2). The results fueled hypothesis-driven experiments to understand the molecular mechanism of *lqfR* function. Secondly, I performed a genetic screen for dominant modifiers of the *lqfR* hypomorphic eye phenotype to find the context of *lqfR* function (Chapter 3). Results from the screen were also used to generate a hypothesis for *lqfR* function, which was that *lqfR* might be required for the Wingless signaling pathway (Chapter 4). Finally, I performed structure/function analysis to find the essential domain or region in LqfR to better understand the function of the protein (Chapter 4).

Chapter 2. *liquid facets-Related* is an essential gene required for cell proliferation, growth, and patterning

Chapter 2, in a slightly different format, has been previously published as "*Drosophila liquid facets-Related* encodes Golgi epsin and is an essential gene required for cell proliferation, growth, and patterning." Ji-Hoon Lee, Erin Overstreet, Erin Fitch, Stephen Fleenor, Janice A. Fischer. Developmental Biology, 2009 Jul 1;331(1):1-13. Erin Overstreet was a previous graduate student in the lab. She generated a *liquid facets-Related* (*lqfR*) null allele with Erin Fitch who was an undergraduate student in the lab. Erin Overstreet performed initial characterization of the phenotype of the null allele and a hypomorphic allele obtained from the Bloomington stock center. Erin Overstreet also generated many useful materials including anti-LqfR antibody and transgenic flies used for the rescue experiments. Stephen Fleenor was an undergraduate student in our lab. He generated the recombinant chromosome of $lqfR^{\Delta 117}$ InR^{339} double knockout under my supervision. I indicated works done by other people in the text clearly. Everything not labeled as done by someone else was done by me.

2.1 INTRODUCTION

Epsins are multi-modular membrane-associated proteins that function in endosome trafficking in yeast and metazoans (reviewed in (Duncan & Payne, 2003; Legendre-Guillemin et al, 2004; Wendland, 2002)). The distinctive feature of all Epsins is an ENTH (epsin N-terminal homology) domain that binds membrane

phosphoinositides (Itoh et al, 2001; Kay et al, 1999; Rosenthal et al, 1999). There are two classes of Epsins: endocytic Epsins, known as vertebrate Epsin-1 (Chen et al, 1998), yeast Ent1p and Ent2p (Wendland et al, 1999), and Liquid facets (Lqf) in *Drosophila* (Cadavid et al, 2000; Overstreet et al, 2003) and nematodes (Tian et al, 2004) and Golgi-associated Epsins, known as yeast Ent3p and Ent5p (Duncan et al, 2003), and vertebrate Epsin-Related (EpsinR), also known as enthoprotin or Clint (Hirst et al, 2003; Kalthoff et al, 2002; Mills et al, 2003; Wasiak et al, 2002). Endocytic or Golgi Epsin ENTH domains prefer to bind the phosophoinositides enriched in the plasma membrane and Golgi membranes, respectively (Duncan & Payne, 2003; Legendre-Guillemin et al, 2004). Both endocytic and Golgi Epsins have a variety of motifs C-terminal to their ENTH domains. Endocytic Epsins have motifs for interaction with ubiquitin, clathrin, the clathrin adapter complex AP-2, and EH-domain containing endocytic factors. Golgi Epsins have clathrin-binding motifs, and also motifs for binding the Golgi-associated clathrin adapter proteins AP-1 and Gga (Duncan & Payne, 2003; Legendre-Guillemin et al, 2004).

Endocytic Epsins have been studied more intensively than Golgi Epsins. Most of the available data supports a model where endocytic Epsin promotes clathrin-dependent endocytosis, acting either as a clathrin adapter, or as an accessory factor for the AP-2 adapter complex (reviewed in (Aguilar & Wendland, 2005; Wendland, 2002)). As a clathrin adapter, through its UIMs, Epsin binds transmembrane proteins that use ubiquitin as an internalization signal, and recruits clathrin and other endocytic factors to the plasma membrane. As an accessory factor, in order to facilitate internalization of transmembrane proteins whose endocytic signals are amino acid motifs in their intracellular domains that bind the AP-2 adapter, Epsin bound to AP-2 would bring clathrin and other proteins to the plasma membrane. Epsin's ENTH domain may also promote vesicle formation by

inducing membrane curvature (Ford et al, 2002). Yeast Epsin ENTH domains also coordinate actin cytoskeleton rearrangement with endocytosis (Aguilar et al, 2006). In yeast and also in vertebrate cell culture, endocytic Epsin functions in internalization of a variety of different cargos (Barriere et al, 2006; Chen et al, 1998; Sigismund et al, 2005; Wang et al, 2006b; Wendland et al, 1999). Although this is probably also the case in *Drosophila*, the only apparent requirement for Lqf is for endocytosis of Notch ligands, which is essential for Notch receptor activation (Overstreet et al, 2003; Overstreet et al, 2004; Wang & Struhl, 2004; Wang & Struhl, 2005). Thus at least in *Drosophila*, endocytic Epsin plays a pivotal role in Notch signaling, and Epsin is therefore critical for virtually all aspects of cell determination and differentiation during development.

Golgi Epsins promote vesicular trafficking mainly between endosomes and the trans-Golgi network (TGN) (reviewed in (Duncan & Payne, 2003; Legendre-Guillemin et al, 2004)). In higher organisms, EpsinR promotes clathrin-coated vesicle formation and trafficking between the TGN and early endosomes, in both directions. One type of cargo known to be transported in an EpsinR-dependent manner from the TGN to the early endosome is lysosomal proteins bound to mannose-6-phosphate receptors on their way to the lysosome. Also, EpsinR-dependent retrograde trafficking from the early endosome to the TGN retrieves mannose-6-phosphate receptors, and also other resident Golgi membrane proteins (Hirst et al, 2003; Mills et al, 2003; Saint-Pol et al, 2004). Yeast Ent3p and Ent5p are required for trafficking of carboxypeptidase S from the TGN to the vacuole, where it is processed into active form, and also for endosome-to-TGN transport of Kex2p, a protease required for α-factor mating pheromone maturation (Duncan et al, 2003). Another type of Golgi Epsin cargo in both yeast and higher eukaryotes is SNARE

proteins. In yeast, SNAREs required for vesicle fusion at late endosomes are transported from the TGN to the late endosome in an Ent3p-dependent manner (Chidambaram et al, 2008). In mammalian cells, although the biological rationale for this is unclear, SNAREs that function at late endosomes appear to depend on EpsinR for early endosome-to-TGN transport (Chidambaram et al, 2008). Yeast Ent3p and Ent5p also function in sorting proteins within the multi-vesicular body, the late endosome whose internal vesicles eventually fuse with the vacuole (Eugster et al, 2004; Friant et al, 2003). Like yeast endocytic Epsins, Ent3p is also a factor in actin cytokeletal organization (Friant et al, 2003).

The mechanism of Golgi Epsin function is probably similar to that of endocytic Epsin (Duncan & Payne, 2003; Legendre-Guillemin et al, 2004), with at least one notable difference. EpsinR is likely the clathrin adapter for SNARE cargo, but unlike endocytic epsin which recognizes ubiquitin internalization signals via its UIMs, EpsinR binds SNARES directly with its ENTH domain (Chidambaram et al, 2004; Hirst et al, 2004; Miller et al, 2007). In the transport of other cargos, EpsinR and also Ent3p/Ent5p may function either as the key clathrin adapter, or as accessory proteins for the AP-1 clathrin adapter complex or Gga adapters (Costaguta et al, 2006; Duncan & Payne, 2003; Legendre-Guillemin et al, 2004).

No analysis of Golgi Epsin function in a developmental context has been reported in a multicellular organism. Only through genetic characterization of the *Drosophila* endocytic Epsin gene, *lqf*, was it revealed that endocytic Epsin plays a critical and specific role in Notch signaling. I wondered whether *Drosophila* Golgi Epsin is also essential, and if it functions in cell patterning. Here, I report an analysis of the mutant phenotype of flies with weak and strong loss-of-function alleles of the Golgi Epsin gene,

which I call *liquid facets-Related (lqfR)*. *lqfR+* was indeed essential for *Drosophila* viability, and that more specifically, *lqfR+* is required for cell proliferation, insulin-independent cell growth, and cell fate determination in the developing eye. In addition, I report that all of the detectable functions of *lqfR+* are independent of the ENTH domain.

2.2 RESULTS

liquid facets-Related encodes two proteins by alternate splicing

The *Drosophila* gene encoding Golgi Epsin (CG42250), located on chromosome 3R at polytene position 94A12, was identified by sequence similarity to the vertebrate gene and referred to as Epsin-2 (Lloyd et al, 2000) or Epsin-like (Tweedie et al, 2009). Because the endocytic Epsin gene is named *liquid facets*, and the vertebrate Golgi Epsin gene is called *epsin-Related*, I call the gene *liquid facets-Related (lqfR)*. The *lqfR* gene contains seven exons. As diagrammed in Fig. 2-1A, *lqfR* mRNA is alternately spliced to generate one transcript (*lqfRa*) that contains all seven exons, and another transcript (*lqfRb*) that lacks exon 6. This model is supported by analysis of mRNA and protein produced by the *lqfR* locus. By RT-PCR of eye disc mRNA or whole adult fly mRNA, Erin Overstreet, a former graduate student, could amplify transcripts in which exons 3 through 6 were joined (*lqfRa*), and also transcripts in which exons 1 through 5 were joined with exon 7 (*lqfRb*) (Data not shown; see Materials and methods). In addition, Erin generated an antibody in guinea pigs to bacterially produced protein encoded by the open-reading frame in exons 1-5, which is expected to recognize the proteins produced by both transcripts. On protein blots of third instar larval eye disc protein extracts, the antibody recognizes two proteins of approximate size 70 kD and 150 kD (Fig. 2-1C)

predicted by the open-reading frames in *lqfRa* and *lqfRb* transcripts (Fig. 2-1B). The antibody is likely to be specific for LqfR protein in this assay, as the levels of both the 70 kD and the 150 kD protein are reduced by a factor of ~1/3 in eye discs homozygous for a hypomorphic allele of *lqfR* called $lqfR^{P3685}$ *(*$lqfR^{P}$*)* (Fig. 2-1C and Materials and methods; see below).

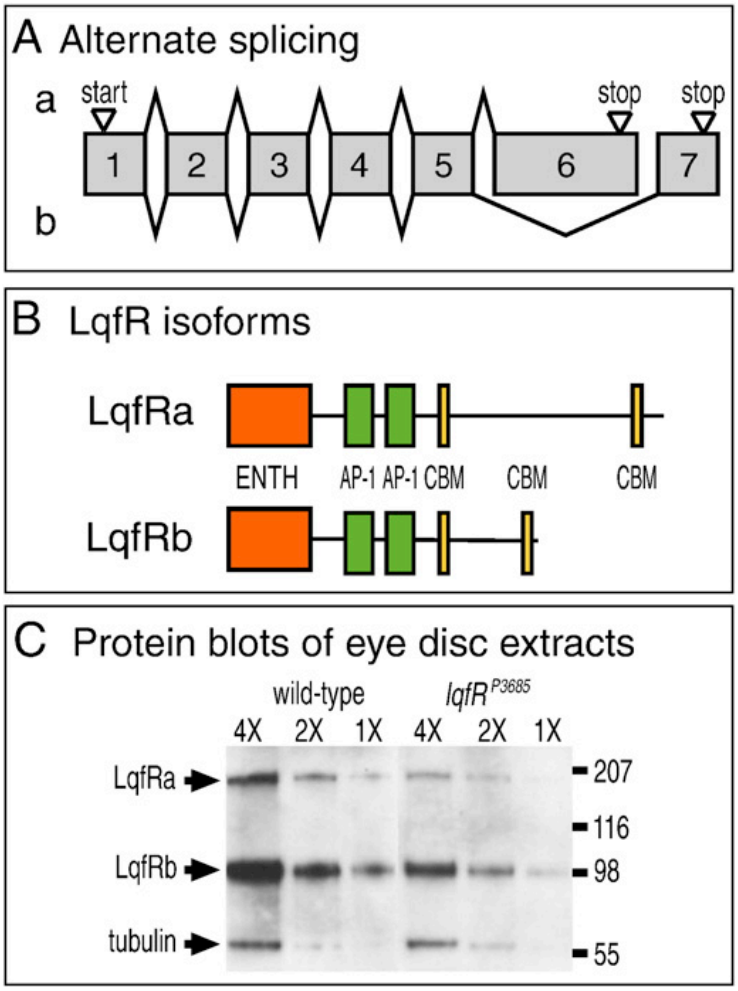

Figure 2-1. Structure of the *lqfR* locus.

(A) A diagram of the two alternate splice forms of *lqfR* mRNA (a and b) is shown. Grey bars are exons 1–7, and the lines connecting them indicate introns. Triangles indicate start and stop codons. (B) Diagram of the two different proteins encoded by the a and b transcripts in (A). Each protein has an epsin N-terminal homology (ENTH) domain, two motifs for interaction with AP-1, and two clathrin-binding motifs (CBM). (C) A blot of eye disc protein extracts from w^{1118} (wild-type) and $lqfR^{P}$ third instar larvae probed with antibodies to LqfR and β-tubulin is shown. Different amounts (1X-4X) of the same extracts were loaded into each of three lanes. The lines and numbers at the right indicate the positions and approximate sizes (kD) of markers. A similar blot probed with preimmune serum from the guinea pig that generated anti-LqfR had no signal. $lqfR^{P3685}$=$lqfR^{P}$. The gene model is based on analysis of mRNA and protein from *lqfR* by Erin Overstreet. Western blot image in (C) was generated by Erin Overstreet.

LqfR is present at the Golgi

Erin Overstreet used the LqfR antibody to detect the protein in developing eyes by immunofluorescence. The *Drosophila* eye develops in third instar larvae from the eye imaginal disc, which consists of a monolayer of columnar epithelial cells (the eye disc proper) that will form the eye, and an overlying layer of squamous epithelial cells, called the peripodial epithelium (Wolff and Ready, 1993). The peripodial epithelium does not contribute structurally to the adult eye, but functions in disc development by signaling to the columnar cells beneath, and is also required for disc eversion during pupation, a process where the disc unfolds to become the adult eye (Gibson & Schubiger, 2001). The LqfR antibody produces no fluorescence above background in eye disc cells homozygous for a null allele of *lqfR* called $lqfR^{s117}$ (Fig. 2-3). By contrast, Erin detects a signal in wild-type eye discs, and she finds that the anti-LqfR signal overlaps significantly with that of two Golgi markers, p120 (Stanley et al, 1997) and Lava lamp (Sisson et al, 2000) (Fig. 2-2). LqfR and p120 accumulate mainly in the peripodial epithelium (Fig. 2-2A-C") and also basally in the eye disc proper (Fig. 2-2A-A"). The LqfR and p120 signals are both diffuse and punctate in the cytoplasm, and remarkably overlapping (Fig. 2-2B-C"). Lava lamp accumulates in puncta throughout the apical/basal plane of the eye disc proper (Fig. 2-2D'). Some of the Lava lamp and LqfR puncta are coincident, and others are adjacent to each other (Fig. 2-2E-F"). She conclude that LqfR is a Golgi protein.

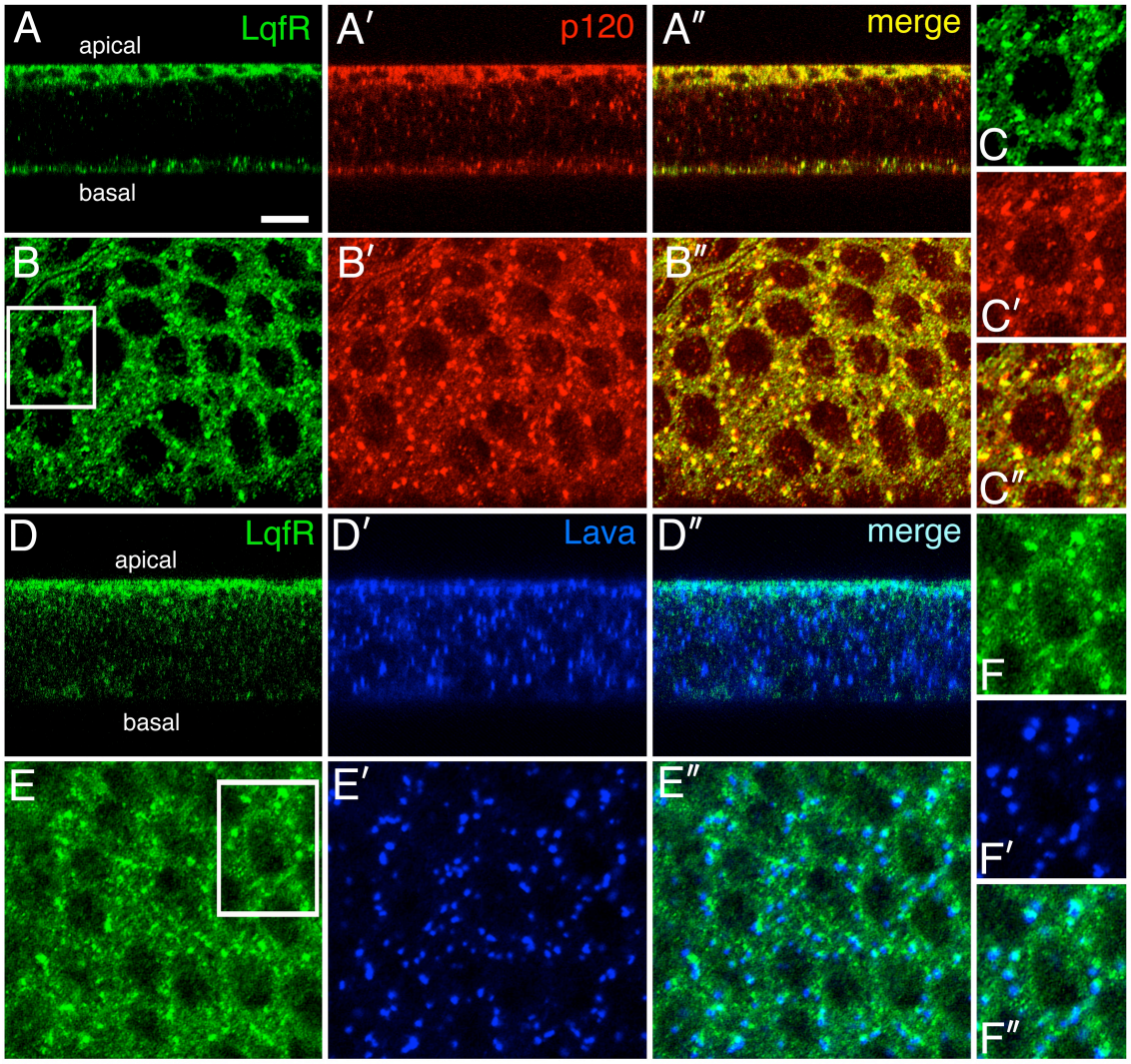

Figure 2-2. Expression pattern and subcellular localization of LqfR in eye discs.

Confocal images of immunolabeled w^{1118} (wild-type) third instar larval eye discs are shown. (A-C") Expression of LqfR and the Golgi protein p120 are shown in Z-sections (A-A") and apical XY-sections (B-B"). In (C-C"), enlargements of the area in the box in (B) are shown. (D-F") Expression of LqfR and the Golgi protein Lava lamp (Lava) are shown in Z-sections (D-D") and apical XY-sections (E-E"). In (F-F"), enlargements of the area in the box in (E) are shown. The apical XY-sections show the peripodial epithelium; the dark circles are nuclei. Scale bar in A: 40 μm in (A-A", D-D"), 20 μm in (B-B", E-E"). These images were generated by Erin Overstreet.

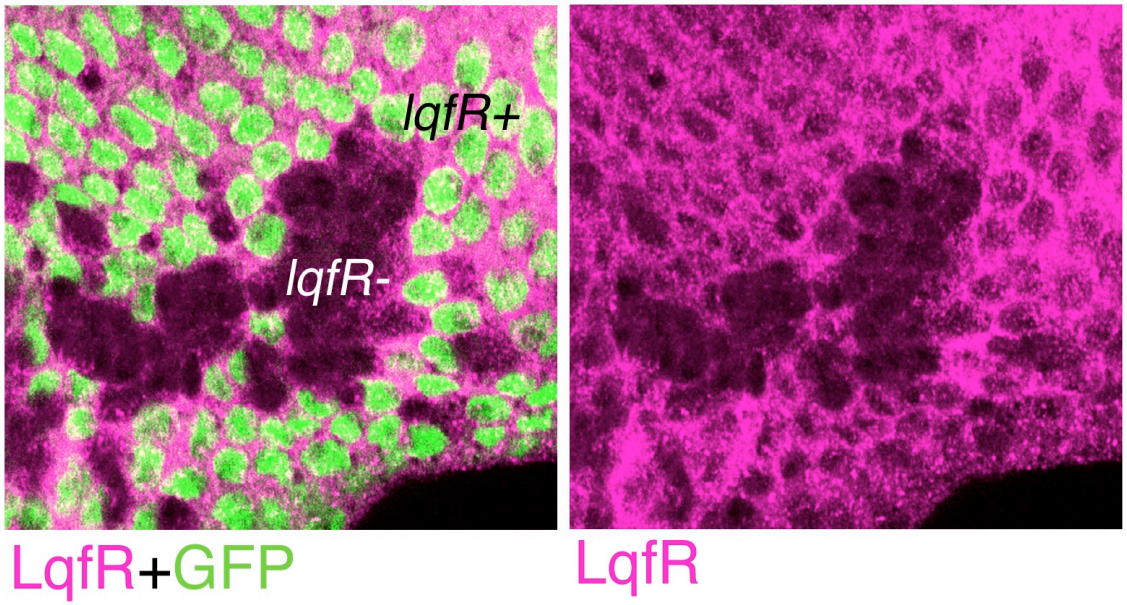

Figure 2-3. Eye disc containing clones of *lqfR*$^{\Delta 117}$ cells immunolabeled with anti-LqfR.

Shown is a confocal image of a third instar larval eye disc of the genotype *ey-flp; FRT82B lqfR*$^{\Delta 117}$*/FRT82B ubi-gfp* containing a clone of *lqfR*$^{\Delta 117}$ cells marked by the absence of GFP expression. Note the absence of LqfR signal within the mutant clone. These images were generated by Erin Overstreet.

lqfR is an essential gene

The Berkeley *Drosophila* Genome Project generated a mutant allele of *lqfR* (called *l(3)03685*) that has a P element insertion in the 5'-untranslated region (Spradling et al, 1999). I refer to this allele as $lqfR^{P}$ (Fig. 2-4A). At 25°C, $lqfR^{P}$ is semi-lethal; most $lqfR^{P}$ homozygotes die fully formed in their pupal cases. Rare escapers eclose and many have obvious morphological defects. The eyes are kidney-shaped and rough, especially at the dorsal/ventral axis (Figs. 2-4B, C). The wings are notched (Figs. 2-4E, F), and the wing hair patterns may suggest planar cell polarity defects (Fig. 2-3). Duplications of the anterior scutellar bristles on the notum are observed also (Fig. 2-4G, H). At 18°C, $lqfR^{P}$ homozygous flies eclose and appear normal morphologically. As described above, $lqfR^{P}$ is hypomorphic; $lqfR^{P}$ homozygotes produce LqfRa and LqfRb proteins at reduced levels. The results of several experiments done by Erin Overstreet indicate that the temperature-sensitive semi-lethality and morphological defects observed in these flies is due to the $lqfR^{P}$ mutation. First, one copy of a transgene containing genomic DNA corresponding to a wild-type *lqfR* gene (*PglqfR+*) complements all defects in the homozygotes (data not shown). Second, a *UAS-lqfRa* transgene (contains a *lqfRa* cDNA) expressed using the ubiquitous *Act5C-gal4* driver (*Act5C>lqfRa*) also complements the $lqfR^{P}$ mutant phenotype observed (data not shown). Finally, precise excision of the P element in $lqfR^{P}$ results in viable flies with apparently normal morphology (Materials and methods).

Erin Overstreet and Erin Fitch mobilized the P element in $lqfR^{P}$ in order to generate a null allele by imprecise excision. In this way, they obtained $lqfR^{x117}$, in which the transcription start site and most of the *lqfR* gene is deleted (Fig. 2-1A). The mutant

phenotype of *lqfR*$^{\Delta 117}$ is more severe than that of *lqfR*^{P}. At 25°C, *lqfR*$^{\Delta 117}$ homozygotes die as third instar larvae, and *lqfR*$^{\Delta 117}$/*lqfR*^{P} animals die as pupae and no escapers are observed. Also, homozygous *lqfR*$^{\Delta 117}$ adult eyes generated using *FLP*/*FRT*-induced mitotic recombination and *GMR-hid* (Stowers & Schwarz, 1999) are much more severely malformed and smaller than *lqfR*^{P} homozygous eyes generated the same way (Fig. 2-4D and data not shown). Finally, unlike *lqfR*^{P} homozygotes, *lqfR*$^{\Delta 117}$ third instar larvae have small salivary glands that have small cells (Fig. 2-6), and no imaginal discs (data not shown). All of the aspects of the mutant phenotype described above are due to loss of *lqfR* function, as they are complemented by one copy of *PglqfR+* or *Act5C>lqfRa* (data not shown).

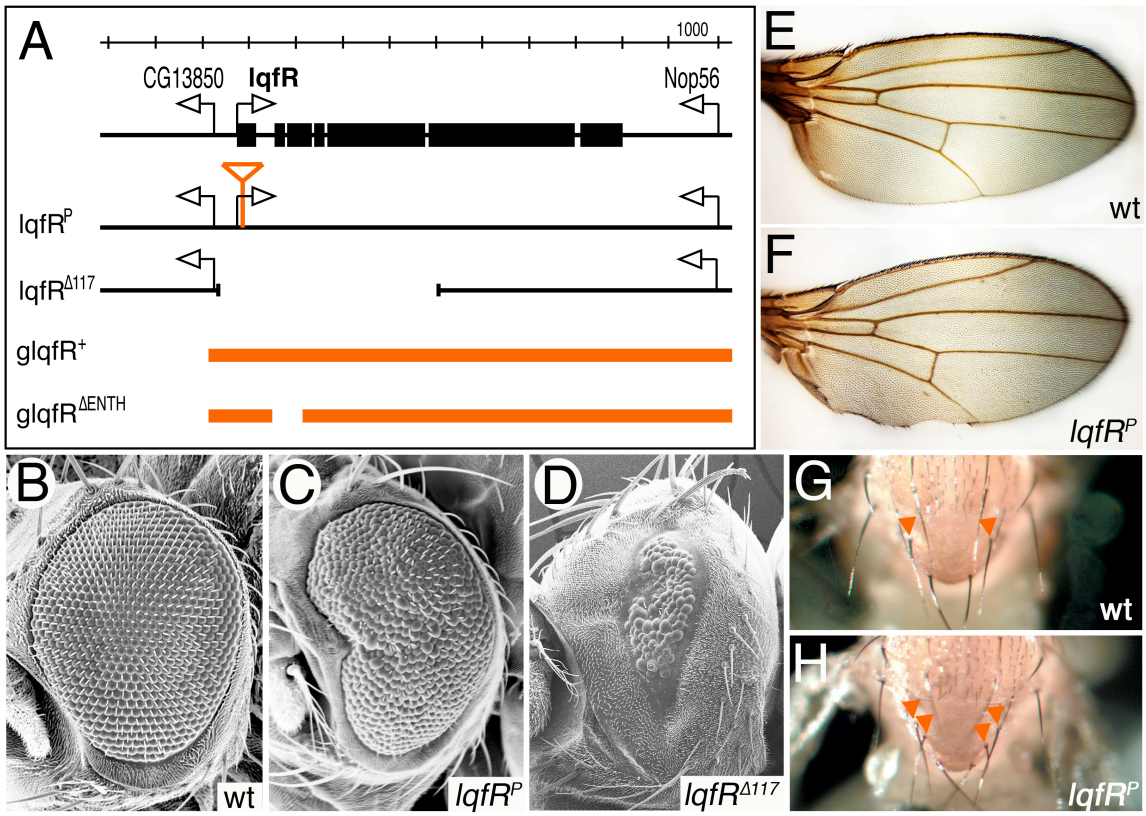

Figure 2-4. Molecular structure and external morphological phenotype of mutant *lqfR* alleles.

(A) A diagram of the *lqfR* genomic DNA region, and the molecular structures of the two mutant alleles used in this work (lqfR^{P} and lqfR$^{\Delta 117}$), and two genomic DNA transgenes (glqfR^{+} and glqfR$^{\Delta ENTH}$) is shown. The scale bar at the top is in increments of 1000 bp. The black bars represent exons, and the arrows indicate the start site and direction of transcription of *lqfR* and flanking genes (Tweedie et al, 2009). The open red triangle indicates the P element insertion site in *lqfR^{P}*, which is 94 bp upstream of the start codon (Tweedie et al., 2009). The extent of the deletion in *lqfR$^{\Delta 117}$* (–469 to +4081 bp relative to the start codon) is indicated by a break in the black line. Red bars indicate the extents of the genomic DNA in each of the transgenes, with a break indicating a deletion. (B–D) Scanning electron micrographs of adult eyes are shown. (E, F) Adult wings are shown. (G, H) The adult notum (dorsal thorax) is shown. Arrows indicate anterior scutellar bristles. (*wt = w^{1118}; lqfR^{P} = FRT82B lqfR^{P}; lqfR$^{\Delta 117}$ = ey-FLP; FRT82B lqfR$^{\Delta 117}$/FRT82B GMR-hid l(3)CL-R^{1}*). *lqfR$^{\Delta 117}$* was generated by Erin Overstreet and Erin Fitch.

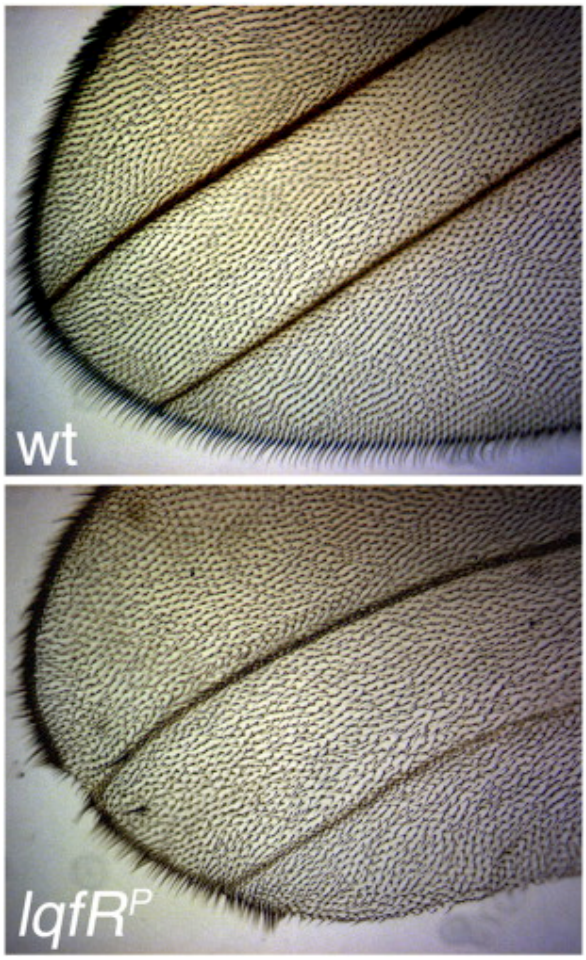

Figure 2-5. Wings of wild-type and *lqfR*^{P} adults.

The dorsal surfaces of distal wing ends are shown. (wt = wild-type).

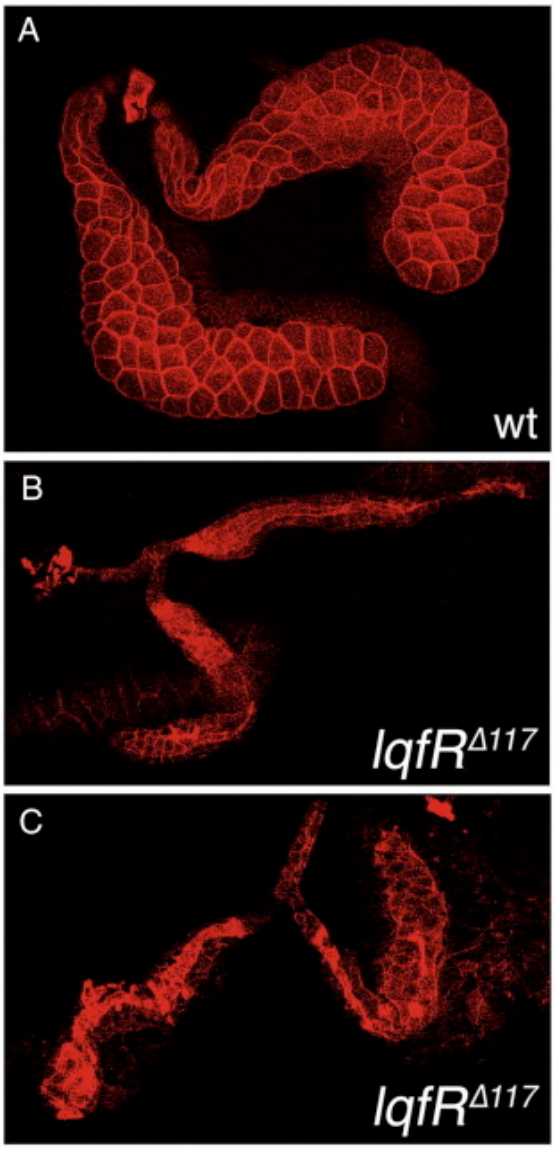

Figure 2-6. Salivary glands of wild-type and *lqfR*$^{\Delta 117}$ third instar larvae.

Shown are light micrographs of salivary glands treated with phalloidin to outline plasma membranes. The tissue in all three panels was photographed at the same magnification. (A) wt = w^{1118}, (B,C) glands from two different homozygous mutant larvae.

***lqfR+* is required for morphogenetic furrow movement and cell patterning**

The kidney shape of *lqfR*^{P} eyes suggests that *lqfR*+ might play a role in controlling movement of the wave of morphogenesis, called the morphogenetic furrow.

Eye disc cells in third instar larvae proliferate until ommatidial assembly begins. The morphogenetic furrow forms at the posterior of the disc and moves anteriorly into the undifferentiated cells, which cease dividing as the furrow approaches. Posterior to the furrow, rows of cells assemble stepwise into ommatidia, beginning with the eight photoreceptor cells (Wolff and Ready, 1993). Kidney-shaped eye have been observed in mutants where furrow movement is hampered (Chanut et al, 2000). To monitor furrow movement in *lqfR*^{P} eye discs, I examined expression of Elav, a nuclear protein expressed in all photoreceptors, beginning at the fourth row of assembling ommatidia posterior to the furrow (Robinow & White, 1991). The idea is that if furrow movement slows in *lqfR* mutant discs, ommatidia closest to the furrow will be at more advanced stages of development than they normally would be. In *lqfR*^{P} eye discs, not only are ommatidia near the furrow abnormally mature, but the rows of assembling ommatidia are strikingly V-shaped, rather than straight as in wild-type discs (Fig. 2-7A, B). I conclude that the kidney shape of *lqfR*^{P} eyes is due to the furrow stopping, first at the dorsal/ventral axis (the equator), and then later more laterally in the disc.

Externally, *lqfR*^{P} eyes are rough along the equator, suggesting that there might be patterning defects in the ommatidia there (Fig. 2-4C). Tangential sections through the equator of *lqfR*^{P} eye reveal ommatidia with a wide variety of defects, including ommatidia with too many or too few photoreceptors, irregular polarity, and ommatidial fusions (Fig. 2-7E, F). Away from the equator, *lqfR*^{P} ommatidia are normal (data not

shown). Dorsal/ventral polarity itself, however, is still present, even in *lqfR*$^{\Delta 117}$ eyes. An enhancer trap insertion in the *mirror* gene, where the *white+* gene is expressed only in cells in the dorsal half of the eye (Brodsky & Steller, 1996), was used as a dorsal marker (Fig. 2-7C). In *lqfR*$^{\Delta 117}$ eyes generated using mitotic recombination and *GMR-hid*, the small eye that remains has dorsal and ventral halves in their normal positions (Fig. 2-7D).

One example of a mutation that results in morphogenetic furrow arrest and kidney-shaped eyes is a dominant gain-of-function allele of the *rough* gene, called *ro*^{DOM}, in which *rough* is overexpressed (Chanut et al, 2000). I wondered whether the *lqfR*^{P} mutant eye phenotype could be caused by *rough* overexpression. To determine if *rough* is overexpressed in *lqfR-* cells, we generated *lqfR*$^{\Delta 117}$ homozygous clones in *lqfR*$^{\Delta 117}$/*lqfR+* eye discs. The eye discs also contain a reporter for *rough* gene expression: a *rough-gfp (ro-gfp)* transgene that expresses GFP under the control of the *rough* promoter (Overstreet et al., 2004). I observed that GFP levels were higher within the *lqfR*$^{\Delta 117}$ clones than in the surrounding *lqfR+* cells (Figs. 2-5G-G''). In order to test if the elevated GFP level within the clones is due to overexpression from the *rough* promoter, or to GFP stabilization, I generated *lqfR*$^{\Delta 117}$ clones in eye discs that express GFP from the ubiquitin promoter. I found that the GFP levels are not elevated in these clones (Fig. 2-6), and thus I conclude that the absence of *lqfR+* activity results in *rough* overexpression.

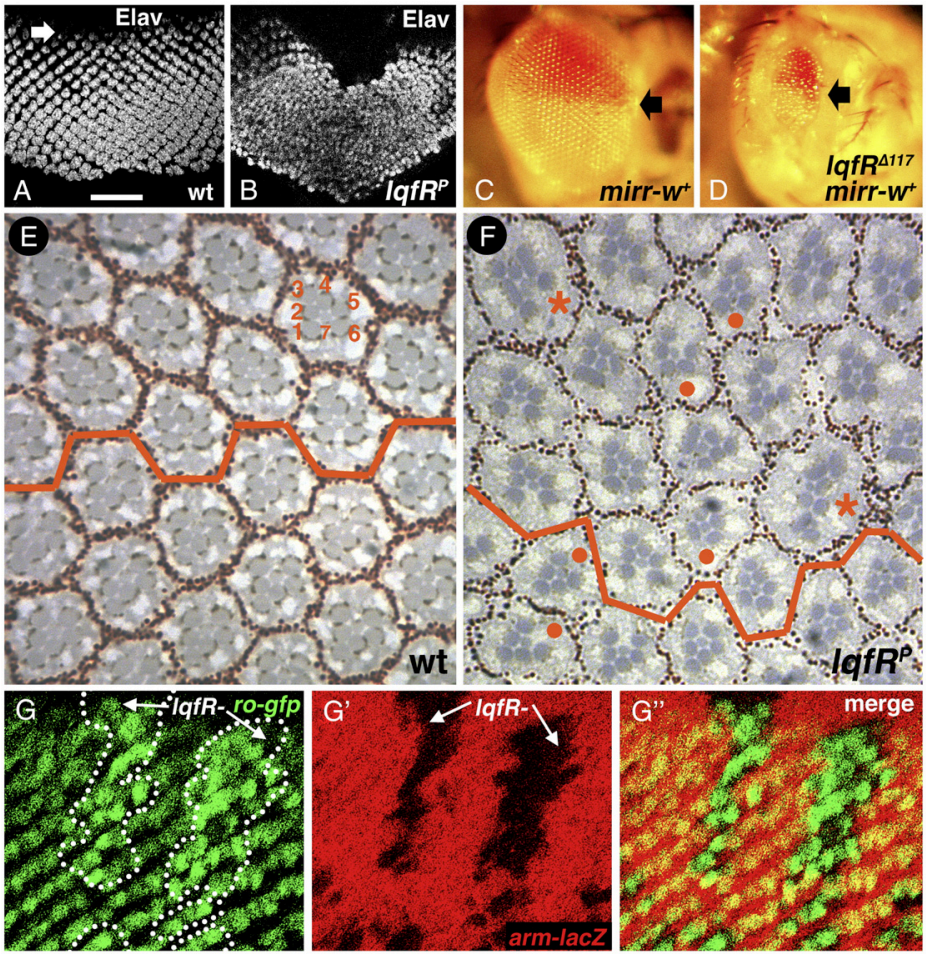

Figure 2-7. Eye development defects in *lqfR* mutants.

(A, B) Confocal images of third instar larval eye discs immunolabeled with anti-Elav which labels R-cell nuclei. The arrow in (A) indicates the morphogenetic furrow. Discs are oriented with anterior at top and posterior at bottom. (C, D) Adult eyes that express w+ under the control of mirror are shown. The arrows indicate the D/V axis. The genotype in (C) is *ey-flp; mirr*^{P69Df7} *FRT82B lqfR*$^{\Delta 117}$*/TM6B*, and in (D) is *ey-flp; mirr*^{P69Df7} *FRT82B lqfR*$^{\Delta 117}$*/FRT82B GMR-hid l(3)CL-R*^{1}. (E, F) Apical sections of adult eyes through the D/V axis, or equator, are marked by the red line. Numbers in (E) are R-cells, and in (F), asterisks indicate ommatidia with additional R-cells, and dots indicate ommatidia missing an R-cell. (G–G″) Confocal images of a third instar larval eye disc (*ey-flp; ro-gfp/+; FRT82B lqfR*$^{\Delta 117}$*/FRT82B arm-lacZ*) immunolabeled with anti-β-galactosidase. GFP expression is shown in (G), and *lqfR*$^{\Delta 117}$ clones are outlined. The clones are marked by the absence of β-galactosidase expression, shown in (G') and (G"). (wt = *w*^{1118}; *lqfR*^{P} = *FRT82B lqfR*^{P}) Scale bar in A: 30 μm in (A, B), 100 μm in (C, D), 10 μm in (E–G″).

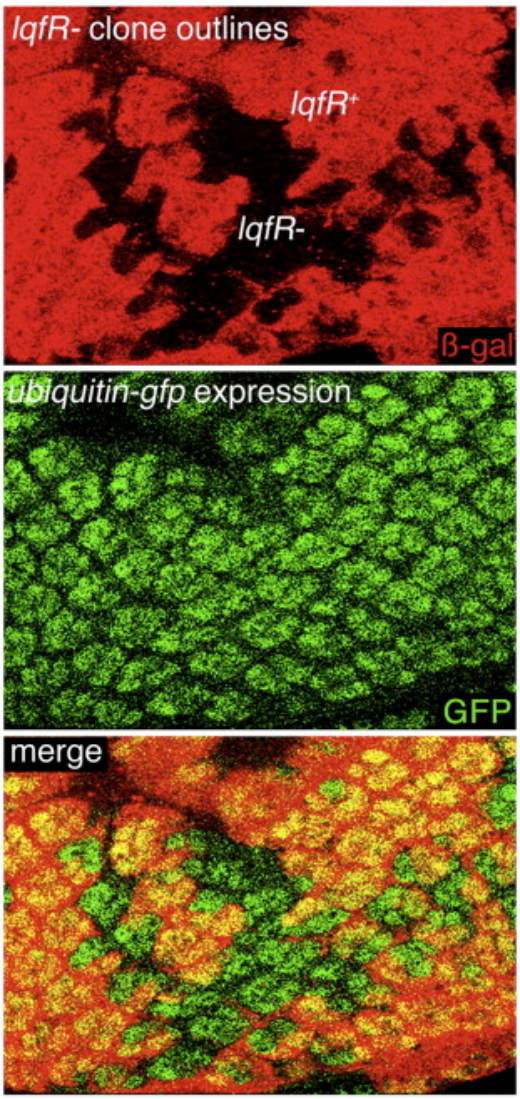

Figure 2-8. GFP expression from a *ubiquitin* promoter in eye discs containing clones of $lqR^{\Delta 117}$ cells.

Shown are confocal images of a third instar larval eye disc of the genotype *ey-flp; ubi-gfp/+; FRT82B* $lqfR^{\Delta 117}$*/FRT82B arm-lacZ*. The $lqfR^{\Delta 117}$ clones are marked by absence of β-gal expression. Note that the level of GFP appears the same inside and outside of the clone.

lqfR+ is required for cell proliferation in the eye imaginal disc

The absence of imaginal discs observed in $lqfR^{\Delta 117}$ larvae is typical of mutants in genes required for cell proliferation (Shearn & Garen, 1974; Shearn et al, 1971). To test if *lqfR*- cells divide more slowly than wild-type cells in the eye disc, I used mitotic recombination in a $lqfR^{\Delta 117}$/*lqfR*+ disc to generate a $lqfR^{\Delta 117}/lqfR^{\Delta 117}$ cell and a *lqfR*+/*lqfR*+ cell, born at the same time (Fig. 2-9A). The descendants of the $lqfR^{\Delta 117}$ homozygous cell and those of its *lqfR*+ homozygous sister are marked so as to distinguish them from each other and also from the $lqfR^{\Delta 117}$/*lqfR*+ background cells that did not undergo mitotic recombination (Fig. 2-9A). The $lqfR^{\Delta 117}$ cell clone is marked by the absence of β-galactosidase (β-gal) expression, and its *lqfR*+ twin spot is marked by a β-gal expression level two-fold higher than that in the background $lqfR^{\Delta 117}$/*lqfR*+ cells (Fig. 2-9A). After several rounds of cell division, the cell number in the mutant clone and twin spot should be similar, unless the mutant has an affect on cell proliferation.

As described above, undifferentiated eye disc cells proliferate as a monolayer until the third instar larval stage when the morphogenetic furrow moves anteriorly across the eye disc. Cell division stops as cells enter the furrow, and then about 4 rows posterior to the furrow, cells not yet recruited into ommatidia undergo one additional division (Wolff and Ready, 1993). Therefore, in the mutant clones and twin spots, mitotic recombination and most subsequent cell division occurred anterior to the morphogenetic furrow. I examined four mutant clones and twin spots posterior to the furrow in third instar eye discs. First, I measured the sizes of the clones and twin spots, and found that the $lqfR^{\Delta 117}$ clones were always smaller than the *lqfR*+ twin spots (Fig. 2-9C and Table 2-

1). To determine if the size difference is due to differences in cell size or cell number, I counted the number of nuclei and found that the mutant clones had proportionally fewer (Fig. 2-9C' and Table 2-1). Thus, the *lqfR*$^{\Delta 117}$ clones are smaller than the wild-type twin spots because they have fewer cells, not because the mutant cells are smaller. One potential caveat to this experiment is that if the β-gal initially present in the *lqfR*$^{\Delta 117}$/*lqfR*+ cell perdures in the *lqfR*$^{\Delta 117}$/*lqfR*$^{\Delta 117}$ daughter cell after mitotic recombination, and remains at detectable levels through several subsequent cell divisions, the clone could appear to have fewer cells than it actually does because the cells in which β-gal persists are indistinguishable from the *lqfR*$^{\Delta 117}$/*lqfR*+ background cells. To determine whether perdurance of β-gal could explain the difference between clone and twin spot size, I generated clones and twin spots in exactly the same manner, except both were *lqfR*+/*lqfR*+. I examined two wild-type clones and wild-type twin spots, and they were the same size and contained the same number of cells (Figs. 2-9B, B' and Table 2-1). Thus, the number of cells in *lqfR*$^{\Delta 117}$ clones is smaller than in their twin spots because the clones are *lqfR*-. I conclude that cells lacking *lqfR*+ either divide more slowly than wild-type cells, or tend to die.

A mutagenesis screen for genes required for imaginal disc development identified a recessive lethal mutation, *l(3)SG62*^{1} (a.k.a. *A9*, and *l(3)XII-10*) that was localized to a map position close to *lqfR*, and like *lqfR* mutants, results in disc-less third instar larvae (Shearn & Garen, 1974; Shearn et al, 1971). I found that *l(3)SG62*^{1} fails to complement *lqfR*$^{\Delta 117}$. Analysis of cell division cycles in *l(3)SG62*^{1} mutants led to the conclusion that

there are mitotic defect including chromosome breakage, condensation defect, and polyploidy (Gatti & Baker, 1989).

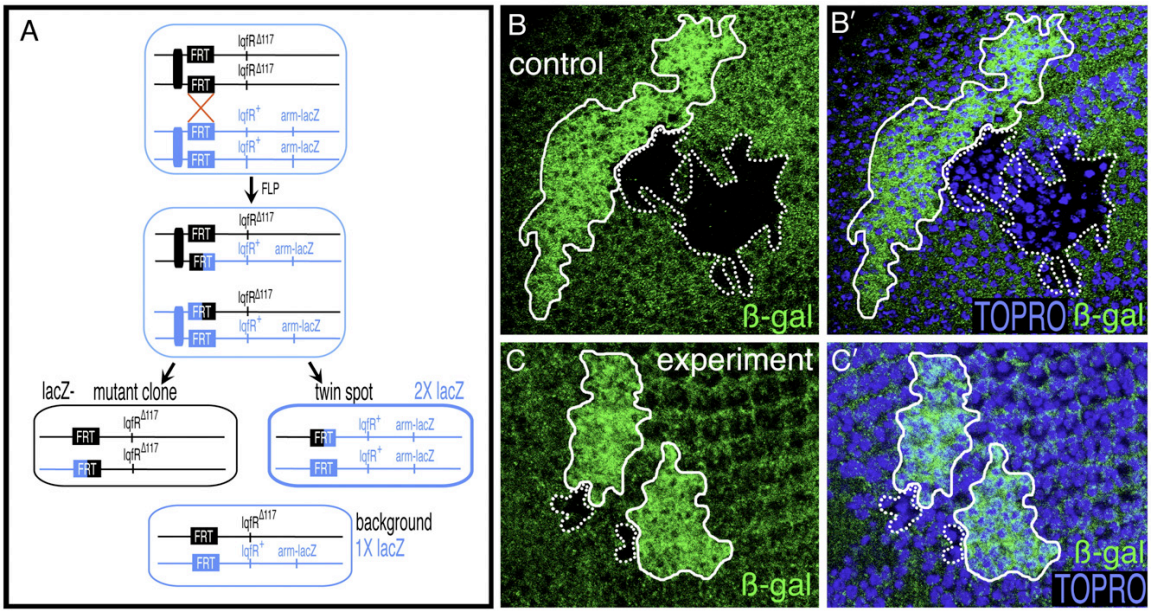

Figure 2-9. Comparison of cell proliferation in *lqfR*+ and *lqfR*– clones.

(A) A diagram of the method used to generate *lqfR*$^{\Delta 117}$ clones and *lqfR*+ twin spots, each marked so as to be distinguished from each other and also the *lqfR*$^{\Delta 117}$/*lqfR*+ background cells. (B, B') Apical confocal images of third instar larval eye discs of the genotype *hs-flp; FRT82B/FRT82B armlacZ*, immunolabeled with anti-βgal and incubated with DNA stain TOPRO-3. A *lqfR*+ clone (*lacZ*–; dotted outline) and *lqfR*+ twinspot (2X*lacZ*; solid outline) are shown. The twin spot is 1.3X larger in area, and has 1.3X as many nuclei as the clone. (C, C′) Apical confocal images of eye discs of the genotype *hs-flp; FRT82B lqfR*$^{\Delta 117}$*/FRT82B arm-lacZ*, treated as in (B,B'). A *lqfR*– clone (*lacZ*–; dotted outline) and *lqfR*+ twinspot (2X*lacZ*; solid outline) are shown. The twin spot is 15X larger in area and has 17X as many nuclei as the clone. Raw data for these and other control and experimental clones, at these and other focal planes, is in Table 2-1.

genotype		area (pixels)	twin/clone	no. nuclei	twin/clone
wt control #1	clone	101180	1.3	105	1.3
	twinspot	126641		136	
wt control #2	clone	118542	1.4	173	1.4
	twinspot	167515		233	
lqfR$^{\Delta 117}$ #1-fp1	clone	6836	3.1	9	2.5
	twinspot	21529		23	
lqfR$^{\Delta 117}$ #1-fp2	clone	8047	2.4	11	2.2
	twinspot	19603		24	
lqfR$^{\Delta 117}$ #1-fp3	clone	9817	2.4	14	1.4
	twinspot	23261		20	
lqfR$^{\Delta 117}$ #2-fp1	clone	10036	5.2	6	3.6
	twinspot	52517		22	
lqfR$^{\Delta 117}$ #2-fp2	clone	11163	4.4	9	2.3
	twinspot	49411		21	
lqfR$^{\Delta 117}$ #2-fp3	clone	17705	2.6	11	2.1
	twinspot	45517		23	
lqfR$^{\Delta 117}$ #3-fp1	clone	5297	15	2	17
	twinspot	77456		34	
lqfR$^{\Delta 117}$ #3-fp2	clone	8001	7.3	6	6.3
	twinspot	58393		38	
lqfR$^{\Delta 117}$ #3-fp3	clone	19091	2.2	14	1.8
	twinspot	42824		25	
lqfR$^{\Delta 117}$ #4-fp1	clone	4065	19	2	20
	twinspot	78851		41	
lqfR$^{\Delta 117}$ #4-fp2	clone	3755	20	3	14
	twinspot	75008		43	
lqfR$^{\Delta 117}$ #1-fp3	clone	9071	7	4	9.3
	twinspot	63313		37	

Table 2-1. Quantifying the areas of *lqfR*$^{\Delta 117}$ (or *lqfR*$^{+}$ control) clones and *lqfR*$^{+}$ twinspots.

The results from two different control (wt) clones and four different *lqfR*$^{\Delta 117}$ clones are shown. The *lqfR*$^{\Delta 117}$ clones were analyzed at 3 different focal planes: fp1 is apical, fp2 is midway, and fp3 is basal.

***lqfR+* is required cell autonomously for insulin-independent cell growth in the eye**

I was curious to determine how the complete absence of *lqfR+* activity would affect cells in the adult eye. I generated marked $lqfR^{\Delta 117}$ homozygous clones in a *lqfR+*/$lqfR^{\Delta 117}$ background in adult eyes. Because *lqfR+* is required for cell proliferation, I expected the clones to be small and they were. I found that ommatidia within the clones composed of all $lqfR^{\Delta 117}$ cells (n=18) were sometimes normally constructed, with eight photoreceptors arranged in a trapezoid, but the mutant ommatidia as a whole and all the R-cell rhabdomeres within them appeared smaller than the wild-type cells surrounding them (Fig. 2-10B). At the clone borders there were ommatidia mosaic for *lqfR-* mutation, because a *glqfR+* transgene complements the clone mutant phenotype (data not shown). I conclude that *lqfR+* is required cell autonomously for cells in the adult eye to attain their normal size.

The appearance of the *lqfR-* retinal clones is smaller to that of mutants in the insulin pathway (Figs. 2-10B, C), a major regulator of cell size (reviewed in (Oldham & Hafen, 2003)). As *lqfR+* function in cell growth is autonomous, its role in the insulin pathway could be in the signal receiving cells, in which the insulin receptor is activated. In the *lqfR-* clones, rhabdomere size appears to be a reflection of cell size. Individual R-cells are not outlined, but their collective cytoplasms, which ring the rhabdomeres, appear reduced in size relative to wild-type in the *lqfR-* ommatidia (Fig. 2-10B). In previous studies of *InR* mutants (Brogiolo et al, 2001), and mutants in other genes in the insulin pathway, similar observations were made of R-cells in mutant clones (see Fig. 2-10C). In these studies, the sizes of mutant cells in other tissues where the cells were outlined were

obviously smaller. Similarly, as described above, I find that *lqfR*$^{\Delta 117}$ salivary glands have small cells (Fig. 2-6). Thus, in the experiments described below, I measured rhabdomere size and used it as indicator of cell size.

I performed a genetic experiment to determine if the small size of *lqfR*$^{\Delta 117}$ cells was due to a defective insulin pathway. Retinal cell clones doubly mutant for an *InR* null and a *lqfR* null allele (*InR*^{339} *lqfR*$^{\Delta 117}$ cells) were generated and compared with *InR*^{339} clones and *lqfR*$^{\Delta 117}$ clones. The *InR*^{339} *lqfR*$^{\Delta 117}$ double knockout chromosome has been generated by Stephen Fleenor. I measured the decrease in rhabdomere size relative to wild-type in each single mutant and in the double mutant. If the *lqfR*- cell size defect is due solely to a malfunction in insulin signaling, then *lqfR*- *InR*- double mutant cells should not be smaller than cells with either mutation alone. Conversely, if *lqfR*+ regulates cell size through a different pathway, then *lqfR*- *InR*- cells could be smaller than *lqfR*- or *InR*- single mutant cells, if the effects of failure of each pathway are additive. I found that *lqfR*$^{\Delta 117}$ R-cell rhabdomeres are on average 45% the size of wild-type (Figs. 2-10A, B), that *InR*^{339} rhabdomeres are on average 30% the size of wild-type (Figs. 2-10A, C). Double mutant *InR*^{339} *lqfR*$^{\Delta 117}$ rhabdomeres are on average 23% of wild-type size (Figs. 2-10A, D), and are significantly smaller than those of either single mutant (Fig. 2-10A). I conclude that the cell growth defect in *lqfR*- retinas cannot be due solely to a role of LqfR in insulin signaling.

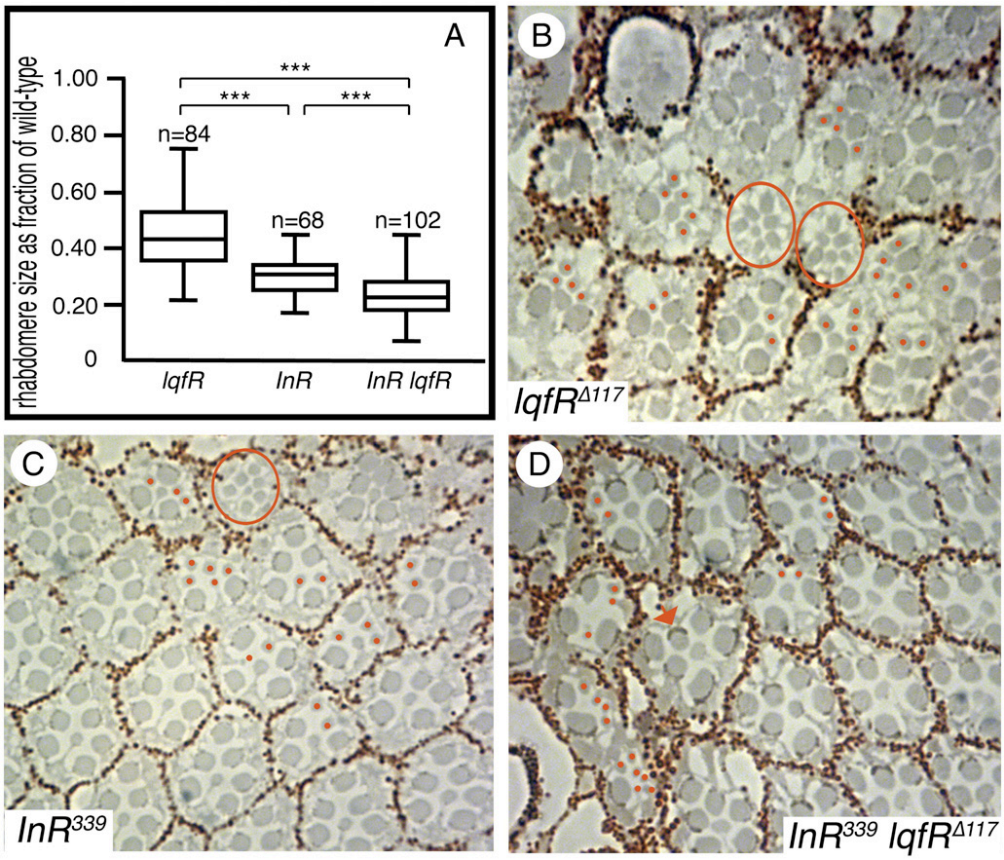

Figure 2-10. Comparison of rhabdomere size in *lqfR*– and *InR*– single and double mutants.

(A) A box plot comparing rhabdomere sizes in $lqfR^{\Delta 117}$, InR^{339}, and $lqfR^{\Delta 117}$ InR^{339} cells. *lqfR* is $lqfR^{\Delta 117}$, and *InR* is InR^{339}. Each ommatidium mosaic for wild-type and mutant R-cells provided a single data point, which was calculated as the average size of the mutant rhabdomeres divided by the average size of the wild-type rhabdomeres (R1–R6 only). The boxes represent the values corresponding to 50% of the data points, and the line within each box is the median. The lines above and below each box extend to the highest and lowest data points. (n=the number of mosaic facets scored, ***p<0.001 by 1-way ANOVA) (B–D) Sections of adult eyes containing facets mosaic for wild-type R-cells and R-cells of the indicated genotypes, that serve as examples of the raw data used to generate the graph in (A). Genetically wild-type R-cells are marked by the presence of pigment granules that appear as black puncta (arrow in panel D). Dots indicate genetically mutant rhabdomeres in mosaic facets, and facets composed of all mutant R-cells are circled. Genotypes are: (B) *ey-flp; FRT82B* $lqfR^{\Delta 117}$*/FRT82B* Pw^{+}; (C) *ey-flp; FRT82B* InR^{339}*/FRT82B* Pw^{+}; (D) *ey-flp; FRT82B* InR^{339} $lqfR^{\Delta 117}$*/FRT82B* Pw^{+}. The $lqfR^{\Delta 117}$ InR^{339} double knockout chromosome was generated by Stephen Fleenor.

LqfR lacking the ENTH domain complements all apparent morphological aspects of the *lqfR* mutant phenotype

Previous research in our lab indicated that an ENTH-less endocytic Epsin (Lqf) protein, when overexpressed, complements all obvious aspects of the *lqf* mutant phenotype (Overstreet et al, 2003). Is LqfR ENTH domain dispensable in *Drosophila* like the ENTH domain of Lqf? Erin Overstreet constructed two transgenes, one that expresses full-length LqfRa fused at the C-terminus to GFP (*UAS-lqfRa-gfp*), and one that expresses an ENTH-less LqfRa-GFP (*UAS-lqfRa$^{\Delta ENTH}$-gfp*). GFP fusions would be useful in case that ENTH-less protein would not function. It could be determined if this was due to its failure to localize to the Golgi. Contrary to this, when overexpressed ubiquitously with an *Act5C-gal4* driver, one copy of either transgene rescues to wild-type all apparent aspects of the mutant phenotype of *lqfR^{a117}* homozygotes (Fig. 2-11A, B, E, F and data not shown) including lethality, and rescues the nearly absent *lqfR^{a117}* homozygous eyes generated using *GMR-hid* (Fig. 2-11G, H, K, L). The full-length GFP-tagged LqfRa protein localizes similarly to the endogenous protein; it is diffuse in the cytoplasm and also in p120-positive puncta (Fig. 2-12). The ENTH-less GFP-tagged LqfRa is more diffuse in the cytoplasm than the full-length protein, but is also present in p120-containing puncta (Fig. 2-12).

In order to determine whether overexpression of the ENTH-less protein was necessary for it to provide all LqfR function, I constructed a genomic DNA transgene similar to *glqfR+* described above, in which the ENTH domain coding sequences are deleted (*glqfR$^{\Delta ENTH}$*, Fig. 2-4A). One copy of a *glqfR$^{\Delta ENTH}$* transgene that is not grossly overexpressed (Materials and methods, Fig. 2-13) also rescues to wild-type the mutant

phenotype of *lqfR*$^{\Delta 117}$ homozygotes, including lethality (Fig. 2-11D and data not shown). I conclude that the ENTH domain of LqfR is dispensable for all of its obvious non-redundant functions in *Drosophila*.

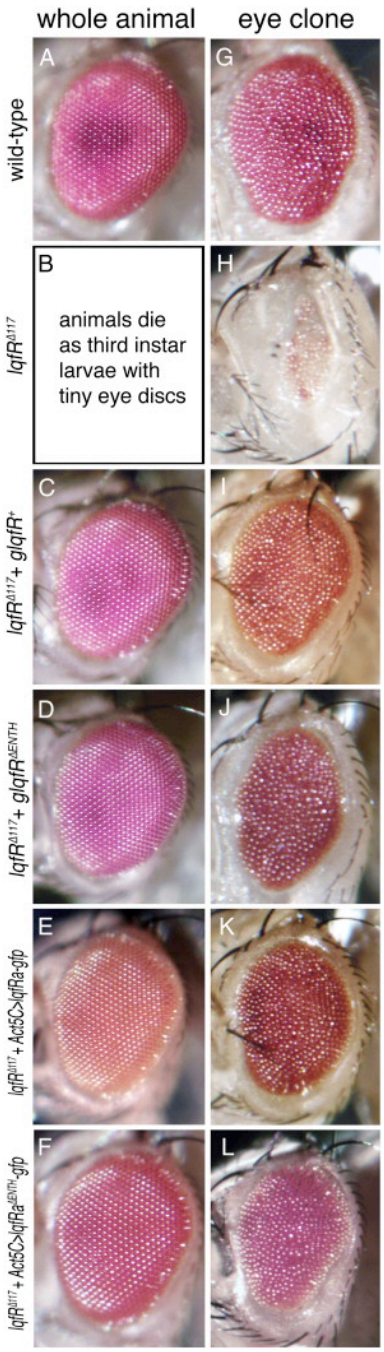

Figure 2-11. Complementation of *lqfR* mutant phenotype by transgenes encoding wild-type and ENTH-less LqfRa.

Adult eyes of eclosed flies are shown in all panels except (B), where adults never eclosed. In (B‑ F), the entire animal is homozygous for $lqfR^{\Delta 117}$, and in (H‑ L), only the eyes are $lqfR^{\Delta 117}$, while the rest of the animal is $lqfR^{\Delta 117}$ /*lqfR*+. In both (B‑ F) and (H‑ L), the animal contains a single copy of the transgene(s) indicated at the left. The genotypes are: (A) OregonR, (B) *FRT82B* $lqfR^{\Delta 117}$, (C) *glqfR+; FRT82B* $lqfR^{\Delta 117}$, (D) $glqf^{\Delta ENTH}$*; FRT82B* $lqfR^{\Delta 117}$, (E) *Act5C-gal4/UAS-lqfRa-gfp; FRT82B* $lqfR^{\Delta 117}$, (F) *Act5C-gal4/UAS-*$lqfRa^{\Delta ENTH}$*-gfp; FRT82B* $lqfR^{\Delta 117}$, (G) *ey-flp; CyO gfp/+; FRT82B Pw+/FRT82B GMR-hid (3)CL-R1*, (H) *ey-flp; CyO gfp/+; FRT82B* $lqfR^{\Delta 117}$ */FRT82B GMR-hid l(3)CL-R1*, (I) *ey-flp; glqfR+/+; FRT82B* $lqfR^{\Delta 117}$*/FRT82B GMR-hid l(3)CL-R1*, (J) *ey-flp;* $glqfR^{\Delta ENTH}$*/+; FRT82B* $lqfR^{\Delta 117}$ */FRT82B GMR-hid l(3)CL-R1*, (K) *ey-flp; Act5C- gal4, UAS-lqfRa-gfp/+; FRT82B* $lqfR^{\Delta 117}$*/FRT82B GMR-hid l(3)CL-R1*, (L) *ey-flp; Act5C-gal4, UAS-*$lqfRa^{\Delta ENTH}$*-gfp/+; FRT82B* $lqfR^{\Delta 117}$*/FRT82B GMR-hid l(3)CL-R1*. The $lqfR^{\Delta 117}$ eyes (and all other morphological aspects of the mutant phenotype) in (C–F) are fully rescued to wild-type by transgene expression. Thus, the eyes in (I–L) would also be expected to be rescued to wild-type. Although they are obviously improved as compared to (H), and appear similar to (G), whether or not the rescue is complete is difficult to assess without the whole animal experiment because the genetically wild-type eyes generated using *FLP/GMR-hid* (G) do not have normal morphology (compare to A).

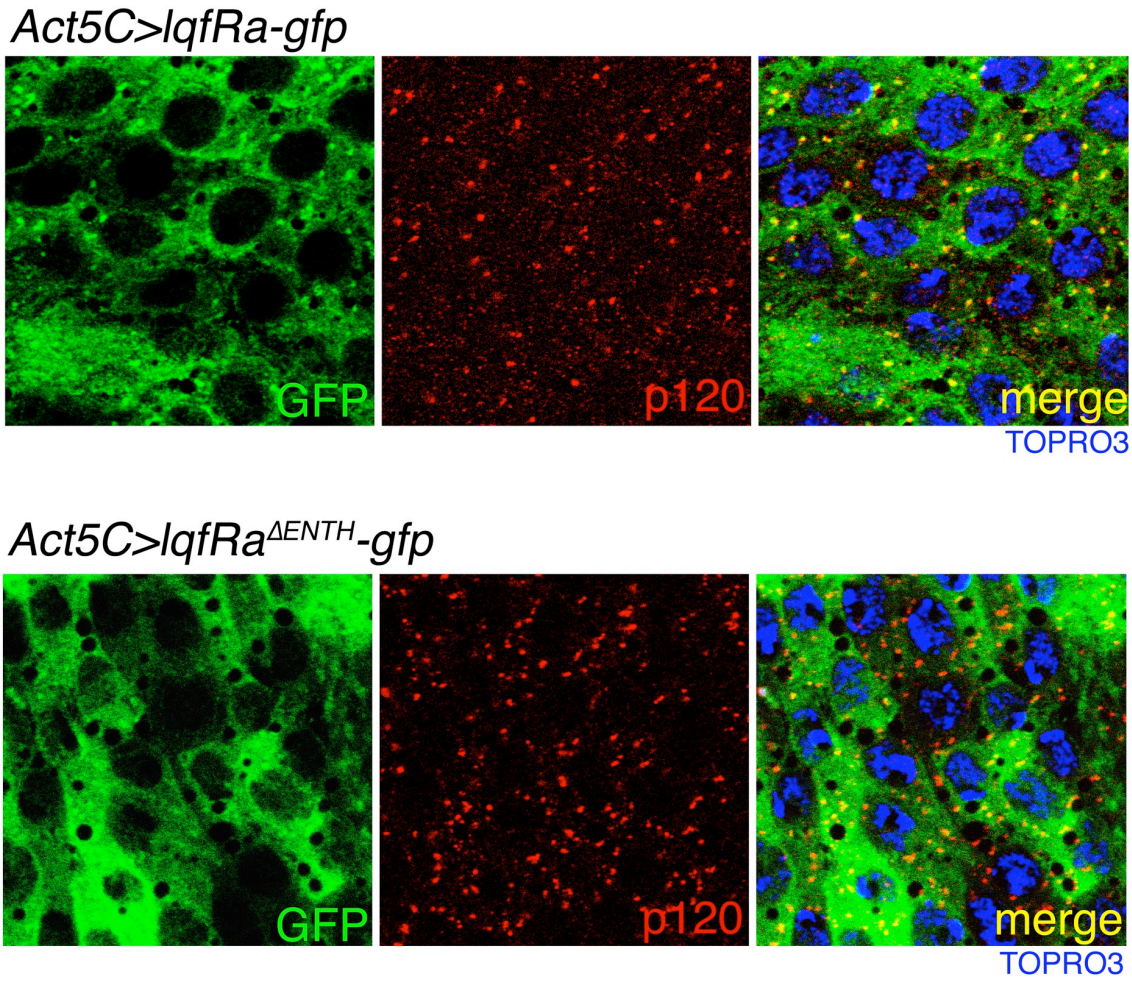

Figure 2-12. Expression of GFP-tagged LqfRa proteins in eye discs.

Confocal images of eye disc peripodial epithelia are shown. Eye discs are labeled with p120 and TOPRO3.

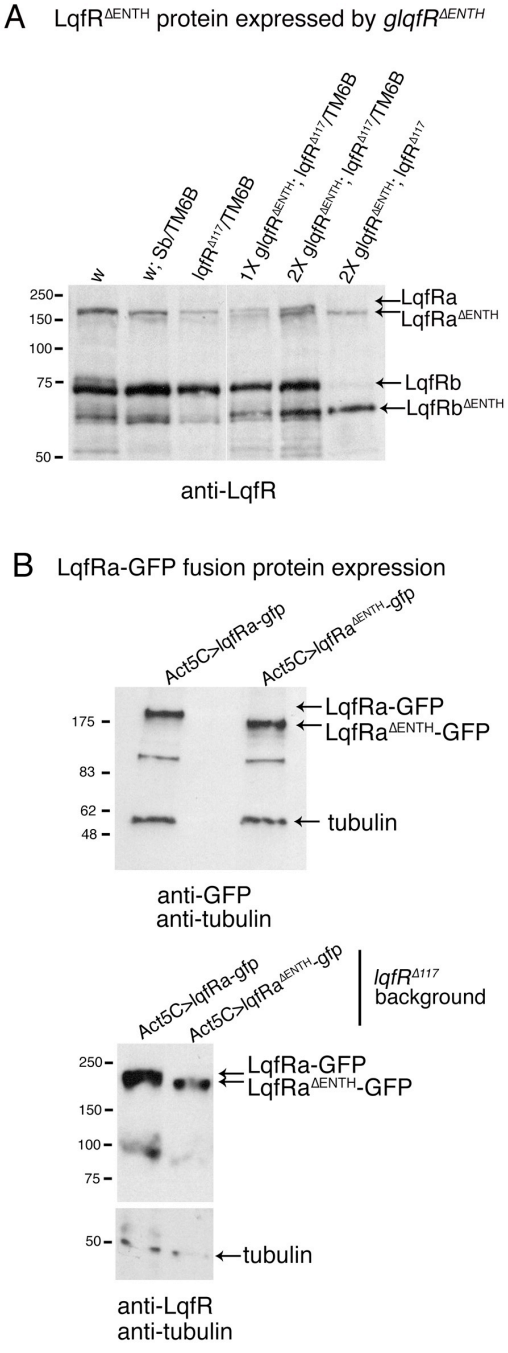

Figure 2-13. Quantifying LqfR$^{\Delta ENTH}$ expressed by *glqfR*$^{\Delta ENTH}$.

Quantifying LqfR$^{\Delta ENTH}$ expressed by *glqfR*$^{\Delta ENTH}$. expressed by *glqfR*$^{\Delta ENTH}$. (A) A blot revealing the LqfR proteins in whole adult fly extracts is shown. 1X and 2X indicate the copy number of the transgene. The signal from anti-LqfR is similar in strength for endogenous LqfRa and transgenic LqfRa$^{\Delta ENTH}$, while the LqfRb$^{\Delta ENTH}$ signal is somewhat weaker than that of endogenous LqfRb. (B) In the top panel, a blot revealing the LqfRa/GFP fusion proteins in eye disc protein extracts is shown. As judged by the signal from anti-GFP relative to anti-tubulin, the levels of LqfRa-GFP and LqfRa$^{\Delta ENTH}$-GFP proteins produced are similar. In the bottom panel, LqfR-GFP fusion proteins produced by the same transgenes as in the panel above are revealed in adult protein extracts using anti-LqfR. The LqfRa signals relative to tubulin are similar for LqfRa-GFP and LqfRa$^{\Delta ENTH}$-GFP.

2.3 DISCUSSION

From this research, flies with null mutations in the Golgi Epsin gene, *lqfR*, have been generated and analyzed for several aspects of their mutant phenotype and also those of hypomorphs. *lqfR* is essential for viability of the organism. Further experiments in the eye imaginal disc revealed that *lqfR* is needed for cell proliferation, insulin-independent cell growth, patterning at the D/V axis, advancement of the morphogenetic furrow, and regulation of expression of the *rough* transcription factor. Finally, all of these functions of *lqfR* are independent of the ENTH domain.

What does the lack of a requirement for the ENTH domain mean?

Endocytic Epsin (Lqf) functions without its ENTH domain, but overexpression of the ENTH-less protein may be required (Overstreet et al., 2003). Here, I found that even when expressed by its own promoter, an ENTH-less *lqfR* gene can substitute for all apparent functions of endogenous *lqfR*. Like Lqf, LqfR is able to localize to the appropriate (Golgi) membrane without the ENTH domain. Also, if the LqfR ENTH domain induces curvature of clathrin-coated vesicles as proposed for the ENTH domain of endocytic Epsin (Ford et al., 2002), this function is not essential to the major role of LqfR in *Drosophila*. The Golgi Epsin ENTH domain also serves as the recognition element for SNARE cargos (Miller et al., 2007), and thus it can be inferred that SNARES are not the cargo relevant to the critical function of LqfR. See chapter 4 for further structure/function analysis.

Is *lqfR* required in a specific signaling pathway?

I think that *lqfR* is likely required for cell signaling because signaling pathways control both cell proliferation/growth and patterning (Baker, 2007), and in the absence of *lqfR*, there are defects in both of these aspects of cell behavior. Also, the observation that expression levels of a transcription factor are altered in *lqfR* mutants is consistent with a signaling pathway defect. Virtually all signaling pathways have an endosomal component (Fischer et al, 2006; Le Roy & Wrana, 2005; Piddini & Vincent, 2003), and moreover, Wnt signaling is known to require endosome-to-TGN trafficking specifically (Belenkaya et al, 2008; Franch-Marro et al, 2008; Port et al, 2008). As a single signaling pathway may control cell proliferation and growth and also patterning, it seems possible, although by no means necessary, that all aspects of the *lqfR* mutant phenotype could be due to misregulation of a single pathway.

Wnt signaling (Wingless (Wg) in *Drosophila*) requires the Golgi transmembrane protein Wntless (Banziger et al, 2006; Bartscherer et al, 2006; Goodman et al, 2006). Wntless is a Golgi protein that promotes secretion of the ligand Wg, and which accompanies Wg to the plasma membrane. Wntless is subsequently endocytosed, and sorted for recycling back to the TGN through the action of the retromer complex (Belenkaya et al, 2008; Franch-Marro et al, 2008; Port et al, 2008). Protein sorting by retromer in the early endosome may be followed by EpsinR-dependent clathrin-coated vesicle formation (Popoff et al, 2007). Thus, it seems possible that along with Wntless and the retromer proteins, LqfR might promote Wg signaling. This idea has been tested in Chapter 4.

Can the *lqfR* mutant eye phenotype be explained by *wg* loss-of-function? (The role of Wg in eye disc morphogenesis is reviewed in (Legent & Treisman, 2008)) Early in eye disc development, Wg and Hh signaling collaborate in the dorsal half of the eye disc to set up the D/V axis. Later, by diffusing from the dorsal and ventral disc margins, Wg organizes the gradients of Dachsous and Four-jointed proteins that in part define planar cell polarity in the eye. Dampening of Wg signaling could lead to patterning disruptions at the equator in weak *lqfR* mutants. Wg emanating from the dorsal and ventral margins also positions the morphogenetic furrow centrally by repressing expression of *decapentaplegic (dpp)* (see below), and promotes proliferation of cells anterior to the morphogenetic furrow that will become head capsule. Reduction of Wg activity in the eye disc results in initiation of ectopic furrows at the lateral margins of the eye disc, and a larger eye at the expense of head tissue. Essentially the opposite is observed in *lqfR* mutant eyes: halting of the furrow and a tiny eye. Also, the cell size defect observed in adult eyes is cell autonomous. Thus, some, but not all aspects of the *lqfR* eye phenotype can be explained easily by weak Wg signaling alone.

One hypothesis that may explain most features of the *lqfR* mutant eye phenotype is overactive Hh signaling. The key observation in support of this idea is that *rough* is overexpressed in *lqfR* eye discs. Excessive Hh signaling results in arrest of the morphogenetic furrow through overexpression of *rough* (Chanut et al, 2000). Morphogenetic furrow progression is controlled mainly by Hh and Dpp (reviewed in Baker, 2007). Posterior to the furrow, differentiating R-cells express Hh, which activates Dpp expression, and both ligands diffuse anteriorly. In cells anterior to the furrow, Dpp arrests the cell cycle in G1, and Hh subsequently initiates R-cell differentiation. Hh

signaling is able to arrest the cell cycle also, but as Dpp diffuses faster than Hh, Dpp normally plays this role. As the R-cells differentiate, they start to express Hh, and this cycle moves the furrow forward. Anterior to the furrow, through Notch, Hh activates expression of the proneural transcription factor Atonal, which is required for subsequent Hh expression by R-cells posterior to the furrow. Rough expression is also activated by Hh, and it blocks Atonal expression in some cells. The ro^{DOM} allele appears to be hypersensitive to Hh activity, and thus Rough is overexpressed and blocks Atonal in too many cells, leading to loss of Hh expression posterior to the furrow, and the furrow stops (Chanut et al., 2000). Thus, overactivity of Hh in *lqfR* discs could result in *rough* overexpression and halting of the furrow. Third, the D/V axis in the eye disc is defined by a stripe of cells in which Notch is activated. Setting up of the Notch stripe requires Hh, which is expressed only dorsally and defines the dorsal half of the eye disc (Legent and Treisman, 2008). Hh overactivity sometimes results in enlargement of the dorsal area of the eye, but not always, and as in *lqfR*, the D/V boundary is still present (Thomas & Ingham, 2003). As Hh can negatively regulate the cell cycle anterior to the furrow (Baker, 2007), it seems that Hh overactivity could account for the cell proliferation defect.

By what mechanism could LqfR negatively regulate Hh signaling? (The mechanism of Hh signaling is reviewed in (Kalderon, 2005; Rohatgi & Scott, 2007).) Hh signaling is transduced by the transmembrane protein Smoothened (Smo), which is negatively regulated (through mechanisms that are not entirely clear) by the Hh receptor Patched (Ptc) when it is not bound to Hh. Binding of Hh to Ptc relieves negative regulation of Smo. Hh/Ptc induces Smo phosphorylation, thereby inducing Smo to switch into active conformation (Zhao et al, 2007). Hh/Ptc also binds the glypican Dally-like

(Dlp), which serves as an endocytosis signal. Hh/Ptc endocytosis results in Smo translocation to the plasma membrane and signaling (Beckett et al, 2008; Gallet et al, 2008). LqfR could regulate Smo negatively through recycling of Ptc to the plasma membrane, or by promoting the transport of Smo or Dlp away from the plasma membrane, possibly to the lysosome instead. This role for LqfR would be similar to that of yeast Ent3p/Ent5p in the multi-vesicular body.

Further experiments are required to determine if LqfR plays any role at all in Wntless endosome-to-TGN recycling, in Hh signaling, or in one or several other pathways. The mutants and phenotypic characterization described here suggest strongly that like Lqf, LqfR is involved in signaling, and provide the tools for testing these and other hypotheses.

Chapter 3. Identification of dominant modifiers of the *liquid facets-Related* hypomorphic phenotype

The experiments in Chapter 3 have been performed as collaborations with Stephen Fleenor, Yoni Bibliowicz, and Erin Overstreet. Erin is a former graduate student who identified *fringe* as a dominant enhancer of the *liquid facets-Related (lqfR)* hypomorphic eye phenotype. Yoni was a rotation student in our lab. Yoni initiated a pilot screen for dominant modifiers of the *lqfR* hypomorphic eye phenotype. Stephen collaborated with me as an undergraduate student to perform a scaled-up screen to identify more dominant modifiers. Stephen also participated in complementation tests and deficiency mapping to identify genes mutated in complementation groups. I indicated each of their contributions in the text. Experiments explained without identifying the contributor were performed by me alone.

3.1 INTRODUCTION

Drosophila liquid facets-Related (lqfR) encodes a single homolog of Golgi Epsin with an ENTH (Epsin N-term homology) domain and putative peptide motifs for protein-protein interaction (see Chapters 1 and 2). *lqfR* also contains an exon, which is a single homolog of a well-conserved gene called *tel2* (see Chapters 1 and 4).

The *lqfR* mutant phenotype shown in Chapter 2 suggests its role in signaling pathway(s) and cell cycle regulation. *lqfR* loss-of-function mutants have defects in proliferation, patterning, and insulin-independent cell growth. A hypomorphic allele $lqfR^{p}$

is semi-lethal when it is homozygous. The escapers frequently have a morphological mutant phenotype, including rough and kidney-shaped eyes. When such eyes of *lqfR*^{P} homozygotes were sectioned tangentially, they showed defects in patterning. Unlike wild-type eyes, *lqfR* hypomorphic eyes have irregularly ordered ommatidia frequently with too many or too few rhabdomeres. There were also planar cell polarity defects. (See Fig. 2-7 in Chapter 2). Signaling pathways including the Notch pathway are known to be crucial for photoreceptor recruitment during the eye development (Roignant & Treisman, 2009). The kidney-shaped eye in the *lqfR* hypomorph is due to a defect in the morphogenetic furrow movement. It has been shown that the Hedgehog signaling pathway directly regulates furrow movement, and Wingless and Dpp signaling pathways are also involved (Dominguez & Hafen, 1997). A *lqfR* null allele, *lqfR*^{s117}, imparts a proliferation defect, suggesting that *lqfR* may have an important role in cell cycle regulation and/or cell survival. Cell proliferation in the eye disc is regulated by Notch and Wingless signaling (Baker, 2007; Giraldez & Cohen, 2003).

Although the *lqfR* mutant phenotype suggests its important function in *Drosophila* development, the mechanism is unknown. To obtain a mechanistic understanding of the *lqfR* function, it would be important to know the context of the *lqfR* function by identifying genes that interact with *lqfR*. With this reason, colleagues and I performed a genetic screen for dominant modifiers of the *lqfR*^{P} eye phenotype. Erin Overstreet found that *lqfR*^{P} eye phenotype could be modified dominantly by a loss-of-function allele of *fringe*, a gene in the Notch signaling pathway. As *lqfR*^{P} homozygotes are semi-lethal, the *GMR-hid* technique has been used to generate homozygous *lqfR*^{P} eyes in the heterozygous background (see Chapter 1). These flies are convenient for use in an

F1 screen of viable adult flies with eye defects. Yoni Bibliowicz initiated a pilot screen and showed that the screen works. Stephen Fleenor collaborated with me to perform a large-scale screen, complementation tests, and mapping. From these screens, 8 lethal complementation groups with multiple members on the third chromosome were identified. *Delta, neuralized, polychaetoid (ZO-1), string (cdc25),* and *altered disjunction (Mps1)* were identified as dominant enhancers from this screen. The possible meaning of these results and future directions are discussed.

3.2 RESULTS

The *lqfR^{P}* eye phenotype as a sensitized background for dominant modifiers

lqfR^{P} is a hypomorph (Chapter 2). The phenotype includes semi-lethality and morphological defects in the eye. The eyes of the mutants have a "rough" surface due to the irregular array of the facets in the compound eye, instead of the smooth and regular array of the wild-type eye. As the eye phenotype of *lqfR^{s117}*, a null allele, is much more severe, it is likely that the *lqfR^{P}* eye phenotype is modifiable and suitable for a dominant modifier screen. To test if the *lqfR^{P}* eye phenotype can be dominantly modified, Erin Overstreet performed a series of candidate-based genetic interaction tests. Genes tested for dominant modification of the *lqfR^{P}* eye phenotype were: *lqf (lqf^{FDD9}, lqf^{L71}), hrs (hrs^{D28}), chico (chico^{1}), Tor (Tor$^{\Delta P}$), aux (aux^{e727}, aux^{ed136}), vn (vn^{G115}, vn^{11749}), hh (hh^{rJ413}, hh^{AC}), fng (fng^{rG554}), syx5 (syx5^{AR113}), Ras (Ras^{e1b}), wg (wg^{I-17}), dpp (dpp^{s-11}), InR (InR^{05545}), gig (gig^{109}), syx1A (syx1A$^{\Delta 229}$),* and *Egfr (Egfr^{tsla})*. Erin found that *fng^{rG554}* dominantly enhanced the *lqfR^{P}* eye phenotype at 23°C. *fringe (fng)* encodes a glycosyltransferase required for restricting Notch activation to the D/V midline in the eye disc. None of the other genes tested t interacted with *lqfR^{P}* in her hands. Her results indicate that the *lqfR^{P}* eye phenotype can be dominantly modified, and this genetic interaction does not happen with random genes required for *Drosophila* eye development. It implies that more specific genetic interactions can be found in larger scale genetic experiments such as mutagenesis screens for dominant modifiers. Her results also suggest that *lqfR^{+}* may have a role in the Notch signaling pathway.

To obtain a better picture of the modification of the *lqfR*^{P} eye phenotype, I confirmed the genetic interaction between *lqfR* and *fng*. For the initial test, I crossed a fly line with the recombinant chromosome, *fng*^{rG554} *lqfR*^{P}, which was generated by Erin, with *lqfR*^{P} heterozygotes to get progeny with the genotype of *fng*^{rG554} *lqfR*^{P}/*lqfR*^{P}. Because the *lqfR*^{P} eye phenotype is temperature sensitive, I incubated the crosses in two temperature conditions, 23°C and 25°C. As expected, the phenotype seemed to be enhanced, but I observed variable expressivity at both temperature and as I anticipated that this may happen in my mutant screen as well, I needed to find a way to quantify this. I decided to score the candidate enhancer mutations by generating several flies with the same genotype (*lqfR*^{P}/ *lqfR*^{P} ; *E*-/*E*+), dividing them into four categories of eye defect severity, and counting the fraction in each category. The four categories are: Normal, Rough, Kidney, and Small (Fig. 3-1). "Normal" mean wild-type. In the "Rough" category, the number of flies with slightly rough eyes with overall wild-type size and shape was recorded. The "Kidney" category is for flies with at least one kidney-shaped eye with overall wild-type size. A "Kidney"-shaped eye was considered more severe than a "Rough" eye because kidney-shaped eyes were almost always rougher than rough oval eyes, in addition to the anterior defect. Lastly, the "Small" category is for flies with at least one more severely enhanced smaller and rougher eye. The data is summarized in Table 3-1. At 23°C, the phenotype of the progeny is shifted to "Kidney" and "Small" categories when one copy of *fng*^{rG554} is added. However, this pattern was not obvious at 25°C. The number of progeny was also significantly decreased at 25°C as expected from the temperature-sensitive semi-lethality of the allele. These results confirm Erin's results that *fng*^{rG554} dominantly enhances the *lqfR*^{P} eye phenotype. The results also indicate that the enhancement can be visualized better at 23°C.

fng^{rG554} is an enhancer trap line with a P element inserted in the *fng* locus, and it is allelic to *fng*^{80}, a null allele (Milan & Cohen, 2000). The *fng*^{rG554} chromosome is homozygous lethal. However, *fng*^{rG554} has not been used as a loss-of-function allele in the literature. To confirm that *fng*^{rG554} is a loss-of-function allele, I obtained *fng*^{13}, which is thought to be a null allele (Grammont & Irvine, 2001; Irvine & Wieschaus, 1994)), and *Df(3L)ri-XT1*, a deficiency line that deletes the *fng* locus. I tested if they fail to complement each other. All three chromosomes were indeed lethal over each other (data not shown). This result indicates that *fng*^{rG554}, as well as *fng*^{13}, is a loss-of-function allele although the strength of the *fng*^{rG554} allele is not tested here.

To confirm the genetic interaction between *lqfR* and *fng*, I tested if *fng*^{13} dominantly modifies the *lqfR*^{P} eye phenotype. I would expect a stronger genetic interaction because *fng*^{13} is presumably a null allele. As both genes are on chromosome 3, I generated *fng*^{13} *lqfR*^{P} recombinant chromosomes. I obtained 3 lines, #2, #13, and #14. Because genetic interactions are sensitive to the genetic background and the *lqfR*^{P} phenotype is variable, I used all three lines for dominant modification tests. Again, I did this test at both 23°C and 25°C. The number of progeny in each category of severity was counted. The numbers from two independent crosses was added and shown in Table 3-1. The result shows that *fng*^{13} is a stronger enhancer of the *lqfR*^{P} phenotype compared to the *fng*^{rG554} allele as expected. *fng*^{13} enhanced at both 23°C and 25°C. However, the number of progeny were fewer at 25°C, which is consistent with the previous results.

The results in this section suggest that the *lqfR*^{P} eye phenotype can be used as a sensitized background for dominant modifier screens. This validation method can also be used in the large-scale genetic screen. Incubation at 23°C would be better than 25°C for this validation assay because *fng*^{rG554}, a presumably weaker allele, did not show dominant

modification at 25°C. Furthermore, even though *fng*^{13} enhanced the eye phenotype at both temperatures, the larger progeny number would make the result of the assay more convincing.

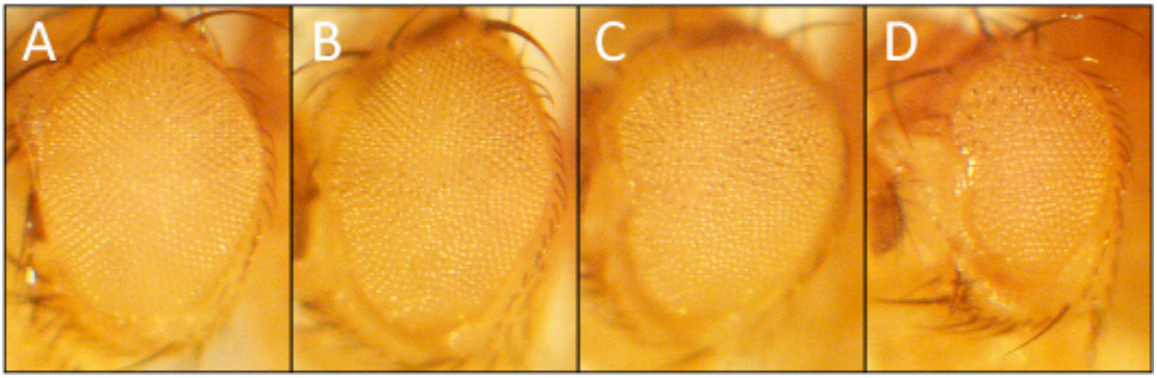

Figure 3-1. Variable eye phenotype of $lqfR^{P}$ with a dominant enhancer, fng^{13}.

(A-D) are images of adult eyes with the same genotype: fng^{13}, $lqfR^{P}/lqfR^{P}$. It shows the variable range of $lqfR^{P}$ eye phenotype with a dominant enhancer, fng^{13}. The variable eye phenotype is categorized into 4 classes based on the severity of the phenotype: (A) "Normal" = almost as good as wild-type. (B) "Rough" = the surface of the eye is rough but the overall size and shape resemble the wild-type. Note the irregular array of facets at the ventral region. (C) "Kidney" = the eye is rough and has an anterior defect shown as a kidney-shaped eye. However, the overall size is comparable to wild-type. (D) "Small" = the size of the eye is severely reduced. There are anterior defects very frequently in flies shown in (D). As the $lqfR^{P}$ eye phenotype with or without one copy of a *fng* loss-of-function allele is variable, the validation has been done by counting the numbers of flies in each category of (A-D). The relative strength of the enhancement might be: Normal < Rough < Kidney < Small. The data is summarized in Table. 3-1.

Genotype	Temp	#Normal(%)	#Rough(%)	#Kidney(%)	#Small(%)	Total(%)	#Crosses
$lqfR^P/lqfR^P$	23°C	32 (27.6%)	58 (50%)	26 (22.4%)	0 (0%)	116 (100%)	3
fng^{rG554} $lqfR^P/lqfR^P$	23°C	18 (18.4%)	30 (30.6%)	32 (32.6%)	18 (18.4%)	98 (100%)	4
$lqfR^P/lqfR^P$	25°C	1 (4%)	6 (24%)	15 (60%)	3 (12%)	25 (100%)	2
fng^{rG554} $lqfR^P/lqfR^P$	25°C	9 (22.5%)	10 (25%)	19 (47.5%)	2 (5%)	40 (100%)	3
$lqfR^P/lqfR^P$	23°C	33 (51.6%)	31 (48.4%)	0 (0%)	0 (0%)	64 (100%)	2
(Line #2) fng^{13} $lqfR^P/lqfR^P$	23°C	7 (8.75%)	25 (31.25%)	29 (36.25%)	19 (23.75%)	80 (100%)	2
(Line #13) fng^{13} $lqfR^P/lqfR^P$	23°C	11 (13.3%)	37 (44.6%)	29 (34.9%)	6 (7.2%)	83 (100%)	2
(Line #14) fng^{13} $lqfR^P/lqfR^P$	23°C	16 (22.2%)	38 (52.8%)	7 (9.7%)	11 (15.3%)	72 (100%)	2
$lqfR^P/lqfR^P$	25°C	0 (0%)	6 (46.1%)	5 (38.5%)	2 (15.4%)	13 (100%)	2
(Line #2) fng^{13} $lqfR^P/lqfR^P$	25°C	0 (0%)	0 (0%)	1 (11.1%)	8 (88.9%)	9 (100%)	2
(Line #13) fng^{13} $lqfR^P/lqfR^P$	25°C	0 (0%)	0 (0%)	1 (8.3%)	11 (91.7%)	12 (100%)	2
(Line #14) fng^{13} $lqfR^P/lqfR^P$	25°C	0 (0%)	3 (12.5%)	6 (25%)	15 (62.5%)	24 (100%)	2

Table 3-1. Validation of genetic interaction between *lqfR* and *fng*.

Results from the experiments to test if strong loss-of-function alleles of *fng* dominantly modify $lqfR^P$ eye phenotype at either 23°C or 25°C. The numbers of progeny correspond to the genotype are shown with percentage. The numbers of progeny from multiple independent crosses with the same genotype at the same condition were added. Normal, Rough, Kidney, and Small indicate categories of severity of the phenotype as shown in Fig. 3-1 (Correspond to (A), (B), (C), and (D), respectively.). "$lqfR^P/lqfR^P$" is the control for background variability.

Pilot screen for dominant modifiers of *lqfR* whole eye clone phenotype

lqfR^{P} homozygotes are semi-lethal. To perform a dominant modifier screen using the validation method I explained earlier, the screen has to be an F2 screen. However, the validation requires a significant amount of time due to the variable expressivity of the *lqfR*^{P} eye phenotype. So, instead of doing an F2 screen, we decided to do an F1 screen by generating whole eye clones of homozygous *lqfR*^{P} in the heterozygous background using the *FLP/FRT GMR-hid* technique. The idea is to express *flp* eye-specifically using either *ey-flp* or *ey-gal4 UAS-flp (EGUF)*, and induce mitotic recombination at the FRT site between 3R chromosome homologs of *FRT82B lqfR*^{P} and *FRT82B lqfR*$^{+}$ *GMR-hid* early in eye development. As a result, while the whole rest of the body is *lqfR*^{P}/*lqfR*$^{+}$ *GMR-hid*, there will be three genotypes of cells in the eye: *lqfR*^{P}/*lqfR*^{P}, *GMR-hid*/*GMR-hid*, and *lqfR*^{P}/*GMR-hid*. *GMR* is a late onset promoter expressed behind of the morphogenetic furrow and hid is a potent apoptosis inducer. Therefore, in the adult eye, cells with GMR-hid will be eliminated and the whole eye will be *lqfR*^{P} homozygous. This method solves the semi-lethality problem.

With the *GMR-hid* technique, the 3R chromosome arm of *FRT82B lqfR*^{P} is homozygosed in the eye. So, if there are other mutations in the chromosome, those mutations will also be homozygosed. These junk mutations can cause eye defects by themselves. To test this possibility, Yoni Bibliowicz double checked the isogenized fly stock to be mutagenized to see if the *lqfR*^{P} phenotype can be rescued by overexpressing *UAS-lqfRa-gfp* using *Act5C-gal4* driver. He found that the phenotype is rescued (data not shown).

The *GMR-hid* technique may cause a similar problem by homozygosing the *FRT82B lqfR*^{P} chromosome during the mutagenesis screen. If the mutagen hits the 3R chromosome and make a mutation in a gene, the mutation will also be homozygosed as well as *lqfR*^{P}. This may result in a misinterpretation of the data especially when the mutagenized gene has a role in the eye development because the purpose of this screen is to identify genes with a dominant effect on the modification of the *lqfR*^{P} phenotype. For this reason, the dominant modifiers on the chromosome 3 screened using *GMR-hid* technique should be validated again for their dominant effects on the modification of the *lqfR*^{P} phenotype. So, this screen is a modified F2 screen when the dominant modifier is on chromosome 3. However, due to the variable expressivity and difficulty of the validation of the phenotype, this strategy has the advantage to save a significant amount of time and labor compared to the F2 screen where all F1 mutant stocks should be validated.

To test if this screen works, Yoni Bibliowicz initiated a pilot screen. First, he tested if the *lqfR*^{P} whole eye clone phenotype resembles that of *lqfR*^{P} homozygotes. Yoni found that, similar to eyes from the homozygotes, the *lqfR*^{P} whole eye clone has moderate roughness and frequent anterior defects (Fig. 3-2). This screen aimed to screen autosomes 2 and 3, which cover approximately 80% of the genome. Ethyl methanesulfonate (EMS) was fed to males of the genotype *'+/+ ; FRT82B lqfR*^{P}*/TM6B'* and they were mated with the females of *'EGUF/EGUF ; FRT82B GMR-hid/TM6B'* (Fig. 3-3). The males mated only for 4 days so that only mutagenized individual sperms were used, but no sperms from mutagenized germ line stem cells were used. Yoni screened 2304 F1 males and found 607 enhancer candidates. F1 progeny are mosaic because EMS hit only one strand of DNA. To observe non-mosaic phenotype, the enhanced 607 F1 males were

backcrossed (Fig. 3-3). 244 F2 males were enhanced. To identify on which chromosome each enhancer is located, segregation tests followed. Enhanced males were crossed with the females of '*EGUF/CyO ; FRT82B GMR-hid/TM6B*' (Fig. 3-3). If the *CyO* progeny from the cross are enhanced, it means that the dominant enhancer is on the chromosome 3. However, if all enhanced progeny are non-*CyO*, it means that the enhancer is on chromosome 2. I took over the enhancers from Yoni when the segregation test was almost completed. Because the segregation test for the chromosome 2 is done by looking at the absence of enhanced *CyO* progeny, the results can be misinterpreted when there are few non-*TM6B* progeny. I repeated the cross for chromosome 2 enhancers until I was sure that the enhancer is really on chromosome 2. The segregation test resulted in 3 enhancers on chromosome 2 and 48 on chromosome 3. Chromosomes with enhancers were saved with *CyO* (chromosome 2) or *TM6B* (chromosome 3) balancers. The result indicates that the screen is biased toward chromosome 3 (see Discussion).

Enhancer candidates on chromosome 3 should be validated for their ability to enhance the $lqfR^{P}$ phenotype dominantly. Flies with the FRT82B $lqfR^{P}$ chromosomes containing an enhancer were crossed with *FRT82B* $lqfR^{P}$*/TM6B* and incubated at 23°C. Non-*TM6B* progeny were screened for validation. For a control, males and females from the *FRT82B* $lqfR^{P}$*/TM6B* stock were crossed (Table 3-2). Although the unexpectedly few progeny from the two control crosses dampened the quality of the result, their eye phenotype was within the expected range: mostly in "Rough" category with little deviation. Out of 48 enhancer candidates, 25 showed this pattern and were eliminated (data not shown). Table 3-2 summarizes the 23 enhancers passed the validation.

I was interested in enhancers that were homozygous lethal so I could make a lethal complementation matrix. I was also interested in enhancers homozygous viable

with an obvious and consistent morphological phenotype. I planned to do gene mapping only with lethal complementation groups with multiple members or homozygous viable enhancers with a morphological phenotype so I could be sure that the gene I was mapping was also the enhancer. Otherwise, I could map based on the enhancement of the $lqfR^{P}$ phenotype, which would be impossible - especially with the variability even within an isogenic background. Furthermore, enhancers not in a complementation group of multiple members might have more than one mutation with cumulative effects, or they could be gain-of-function mutations. On the other hand, if an enhancer was found as non-complementing with another enhancer, it is likely that the lethal gene enhanced the $lqfR^{P}$ phenotype because it is unlikely that EMS hit same two genes (one for lethality and one for enhancement) in both non-complementing enhancer strains.

For these reasons, I first observed homozygous phenotypes of the enhancer chromosomes. Three enhancers on chromosome 2 were all homozygous viable without obvious mutant phenotypes. I did not pursue them anymore. To observe the phenotype of the enhancers on chromosome 3, a transgene containing a *lqfR* genomic fragment was added on chromosome 2 in each strain to rescue the $lqfR^{P}$ phenotype. Among 23 enhancers on chromosome 3, 20 were homozygous lethal and 3 were homozygous viable with morphological phenotype (Fig. 3-4). The phenotypes of 3 homozygous viable enhancers, 359, 37104, and 37105, are shown in Fig. 3-5: 359 homozygotes had a rough eye phenotype (Fig. 3-5C), 37104 homozygotes had a rough eye phenotype and a notched wing phenotype (Fig. 3-5B, G), and 37105 homozygotes had a notum bristle phenotype. The number of macrochaete was increased (Fig. 3-5E, E').

All 23 enhancers on chromosome 3 were then tested for complementation. I found one lethal and one semi-lethal complementation group, each with 2 members (Fig. 3-4).

Two homozygous lethal enhancers, 368 and 3234, failed to complement each other. A homozygous viable enhancer (359) failed to complement a homozygous lethal enhancer (3518). As *fringe* is on chromosome 3, all 23 enhancers on chromosomes 3 were tested for complementation with fng^{13}. All of them complemented.

Two lethal complementation groups and two homozygous viable enhancers with a mutant phenotype were further pursued to ultimately identify the genes mutated. I planned to perform meiotic mapping first to roughly narrow down the location of the enhancers, and then do deficiency mapping using multiple overlapping deficiency lines covering the region identified from meiotic mapping. After deficiency mapping, genes within the region would be further tested either with specific mutants if they exist or by sequencing.

I performed the meiotic mapping for each of the complementation groups and homozygous viable enhancers with phenotype. I will explain the mapping for the lethal complementation group with enhancers 368 and 3234 first (Fig. 3-6). The chromosome 3 containing 368 was crossed with the multiply marked chromosome 3 (MM3). MM3 has recessive markers, *roughoid (ru), hairy (h), thread (th), curled (cu), stripe (st), and ebony (e)*. The virgin female progeny of '*MM3/368*' were crossed with males of '*MM3, Pr/TM6B*'. Recombination happened in the germline of '*MM3/368*' females. From their progeny, I saved 5 males with each of two parental chromosomes (the one with all recessive markers and the one without any recessive markers) and 10 single recombinant chromosomes over '*MM3, Pr'* chromosome (Fig. 3-6). Each of the male was crossed with females of '*glqfR+/CyO ; 3234/TM6B*'. The lethality of the progeny was recorded for each cross (Table 3-3). As a result, the location of the enhancer in this complementation group was mapped to the right side of *e* (toward the telomere). The complementation

group with 3518 and 359 was mapped in the same way. The gene was mapped between *cu* and *sr* based on semi-lethality and the rough eye phenotype of escapers (Table 3-4). 37104 was mapped in a similar way with its homozygous phenotype of rough eyes and notched wings. As a result, 37104 was mapped to between *th* and *cu* (Table 3-5). Finally, 37105 was mapped based on its homozygous notum bristle phenotype. The location of the gene was mapped to between *th* and *cu* as well (Table 3-6). Further deficiency mapping for each enhancers will be explained below.

Based on the results of the pilot screen so far, this genetic screen seemed to work well. At least 4 different dominant enhancers were isolated from this screen and roughly mapped. However, unexpectedly, this screen using *FLP/FRT GMR-hid* technique seemed to be biased toward the 3R chromosome where the mitotic recombination was induced. Three enhancers were found on chromosome 2, while 48 were found on chromosome 3. Also, out of 4 groups meiotically mapped, 2 were on 3R and 2 were mapped to a region where half of it was 3R.

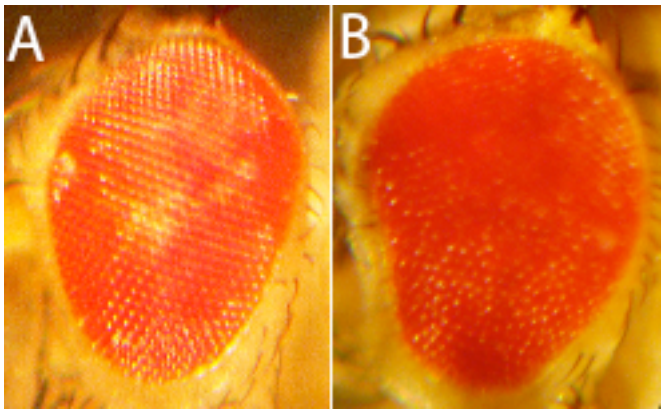

Figure 3-2. The *lqfR*^{P} whole eye clone resembles the *lqfR*^{P} homozygous eye phenotype.

A wild-type (Oregon R) adult eye (A) and a *lqfR*^{P} whole eye clone (B) are compared. The *lqfR*^{P} whole eye clones show rough eyes with a frequent anterior defect similar to the *lqfR*^{P} homozygous eye phenotype.
The genotype of the fly in (B) is:
ey-gal4 UAS-flp/+;FRT82B lqfR^{P}*/FRT82B GMR-hid, cl.*
These images were generated by Yoni Bibliowicz.

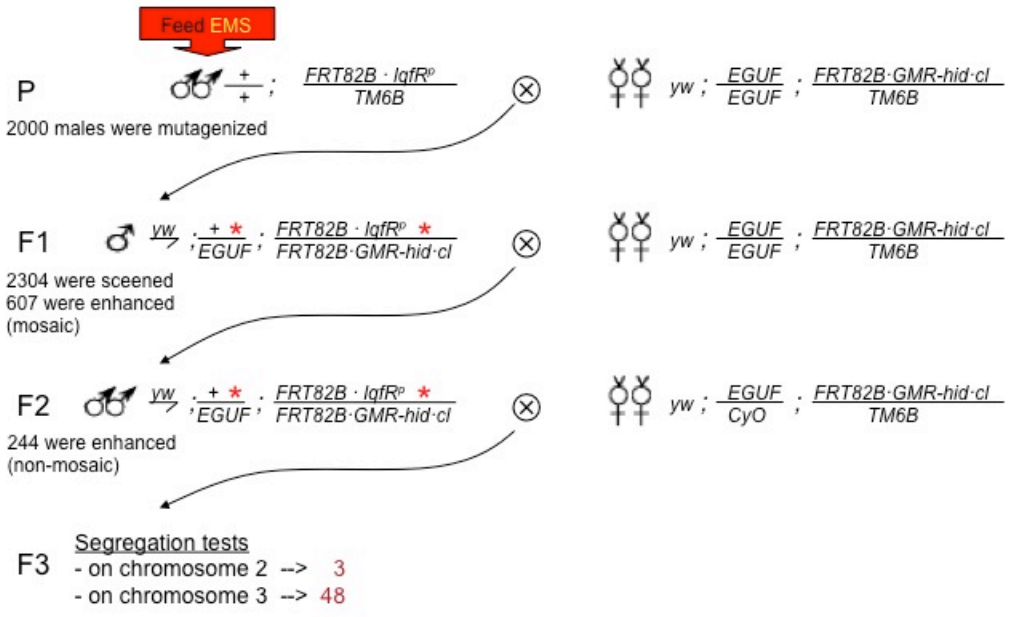

Figure 3-3. Cross scheme for the pilot screen.

A simplified cross scheme for the pilot screen was shown. 2000 males were mutagenized, 2304 F1 were screened, and 607 with enhanced mosaic eyes were identified. From a backcross, 244 with non-mosaic enhanced eyes were isolated. Segregation tests were followed. 3 enhancers from chromosome 2, 48 enhancers from chromosome 3 were isolated.
Abbreviations: *EGUF=eyeless-Gal4 UAS-flp*; *=possible mutations; *cl= l(3)CL-R1*.

Name	#Normal	#Rough	#Kidney	#Small	Total
Control 1	0	5	1	0	6
Control 2	2	5	0	0	7
356	0	4	9	10	23
358	2	7	7	1	17
359	0	5	2	1	8
3513	0	2	1	0	3
3514	0	9	8	5	22
3515	0	4	5	1	10
3518	0	2	12	5	19
362	1	10	3	1	16
368	0	1	2	1	4
3610	0	9	5	1	15
372	0	1	2	0	3
37102	0	3	4	3	10
37104	2	2	3	3	10
37105	0	3	3	2	8
37106	0	10	2	1	13
37107	0	0	1	3	4
387	0	12	4	3	19
388	2	2	0	6	10
389	0	0	0	1	1
3813	0	1	1	6	8
386	3	0	1	4	8
3223	0	6	0	8	14
3234	0	0	4	22	26

Table 3-2. Validation of dominant enhancers from the pilot screen.

Results from the validation test were shown. Among the progeny of the cross '*lqfR*^{P}*/TM6B* X *enhancer lqfR*^{P}*/TM6B*' incubated at 23°C, the number of non-*TM6B* progeny were recorded in each category for severity (Normal < Rough < Kidney < Small). The results from two control crosses with males and females of '*lqfR*^{P}*/lqfR*^{P}' were also shown.

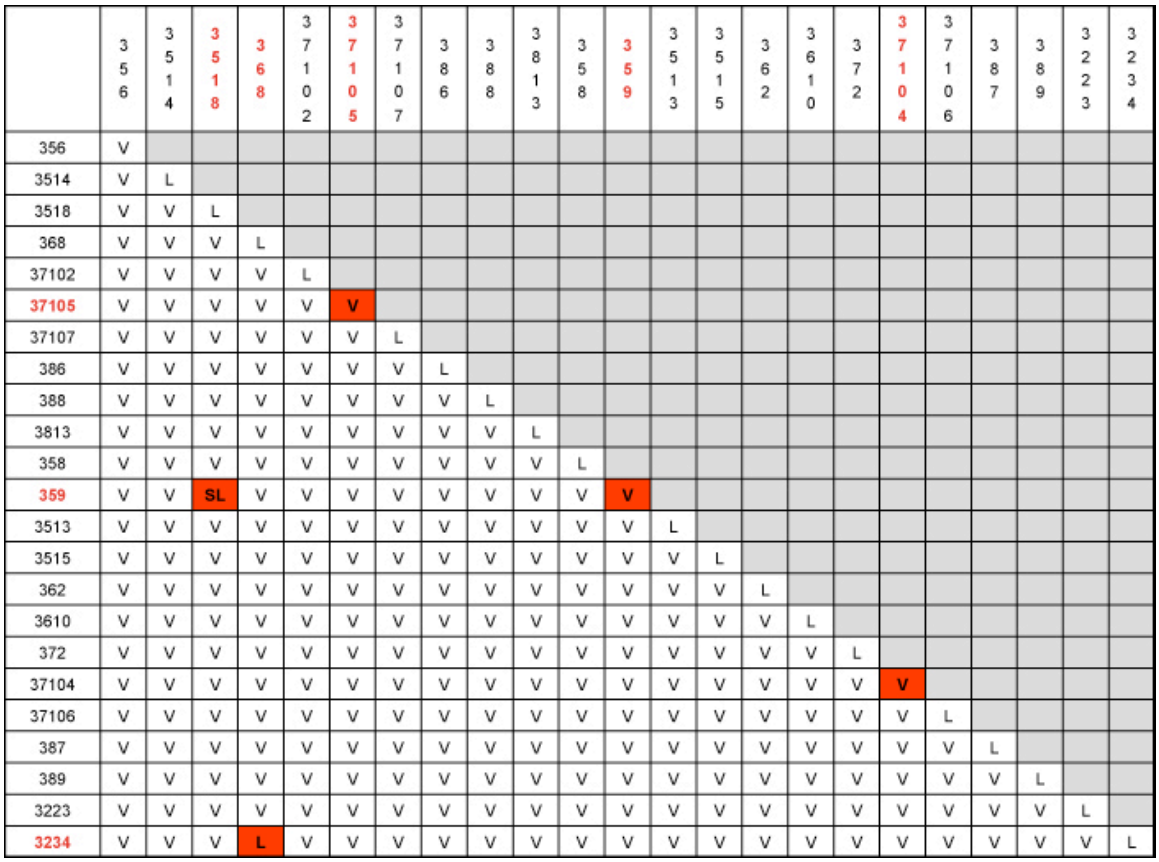

	356	3514	3518	368	37102	37105	37107	386	388	3813	358	359	3513	3515	362	3610	372	37104	37106	387	389	3223	3234
356	V																						
3514	V	L																					
3518	V	V	L																				
368	V	V	V	L																			
37102	V	V	V	V	L																		
37105	V	V	V	V	V	V																	
37107	V	V	V	V	V	V	L																
386	V	V	V	V	V	V	V	L															
388	V	V	V	V	V	V	V	V	L														
3813	V	V	V	V	V	V	V	V	V	L													
358	V	V	V	V	V	V	V	V	V	V	L												
359	V	V	SL	V	V	V	V	V	V	V	V	V											
3513	V	V	V	V	V	V	V	V	V	V	V	V	L										
3515	V	V	V	V	V	V	V	V	V	V	V	V	V	L									
362	V	V	V	V	V	V	V	V	V	V	V	V	V	V	L								
3610	V	V	V	V	V	V	V	V	V	V	V	V	V	V	V	L							
372	V	V	V	V	V	V	V	V	V	V	V	V	V	V	V	V	L						
37104	V	V	V	V	V	V	V	V	V	V	V	V	V	V	V	V	V	V					
37106	V	V	V	V	V	V	V	V	V	V	V	V	V	V	V	V	V	V	L				
387	V	V	V	V	V	V	V	V	V	V	V	V	V	V	V	V	V	V	V	L			
389	V	V	V	V	V	V	V	V	V	V	V	V	V	V	V	V	V	V	V	V	L		
3223	V	V	V	V	V	V	V	V	V	V	V	V	V	V	V	V	V	V	V	V	V	L	
3234	V	V	V	L	V	V	V	V	V	V	V	V	V	V	V	V	V	V	V	V	V	V	L

Figure 3-4. The complementation matrix of enhancers on chromosome 3 from the pilot screen.

23 third chromosome enhancers from the pilot screen were tested for complementation. 2 complementation groups with 2 members were found (359/3518 and 368/3234). 359/3518 was semi-lethal (SL). 368/3234 was lethal (L). 359 had homozygous phenotype. 2 other enhancers with morphological phenotype were also found (37104 and 37105). V=viable; L=lethal; SL=semi-lethal.

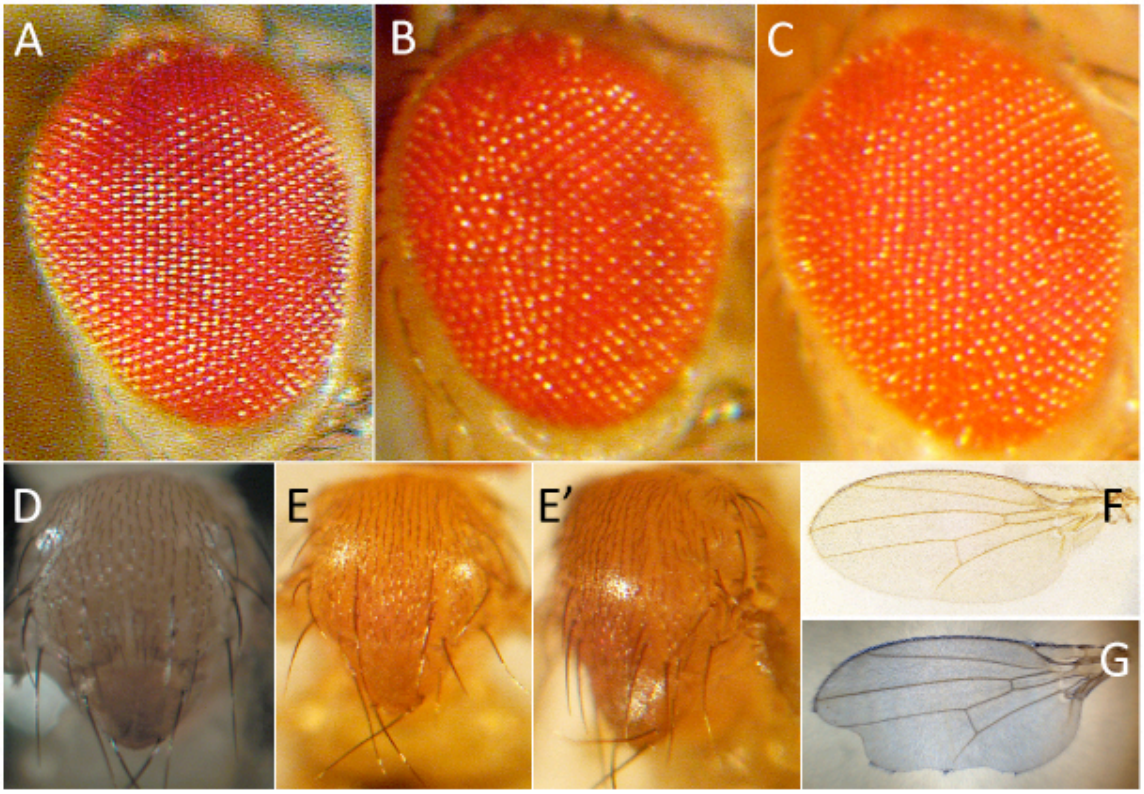

Figure 3-5. Phenotypes of homozygous viable enhancers from the pilot screen.

Images of adult morphological phenotypes of dominant enhancers as well as wild-type controls were shown. (A) is an eye of Oregon R as a control for (B) and (C). Rough eye phenotypes of 37104 (B) and 359 (C) homozygotes. Note the regular array of facets in (A) and irregularly ordered facets in (B) and (C). (D) is a wild-type (w^{1118}) notum to compare with that of 37105 homozygotes (E, E'). The number of macrochaete in (E, E') was increased. (F) is a wild-type (w^{1118}) wing to compare with a notched wing of a 37104 homozygote (G). These phenotypes were consistent.

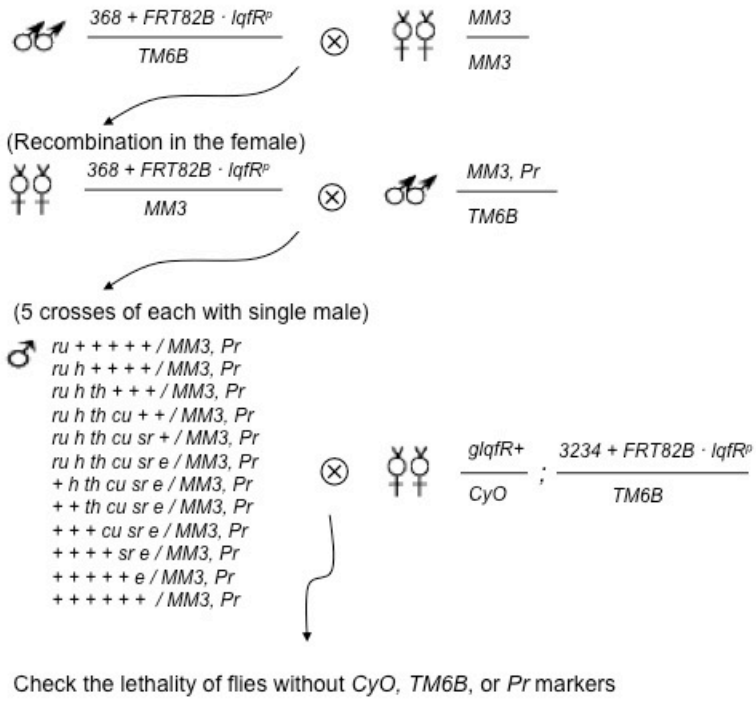

Figure 3-6. An example of the cross scheme for meiotic mapping.

The cross scheme for the meiotic mapping of the complementation group with 368 and 3234 was shown as an example. Virgin female progeny without *TM6B* were collected from the Parental cross. *Pr (Prickly)* is a homozygous lethal dominant marker. The complementation group with 359 and 3518 was mapped in the same way, where 3518 was recombined with MM3 and 359 was crossed with the recombinants in the next generation. For homozygous viable enhancers with phenotype, 37104 and 37105, they were recombined with MM3 and the same chromosomes were crossed again in the next generation. 5 single male progeny with appropriate phenotypes from the F1 cross were each crossed and the rough location of the gene with lethality or phenotype was identified in the next generation.
Abbreviations: MM3 = multiply marked chromosome 3; *glqfR+ = lqfR* genomic fragment; *ru = roughoid; h = hairy; th = thread; cu = curled; sr = stripe; e = ebony: Pr = Prickly*.

Recombinants (MM3 + 368)	Recombinants / 3234	
	Lethal (# lines with few sick escapers)	Viable
ru +++++	5 (1)	0
ru h ++++	5 (5)	0
ru h th +++	5 (2)	0
ru h th cu ++	5	0
ru h th cu sr +	4	0
ru h th cu sr e	0	5
+ h th cu sr e	0	5
++ th cu sr e	0	5
+++ cu sr e	0	5
++++ sr e	0	5
+++++ e	0	5
++++++	4 (1)	1

Table 3-3. Meiotic mapping for the complementation group with 368 and 3234.

Results of the meiotic mapping for the complementation group with 368 and 3234. The cross scheme was as shown in Fig. 3-6. Genotypes in each cell in the first row indicate males with either parental or single recombinant chromosomes from females of '*368/MM3*' (see Fig. 3-6). For example, '*ru* + + + + +' means the male progeny with a recombinant chromosome 3 recombined in between *ru* and *h* markers. The piece of chromosome from the recombination point to the left is from *MM3,* and the piece of chromosome from the recombination point to the right (denoted as +) is from *368*. The second and third column show the results from the cross between the males shown in the first column and females of '*glqfR*$^{+}$*/CyO ; 3234/TM6B*' (Fig. 3-6). For each genotype, 4~5 single males (with the recombined chromosome 3) were crossed. The phenotype in this complementation group is lethality. When I found a few small and sick escapers, I recorded it as lethal and put the number of such cases in the parenthesis. This result indicates that the mutated gene is telomeric from *e*.

Recombinants (MM3 + 3518)	Recombinants / 359	
	Lethal or with phenotype	Viable and no phenotype
ru +++++	5	0
ru h ++++	5	0
ru h th +++	5	0
ru h th cu ++	3	0
ru h th cu sr +	0	2
ru h th cu sr e	0	5
+ h th cu sr e	0	5
++ th cu sr e	0	5
+++ cu sr e	0	4
++++ sr e	1	4
+++++ e	4	0
++++++	5	0

Table 3-4. Meiotic mapping of the complementation group with 3518 and 359.

Results of the meiotic mapping for the complementation group with 3518 and 359. The cross scheme was as shown in Fig. 3-6. Genotypes in each cell in the first row indicate males with either parental or single recombinant chromosomes from females of '*3518/MM3*' (see Fig. 3-6). For example, '*ru* + + + + +' means the male progeny with a recombinant chromosome 3 recombined in between *ru* and *h* markers. The piece of chromosome from the recombination point to the left is from *MM3*, and the piece of chromosome from the recombination point to the right (denoted as +) is from *3518*. The second and third column show the results from the cross between the males shown in the first column and females of '*glqfR*$^{+}$*/CyO ; 359/TM6B*' (Fig. 3-6). For each genotype, 2~5 single males (with the recombined chromosome 3) were crossed. The phenotype of this complementation group is semi-lethality with the rough eye phenotype in the escapers. This result indicates that the mutated gene exists between *cu* and *sr*.

Recombinants (MM3 + 37104)	Recombinants / 37104	
	With phenotype	Without phenotype
ru +++++	5	0
ru h ++++	5	0
ru h th +++	3	2
ru h th cu ++	0	5
ru h th cu sr +	0	5
ru h th cu sr e	0	5
+ h th cu sr e	0	5
++ th cu sr e	0	5
+++ cu sr e	0	5
++++ sr e	5	0
+++++ e	5	0
++++++	5	0

Table 3-5. Meiotic mapping of 37104.

Results of the meiotic mapping for 37104. The cross scheme was as shown in Fig. 3-6. Genotypes in each cell in the first row indicate males with either parental or single recombinant chromosomes from females of '*37104*/*MM3*' (see Fig. 3-6). For example, '*ru* + + + + +' means the male progeny with a recombinant chromosome 3 recombined in between *ru* and *h* markers. The piece of chromosome from the recombination point to the left is from *MM3*, and the piece of chromosome from the recombination point to the right (denoted as +) is from *37104*. The second and third column show the results from the cross between the males shown in the first column and females of '*glqfR*$^{+}$/*CyO* ; *37104*/*TM6B*' (Fig. 3-6). For each genotype, 5 single males (with the recombined chromosome 3) were crossed. The homozygous phenotype of 37104 is rough eyes and notched wings. This result indicates that the mutated gene exists between *th* and *cu*.

Recombinants (MM3 + 37105)	Recombinants / 37105	
	With phenotype	Without phenotype
ru +++++	5	0
ru h ++++	5	0
ru h th +++	3	2
ru h th cu ++	0	5
ru h th cu sr +	0	5
ru h th cu sr e	0	5
+ h th cu sr e	0	5
++ th cu sr e	0	5
+++ cu sr e	2	3
++++ sr e	5	0
+++++ e	5	0
++++++	5	0

Table 3-6. Meiotic mapping of 37105.

Results of the meiotic mapping for 37105. The cross scheme was as shown in Fig. 3-6. Genotypes in each cell in the first row indicate males with either parental or single recombinant chromosomes from females of '*37105/MM3*' (see Fig. 3-6). For example, '*ru* + + + + +' means the male progeny with a recombinant chromosome 3 recombined in between *ru* and *h* markers. The piece of chromosome from the recombination point to the left is from *MM3*, and the piece of chromosome from the recombination point to the right (denoted as +) is from *37105*. The second and third column show the results from the cross between the males shown in the first column and females of '*glqfR*$^{+}$*/CyO ; 37105/TM6B*' (Fig. 3-6). For each genotype, 5 single males (with the recombined chromosome 3) were crossed. The homozygous phenotype of 37105 is increased notum bristles and slightly rough eyes. This result indicates that the mutated gene exists between *th* and *cu*.

A Large-scale screen

The pilot screen identified 4 complementation groups of dominant enhancers. To scale it up, Stephen Fleenor and I performed a large-scale screen with a similar cross scheme (Fig. 3-7). The difference between the pilot screen and this one is that we used *ey-flp* on the X chromosome instead *EGUF* on chromsosome 2 to avoid possible false positive from *gal4* expression. We screened 7423 more F1. Overall 9727 F1 were screened including the pilot screen. At the end of the crosses shown in Fig. 3-7, 5 enhancers on chromosome 2 and 213 enhancer candidates on chromosome 3 were identified. The enhancer candidates on chromosome 3 were identified based on their ability to enhance the $lqfR^{P}$ phenotype with their chromosome 3R homozygosed, so they should be further validated.

For the validation for enhancer candidates on chromosome 3, I used two criteria. The first criterion was, as explained previously, the ability to dominantly enhance the eye $lqfR^{P}$ phenotype with 4 categories of expressivity. The second new criterion was the ability to dominantly enhance the semi-lethality of $lqfR^{P}$. I included this criterion because while I was performing validation of 213 enhancers, I noticed that strong dominant enhancers of the eye phenotype frequently enhance lethality as well (for example, A56 in Table 3-7), although some enhancer candidates dominantly enhanced only lethality but not the eye phenotype (for example, C13 in Table 3-7). However, the lethality of $lqfR^{P}$ might be due to other junk mutations in the background. Previously Yoni confirmed that the eye phenotype was completely rescued by overexpressing *UAS-lqfRa-gfp* but he did not determine if the semi-lethality was also rescued. To test if the semi-lethality of $lqfR^{P}$ was due to the mutation in *lqfR*, Stephen made cross with males and females of '$glqfR^{+}$;

FRT82 lqfR^P/TM6B' and observed the ratio of non-*TM6B* progeny and *TM6B* progeny. As *TM6B* is homozygous lethal, if semi-lethality was completely rescued by *glqfR*+, the expected ratio of '*lqfR^P* homozygotes/total' should be about 1/3. Indeed, he found 16 (*lqfR^P* homozygotes) / 47 (total), which is ~34%. However, when I made 8 control crosses with males and females of '*FRT82 lqfR^P/TM6B*' in the same condition while I was validating the chromosome 3 enhancers, the overall ratio was 307/1811, which is ~17% (Table 3-7). These results support that using both criteria is reasonable.

One technical problem of the validation method was that the *lqfR^P* homozygotes were very sick and died in the liquefied food in the vial right after eclosion. The food liquefies due to the larvae. So, I modified the validation methodology to overcome this problem. After I made a cross, I kept the parents for one day in a vial to lay eggs. After 24 hours, the parents were removed to a fresh vial and let them lay eggs for one day. I kept doing it until I make 5 vials from the same parents. In this way, I could keep the number of progeny in each vial low and the food dry. As shown in Table 3-7, the overall number of progeny was significantly increased.

I set up the cut-off value for % '*enhancer lqfR^P/lqfR^P*' progeny as 10% or below. With this method, 213 enhancer candidates on chromosome 3 were validated, with a total of 33 dominant enhancers isolated (Table 3-7). Candidates that dominantly enhanced the *lqfR^P* semi-lethality much lower than 10% but did not enhance the eye phenotype were also included in 33. Candidates that did not enhance the lethality but significantly enhanced the eye phenotype were not found. I also retested 8 enhancers found from the pilot screen with the new validation method. Although the eye phenotype was dominantly enhanced in most of them, none of them enhanced the lethality (Table 3-7). As they were

screened for the enhancement of the eye phenotype but not lethality, the results are not unreasonable.

Before the enhancers were tested for complementation, the homozygous lethality was tested first. For the chromosome 2 enhancers, chromosome 2 was balanced with *CyO* and chromosome 3 with $lqfR^{P}$ was replaced with the wild-type chromosome 3. I found that all 5 enhancers were homozygous lethal. For the chromosome 3 enhancers, chromosome 2 with *glqfR+* was added to rescue the $lqfR^{P}$ phenotype. All 33 of chromosome 3 enhancers were homozygous lethal.

I performed complementation tests for dominant enhancers on chromosome 2. Three complementation groups were identified: one with 3 members, E11, I44, and D131, and two groups each with one member, D200 and G150 (Fig. 3-8). Both D200 and G150 were lost after several generations because females of them balanced with *CyO* were almost infertile. All of the 5 enhancers on the second chromosome had slight dominant rough eye phenotype (data not shown).

Stephen performed complementation tests for dominant enhancers on chromosome 3. Seven lethal complementation groups with multiple members were found (Fig. 3-9). Group 1 has three members, G160, G161, and G146. G146 and G160 were semi-lethal *in trans* to each other, but all other combinations were lethal. A56, G215, and H49 are members in group 2. They were all lethal *in trans* each other. Group 3 had 4 members, G47, H19, D110 and 37105. 37105 was isolated from the pilot screen. 37105 was homozygous viable with a morphological mutant phenotype, which is increased bristles on the notum (Fig. 3-5E, E'). G47/D110 and G47/H19 were lethal, G47/37105 and D110/37105 were semi-lethal, and H19/G47 and H19/37105 were viable. Escapers frequently had the notum bristle phenotype. They frequently had slightly rough eyes as

well. Lethal complementation group 4 had 2 members, K31 from the large-scale screen and 3513 from the pilot screen. In group 5, one of the member C13 was lethal or semi-lethal with many enhancers, but these enhancers lethal or semi-lethal *in trans* to C13 were not lethal with each others except with C13. This suggests that the lethality with C13 might be due to a dominant effect of C13 rather than they are all allelic. Therefore, group 5 was not pursued for mapping for the time being. Group 6 and 7 were two complementation groups originally from the pilot screen. They were retested this time. Group 6 was with 3518 and 359, and group 7 was with 3234 and 368. In group 7, the lethality *in trans* to each other was temperature sensitive. 3234/368 was strictly lethal at 25°C but completely viable at 23°C. A homozygous viable enhancer with a morphological mutant phenotype 37104 from the pilot screen comprised group 8.

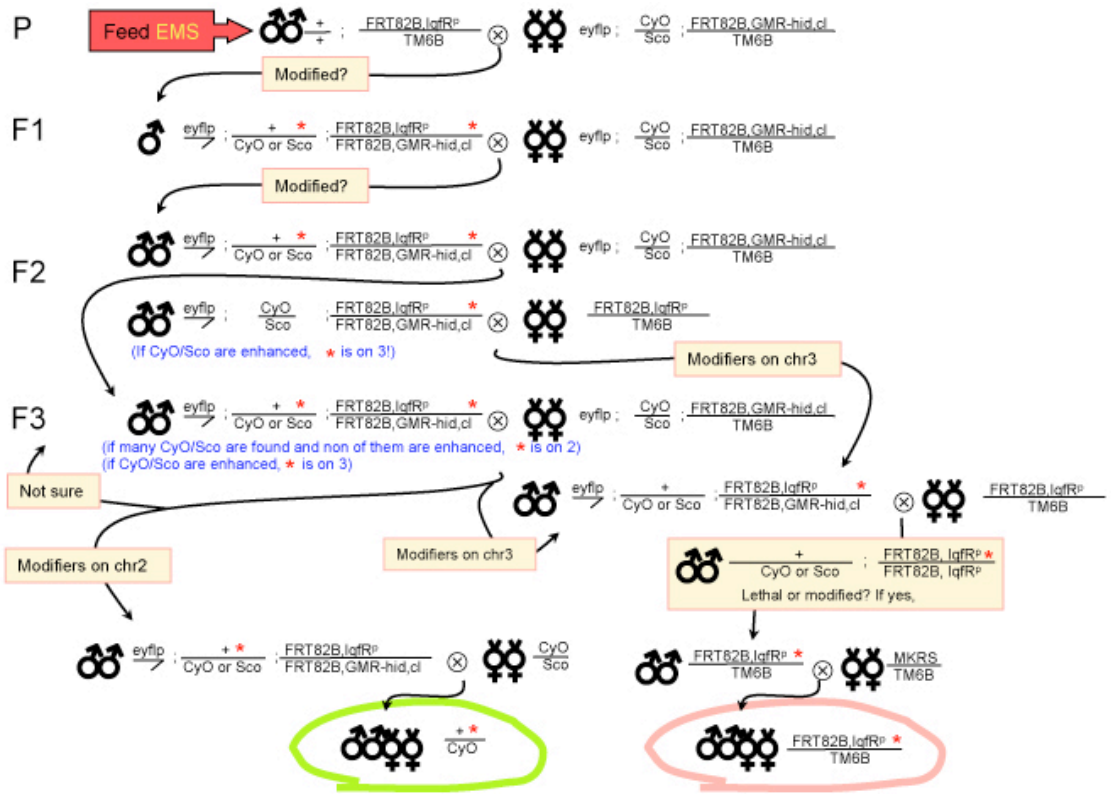

Figure 3-7. Cross scheme for the large-scale screen.

Shown is the cross scheme used for the large-scale screen modified from the pilot screen. Here *ey-flp* was used to induce eye specific recombination instead of *EGUF*. F1 males are mosaic because EMS hit just one strand of the DNA. F2 males are non-mosaic.
* = a marker for the mutagenized enhancer in the chromosome.
I collaborated with Stephen Fleenor for this screen.

Name	non-*TM6B*/total (%)	#Normal	#Rough	#Kidney	#Small
Control 1	60/396 (15.2%)	33	19	5	3
Control 2	65/380 (17.1%)	51	13	1	0
Control 3	33/210 (15.7%)	9	13	10	1
Control 4	52/238 (23.5%)	11	18	17	6
Control 5	47/263 (18.6%)	15	16	14	2
Control 6	6/56 (10.7%)	1	2	2	1
Control 7	24/153 (13.7%)	3	10	11	0
Control 8	20/115 (17.4%)	4	7	7	2
D 29	7/361 (1.9%)	5	1	0	1
A 56	24/327 (7.3%)	0	1	9	14
C 13	2/243 (0.8%)	2	0	0	0
D 110	4/233 (1.7%)	1	2	1	0
D 191	3/236 (1.3%)	0	2	1	0
E 85	14/158 (8.9%)	1	5	7	1
E 92	5/247 (2.0%)	0	1	3	1
E 119	23/237 (9.7%)	15	5	3	0
F 2	15/264 (5.6%)	10	2	3	0
F 91	9/148 (6.1%)	2	5	1	1

Table 3-7. Validation of dominant enhancers from the large-scale screen.

Results from the validation test were shown. Only 33 dominant enhancers chosen from 213 candidates based on their ability to dominantly enhance the eye and lethality phenotype of *lqfR*^{P} were shown here. Among the progeny of the cross '*lqfR*^{P}/*TM6B* X *enhancer lqfR*^{P}/*TM6B*' incubated at 23°C, the number of non-*TM6B* progeny were recorded in each category for severity (Normal < Rough < Kidney < Small). The ratio of '(non-TM6B)/(TM6B + non-TM6B)' was also recorded for each cross to show enhancement of the lethality. The results from eight control crosses with males and females of '*lqfR*^{P}/*lqfR*^{P}' were also shown. 8 enhancers identified from the pilot screen were also validated again here. Note that the proportions of viable non-TM6B progeny in each pilot screen enhancers are pretty higher compared to the enhancers from large-scale screen. (The previous validation for enhancer candidates from the pilot screen was based on the ability to enhance the eye phenotype, but not the lethality.) Enhancers from the pilot screen were named only with numbers (ex. 3513) and those from large-scale screen were named with a capital letter and number (ex. D29).

Name	non-*TM6B*/total (%)	#Normal	#Rough	#Kidney	#Small
G 2	2/218 (0.9%)	0	0	2	0
G 47	1/197 (0.5%)	0	0	1	0
G 54	13/257 (5.1%)	3	5	2	3
G 61	11/163 (6.7%)	4	4	2	1
G 115	1/182 (0.5%)	0	0	1	0
G 127	9/105 (8.6%)	0	1	5	3
G 136	10/140 (7.1%)	0	2	5	3
G 146	11/225 (4.9%)	0	5	5	1
G 156	2/116 (1.7%)	0	0	2	0
G 160	19/193 (9.8%)	0	4	5	10
G 161	19/261 (7.3%)	0	4	5	10
G 207	10/157 (6.4%)	6	3	1	0
G 215	17/191 (8.9%)	10	3	5	0
H 49	13/183 (7.1%)	4	5	2	2
I 28	0/209 (0%)	0	0	0	0
I 36	11/238 (4.6%)	0	5	5	1
I 63	15/182 (8.2%)	2	8	2	3
I 75	22/263 (8.4%)	0	4	14	4
I 81	26/341 (7.6%)	6	3	9	4
J 5	12/151 (7.9%)	3	5	3	1
J 8	17/179 (9.5%)	0	3	9	5
J 33	0/248 (0%)	0	0	0	0
K 31	5/148 (3.4%)	0	0	3	2
3513	113/324 (34.9%)	10	34	65	4
372	51/245 (20.1%)	1	26	22	3
37107	44/238 (18.5%)	5	10	20	9
389	53/195 (27.2%)	1	9	38	5
3813	79/168 (47%)	37	15	20	5
386	101/281 (35.9%)	18	27	42	14
3232	51/187 (27.3%)	7	17	21	6
368	75/212 (35.4%)	20	30	22	2

Table 3-7. (Continued) Validation of dominant enhancers of *lqfR*^{P} phenotype.

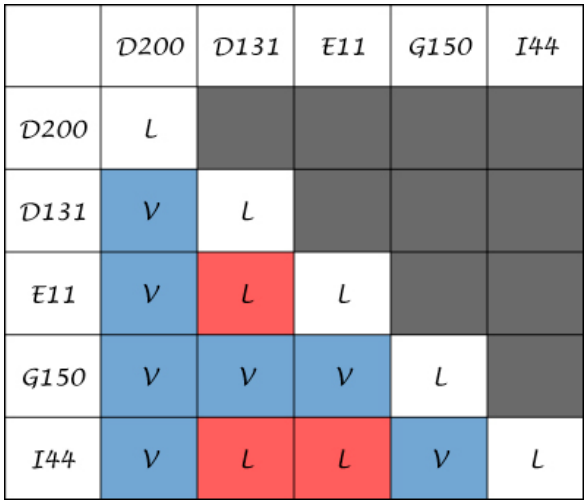

Figure 3-8. The complementation matrix of enhancers on chromosome 2 from the large-scale screen.

Five second chromosome enhancers from the screen were tested for complementation. One complementation group with 3 members was found (D131, E11, and I44). Two groups each with one member (D200 and G150) were also found. D200 and G150 were almost infertile and lost.
Abbreviations: V=viable; L=lethal.

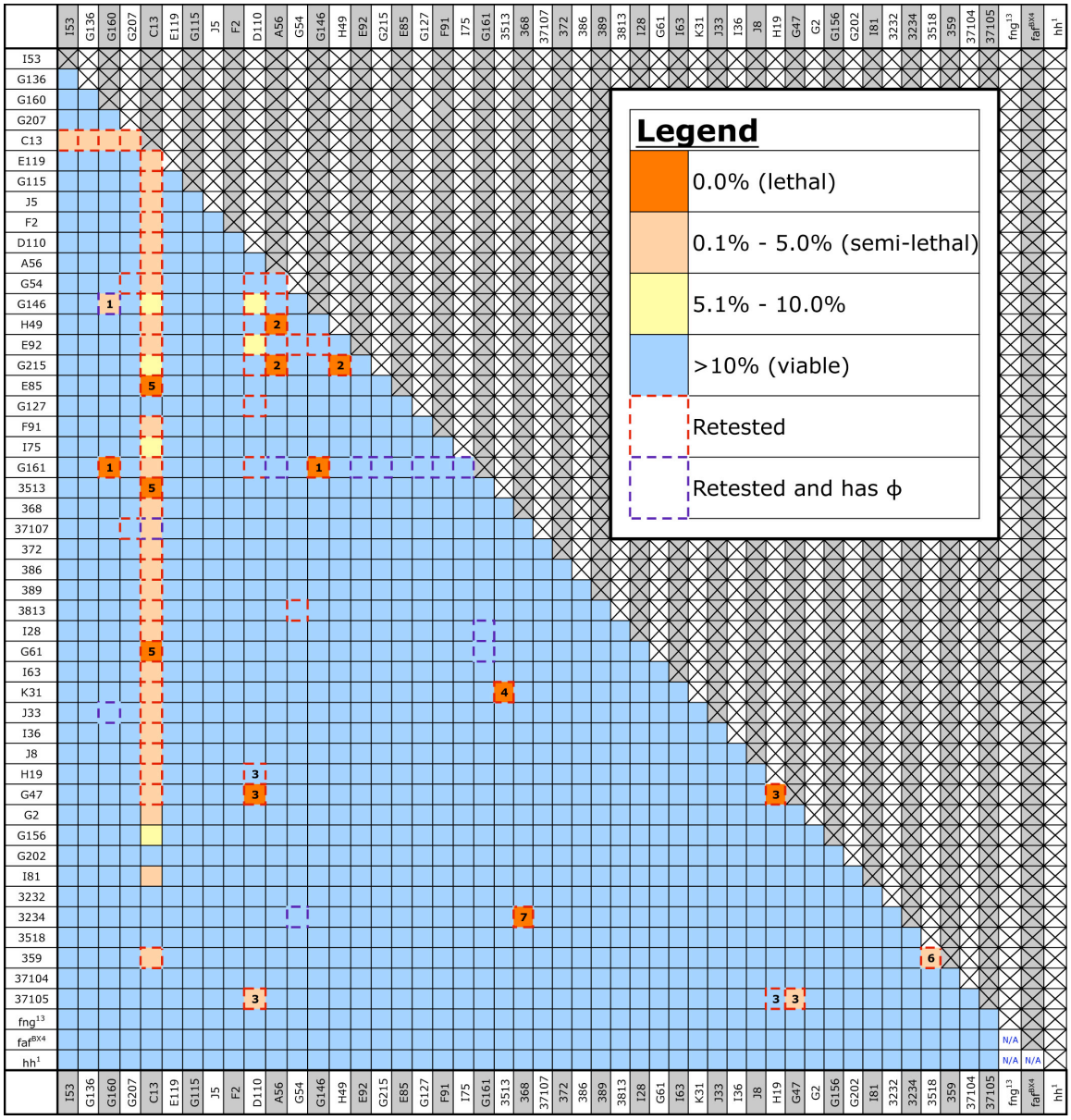

Figure 3-9. The complementation matrix for enhancers on chromosome 3.

47 third chromosome enhancers were tested for complementation. 33 were from the large-scale screen and 14 were from the pilot screen. 7 complementation groups with more than one member were found. Colors indicate levels of lethality as explained in the legend in the figure. Numbers in the cell indicate the number of complementation groups. Strong loss-of-function alleles of *fng*, *faf*, and *hh* were also tested for complementation. Stephen Fleenor performed this complementation tests and generated this image.

Identification of the complementation group on chromosome 2 as *Star*

Stephen and I performed meiotic mapping for the chromosome 2 complementation group with 3 members. Multiply marked chromosome 2 with recessive markers, *aristaless (al), dumpy (dp), black (b), curved (c),* and *plexus (px)*, was recombined with *D131*. The recombinant chromosomes were tested for their lethality over *I44*. As shown in Table 3-8, *'+ dp b c px'* recombinants over I44 were either lethal and viable. This indicates that the enhancer exists between *al* and *dp* (Table 3-8).

Stephen then performed deficiency mapping to further narrow down the location of the enhancer in this group. He obtained flies with molecularly known legions on the chromosome 2 between *al* and *dp* and crossed with D131. Among them, two deficiency lines were lethal over D131: *Df(2L)Exel6003* and *Df(2L)Exel6004*. *Df(2L)Exel6003* has deletion between 21E2 and 21E4, and *Df(2L)Exel6004* has deletion between 21E4 and 21F1. They do not overlap, but the 3'-end of *Df(2L)Exel6003* and the 5'-end of *Df(2L)Exel6004* are exactly the same. The only gene deleted by both of the deficiency lines was *Star*. With this information, I conclude that the gene mutated in this complementation group is *Star*.

Recombinants (MM2 + D131)	Recombinants / I 44	
	Lethal	Viable
al + + + +	0	8
al dp + + +	0	9
al dp b + +	0	2
al dp b c +	0	2
al dp b c px	0	5
+ *dp b c px*	4	2
+ + *b c px*	8	0
+ + + *c px*	7	0
+ + + + *px*	9	1*
+ + + + +	5	0

Table 3-8. Meiotic mapping for the complementation group on chromosome 2.

Shown is the result of the meiotic mapping for the complementation group on chromosome 2 with D131, I44, and E11. The cross scheme is essentially the same as in Fig. 3-6 except MM2, instead of MM3, was used here. Genotypes in each cell in the first row indicate males with either parental or single recombinant chromosomes from females of '*D131/MM2*'. For example, '*al* + + + +' means the male progeny with a recombinant chromosome 3 recombined in between *al* and *dp* markers. The piece of chromosome from the recombination point to the left is from *MM2,* and the piece of chromosome from the recombination point to the right (denoted as +) is from *D131*. The second and third columns show the results from the cross between the males shown in the first column and females of '*I44/CyO*'. For each genotype, 2~10 single males (with the recombined chromosome 2) were crossed. The phenotype in this complementation group is lethality. * is thought to be due to double cross over between *al* and *dp*.
Abbreviations: MM2=multiply marked chromosome 2; *al=aristaless; dp=dumpy; b=black; c=curved; px=plexus*.

Identification of Group 1 on chromosome 3 as *Delta*

I performed meiotic mapping for the complementation group 1 on chromosome 3 with G161, G160, and G146 as explained earlier (see also Fig. 3-6). The *G161* chromosome was recombined with the chromosome with *MM3*, and then the recombinant chromosomes were tested for the lethality over G160. As shown in Table 3-9, this meiotic mapping indicated that the gene mutated in this group is located between *sr* and *e*. Followed was a deficiency mapping. I obtained deficiency lines covering the region between *sr* and *e* and crossed with the three members in the group. As a result, I found that 3 deficiency lines, *Df(3R)Dl-KX23* (deletes from 91C7-D3 to 92A5-8), *Df(3R)Dl-BX12* (deletes from 91F1-2 to 92D3-6), and *Df(3R)Cha9* (deletes from 91C7 to 92A2), were lethal over all three members. This result narrows down the region from 91F1-2 to 92A2, which includes more than 30 genes mapped to the sequence including *Delta*. *Delta* was a good candidate for the mutated gene because G160 and G161 have dominant wing phenotype similar to that of *Delta*. *Delta (Dl)* amorphic alleles Dl^{9P} and Dl^{B2} were tested for complementation. All three members fail to complement with both null alleles of *Delta*. With this information, I concluded that the Group 1 on chromosome 3 was *Delta*.

Recombinants (MM3 + G161)	Recombinants / G160	
	Lethal	Viable
ru +++++	5	0
ru h ++++	5	0
ru h th +++	5	0
ru h th cu ++	5	0
ru h th cu sr +	3	2
ru h th cu sr e	0	5
+ h th cu sr e	0	7
++ th cu sr e	0	5
+++ cu sr e	0	7
++++ sr e	0	5
+++++ e	3	2
++++++	5	0

Table 3-9. Meiotic mapping for Group 1 with G161, G160 and G146.

Results of the meiotic mapping for the Group 1 with G161, G160, and G146. The cross scheme is essentially the same as Fig. 3-6. MM3 was recombined with G161. Genotypes in each cell in the first row indicate males with either parental or single recombinant chromosomes from females of '*G161/MM3*'. For example, '*ru* + + + + +' means the male progeny with a recombinant chromosome 3 recombined in between *ru* and *h* markers. The piece of chromosome from the recombination point to the left is from *MM3*, and the piece of chromosome from the recombination point to the right (denoted as +) is from *G161*. The second and third column show the results from the cross between the males shown in the first column and females of '*glqfR*$^{+}$*/CyO ; G160/TM6B*'. For each genotype, 5~7 single males (with the recombined chromosome 3) were crossed. This result indicates that the mutated gene exists between *sr* and *e*.

Identification of Group 2 on chromosome 3 as *neuralized*

The strongest enhancer in Group 2 is A56 (Table 3-7). *A56* was chosen for recombination with *MM3*. The recombinant chromosomes were tested for lethality over *H49*. The result from these crosses indicated that the gene affected in this group is in between *th* and *cu*, but closer to *cu* (Table 3-10). I performed deficiency mapping with deficiency lines covering from the centromere to *cu*, and found that all three members were lethal over *Df(3R)BSC24,* which has deletion region between 85B7 and 85D15. This region includes many genes including *neuralized (neur)*, which is a good candidate because *neur* encodes an E3 ligase required for Notch signaling and I already found other Notch signal components *fringe* and *Delta* as dominant enhancers. I crossed all three Group 2 members with two loss-of-function alleles $neur^{1}$ and $neur^{11}$. I found that they did not complement in all combinations. I concluded that members in Group 2 had mutations in *neur*.

Recombinants (MM3 + A56)	Recombinants / H49	
	Lethal	Viable
ru +++++	5	0
ru h ++++	7	0
ru h th +++	5	0
ru h th cu ++	0	6
ru h th cu sr +	0	5
ru h th cu sr e	0	5
+ *h th cu sr e*	0	6
++ *th cu sr e*	0	8
+++ *cu sr e*	3	2
++++ *sr e*	5	0
+++++ *e*	5	0
++++++	5	0

Table 3-10. Meiotic mapping for Group 2 with A56, H49 and G215.

Results of the meiotic mapping for the Group 2 with A56, H49, and G215. The cross scheme is essentially the same as Fig. 3-6. MM3 was recombined with A56. Genotypes in each cell in the first row indicate males with either parental or single recombinant chromosomes from females of '*A56/MM3*'. For example, '*ru* + + + + +' means the male progeny with a recombinant chromosome 3 recombined in between *ru* and *h* markers. The piece of chromosome from the recombination point to the left is from *MM3*, and the piece of chromosome from the recombination point to the right (denoted as +) is from *A56*. The second and third column show the results from the cross between the males shown in the first column and females of '*glqfR*$^{+}$*/CyO ; H49/TM6B*'. For each genotype, 5~8 single males (with the recombined chromosome 3) were crossed. This result indicates that the mutated gene exists between *th* and *cu*.

Identification of Group 3 on chromosome 3 as *polychaetoid*

Group 3 has 4 members, G47, H19, D110 and 37105. Among them, 37105 was identified from the pilot screen. 37105 was homozygous viable with the morphological mutant phenotype of increased notum bristles. I explained earlier the meiotic mapping of 37105 based on the phenotype (Table 3-6). Based on this result the gene with this phenotype exists in between *th* and *cu*. Because it was mapped to the same region as Group 2, the same Deficiency line set was used for Deficiency mapping. 37105 was semi-lethal over *Df(3R)p-XT103* and *Df(3R)BSC506*. All other members in the group showed either semi-lethality or the notal bristle phenotype. These results indicated that the mutation exists in between 85B1 to 85C2. This region included many small genes but the biggest one was *polychaetoid (pyd)*. Two available *pyd* alleles pyd^{1} and pyd^{14} were crossed with members of group 3 and identified as allelic based on the appearance of the notal bristle phenotype. I concluded that Group 3 members had mutations in *pyd*.

Identification of Group 4 on chromosome 3 as *string*

Group 4 members are K31 and 3513. I performed meiotic mapping for this group. The result is shown in Table 3-11. In the result, in all cases of parental and recombinant chromosomes, some were viable and some others were lethal. This happens when the mutation exists far away from *e* toward telomere because between *e* and telomere is a fairly large piece of genomic DNA. From a deficiency mapping using deficiency lines covering this area, Stephen found that Group 4 members are lethal *in trans* to *Df(3R)BSC501* (from 98F10 to 99B9), *Df(3R)Exel6212* (from 99A1 to 99A5), *Df(3R)ED6310* (from 98F12 to 99B2), *Df(3R)BSC486* (from 99A1 to 99B10), and

Df(3R)ED6316 (from 99A5 to 99C1). *Df(3R)Exel6212* and *Df(3R)ED6316* overlapped in very small region in 99A5 that deletes *string (stg)* in ~3/4 of the *5'UTR*. A *stg* amorphic allele, stg^4, was lethal *in trans* to each of group 4 members. I concluded that Group 4 members have mutations in *string*.

Recombinants (MM3 + K31)	Recombinants / 3513	
	Lethal	Viable
ru +++++	3	2
ru h ++++	4	3
ru h th +++	1	5
ru h th cu ++	6	2
ru h th cu sr +	5	1
ru h th cu sr e	3	4
+ *h th cu sr e*	2	3
++ *th cu sr e*	1	5
+++ *cu sr e*	0	6
++++ *sr e*	2	4
+++++ *e*	2	3
++++++	8	4

Table 3-11. Meiotic mapping for Group 4 with K31 and 3513.

Results of the meiotic mapping for the Group 4 with K31 and 3513. The cross scheme is essentially the same as Fig. 3-6. MM3 was recombined with K31. Genotypes in each cell in the first row indicate males with either parental or single recombinant chromosomes from females of '*K31*/*MM3*'. For example, '*ru* + + + + +' means the male progeny with a recombinant chromosome 3 recombined in between *ru* and *h* markers. The piece of chromosome from the recombination point to the left is from *MM3*, and the piece of chromosome from the recombination point to the right (denoted as +) is from *K31*. The second and third column show the results from the cross between the males shown in the first column and females of '*glqfR*$^{+}$/*CyO ; 3513*/*TM6B*'. For each genotype, 5~12 single males (with the recombined chromosome 3) were crossed. This result indicates that the mutated gene is telomeric from *e*.

Identification of Group 6 on chromosome 3 as *altered disjunction*

3518 and 359 are members of Group 6. They were identified from the pilot screen and I showed the meiotic mapping for this group earlier (Table 3-4). The result indicated that the mutation is between *cu* and *sr*. From the deficiency mapping with deficiency lines covering this region, Stephen found that *Df(3R)BSC790* and *Df(3R)ED5780* were lethal in trans to both group 6 members. This region includes two uncharacterized protein coding genes, three tRNA's and two other genes, *aluminum tubes* and *altered disjunction (ald)*. A loss-of-function allele of *ald*, $Mps1^{1}$, was lethal over the group 6 members. I concluded that Group 6 members are *ald* mutants.

Group 7 on chromosome 3 is mapped to 93F13-14

Group 7 members are 368 and 3234. The meiotic mapping has been shown in Table 3-4. The result indicated that the gene mutated in 368 and 3234 exist telomeric to *e*, but probably close to *e*. From deficiency mapping, Stephen identified *Df(3R)BSC677*, *Df(3R)ED6076*, and *Df(3R)BSC678* as lethal in trans to group 7 members. These data narrowed down the region to between 93F13 and 93F4. This region includes 15 genes: 4 gustatory receptor genes, 8 uncharacterized genes (*CG6569, CG31174, CG31431, CG31178, CG6656, CG34148, CG33092,* and *CG31465*), and 3 known genes (*glec*, *lsn*, and *Cby*). *lsn*, also known as *vps22,* encodes a component of ESCRT II, which regulates protein sorting at early endosomes (Herz et al, 2009). As Golgi Epsin has been shown to function in Golgi-endosome trafficking (Chidambaram et al, 2008; Copic et al, 2007), *lsn* seemed to be a good candidate for a dominant enhancer for the $lqfR^{P}$ phenotype. A strong loss-of-function, thought to be a null (Herz et al, 2009), allele of *lsn*, $lsn^{5F8\text{-}3}$, was tested

for lethality in trans to Group 7 members. $lsn^{5F8\text{-}3}$ complemented with both Group 7 members. Strong loss-of-function alleles of other genes in the region were not available.

Group 8 on chromosome 3 is within 77F1-2

37104 is a single member of Group 8. 37104 was isolated from the pilot screen. The meiotic mapping was done with its rough eye and notched wing phenotype (Table 3-5). The result indicated that the mutation is between *th* and *cu*. Stephen performed a deficiency mapping for this group and found that *Df(3L)BSC797* is lethal *in trans* to *37104*, but is viable with other overlapping deficiency lines *Df(3L)BSC452* and *Df(3L)BSC449*. These data narrowed down the region to 77F1-2, which includes 6 genes: *Pka-R1, CSN3, CG3288, CG13255, CG11456,* and *CG32432*. Further analysis is required to identify the affected gene in *37104*.

3.3 DISCUSSION AND FUTURE DIRECTION

Here I described screens for dominant modifiers of the *lqfR*^{P} phenotype. Erin Overstreet first recognized that the *lqfR*^{P} eye phenotype could be modified dominantly with a loss-of-function allele of *fringe*. Although the expressivity of the *lqfR*^{P} phenotype was variable, the phenotype tended to be shifted toward more severe defects when it was enhanced by heterozygous mutations in other genes. With this assay combined with *FLP/FRT GMR-hid* technique, I could collaborate with Yoni Bibliowicz and Stephen Fleenor to perform EMS mutagenesis screens for dominant modifiers of the *lqfR*^{P} phenotype. This screen identified complementation groups mapped to *Delta, neuralized, polychaetoid (ZO-1), string (cdc25),* and *altered disjunction (Mps1)*.

Originally I aimed to screen for both dominant enhancers and dominant suppressors. However, I ended up having only enhancers. This might be due to the mild eye phenotype of *lqfR*^{P}. When the candidates of modifiers were screened, real dominant suppressors might have been lost because they were indistinguishable from the background. However, it would also be formally possible that LqfR in the biological context somehow does not have as many negative regulators as positive ones.

Also, I originally aimed to screen all autosomes, but the screen turned out to be biased to chromosome 3 especially to 3R. From the large-scale screen, while 33 enhancers were identified from chromosome 3, only five were identified from chromosome 2. Among seven complementation groups on chromosome 3, six were mapped to 3R and only one was mapped to 3L. It seems very likely that this bias was originated by homozygosing chromosome 3R with *FLP/FRT GMR-hid* technique. When the chromosome 3R were homozygosed, genes on 3R mutated by EMS were also

homozygous. If such homozygous mutants affected eye development, the phenotype would turn out to be very enhanced in the F1 and F2. This enhancement is an additive effect and has nothing to do with the function of *lqfR*. However, when they were screened, flies with strongly enhanced eyes would be more easily recognized compared to slightly enhanced "real" dominant enhancers on chromosome 2 or chromosome 3L. As a result, this screen may have been a two-step screen: first step for genes on 3R with a recessive eye phenotype, and second step for genes, among what has already been screened, with the ability to modify the $lqfR^{P}$ phenotype dominantly with the validation method.

Among the dominant enhancers mapped to the gene were *polychaetoid (pyd)*. *pyd* is a *Drosophila* homolog of mammalian *ZO-1* (Seppa et al, 2008). *ZO-1* encodes a member of the MAGUK (membrane-associated guanylate kinase homologs) family that is characterized by multiple binding domains such as PDZ domains, SH3 domain, and guanylate kinase homologous domain (Funke et al, 2005). ZO-1 interacts with occludin and α-catenin, which are localized to tight junction and adherens junction, respectively, and connects them to actin-based cytoskeleton (Fanning et al, 1998; Itoh et al, 1997). *Drosophila* Pyd co-localizes with E-cadherin at the adherens junction (Seppa et al, 2008). Interestingly, when Pyd is depleted, E-cadherin levels at the plasma membrane increase in the developing eyes of pupa (Seppa et al, 2008). Although the mechanism is not clear, it seems that it is not due to defects in the endocytosis because no genetic interactions were identified between *pyd* and genes for endocytosis machineries (Seppa et al, 2008). As *pyd* is found as a dominant enhancer of *lqfR*, I thought it would be interesting if *lqfR* mutants have a similar E-cadherin localization defect. This idea and known Golgi Epsin

function from other species led me to hypothesize that LqfR may have a role in E-cadherin trafficking. In chapter 4, I show that E-cadherin level is indeed increased in *lqfR* null clones in eye discs, as well as other experimental results consistent with the hypothesis.

From this screen, core components of the Notch signaling pathway, *Delta* and *neuralized*, were identified as dominant enhancers of the $lqfR^{P}$ phenotype. In fact, this screen project could be initiated based on the data that yet another important regulator of the Notch signaling pathway, *fringe*, dominantly enhance the $lqfR^{P}$ eye phenotype. These results suggest an interesting possibility that *lqfR+* may play a role in the Notch signaling pathway. $lqfR^{P}$ homozygotes showed rough eye phenotype and images from their sectioned eyes showed patterning defects including irregular numbers of photoreceptors in each ommatidium. Although I admit that there must be many different ways to explain the phenotype, this phenotype was often found when Notch signal activity was not regulated properly (Eun et al, 2008; Eun et al, 2007). In chapter 4, I show some follow-up experiments to test the possibility that *lqfR* might have a role in the Notch signaling pathway. I found that, in the *lqfR* null clones in eye discs, the Notch receptor level was increased and the expression level of a Notch target *mβ-lacZ* was upregulated (see Chapter 4, Discussion). More experiments would be required to fully understand the relationship between the function of *lqfR* and the Notch signaling pathway and the mechanistic basis of the phenomena I discovered.

One of the most interesting finding from this screen might be the identification of cell cycle regulators, *string* and *altered disjunction*, as dominant enhancers of the $lqfR^{P}$ phenotype because the *lqfR* mutant phenotype strongly suggested that *lqfR* has a role in

cell proliferation (see Chapter 2). First of all, the whole eye clones composed of *lqfR* null cells were extremely reduced suggestive of its role in proliferation during the eye development (Fig. 2-4D). As the strength of a dominant enhancer increased, the $lqfR^{P}$ hypomorphic eyes became smaller, which suggests that the organ size and the *lqfR*+ activity have correlation (Fig. 3-1, Tables 3-1, 3-2, and 3-7). Furthermore, when *lqfR* null clones and their twin spots were compared, it became obvious that *lqfR*+ somehow plays a critical role in the proliferation of the developing *Drosophila* eye (Fig. 2-9). The "no disc" phenotype of $lqfR^{s117}$ larvae also strongly suggested that *lqfR*+ plays a role in cell proliferation (Gatti & Baker, 1989; Shearn et al, 1971) (see Chapter 2).

One way to explain the proliferation defect in *lqfR* mutants could be cell cycle delay. Consistent with this, this screen isolated *string (stg)* as dominant enhancers of the $lqfR^{P}$ phenotype, which suggests that the function of *lqfR*+ has to do with cell cycle regulation. Stg is a *Drosophila* homolog of Cdc25. Cdc25 functions as an M phase inducer by activating Cdc2, cyclin-dependent kinase (Cdk) 1, by dephosphorylating inhibitory phosphorylation on a Tyr residue by Wee1 and Mik1 (Millar et al, 1991; Russell & Nurse, 1986; Walworth, 2001). The expression of *stg* overcomes the inhibitory phosphorylation of Cdk1 in *Drosophila* as well (Edgar & O'Farrell, 1990). As *stg* genetically interacted with *lqfR*, it would be interesting to further analyze the role of *lqfR* in the context of cell cycle regulation (see below).

As cell cycle regulation is closely related to the DNA damage checkpoint pathway, Cdc25 also plays a role in cell cycle delay in the context of DNA damage response. DNA damage activates Chk1, and Chk1 phosphorylates Cdc25. This event causes Cdc25 to bind to 14-3-3 protein and, as a consequence, the nuclear entry of Cdc25

is blocked, which means no Cdc2 activation in the nucleus (Walworth, 2001). This is interesting to me because my structure/function analysis of *lqfR* indicates that *lqfR* functions as a *Drosophila tel2* homolog (see Chapter 4). *tel2* has been shown to be important in DNA damage response and genome stability (Ahmed et al, 2001; Anderson et al, 2008; Hurov et al, 2010). Gatti and Baker analyzed complementation groups identified from mutagenesis screens for mutant larvae with the "no disc" phenotype to know their roles in cell cycle regulation (Gatti & Baker, 1989). Interestingly, they showed that *l(3)XII-10*, which is an allele of *lqfR* (see Chapter 2), had mitotic defects. The mitotic defects included chromosome breakage, defects in chromosome condensation, and polyploidy (Gatti & Baker, 1989). This seems to have a connection with the known function of *tel2* in genome stability, and *stg* has been identified from my dominant modifier screen maybe in this context. Further analysis of the function of *lqfR* in DNA damage response and genome stability would be an interesting future direction of this project.

This screen also identified a genetic interaction between *lqfR* and *ald*. *ald* encodes a single *Drosophila* homolog of Mps1, which has been shown to be important in the mitotic spindle checkpoint (Hardwick et al, 1996). Mps1 is the most upstream among known regulators in spindle checkpoint cascade (Hardwick et al, 1996). Genetic studies using *Drosophila* showed that an *ald* loss-of-function mutant had a mitotic spindle checkpoint defect (Fischer et al, 2004). They also showed that Ald is responsible for a developmental cell cycle arrest (Fischer et al, 2004). It would be interesting if *lqfR* has a role in the context of *ald* function.

Are there other cell cycle regulators, which might provide clues to understand the function of *lqfR*? To address this question, I previously performed a set of

immunostaining experiments to find important cell cycle regulators whose expression level change in *lqfR* null clones in the eye discs. Among cell cycle regulators tested, the protein level of Cyclin E was most obviously reduced (Fig. 3-10). The expression level of an E2F activity reader, *PCNA-gfp*, was also decreased (Fig. 3-11). I think these results might be relevant to the genetic screen that identified *stg* as a dominant modifier of the $lqfR^{P}$ phenotype. Cyclin E is a key regulator of the cell cycle that shows genetic interaction with *stg* (Secombe et al, 1998). Both Cyclin E and Stg are expressed to accelerate cell cycle in the context of *Drosophila* wing development (Neufeld et al, 1998). E2F regulates expression of both Cyclin E and Stg in this context (Neufeld et al, 1998). It would be an intriguing question how this genetic program of cell cycle regulation is affected by the function of *lqfR*.

Genetic and phenotypic evidence so far strongly suggest that *lqfR* might play a role in cell cycle regulation. However, no direct evidence has been shown to prove that *lqfR*+ is required for cell cycle progression. To address this question, I performed experiments to test if *lqfR* null cells have defects in the progression of S phase of the cell cycle using clonal assay. When dissected eye discs with $lqfR^{\Delta 117}$ clones prepared with the procedure of incubating for 2 hours in the Schneider's media with BrdU, the proportion of $lqfR^{\Delta 117}$ cells with the incorporation of BrdU seemed to be decreased (data not shown). However, due to small sizes of the null clones and unequal cell cycle status among the cells in the tissue, it was difficult to measure the defect quantitatively. One possible way to avoid this problem would be to switch to use the whole larval brain instead of eye discs with mutant clones. Although $lqfR^{\Delta 117}$ larva does not produce noticeable imaginal discs, it still has relatively smaller brain. If dissected larval brains are given the

Schneider's media with BrdU in a time-course manner, the cell cycle defect of *lqfR*$^{\Delta 117}$ would be revealed.

Would the cell cycle defect be the cause of the *lqfR* phenotype, or a consequence of other defect(s)? This is a difficult question to answer. Based on the known function of *tel2* (see Chapters 1), which is homologous to *lqfR* (Chapter 4), *lqfR* might somehow be directly required for genome stability. If this is true, cell cycle defects in *lqfR* mutants could be a consequence of genome instability. Accumulation of genome instability in *lqfR*$^{\Delta 117}$ may have caused cell cycle delay, increased programmed cell death, and ultimately visualized as a proliferation defect. Consistently, I observed increased apoptosis in *lqfR*$^{\Delta 117}$ cells (Fig. 3-12). It would be intriguing to further develop this hypothesis.

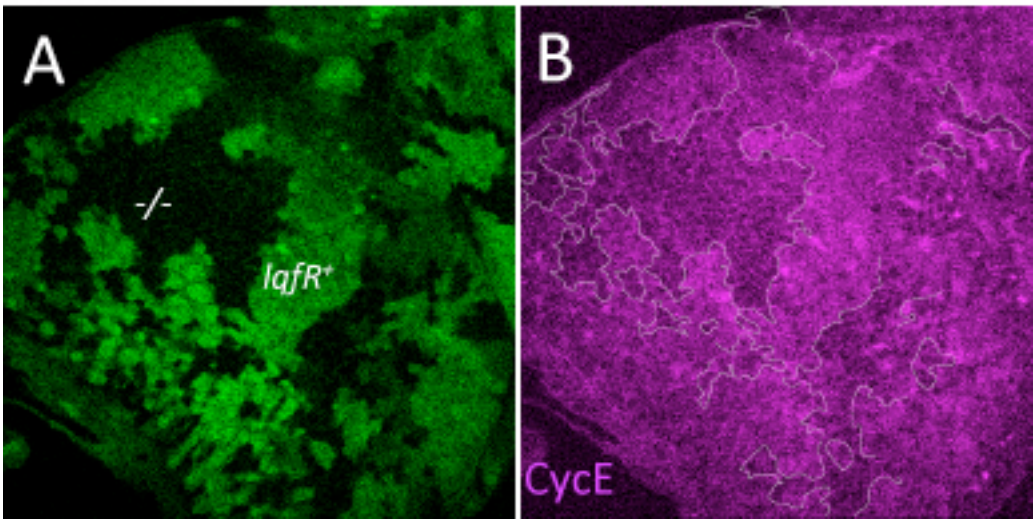

Figure 3-10. Decreased Cyclin E level in *lqfR* null clones.

Confocal images of an eye disc with $lqfR^{\Delta 117}$ clones immunostained with anti-Cyclin E (purple). $lqfR^{\Delta 117}$ clones are marked with the absence of GFP (green). White line in (B) denotes clone boundary. Genotype is: *ey-flp;;FRT82B* $lqfR^{\Delta 117}$*/FRT82B ubi-gfp*.

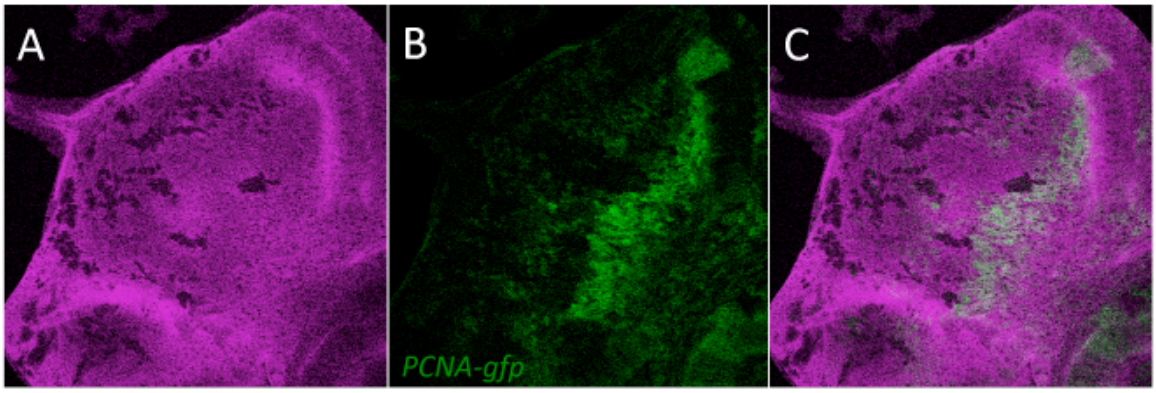

Figure 3-11. Decreased *PCNA-gfp* expression level in *lqfR* null clones.

Confocal images of an eye disc with $lqfR^{\Delta 117}$ clones with the expression of PCNA-gfp (green) (B). $lqfR^{\Delta 117}$ clones are marked with the absence of β-galactosidase (purple) (A). (C) is the merged image of (A) and (B). Genotype is: *ey-flp/PCNA-gfp;;FRT82B* $lqfR^{\Delta 117}$*/FRT82B armadillo-lacZ*.

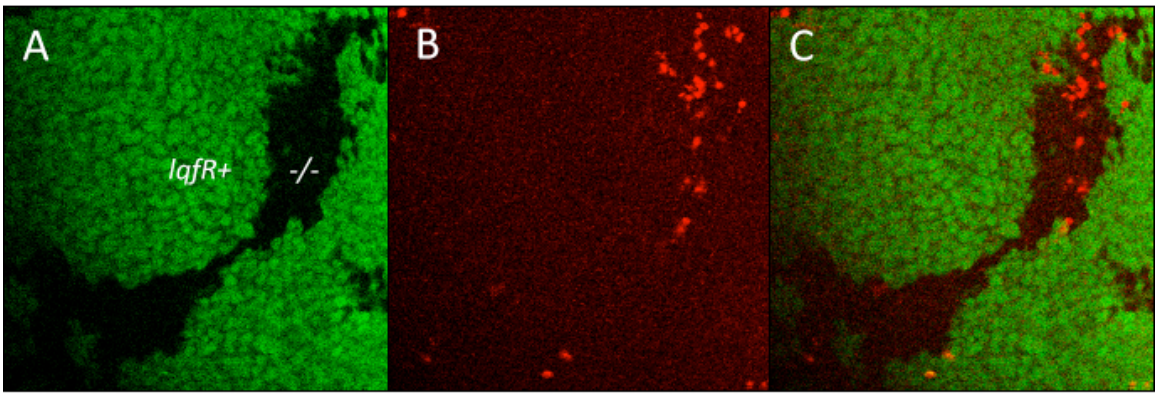

Figure 3-12. Increased apoptosis in *lqfR* null clones.

Confocal images of an eye disc with $lqfR^{\Delta 117}$ clones immunostained with anti-activated caspase 3 antibody (red) (B). $lqfR^{\Delta 117}$ clones are marked with the absence of GFP (green) (A). (C) is a merged image of (A) and (B). Genotype is: *ey-flp;;FRT82B* $lqfR^{\Delta 117}$*/FRT82B ubi-gfp*.

Chapter 4. Liquid facets-Related in the Wingless signaling pathway

4.1 INTRODUCTION

Proliferation is an important issue in many fields of biology. However, it is particularly important in early development. It causes serious defects including lethality if proliferation is not properly regulated during development. The canonical Wingless signaling pathway, which requires Armadillo as a transcriptional activator, plays important roles in proliferation regulation in developing animals including *Drosophila*. Blocking Wingless signaling with loss-of-function mutations in *armadillo (arm)* frequently causes lethality in embryogenesis because the signal activity is needed for segment polarity (Wieschaus & Riggleman, 1987). However, homozygotes of a hypomorphic allele $arm^{H8.6}$ survive up to the pupal stage with no obvious adult cuticle, and late third instar larvae have extremely reduced imaginal discs (Peifer et al, 1991). The "no disc" phenotype is typical in mutants for genes that regulate proliferation (Gatti & Baker, 1989; Shearn et al, 1971). Mutant clones for positive regulators of the Wingless signaling pathway in imaginal discs shows proliferation defects and increased apoptosis (Giraldez & Cohen, 2003).

In the canonical Wingless signaling pathway, Wingless ligand binds to its receptors Frizzled and Arrow ultimately to inhibit the phosphorylation and degradation of Armadillo (Peifer et al, 1994). In other words, Wingless signal activity that leads to target gene expression in the cell is determined by the cytosolic concentration of Armadillo. Armadillo also binds to E-cadherin and serves as a component of the adherens junction. There are at least two pools of Armadillo in the cell: cytosolic Armadillo that serves as

the transcriptional coactivator and membrane-bound Armadillo that is a part of the adherens junction. Membrane bound Armadillo cannot turn on Wingless target gene expression (Cox et al, 1999). Therefore, in addition to the activity of core components of the Wingless signaling pathway, the cellular level of E-cadherin is also an important factor for cytosolic Armadillo level control. Overexpression of E-cadherin decreases Wingless signaling activity both in the developing *Drosophila* wing and in a colorectal cancer cell line SW480 (Gottardi et al, 2001; Sanson et al, 1996). Conversely, accumulation of Armadillo in the cell by expressing either a dominant negative mutant form of Zest-white-3 (GSK3) or constitutively active Armadillo with its N-terminus deleted increase E-cadherin levels (Yanagawa et al, 1997). Interestingly, RNAi-induced knockdown of *polychaetoid*, a mammalian *ZO-1* homolog, increased E-cadherin levels at the plasma membrane in developing *Drosophila* eyes (Seppa et al, 2008). The mechanism of changes in the E-cadherin level or the relationship between *polychaetoid* and the Wingless signaling pathway are unknown.

In this chapter, I show that *lqfR* has a role in the Wingless signaling pathway. LqfR is a single *Drosophila* homolog of Golgi epsin and localizes at the Golgi (chapter 2). It has been shown earlier that the absence of yeast Golgi Epsins Ent3p and Ent5p cause an increase of Chs3p (chitin synthase) at the plasma membrane suggestive of the role of Golgi Epsins in Golgi-to-endosome trafficking (Copic et al, 2007). In genetic screens for dominant modifiers of *lqfR* hypomorph, *polychaetoid* was identified as an enhancer (Chapter 3). In the absence of *polychaetoid*, E-cadherin increases at the plasma membrane in developing *Drosophila* eye (Seppa et al, 2008). I found that the levels of E-cadherin as well as Armadillo are increased in *lqfR* null clones in eye discs. With this observation I hypothesized that LqfR regulates E-cadherin trafficking from the Golgi to

endosomes. Increased E-cadherin has been shown to antagonize Wingless signaling activity due to its binding with Armadillo (Gottardi et al, 2001; Sanson et al, 1996). I show that *lqfR* interacts with genes for Wingless ligand and Armadillo. I also show that the expression level of *dachsous*, a transcriptional target of the Wingless signaling pathway, is decreased in *lqfR* null clones. Consistent with the hypothesis, LqfR associates with E-cadherin, Armadillo, and α-catenin. However, inconsistent with the hypothesis, a structure/function assay indicates that the essential function of *lqfR* comes from its *exon 6*, which is not conserved in Golgi epsin genes in other species. Exon 6 corresponds to a separate gene called *tel2* in vertebrates. Finally, I suggest two alternative hypotheses for the future direction of *lqfR* research.

4.2 RESULTS

Increased E-cadherin and Armadillo at the plasma membrane in *lqfR* null clones

It has been shown that when *polychaetoid (pyd)* is absent, E-cadherin levels at the plasma membrane increase in developing *Drosophila* eye (Seppa et al, 2008). Since *pyd* has been found as a dominant enhancer of *lqfR* hypomorph (Chapter 3), I wondered if *lqfR* null clones would also have altered levels of E-cadherin. At the apical area where the adherens junction is located, the level of E-cadherin in $lqfR^{\Delta 117}$ clones in eye discs was similar to that in the adjacent wild type cells (date not shown). However, from the sub-apical to baso-lateral area where E-cadherin levels are much lower than that in the adherens junction region in wild type cells, the E-cadherin level at the plasma membrane is much higher in $lqfR^{\Delta 117}$ clones compared to adjacent wild type area (Fig. 4-1). The

difference in the E-cadherin level between wild type cells and cells in *lqfR*$^{\Delta 117}$ clones is most dramatic near the morphogenetic furrow where E-cadherin level is overall increased. Because *lqfR* encodes *Drosophila* Golgi Epsin, this result suggests that Golgi Epsin can directly regulate E-cadherin trafficking to the plasma membrane. In support of this idea, it has been shown previously that yeast Golgi Epsins Ent3p and Ent5p are important in Chs3p trafficking and when Golgi Epsin is depleted Chs3p levels at the plasma membrane increase suggesting the role of Golgi Epsin in Golgi to endosome trafficking (Copic et al, 2007).

The increase of E-cadherin at the plasma membrane in *lqfR*$^{\Delta 117}$ clones may be due to increased gene expression. An enhancer trap, *shotgun-lacZ*, has been shown to express β-galactosidase under the control of the E-cadherin gene *shotgun* in eye discs (Brown et al, 2006). To test if shotgun expression is increased in *lqfR*$^{\Delta 117}$ clones, I compared the expression level of *shotgun-lacZ* in the *lqfR*$^{\Delta 117}$ clones with that of neighboring wild type cells. Interestingly, the expression of *shotgun-lacZ* was not increased but somewhat decreased (Fig. 4-2). This result indicates that the increased E-cadherin level is not due to increased gene expression, which is consistent with my model that *lqfR* is required directly for E-cadherin trafficking.

Armadillo is an adherens junction component and a direct binding partner of E-cadherin. Since the level of E-cadherin is increased in *lqfR*$^{\Delta 117}$ cells, I wanted to know if the Armadillo level is also increased in a LqfR deficient condition. As expected, the Armadillo signal was higher in *lqfR*$^{\Delta 117}$ clones compared to adjacent wild type cells from the sub-apical to baso-lateral region (Fig. 4-3). However, there was no difference in the

level of Armadillo at the adherens junction between *lqfR*$^{\Delta 117}$ clones and wild type cells (data not shown). Once again, these data shows that the E-cadherin complex levels are generally increased in cells without LqfR function, which suggests that E-cadherin trafficking is regulated by Golgi Epsin function.

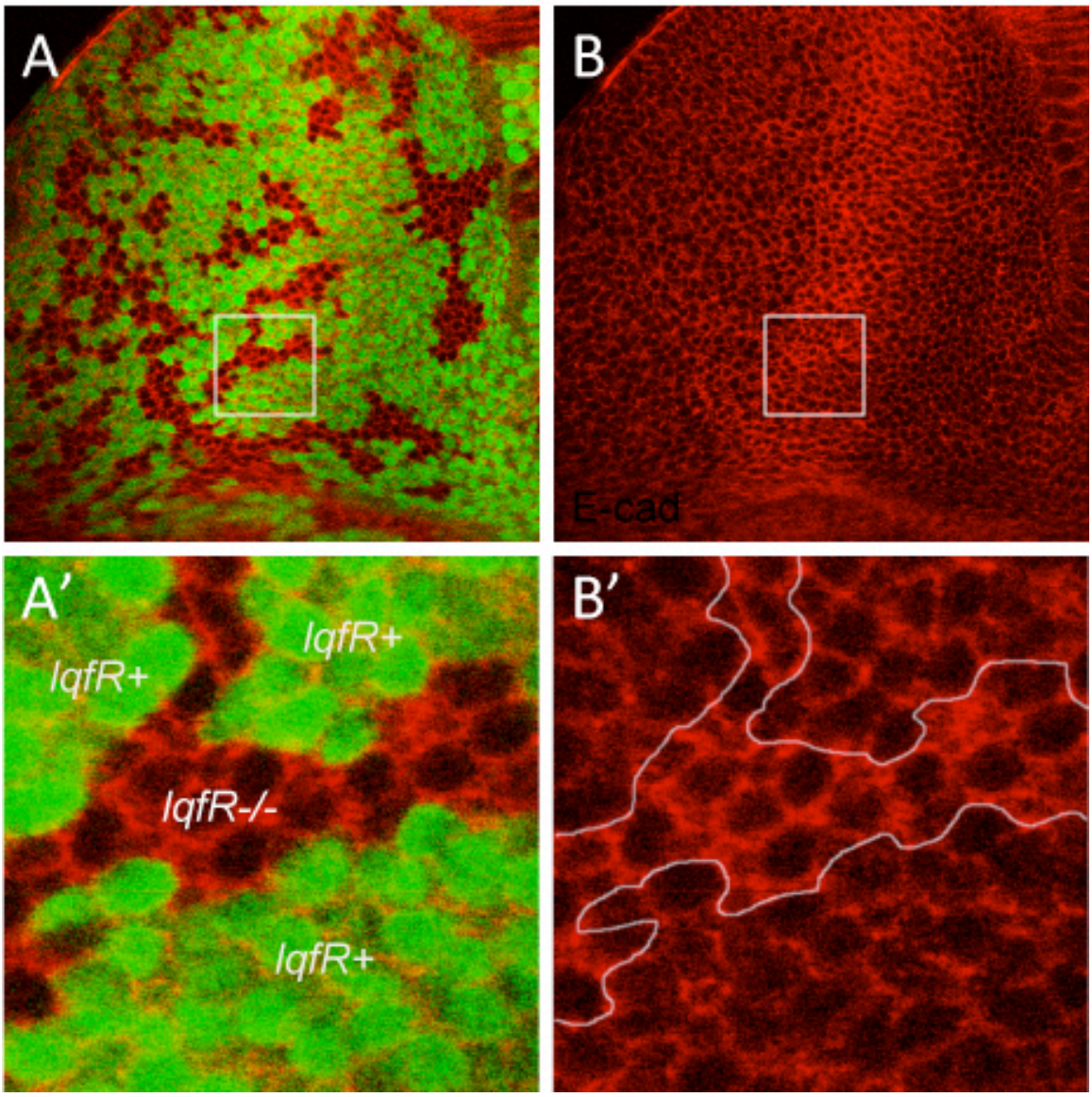

Figure 4-1. Increased E-cadherin level at the plasma membrane in *lqfR* null clones.

Confocal images of an eye disc with *lqfR*$^{\Delta 117}$ clones immunostained with anti-E-cadherin (red). *lqfR*$^{\Delta 117}$ clones are marked with the absence of GFP (green). Area marked with white squares in (A) and (B) are magnified in (A') and (B'). Note that E-cadherin levels are normally increased at the morphogenetic furrow due to increased gene expression as shown in (B). White line in (B') denotes clone boundary. Genotype is: *ey-flp;;FRT82B lqfR*$^{\Delta 117}$*/FRT82B ubi-gfp*.

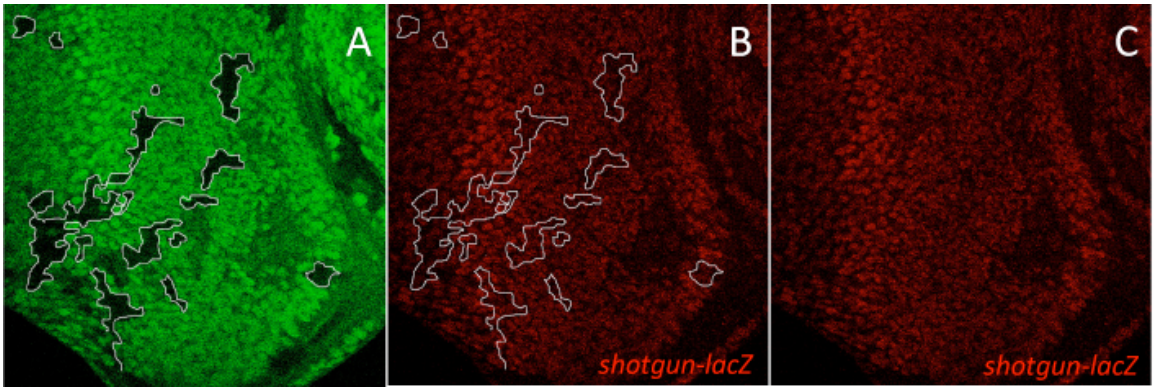

Figure 4-2. E-cadherin gene expression is not increased in *lqfR* null clones.

Confocal images of an eye disc with *shotgun-lacZ* enhancer trap and $lqfR^{s117}$ clones. *shotgun-lacZ* expression level was visualized by immunostaining with anti-β-galactosidase shown in red (B-C). $lqfR^{s117}$clones are marked with the absence of GFP (A). Note that *shotgun-lacZ* expression level is normally increased at the morphogenetic furrow as shown in (B-C). White line in (B) denotes clone boundary. (B) and (C) are the same images except the clone marker is erased in (C). Genotype is: *ey-flp ; shotgun-lacZ/+ ; FRT82B* $lqfR^{s117}$*/FRT82B ubi-gfp*.

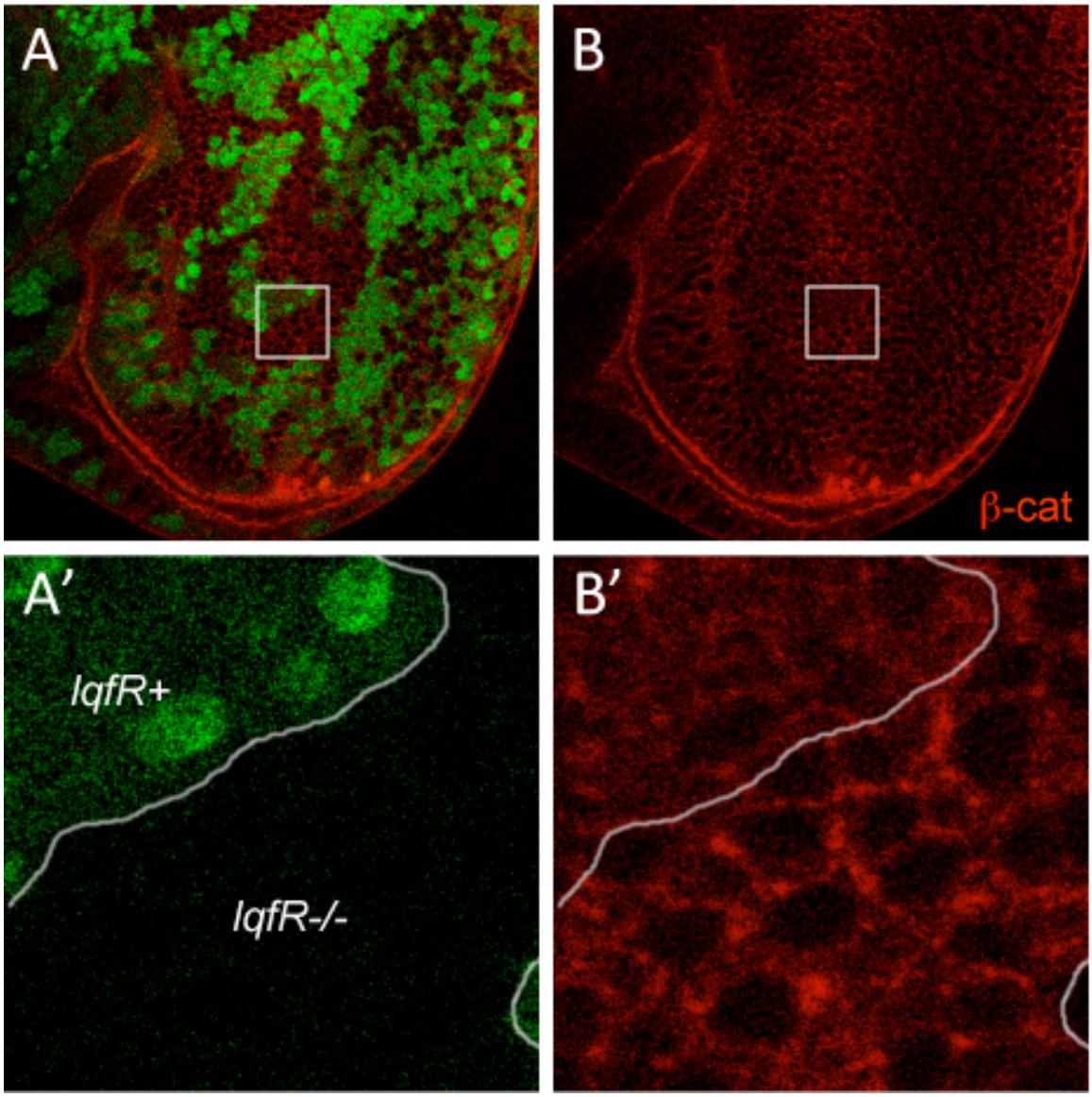

Figure 4-3. Increased Armadillo level at the plasma membrane in *lqfR* null clones.

Confocal images of an eye disc with *lqfR*$^{\Delta 117}$ clones immunostained with anti-Armadillo (red). *lqfR*$^{\Delta 117}$clones are marked with the absence of GFP (green). Area marked with white squares in (A) and (B) are magnified in (A') and (B'). Note that Armadillo levels are normally increased at the morphogenetic furrow as shown in (B). White lines in (A') and (B') denote clone boundary. Genotype is: *ey-flp;;FRT82B lqfR*$^{\Delta 117}$*/FRT82B ubi-gfp*.

***wingless* and *armadillo* dominantly enhance *lqfR* phenotype**

Armadillo, an adherens junction component, also plays a key role in Wingless signaling as a transcriptional co-activator. When Wingless signal is turned on, cytosolic Armadillo is stabilized and accumulates in the cell to enter into the nucleus and turn on target gene transcription by binding with Pangolin, a DNA binding protein. So, the level of E-cadherin, an Armadillo binding protein, is important for Wingless signal activity. It has been shown from research in *Drosophila* and in the colorectal cancer cell line SW480 that increased E-cadherin decreases proliferation by decreasing the Wingless signaling activity through Armadillo (Gottardi et al, 2001; Sanson et al, 1996). To test if increased levels of E-cadherin and Armadillo at the plasma membrane in $lqfR^{\Delta 117}$ clones have functional significance, I performed genetic interaction experiments with strong loss-of-function alleles of genes for Wingless and Armadillo.

To test if *wingless* dominantly enhances thr *lqfR* hypomorphic phenotype, I used two amorphic alleles of wingless, wg^{l-17} and wg^{l-8}, with the $lqfR^{P}/lqfR^{\Delta 117}$ background. First, wg^{l-17}*/CyO-gfp ;* $lqfR^{P}$*/TM6B* males were crossed with +/+ *;* $lqfR^{\Delta 117}$*/TM6B* females. *Non-TM6B* progeny with or without *CyO-gfp* were compared. The *CyO-gfp* chromosome also has a w^{+} marker that was useful for identification of the genotype when the progeny were dead or alive but did not unfold their wings. The eyes of *CyO-gfp/+ ;* $lqfR^{P}/lqfR^{\Delta 117}$ flies are variable, from normal to slightly rough to kidney-shaped, but most escapers have slightly rough eyes (Fig. 4-4A). However, when one copy of wg^{l-17} was introduced, the eyes became much more defective, ranging from kidney-shaped to almost no eyes as well as defects in head epidermis (Fig. 4-4B, C, and data not shown). Similarly, wg^{l-8} dominantly enhanced *lqfR* hypomorphs (data not shown).

armadillo loss-of-function alleles, arm^{3} and arm^{8}, were also tested for dominant modification of *lqfR* hypomorphs. arm^{3}/*FM7 ;;* $lqfR^{\Delta 117}$/*TM6B* females were crossed with w^{1118}/*Y ;;* $lqfR^{P}$/*TM6B*. The *FM7* chromosome and the arm^{3} chromosome can be distinguished in the progeny as *FM7* is w^{-} and the arm^{3} chromosome is w^{+}. Among the progeny, 17 *non-TM6B* pupae were transferred to a new vial to keep them safe, but none of them eclosed. When thye were dissected from their pupal cases, I found that the *lqfR* hypomorphic phenotype was strongly enhanced (Fig. 4-5). The eyes were small and sometimes missing and their heads were small. There were also defects in the head cuticle, wings, and legs. A hypomorphic allele, arm^{8}, also dominantly enhanced the *lqfR* hypomorph strongly, consistent with the results from arm^{3} (data not shown). The fact that both *wingless* and *armadillo* dominantly enhance the *lqfR* hypomorphic phenotype strongly suggests that *lqfR* functions in the context of Wingless signaling pathway. This conclusion is consistent with the observations that E-cadherin and Armadillo levels at the plasma membrane increase in *lqfR* null cells.

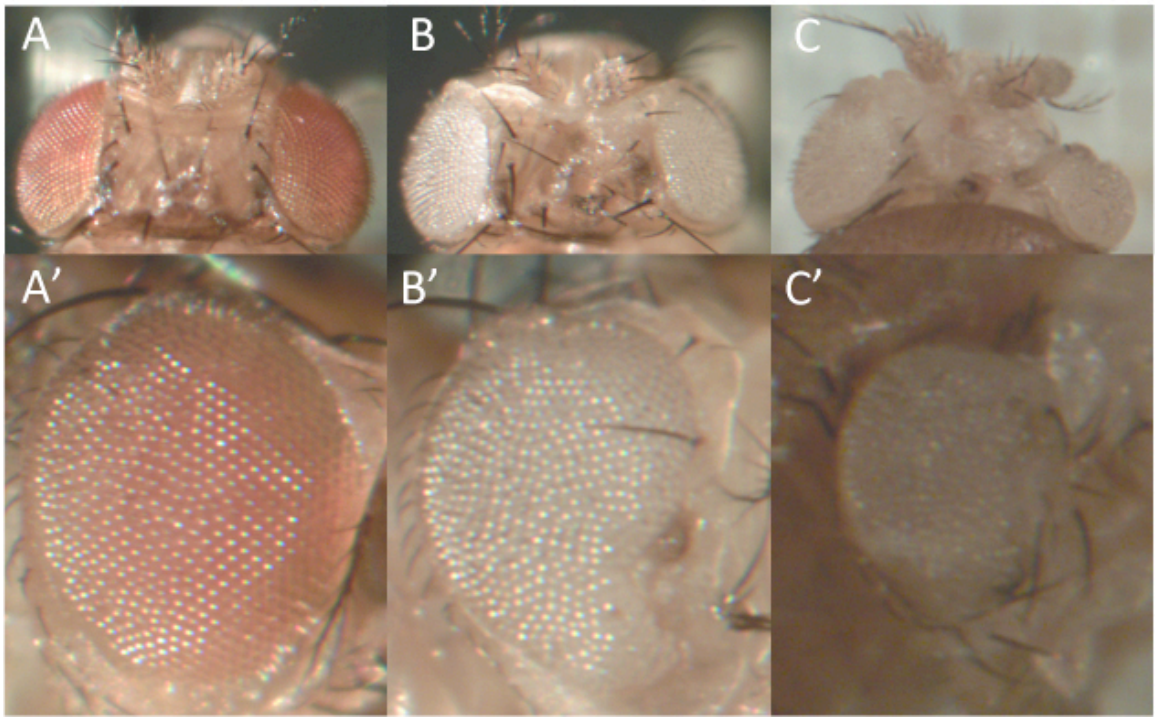

Figure 4-4. *wingless* dominantly modifies *lqfR* hypomorph.

Images are dorsal view of heads (A-C) and eyes (A'-C') of 3 adult flies. (A, A') are images from same animal, so as (B, B'), and (C, C'). Flies shown here are siblings of the cross: $wg^{l\text{-}17}$/*CyO-gfp* ; $lqfR^{P}$/*TM6B* X $lqfR^{\Delta 117}$/*TM6B*. (A, A') are a progeny with the genotype, *CyO-gfp*/+ ; $lqfR^{P}/lqfR^{\Delta 117}$ showing the *lqfR* hypomorphic background to compare with enhanced phenotype in (B, B') and (C, C'). Eye color is from *w+* in *CyO-gfp* chromosome. White eye indicates that the fly is inherited $wg^{l\text{-}17}$, not *CyO-gfp*. (B,B') and (C,C') are two examples of the same genotype: $wg^{l\text{-}17}$/+ ; $lqfR^{P}/lqfR^{\Delta 117}$. A head cuticle defect is shown in (B) and (C).

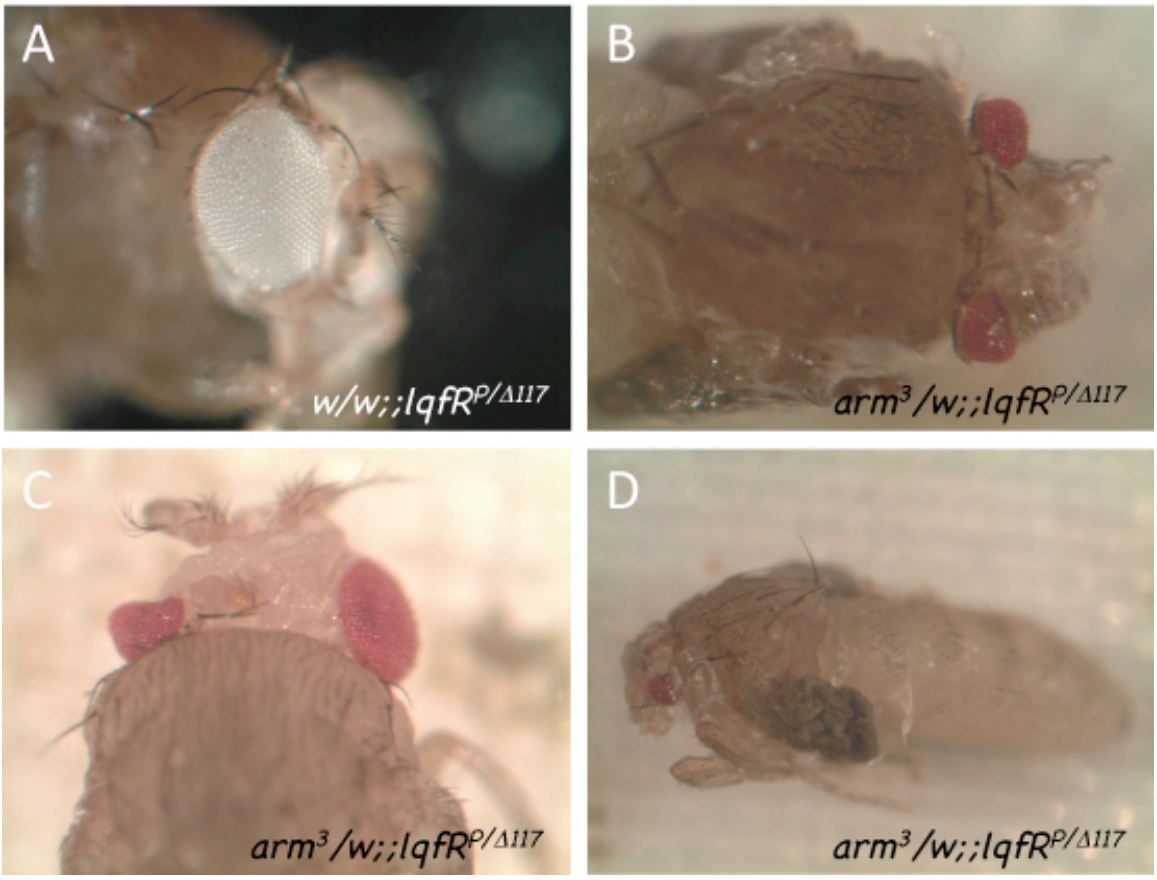

Figure 4-5. *armadillo* dominantly modifies *lqfR* hypomorph.

Images of an adult fly (A) or pharates (B-D). (A) shows the *lqfR* hypomorphic background with the genotype of: *w/w ; $lqfR^{P}$/$lqfR^{\Delta 117}$*. (B-D) are pharates dead in the pupal case with genotype of: *arm^{3}/w ; $lqfR^{P}$/$lqfR^{\Delta 117}$*. Notice that pharates in (B-D) have severely enhanced eye defects and severely shrunken heads with strong head cuticle defects.

Target gene expression is reduced in *lqfR* null cells

Genetic interactions between *lqfR* and genes for Wingless signaling suggest that *lqfR* may serve as a positive regulator of Wingless signaling. To test this idea, the expression level of a Wingless signal target gene, *dachsous,* was monitored in eye discs within *lqfR* null clones. It has been shown that *dachsous* expression, monitored with a *dachsous-lacZ* enhancer trap, is regulated by Wingless signal activity (Yang et al, 2002). Wingless ligand is expressed at the margin area farthest from the D/V midline and forms gradient highest at the margin and lowest at the D/V midline. The expression pattern of *dachsous* recapitulates the Wingless gradient. Furthermore, *dachsous* is ectopically expressed in clones overexpressing *armadillo* in eye discs, and not expressed in *armadillo* null clones, indicating that *dachsous* is a transcriptional target of Wingless (Yang et al, 2002). Using the same *dachsous-lacZ* enhancer trap, I found that *dachsous* expression is reduced in $lqfR^{a117}$ clones in eye discs (Fig. 4-6). This result is consistent with my model to explain genetic interaction results and increased E-cadherin and Armadillo at the plasma membrane in *lqfR* null cells.

Dachsous is an atypical cadherin that interacts with another atypical cadherin, Fat, in an adjacent cell. The Fat-Dachsous interaction and the steep gradient are important in planar cell polarity regulation as well as organ growth (Brittle et al, 2010; Simon, 2004). Specifically, Fat is an important upstream regulator of a recently recognized organ size regulation mechanism called the Hippo pathway (Silva et al, 2006). To test the functional relevance of reduced *dachsous* expression levels in *lqfR* null clones, I performed genetic interaction tests between *dachsous* and *lqfR*. A strong loss-of-function allele, ds^{38K}, was tested for dominant modification of the *lqfR* hypomorphic phenotype. I found that ds^{38K}

dominantly enhanced the *lqfR*^{P}/*lqfR*$^{\Delta 117}$ phenotype strongly (Fig. 4-7). This result further supports that LqfR functions in the context of Wingless signaling and its transcriptional targets.

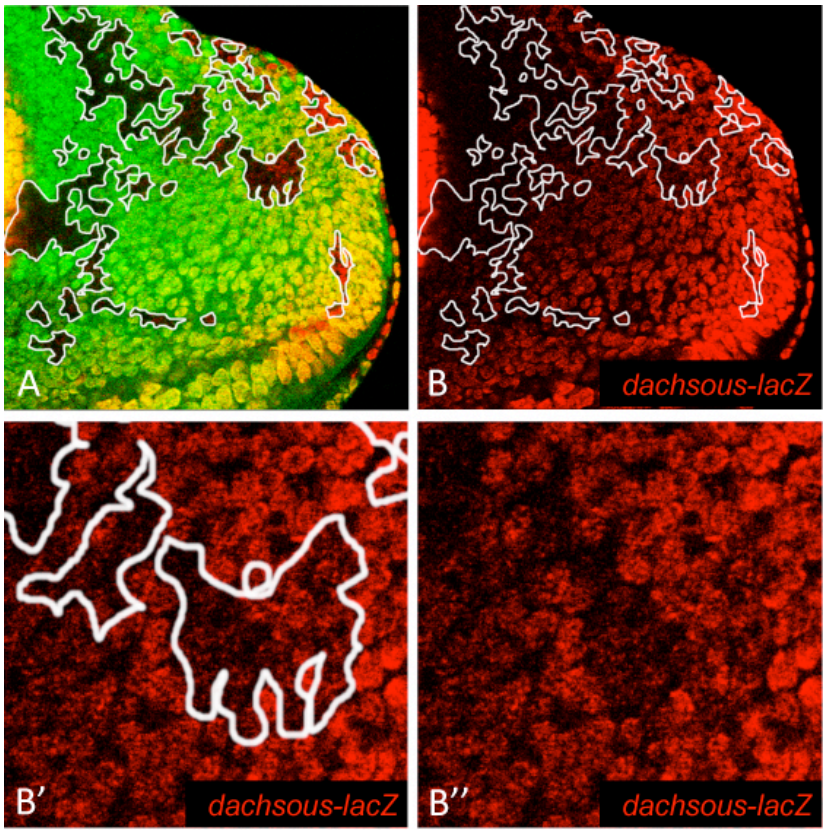

Figure 4-6. *dachsous* gene expression is reduced in *lqfR* null clones.

Confocal images of an eye disc with a *dachsous-lacZ* enhancer trap and $lqfR^{\Delta 117}$ clones. The *dachsous-lacZ* expression level was visualized by immunostaining with anti-β-galactosidase shown in red. $lqfR^{\Delta 117}$ clones are marked by the absence of GFP (green) (A). Note that *dachsous-lacZ* is expressed in a gradient highest at the margins and lowest at the D/V midline (B). The white line in (B) and (B') denote a clone boundary. (B') and (B'') are the same images except the clone marker is erased in (B''). Genotype is: *ey-flp ; dachsous-lacZ/+ ; FRT82B* $lqfR^{\Delta 117}$*/FRT82B ubi-gfp*.

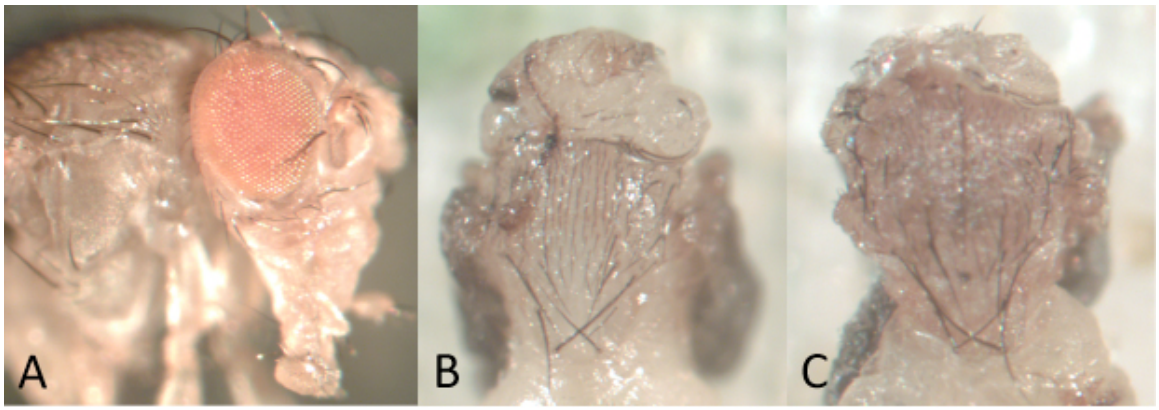

Figure 4-7. *dachsous* dominantly modifies *lqfR* hypomorphic phenotypes.

Images of an adult fly (A) or pharates (B-C). (A) shows the *lqfR* hypomorphic background with the genotype of: *w*/*w* $lqfR^{P}/lqfR^{\Delta 117}$. (B) and (C) are pharates dead in the pupal case with genotype of: arm^{3}/*w* ; $lqfR^{P}/lqfR^{\Delta 117}$. Notice that pharates in (B) and (C) have severely enhanced eyes and severely shrunken heads with head cuticle defects.

LqfR associates E-cadherin, Armadillo, and α-catenin

If the increased E-cadherin complex in *lqfR* null cells is due to a failure of a direct function of LqfR in E-cadherin trafficking from the Golgi to endosomes (as Ent3p and Ent5p are likely to be required for Chs3p trafficking from the Golgi to endosomes in yeast (Copic et al, 2007)), it expected that LqfR would interact physically with the E-cadherin complex. To test this idea, I performed a co-immunoprecipitation assay utilizing fly lines with the transgenes *UAS-lqfRa* (full-length a-form cDNA) and *UAS-lqfR*^{ENTH} (ENTH domain only) each with *gfp* attached at the 3'-end, and overexpressed in the embryo with an *Act5C-gal4* driver. Immunoprecipitation was done with an anti-GFP antibody, and endogenous E-cadherin, Armadillo, and α-catenin were detected with specific antibodies in the Western blot (Fig. 4-8). With this assay, I found that all E-cadherin complex components tested, E-cadherin, Armadillo, and α-catenin, were specifically co-immunoprecipitated with LqfRa-GFP but not as much with LqfR^{ENTH}-GFP (Fig. 4-8). This result is again consistent with the model that LqfR may be required for E-cadherin trafficking at the Golgi (Fig. 4-9).

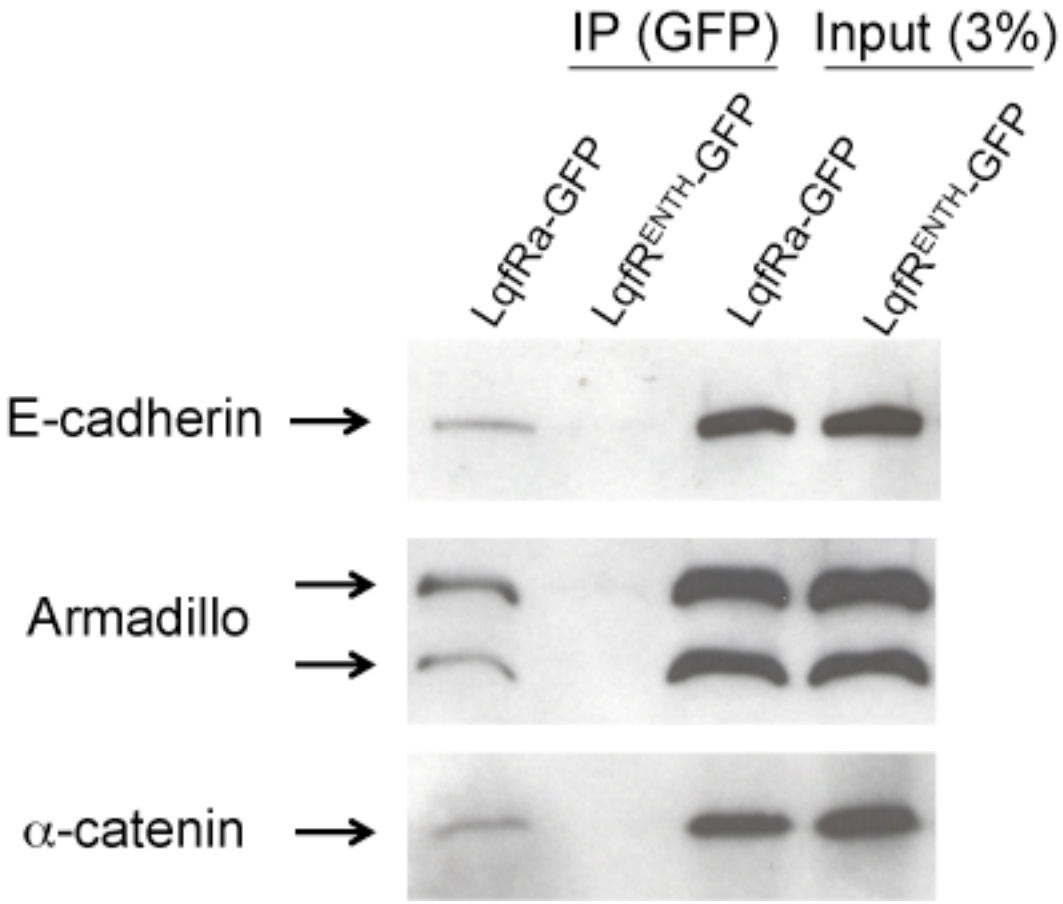

Figure 4-8. LqfRa associates with E-cadherin, Armadillo, and α-catenin.

Co-immuno precipitation with extracts from embryos overexpressing either *lqfRa-gfp* (lane 1) or *lqfR^{ENTH}-gfp* (lane 2) with *Act5C-gal4* using GFP-trap (Chromotek) followed by Western blots. Specific antibodies against E-cadherin, Armadillo, or α-catenin were used to detect endogenous proteins. Compare first and second lanes for protein bands in each Western blot. Third and fourth lanes are 3% of inputs of embryo extract with genotype shown above to show that equal amount of embryo extract have been used in each sample.

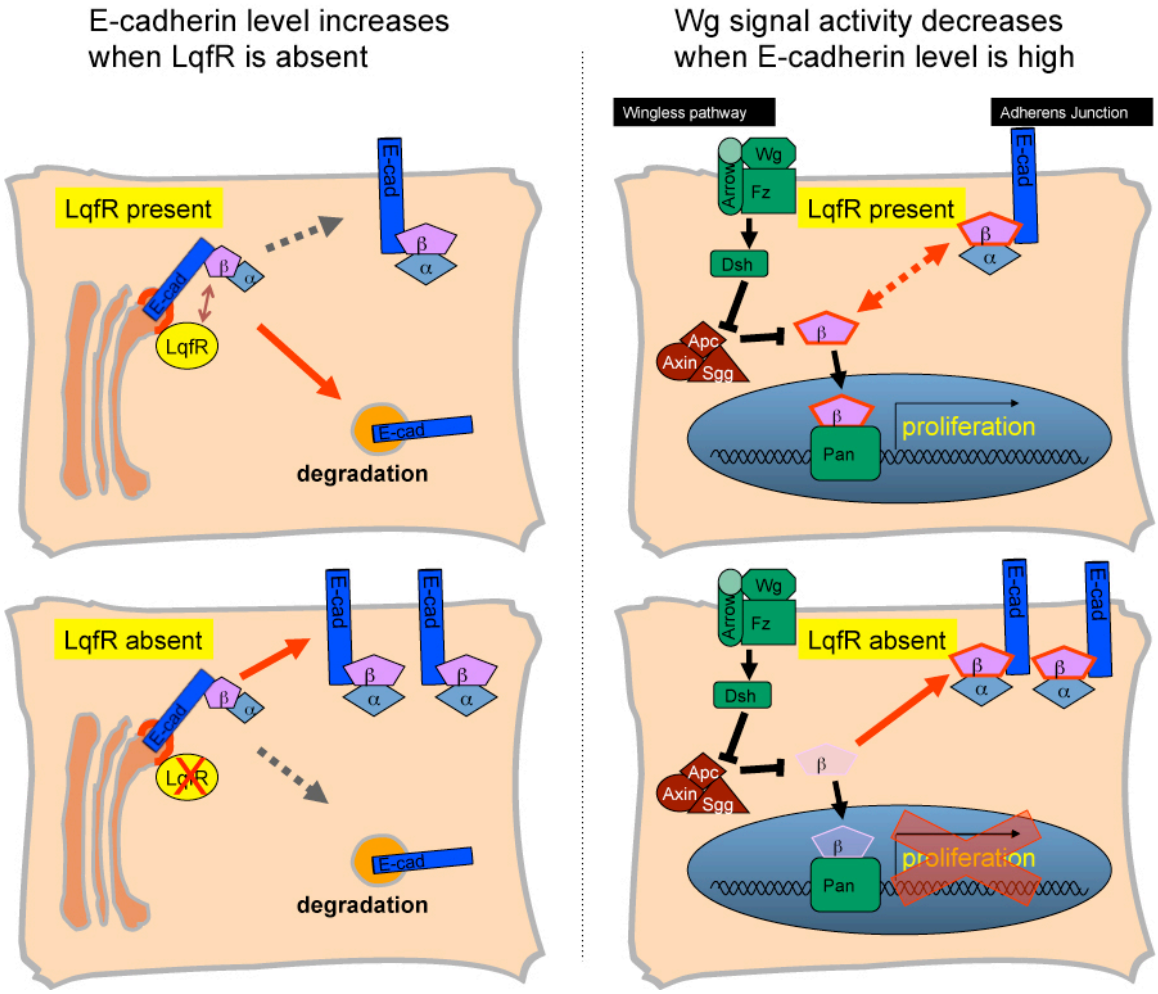

Figure 4-9. The original model for the molecular function of LqfR.

Left panel explains the increased levels of E-cadherin and Armadillo at the plasma membrane. I hypothesized that LqfR may function as a clathrin adaptor at the Golgi to regulate E-cadherin trafficking from the Golgi to endosomes with the assumption that LqfR is the fly Golgi Epsin based on its sequence homology. It has been shown that Golgi Epsin functions in Golgi-to-endosome trafficking (Copic et al, 2007). Right panel is to explain that increased E-cadherin level antagonizes with the Wingless signaling pathway because increased E-cadherin binds to Armadillo and titrates it out. This results in reduced target gene expression and physiological consequences including reduced proliferation. The relationship between increased E-cadherin and the Wingless signal activity has been shown before (Gottardi et al, 2001; Sanson et al, 1996). After a structure/function assay shown below, this model was revised (see Fig. 4-19).

lqfR exon 6* is necessary and sufficient for the function of *lqfR

If the direct role of LqfR in the Wingless signaling pathway is to mediate the trafficking of E-cadherin, known domains and motifs for trafficking in LqfR protein should play critical roles in the function of *lqfR*, which is inferred from the mutant phenotype. To understand the mechanism of LqfR function, I performed structure/function analysis. I generated *UAS* transgenic fly lines with deletions in *lqfRa* cDNA. A *6Xmyc* tag is present in each transgene at the 5'-end. These transgenes were expressed ubiquitously with *Act5C-gal4* or eye specifically with *ey-gal4* to test their ability to rescue the *lqfR* null phenotype either in the whole body or in the eye only. Transgenes in this study are summarized in Figure 4-10.

First, constructs with *lqfRa* full-length, $lqfRa^{\Delta ENTH}$, and $lqfR^{ENTH}$ were overexpressed with *Act5C-gal4* to test their ability to rescue the lethality and morphological defects (Fig. 4-10B). As expected and consistent with results in chapter 2, where I used transgenes with *gfp* at 3'-end, *lqfRa* full-length and $lqfRa^{\Delta ENTH}$ with *6Xmyc* at the 5'-end rescued the *lqfR* null phenotype completely including lethality and morphological defects seen in a few mutant escapers. However, although all escapers were externally undistinguishable from wild-type flies, there were still many progeny that did not eclose and died in the pupal case. Although the reason is not clear, this is not due to the lack of the ENTH domain because the number of escapers with *A5C-gal4>*$lqfRa^{\Delta ENTH}$ is not smaller than with *A5C-gal4>lqfRa* full-length (data not shown). In contrast, *A5C-gal4>*$lqfR^{ENTH}$ did not rescue the *lqfR* null phenotype at all. Larvae with *A5C-gal4>*$lqfR^{ENTH}$ in a $lqfR^{\Delta 117}$ homozygous background die as third instar larvae and do

not pupate just as in *lqfR*$^{\Delta 117}$ homozygotes without the construct (chapter 2). These data confirm the conclusion from chapter 2 that the ENTH domain is not required for the function of LqfR.

Secondly, each of *lqfR exons 1-5* and *lqfR exon 6* was overexpressed with *A5C-gal4* in a *lqfR* null background to test their ability to rescue the null phenotype (Fig. 4-11 C). *lqfR exons 1-5* are found in both alternatively spliced transcripts in *lqfR*, and they contain the ENTH domain and putative γ-ear binding motifs and a clathrin binding motif, while *exon 6* exists only in *lqfRa*, the longer transcript (Fig. 2-1A). *Exon 6* is not conserved in Golgi epsin genes from other species. If LqfR functions as part of the trafficking machinery, it is expected that *A5C-gal4>lqfR exons 1-5* may rescue the null phenotype and *A5C-gal4>lqfR exon 6* may not. Surprisingly, I obtained exactly the opposite results. *A5C-gal4>lqfR exon 6* completely rescued the null phenotype as well as the full-length, but *A5C-gal4>lqfR exons 1-5* did not rescue at all. This unexpected result is against the trafficking model (Fig. 4-9) and suggests that the essential function of LqfR has nothing to do with Golgi Epsin.

Secondary structure prediction data suggest that *exon 6* encodes a protein with a HEAT repeat structure. Based on the predicted structure, I generated a series of overlapping constructs with different deletions in *exon 6* (Fig. 4-10D) to test their ability to rescue *lqfR* null phenotype. Out of 6 deletion constructs, none of them was able to rescue the null phenotype (Table 4-1). These results indicate that at least both ends of *exon 6* (corresponds to a.a.494-690 and a.a.1257-1415) are essential for LqfR function. It is possible that *exons 1-5* cannot rescue the *lqfR* null phenotype alone, but may have some activity redundant with parts of *exon 6*. To test this idea, transgenic lines with *exon*

1-5 fused with *exon 6* deletion constructs have been generated (Fig. 4-10E) and tested for their ability to rescue the *lqfR* null phenotype, but none of them were able to rescue to provide any rescuing activity.

There are two transcripts of *lqfR*: *lqfRa* and *lqfRb*. Previous experiments have been done only with *lqfRa* that includes *exon 6* (Fig. 2-1). To test if *lqfRb* can rescue the *lqfR* null phenotype, I generated *UAS-lqfRb* with a *6Xmyc* tag at the 5'-end (Fig. 4-10A). I wanted to test two lines of flies overexpressing *6Xmyc-lqfRb* with *Act5C-gal4* for their ability to rescue the null phenotype. However, I could not obtain the results because overexpression of *lqfRb* itself caused lethality in both lines. So, instead of using *Act5C-gal4* to express the construct ubiquitously, I used an eye specific driver *ey-gal4* that is expressed from the early stages of eye development. Previous rescue experiments using *lqfRa* constructs were retested here as well as *lqfRb*. Consistent with previous results using *Act5C-gal4*, *lqfRa* full-length, $lqfRa^{\Delta ENTH}$, and *lqfR exon 6* expressed with *ey-gal4* rescued the small eye phenotype of *lqfR* null whole eye clone (Fig. 4-11, A, C-F), but *lqfR exons 1-5* or $lqfR^{ENTH}$ did not (Fig. 4-11, I-L). Interestingly, *ey-gal4>6xMyc-lqfRb* was viable and did not rescue the *lqfR* null whole eye phenotype (Fig. 4-11, G-H). The inability of $lqfR^{ENTH}$, *lqfR exons 1-5*, and *lqfRb* to provide any activity could be due to extremely low expression levels. To test this possibility, I performed Western blotting using $lqfR^{\Delta 117}/lqfR^{+}$ heterozygotes expressing the constructs with *ey-gal4* (Fig. 4-12). The results indicates that those constructs did not rescue the null phenotype were expressed well compared to those that rescued the null phenotype. These data indicate that the essential function of *lqfR* is not to provide Golgi epsin, and *lqfR exon 6* is necessary and sufficient for the function of *lqfR* in *Drosophila* development.

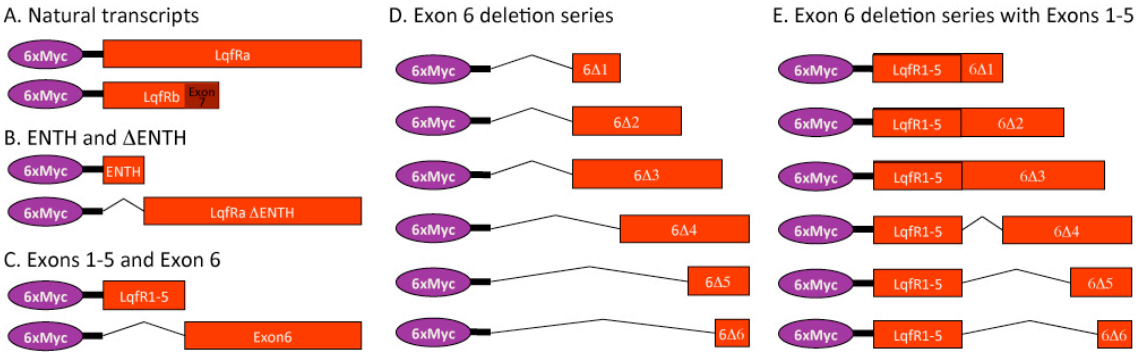

Figure 4-10. *UAS-lqfR* constructs for structure/function analysis.

Schematic view of *UAS-lqfR* constructs. All constructs are with 6xMyc tags at the 5'-end. (A) shows two naturally occurring transcripts from alternative splicing (see Fig. 2-1). (B) shows constructs with gene region for ENTH domain or everything except ENTH. (C) shows constructs with only exons 1-5 or exon 6. Exons 1-5 exist in both *lqfRa* and *lqfRb*, but exon 6 exists only in *lqfRa*. (D) shows a series of exon 6 deletion constructs. (E) shows same constructs as in (D) except that they are fused with exons 1-5.

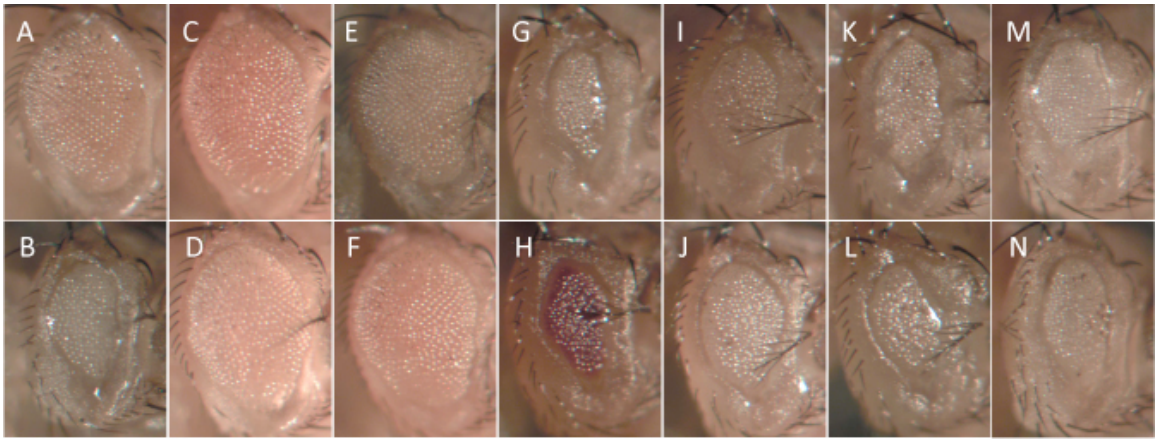

Figure 4-11. Exon 6 is necessary and sufficient for *lqfR* function.

Whole eye clones of *lqfR* null with (A-L) or without (M-N) *UAS-lqfR* constructs in *EGUF; FRT82 lqfR$^{\Delta 117}$/FRT82B GMR-hid* background. *ey-gal4* drives the expression of both *UAS-flp* and *UAS-lqfR* eye specifically. *EGUF=ey-gal4, UAS-flp*.
Genotypes are:
(A) *EGUF/UAS-lqfRa (12) ; FRT82B lqfR$^{\Delta 117}$/FRT82B GMR-hid* ;
(B) *EGUF/UAS-lqfRa(59) ; FRT82B lqfR$^{\Delta 117}$/FRT82B GMR-hid* ;
(C) *EGUF/UAS-lqfRa$^{\Delta ENTH}$ (32) ; FRT82B lqfR$^{\Delta 117}$/FRT82B GMR-hid* ;
(D) *EGUF/UAS-lqfRa$^{\Delta ENTH}$ (72) ; FRT82B lqfR$^{\Delta 117}$/FRT82B GMR-hid* ;
(E) *EGUF/UAS-lqfRa exon 6 (8) ; FRT82B lqfR$^{\Delta 117}$/FRT82B GMR-hid* ;
(F) *EGUF/UAS-lqfRa exon 6 (17) ; FRT82B lqfR$^{\Delta 117}$/FRT82B GMR-hid* ;
(G) *EGUF/UAS-lqfRb (36) ; FRT82B lqfR$^{\Delta 117}$/FRT82B GMR-hid* ;
(H) *EGUF/UAS-lqfRb (57) ; FRT82B lqfR$^{\Delta 117}$/FRT82B GMR-hid* ;
(I) *EGUF/UAS-lqfR exons 1-5 (43) ; FRT82B lqfR$^{\Delta 117}$/FRT82B GMR-hid* ;
(J) *EGUF/UAS-lqfR exons 1-5 (53) ; FRT82B lqfR$^{\Delta 117}$/FRT82B GMR-hid* ;
(K) *EGUF/UAS-lqfR$^{\Delta ENTH}$ (8) ; FRT82B lqfR$^{\Delta 117}$/FRT82B GMR-hid* ;
(L) *EGUF/UAS-lqfR$^{\Delta ENTH}$ (40) ; FRT82B lqfR$^{\Delta 117}$/FRT82B GMR-hid* ;
(M, N) *EGUF/+ ; FRT82B lqfR$^{\Delta 117}$/FRT82B GMR-hid*.

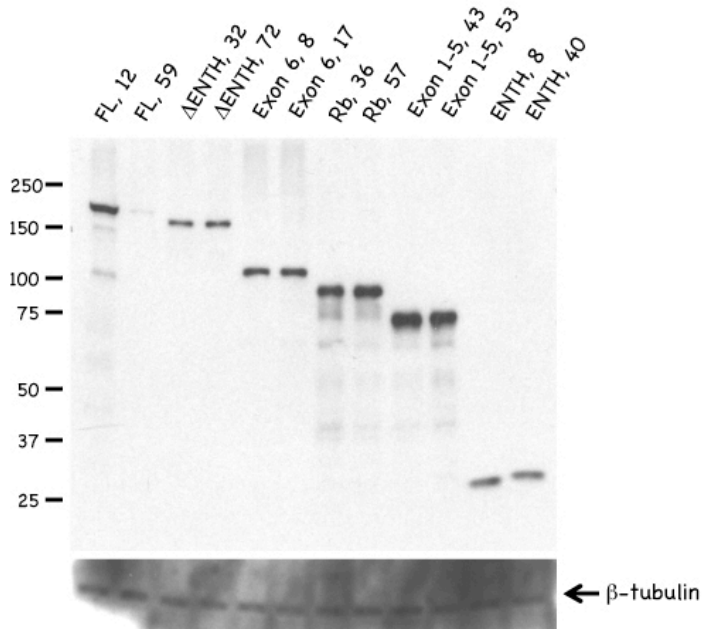

Figure 4-12. Expressed protein levels of *UAS-lqfR* constructs shown in Fig. 4-11.

Expressed protein levels of *UAS-lqfR* constructs in adult flies in Western blot using anti-Myc antibody are shown. Flies used for the Western blot are siblings of flies shown in Fig. 4-11 with *TM6B* chromosomes instead of *FRT82B GMR-hid*. Expression levels of two lines per each *UAS-lqfR* constructs are shown here. As a loading control, β-tubulin is stained with specific antibody using the same nitrocellulose filter. Note the low protein level in lane 2 (labeled as FL, 59) that expresses *lqfRa* full length. This transgene did not rescue the null (see Fig. 4-11B).
Genotypes are:
(lane 1) *EGUF/UAS-lqfRa (12) ; FRT82B lqfR$^{\Delta 117}$/TM6B*;
(lane 2) *EGUF/UAS-lqfRa (59) ; FRT82B lqfR$^{\Delta 117}$/ TM6B*;
(lane 3) *EGUF/UAS-lqfRa$^{\Delta ENTH}$ (32) ; FRT82B lqfR$^{\Delta 117}$/ TM6B*;
(lane 4) *EGUF/UAS-lqfRa$^{\Delta ENTH}$ (72) ; FRT82B lqfR$^{\Delta 117}$/ TM6B*;
(lane 5) *EGUF/UAS-lqfRa exon 6 (8) ; FRT82B lqfR$^{\Delta 117}$/ TM6B*;
(lane 6) *EGUF/UAS-lqfRa exon 6 (17) ; FRT82B lqfR$^{\Delta 117}$/ TM6B*;
(lane 7) *EGUF/UAS-lqfRb (36) ; FRT82B lqfR$^{\Delta 117}$/ TM6B*;
(lane 8) *EGUF/UAS-lqfRb (57) ; FRT82B lqfR$^{\Delta 117}$/ TM6B*;
(lane 9) *EGUF/UAS-lqfR exons 1-5 (43) ; FRT82B lqfR$^{\Delta 117}$/ TM6B*;
(lane 10) *EGUF/UAS-lqfR exons 1-5 (53) ; FRT82B lqfR$^{\Delta 117}$/ TM6B*;
(lane 11) *EGUF/UAS-lqfR^{ENTH} (8) ; FRT82B lqfR$^{\Delta 117}$/ TM6B*;
(lane 12) *EGUF/UAS-lqfR^{ENTH} (40) ; FRT82B lqfR$^{\Delta 117}$/ TM6B*.

LqfR exon 6 is localized in the nucleus and at the perinuclear region, but not at the Golgi

As shown earlier in chapter 2, LqfR is a Golgi protein. This result is from immunostaining experiments using anti-LqfR antibody that has been generated with bacterially expressed antigen encoded by exons 1-5. Although the known functions of Golgi Epsins in other model organisms and the homology of LqfR with Golgi Epsin suggest so, the localization of LqfR at the Golgi does not necessary mean that LqfR plays its essential role at the Golgi. As previous structure/function analyses argue against the idea that the *lqfR* mutant phenotype is caused by the loss of the Golgi Epsin functions of the LqfR protein but instead are caused by loss of the Exon 6 function, I tested the cellular localization of overexpressed LqfR exon 6 tagged with 6xMyc in the eye disc using anti-Myc antibody. Surprisingly, LqfR exon 6 was in the nucleus with the strongest signal at the perinuclear region (Fig. 4-13A). Co-staining with the antibody against LqfR exons 1-5 showed that while the majority of LqfR exon 6 exists in the nucleus and there is also a small amount in the cytosol, the Exon 6 cytosolic protein does not colocalize significantly with LqfR at Golgi punctae (Fig. 4-13C). This result suggests that Exon 6-containing LqfR protein may not function at the Golgi.

To further characterize the essential region in LqfR exon 6 for nuclear localization, I observed the cellular localization of 6xMyc-LqfR exon 6 deletion constructs with anti-Myc antibody. While Exon6Δ1 and Exon6Δ2 are localized at the cytosol, Exon6Δ3, Exon6Δ4, and Exon6Δ5 are localized in the nucleus, suggesting that the a.a.986-1256 region is essential for nuclear localization (Fig. 4-14).

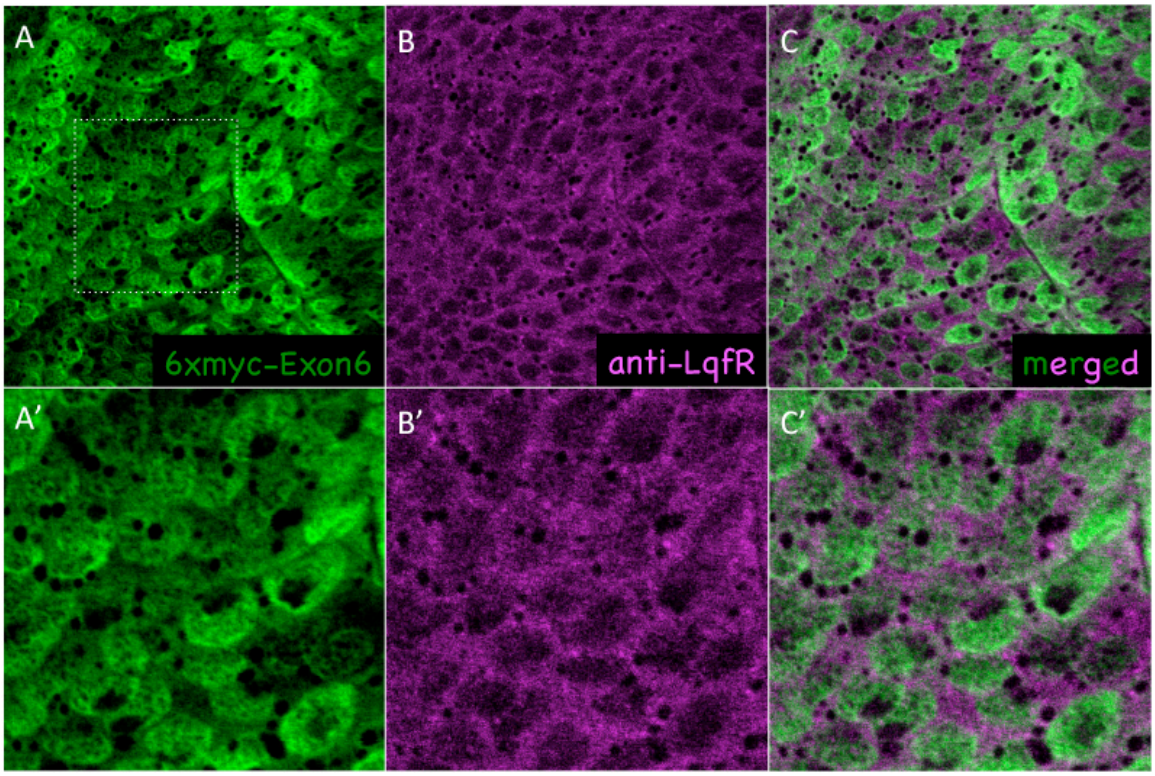

Figure 4-13. LqfR exon 6 localizes in the nucleus, but not at the Golgi.

Confocal images of an eye disc overexpressing *UAS-lqfRa exon 6* with *Act5C-gal4* driver immunostained with anti-Myc (green) and anti-LqfR (purple) antibodies. Vast majority LqfRa exon 6 exists in the nucleus (A), while anti-LqfR generated with antigen from exons 1-5 mainly localize at the Golgi punctae (B). Area marked with white square with dotted line in (A), (B), and (C) are magnified in (A'), (B'), and (C'), respectively.

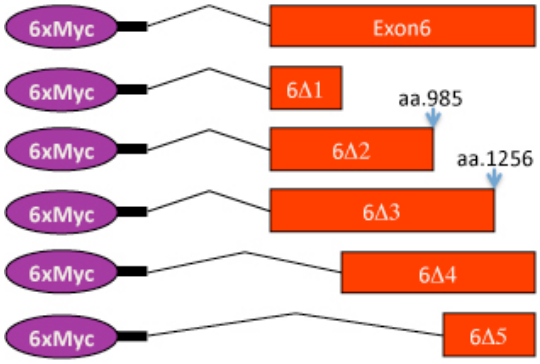

Major localization	
LqfRa-Exon 6	Nucleus (> Cytoplasm)
LqfRa-Exon6-Δ1	Cytoplasm (+ Nucleus)
LqfRa-Exon6-Δ2	Cytoplasm (> Nucleus)
LqfRa-Exon6-Δ3	Nucleus (> Cytoplasm)
LqfRa-Exon6-Δ4	Nucleus (> Cytoplasm)
LqfRa-Exon6-Δ5	Nucleus (> Cytoplasm)

Figure 4-14. Localization of 6xMyc-LqfR deletion constructs.

A summary of localization tests for 6xMyc-LqfR constructs. Nuclear localization is tested with TO-PRO3.

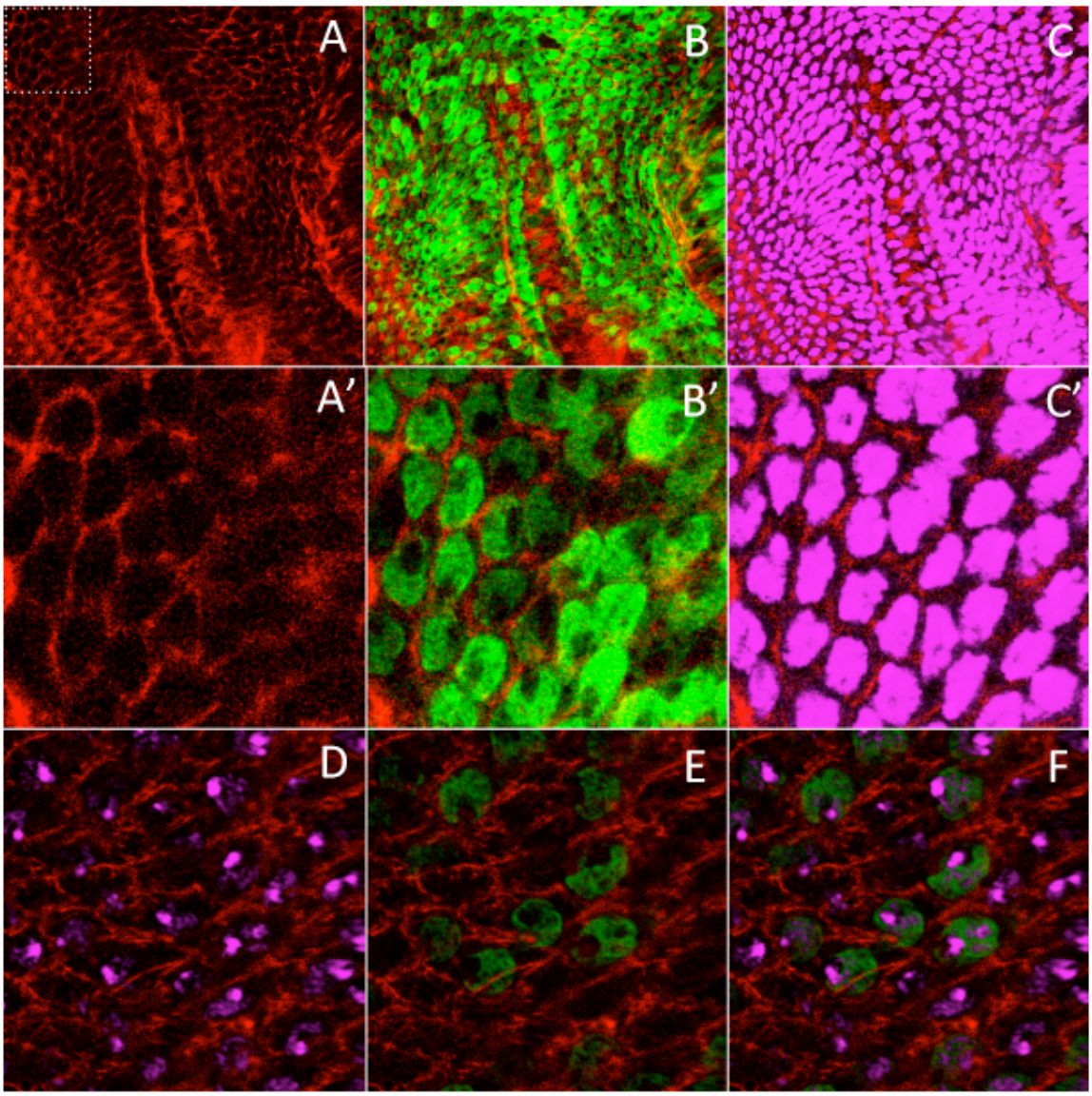

Figure 4-15. Nuclear localization of 6xMyc-LqfRa exon 6.

Confocal images of eye discs overexpressing *UAS-6Xmyc-lqfRa exon 6* with *Act5C-gal4* driver. (A) is phalloidin (red) staining showing the plasma membrane. (B) is a merged image with both phalloidin (red) and 6XMyc-LqfRa exon 6 (green). (C) is a merged image with both phalloidin (red) and TO-PRO3 (purple), which stains DNA. The area in the square with dotted line in (A) is magnified in (A'), (B'), and (C'). Another confocal image taken with lighter laser intensity is shown in (D), (E), and (F). Red is phalloidin, green is 6xMyc-LqfRa exon 6, and purple is TO-PRO3. Note that 6xMyc-LqfRa exon 6 and DNA do not co-exist in the nucleus.

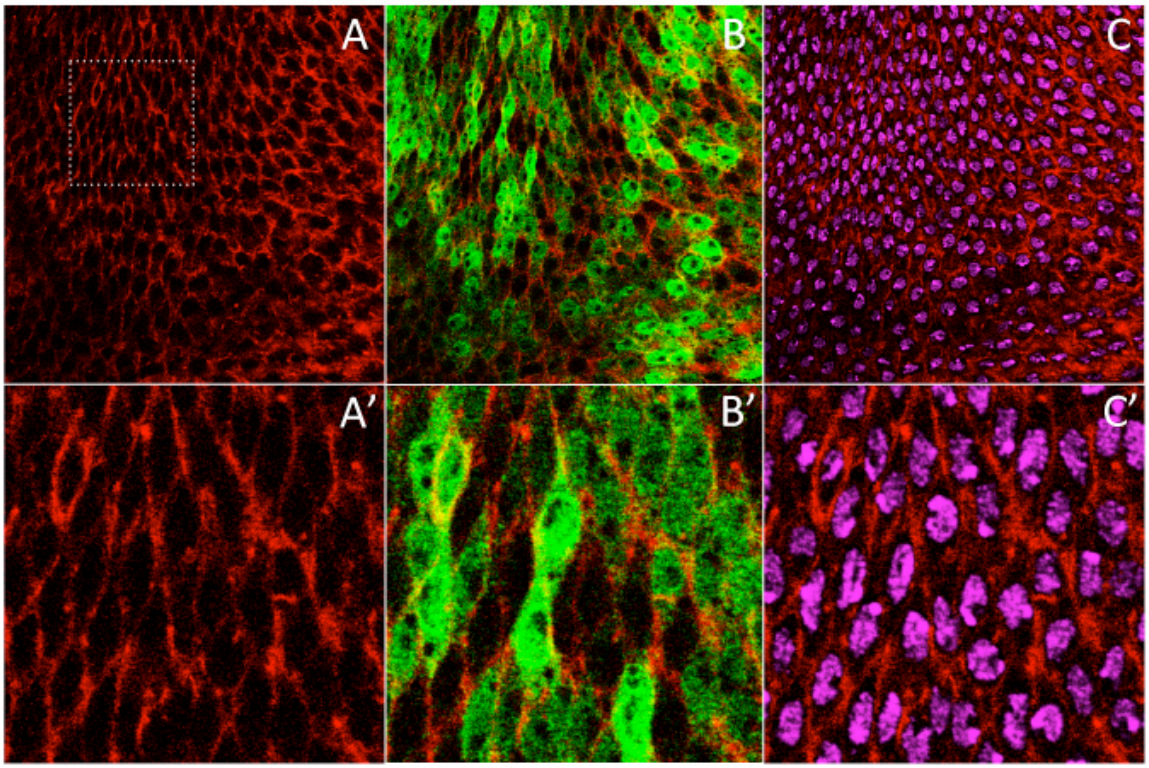

Figure 4-16. Localization of 6xMyc-LqfRa exon 6Δ1.

Confocal images of eye discs overexpressing *UAS-6Xmyc-lqfRa exon 6Δ1* with *Act5C-gal4* driver. (A) is phalloidin (red) staining showing the plasma membrane. (B) is a merged image with both phalloidin (red) and 6XMyc-LqfRa exon 6 Δ1 (green). (C) is a merged image with both phalloidin (red) and TO-PRO3 (purple), which stains DNA. The area in the square with dotted line in (A) is magnified in (A'), (B'), and (C').

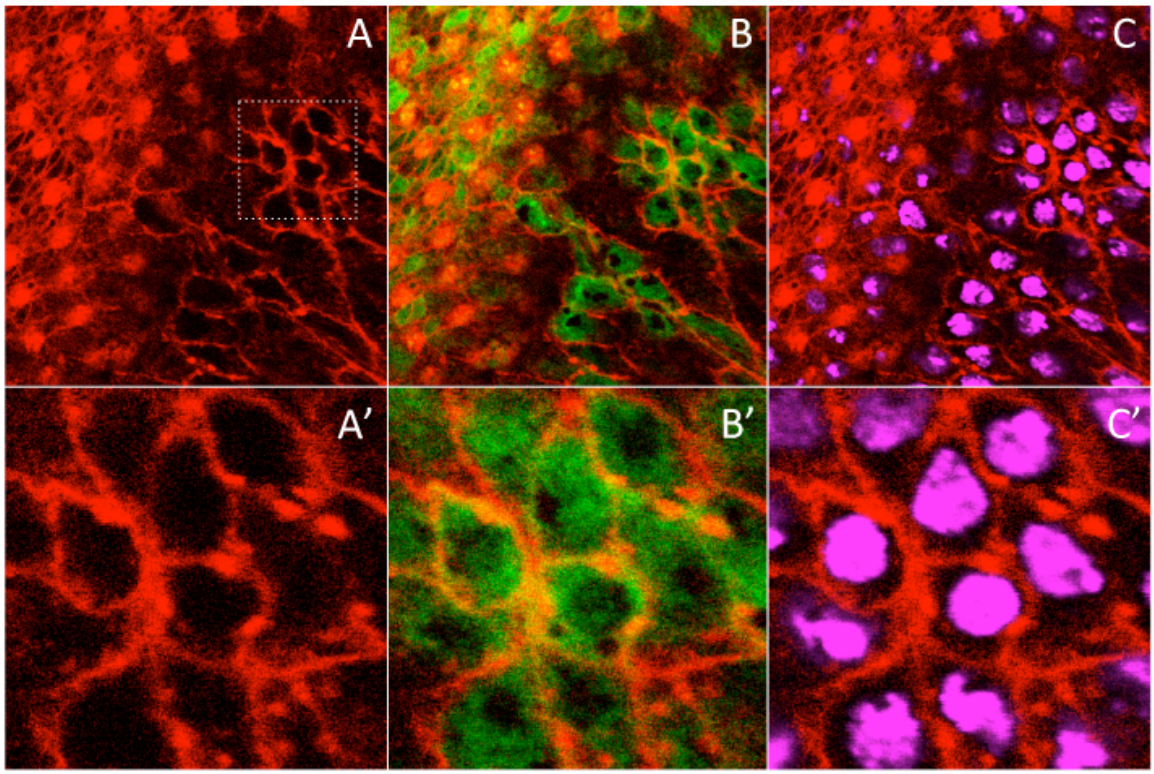

Figure 4-17. Localization of 6xMyc-LqfRa exon 6Δ2.

Confocal images of eye discs overexpressing *UAS-6Xmyc-lqfRa exon 6Δ2* with *Act5C-gal4* driver. (A) is phalloidin (red) staining showing the plasma membrane. (B) is a merged image with both phalloidin (red) and 6XMyc-LqfRa exon 6 Δ2 (green). (C) is a merged image with both phalloidin (red) and TO-PRO3 (purple), which stains DNA. The area in the square with dotted line in (A) is magnified in (A'), (B'), and (C').

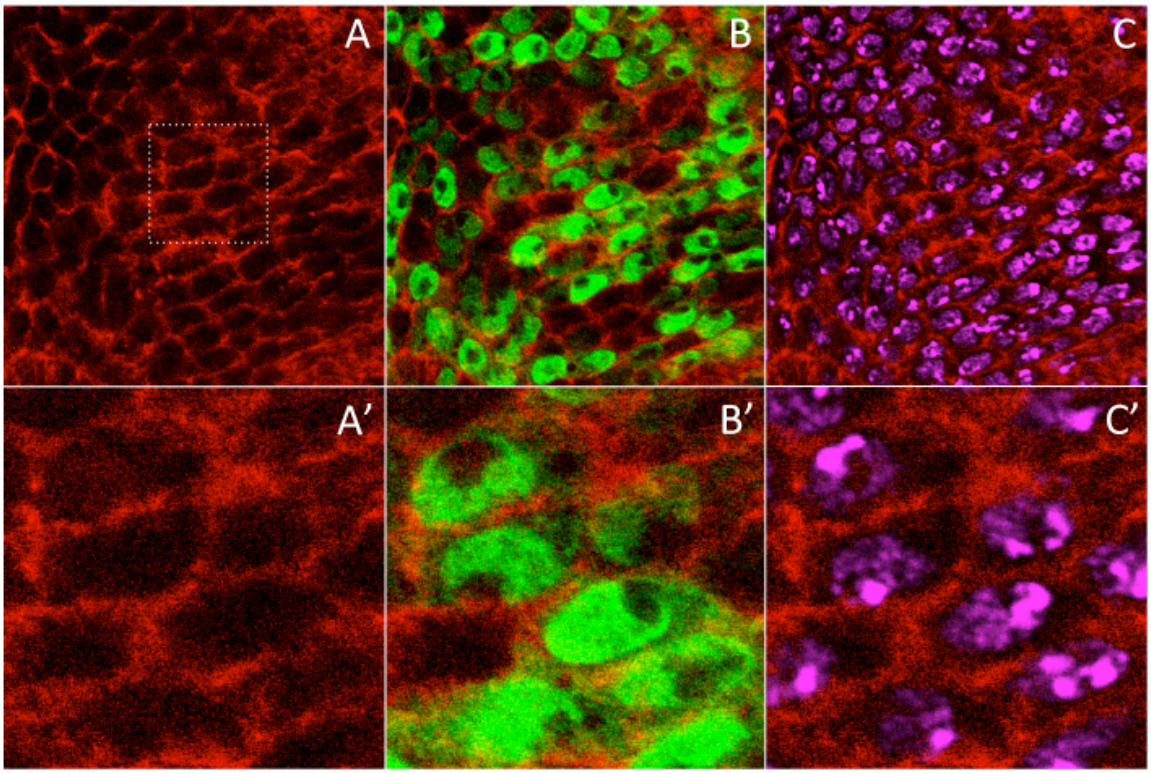

Figure 4-18. Localization of 6xMyc-LqfRa exon 6Δ3.

Confocal images of eye discs overexpressing *UAS-6Xmyc-lqfRa exon 6Δ3* with *Act5C-gal4* driver. (A) is phalloidin (red) staining showing the plasma membrane. (B) is a merged image with both phalloidin (red) and 6XMyc-LqfRa exon 6 Δ3 (green). (C) is a merged image with both phalloidin (red) and TO-PRO3 (purple), which stains DNA. The area in the square with dotted line in (A) is magnified in (A'), (B'), and (C').

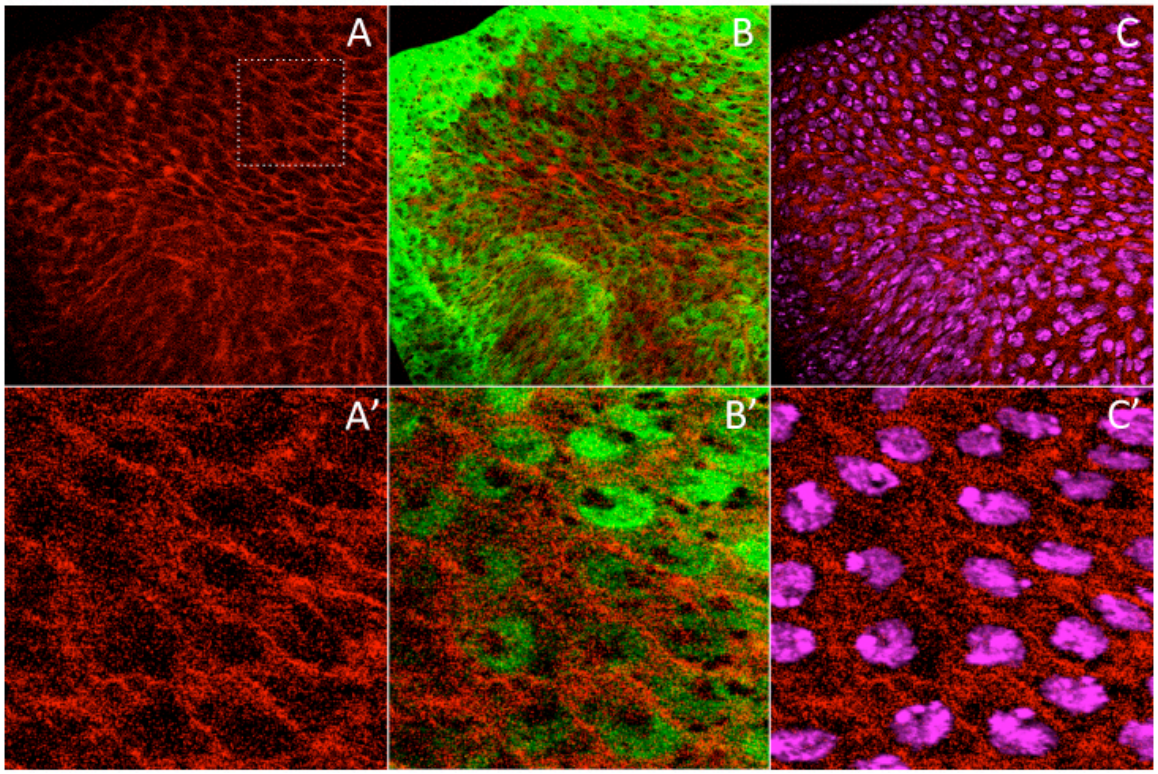

Figure 4-19. Localization of 6xMyc-LqfRa exon 6Δ4.

Confocal images of eye discs overexpressing *UAS-6Xmyc-lqfRa exon 6Δ4* with *Act5C-gal4* driver. (A) is phalloidin (red) staining showing the plasma membrane. (B) is a merged image with both phalloidin (red) and 6XMyc-LqfRa exon 6 Δ4 (green). (C) is a merged image with both phalloidin (red) and TO-PRO3 (purple), which stains DNA. The area in the square with dotted line in (A) is magnified in (A'), (B'), and (C').

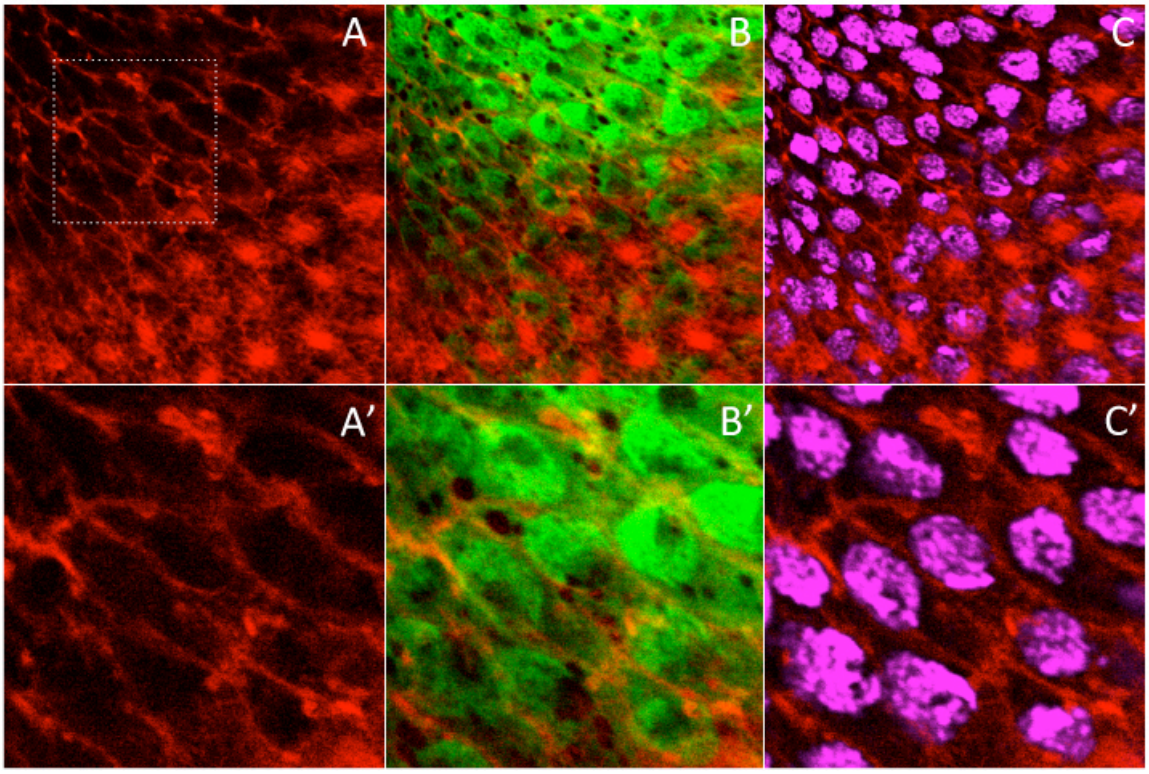

Figure 4-20. Localization of 6xMyc-LqfRa exon 6Δ5.

Confocal images of eye discs overexpressing *UAS-6Xmyc-lqfRa exon 6Δ5* with *Act5C-gal4* driver. (A) is phalloidin (red) staining showing the plasma membrane. (B) is a merged image with both phalloidin (red) and 6XMyc-LqfRa exon 6 Δ5 (green). (C) is a merged image with both phalloidin (red) and TO-PRO3 (purple), which stains DNA. The area in the square with dotted line in (A) is magnified in (A'), (B'), and (C').

Overexpressed *lqfRa* full length or exon 6 rescue the "elevated E-cadherin" phenotype

In previous sections, I showed that the morphological phenotype of *lqfR* null mutants has been rescued by overexpressing *lqfRa exon 6* as well as *lqfRa* full-length. Is the "elevated E-cadherin" phenotype shown in *lqfR* null clones in eye discs also rescued by the overexpression of these constructs? This is interesting question because, although there is evidence consistent with the idea, it is formally possible that the increased E-cadherin is due to the function of Golgi Epsin, but not relevant to the essential function of *lqfR*. If this is true, I would expect to see increased E-cadherin complex levels in *lqfR* null clones with the overexpression of *lqfRa exon 6* but not with *lqfRa* full-length. However, if the E-cadherin level change in *lqfR* null clones is functionally relevant, I would expect to see no difference in E-cadherin level inside or outside of *lqfR* null clones with the overexpression of either *lqfRa* full-length or *lqfRa exon 6*. The results support the latter. When *lqfRa* full-length cDNA or *lqfRa exon 6* was overexpressed with *Act5C-gal4*, there was no obvious difference in the E-cadherin level or Armadillo level inside and outside of *lqfR* null clones (Fig. 4-21). With the overexpression of the full-length or exon 6, the *lqfR* null clone size was also dramatically increased indicating that the proliferation defect of *lqfR* null mutants is also rescued (Fig. 4-21). These results again support that *lqfR exon 6* is necessary and sufficient for the function *lqfR*.

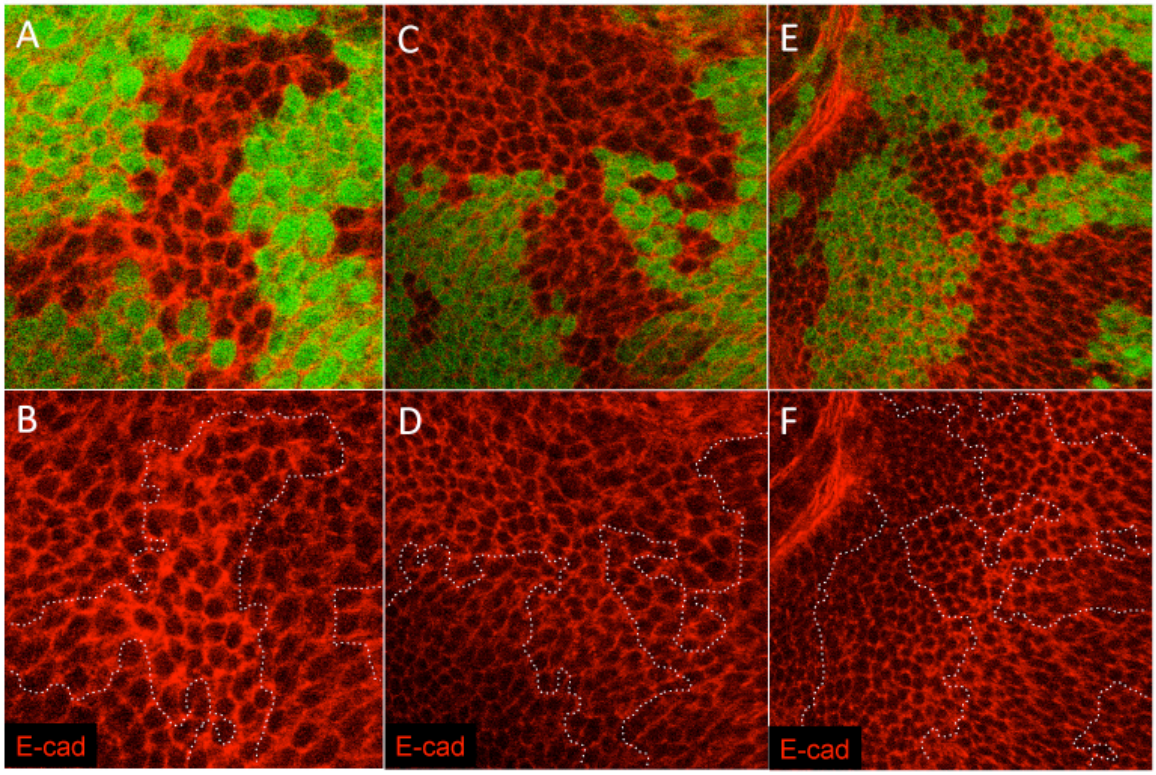

Figure 4-21. Overexpression of either full-length or exon 6 of *lqfRa* rescues increased E-cadherin in *lqfR* null clones.

Confocal images of eye discs with $lqfR^{\Delta 117}$ clones without a construct (A, B), with *lqfRa* full-length (C, D), or with *lqfRa* exon 6 (E, F) immunostained with anti-E-cadherin (red). $lqfR^{\Delta 117}$ clones are marked with the absence of GFP (green). Note that E-cadherin levels are normally increased at the morphogenetic furrow due to increased gene expression as shown in (B). Dotted line in (B) marks the clone borders.
Genotypes are:
(A, B) *ey-flp;; FRT82B* $lqfR^{\Delta 117}$*/FRT82B ubi-gfp ;*
(C, D) *ey-flp; Act5C-gal4 UAS-lqfRa (12)/+ ; FRT82B* $lqfR^{\Delta 117}$*/FRT82B ubi-gfp ;*
(E, F) *ey-flp; Act5C-gal4 UAS-lqfRa exon 6 (8)/+ ; FRT82B* $lqfR^{\Delta 117}$*/FRT82B ubi-gfp.*

lqfR is not required for Wingless secretion

Wntless is a transmembrane protein required for Wingless ligand secretion. Wntless binds to Wingless at the Golgi and brings it to the plasma membrane for Wingless secretion. After releasing Wingless ligand, Wntless is endocytosed to early endosomes and recycled back to the Golgi. The retrograde trafficking of Wntless from early endosome to the Golgi is essential for Wingless secretion, and the retromer complex plays an essential role in this retrograde Wntless trafficking. In mutant clones with strong loss-of-function alleles of genes encoding retromer complex proteins, Wingless ligand cannot be secreted but accumulated inside of the cell (Belenkaya et al, 2008; Franch-Marro et al, 2008; Port et al, 2008).

It has been shown previously that Golgi Epsin also plays a role in endosome-to-Golgi retrograde trafficking (Saint-Pol et al, 2004). It has also been shown that the retromer complex and clathrin-mediated Golgi Epsin activity work together to accomplish the retrograde trafficking of cargos (Popoff et al, 2007). If this is generally true, *Drosophila* Golgi Epsin LqfR may turn out to be essential for Wingless secretion as the retromer complex is. If so, it may also explain the observation that *lqfR* is required for the Wingless signaling pathway.

As a positive control, I repeated what has been done with $vps35^{E42}$, a strong loss-of-function allele for a component of the retromer complex, to show that the retromer complex is essential for Wingless secretion (Popoff et al, 2007). Mitotic clones homozygous for $vps35^{E42}$ generated in wing discs indeed accumulated Wingless (Fig. 4-22A, A'). However, Wingless did not accumulate in $lqfR^{\Delta 117}$ clones in wing discs (Fig. 4-

22B, B'). This result indicates that the Wingless signal defect in *lqfR* null clones is not due to Wingless secretion defect originating from the function of LqfR as Golgi Epsin.

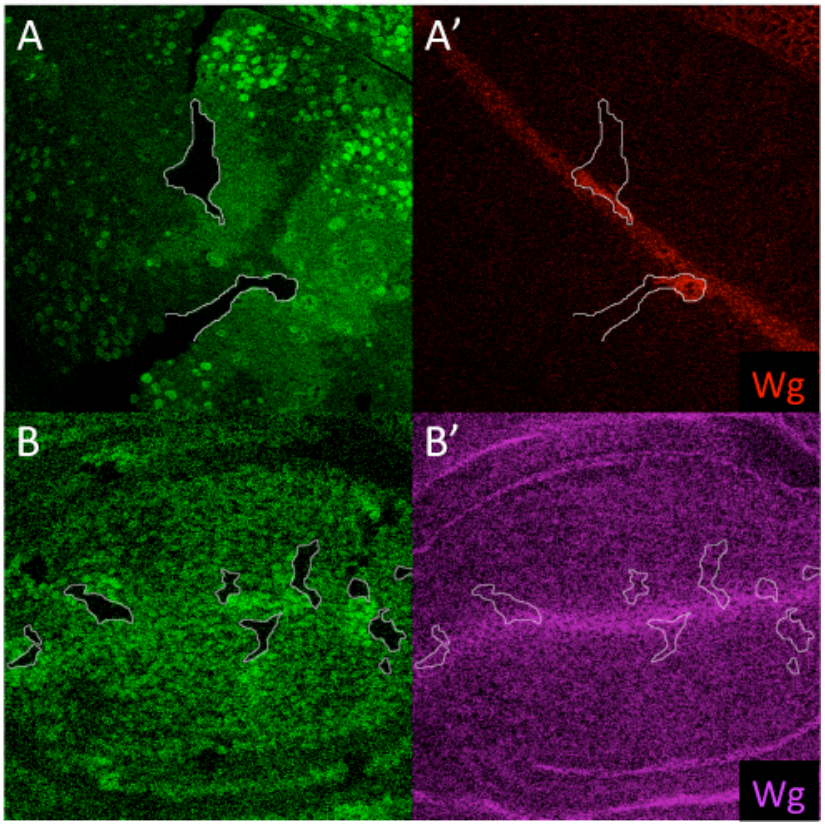

Figure 4-22. *lqfR* is not required for Wingless secretion.

Confocal images of wing discs with *vps35*^{E42} clones (A, A') or *lqfR*^{s117} clones (B, B') immunostained with anti-Wingless (red in A', purple in B'). *lqfR*^{s117} clones are marked with the absence of GFP. White lines marks clone boundary.
Genotypes are:
(A, A') *hs-flp; FRT42D vps35*^{E42}*/FRT42D ubi-gfp ;*
(B, B') *hs-flp;; FRT82B lqfR*^{s117}*/FRT82B ubi-gfp*.

4.3 DISCUSSION AND FUTURE DIRECTION

In this chapter, I show that *lqfR* has a role in the Wingless signaling pathway. Genetic interactions between *lqfR* and two key players in the Wingless signaling pathway, *wingless* and *armadillo*, suggest that *lqfR* has a role in the context of this signaling pathway. Consistent with this, one of the Wingless targets in this context, *dachsous*, is not expressed in *lqfR* null cells as much as in wild type neighbors. Increased levels of E-cadherin and Armadillo at the plasma membrane in *lqfR* null clones as well as the known function of Golgi Epsin in other model organisms led me to hypothesize that LqfR functions as *Drosophila* Golgi Epsin to regulate E-cadherin trafficking from the Golgi to endosomes for E-cadherin degradation bypassing the plasma membrane. Consistent with this hypothesis, LqfR associates with E-cadherin, Armadillo, and α-catenin in fly embryo.

However, the structure/function analysis identifies that the essential function of *lqfR* comes from its *exon 6*. This result argues against my original hypothesis that LqfR functions as the Golgi Epsin because exon 6 is not conserved in Golgi epsin genes in other species including yeast, nematode, fish, and mammals. One of the characteristics of LqfR that suggests its role as a *Drosophila* Golgi Epsin is its localization at the Golgi. However, *lqfR exon 6* encodes a protein that localizes in the nucleus but not at the Golgi. These findings indicate that LqfR does not need to be at the Golgi for its function, arguing against the idea that the essential function of LqfR is due to its role as a clathrin adapter at the Golgi. In fact, I could not identify any genes required for vesicular trafficking from the dominant modifier screen shown in chapter 3. Because Golgi Epsin requires clathrin for its function and the phenotypes of mutants in genes for clathrin-

dependent trafficking proteins are usually sensitive to the amount of *chc (clathrin heavy chain)* expression (Banks et al, 2011; Eun et al, 2007), I also specifically tested if *chc* mutants dominantly enhance the *lqfR* hypomorphic phenotype. *lqfR* did not genetically interact with *chc* (data not shown).

The nuclear localization of 6xMyc-tagged LqfR exon 6 is an unexpected result. LqfR was localized at the Golgi when eye discs were immunostained with anti-LqfR antibody. The antibody was generated with a bacterially expressed antigen encoded with *lqfR exons 1-5*. LqfR exons 1-5 include the ENTH domain and peptide motifs for interactions with proteins at the Golgi for clathrin-coated vesicle formation. Exons 1-5 are encoded in both LqfRa and LqfRb. Because LqfRb is much highly expressed compared to LqfRa in eye discs (Fig. 2-1C), a large portion of the Golgi localized protein detected by anti-LqfR antibody is probably LqfRb. However, LqfRa is also expressed in the eye disc although the level is lower than LqfRb. So, it is unlikely that LqfRa exist in the nucleus, but is not detected due to the low expression level. One possibility is that LqfRa is post-translationally cleaved to produce LqfR exon 6, which resembles Tel2. Anti-LqfR antibody cannot detect this hypothetical protein. To test this idea, a new antibody has to be generated with epitopes in LqfR exon 6.

The exon 6 in *lqfR* is a single homolog of a gene called *tel2,* which is conserved well from yeast to human (see chapter 1 section 1.4). *tel2* is essential in all model organisms tested including yeast, nematode, and mouse. Thus it seems likely that *Drosophila* also needs to have *tel2* function. Like *tel2*, *lqfR* is essential. *exon 6* is necessary and sufficient for all essential function of *lqfR,* which supports the idea that *lqfR*, in addition to encoding Golgi Epsin, also encodes Tel2. The role of Golgi Epsin encoded by *lqfR* in *Drosophila* needs to be investigated further. However, it is clear that

Golgi Epsin function from *lqfR* is not essential for any developmental functions. The *lqfR exon 6* was not predicted as a homolog of *tel2* when I began to study *lqfR* probably due to low amino acid sequence similarity. When Tel2 amino acid sequences from different species were aligned with what exon 6 encodes, identical residues range about 11~19% (11% between fly and *S. cerervisiae,* 19% between fly and human). However, a recent crystal structure of yeast Tel2 (Takai et al, 2010) allowed much more accurate prediction of the critical amino acid sequence similarities that allowed identification of *lqfR exon 6* as a *tel2* homolog. With this reason, I will call this gene *lqfR*/*tel2* now.

Does Tel2 function in the context of the Wingless signaling pathway? In a genetic study using *C. elegans*, *tel2* phenocopied *wnt* and *frizzled* (Moser et al, 2009), although further study to understand the relationship between *tel2* and the Wnt signaling pathway is remained to be done.

I showed that *lqfR*/*tel2* has a role in the Wingless signaling pathway. If LqfR/Tel2 does not function as Golgi Epsin, what would be the molecular mechanism of LqfR/Tel2 function in the Wingless signaling pathway? One interesting observation is that Armadillo levels are increased in the *lqfR* null cells, yet the transcriptional activity of Armadillo is decreased. I initially hypothesized that increased Armadillo is a secondary effect of the increased E-cadherin level at the plasma membrane due to a trafficking defect caused by the absence of Golgi Epsin. However, it is also possible that increased Armadillo in the cytosol resulted in the increase of E-cadherin (Yanagawa et al, 1997). Then, what would be the driving force that increases Armadillo at the cytoplasm and decreases its transcriptional activity in *lqfR* null cells? I present two alternative hypotheses, which are not mutually exclusive each other.

One hypothesis is that *lqfR*+ is required for nuclear access or retention of Armadillo (Fig. 4-25A). First, LqfR may be required for facilitating nuclear import of Armadillo. Unlike many nuclear proteins, Armadillo does not have a known nuclear localization signal. An *in vitro* nuclear localization assay with permeabilized cells provided evidence that β-catenin enters the nucleus by itself (Fagotto et al, 1998). Nuclear import of purified β-catenin was not inhibited by NLS peptides. β-catenin nuclear import did not require other proteins such as importins/karyopherins or nuclear binding partner TCF/LEF-1 (Fagotto et al, 1998). However, when the purified β-catenin was mixed with a cytosol preparation, its nuclear import was inhibited (Fagotto et al, 1998), which leaves open the possibility that β-catenin nuclear import *in vivo* is regulated in a manner different from that suggested by the *in vitro* results. To my knowledge, it has not been proven that β-catenin requires no other factors for its nuclear entry *in vivo*. Tel2 protein consists of a HEAT repeat structure and most resembles importin-β (Anderson et al, 2008; Takai et al, 2010). My preliminary *in vitro* interaction data shows that LqfR interacts directly with Armadillo and α-catenin. LqfR exon 6 is primarily localized to the nucleus and peri-nuclear region. I also observed that LqfRa-GFP with GFP in its C-terminal side is localized at the peri-nuclear region as well as at the Golgi. Further co-localization experiments showed LqfR-GFP signal near the nucleus is punctate with a pattern similar to that of a nuclear pore marker. Further experiments should be done to test this idea. An assay to test for reduced nuclear localization of Armadillo in *lqfR* null cell should be done. It would be also interesting to test if LqfR/Tel2 is similar to importins in its molecular characteristics such as binding to RAN and nuclear pore

components. Alternatively, LqfR may also be required for stabilization of Armadillo in the nucleus. Nuclear export of β-catenin is important in the Wingless signal activity control. The adenomatous polpyposis coli (APC) protein plays an important role in β-catenin nuclear export with its nuclear export signal at the C-terminus (Rosin-Arbesfeld et al, 2000). Nuclear localization of Armadillo is also regulated by Axin and dTCF/Pangolin, which tether and stabilize Armadillo at the cytosol and in the nucleus, respectively (Tolwinski & Wieschaus, 2001). Perhaps LqfR/Tel2 facilitates or inhibits the interaction between Armadillo and these proteins to increase nuclear localization of Armadillo. Somewhat analogous to this idea, yeast Tel2 has been shown to be required for Tel1 recruitment to the sites of DNA damage, which is a crucial step for Tel1 function (Anderson et al, 2008). If Armadillo needs LqfR/Tel2 function to be stabilized in the nucleus, *lqfR/tel2* null clones should show reduced level of nuclear Armadillo compared to their wild type neighbors, but will not show importin-like molecular characteristics. It would be interesting to characterize the function of *lqfR/tel2* further if this were the case.

Another hypothesis to explain increased Armadillo levels at the plasma membrane and decreased transcriptional activity is that the Notch signaling pathway requires *lqfR/tel2* function and the role of *lqfR/tel2* in the Wingless signaling pathway is through the Notch signaling pathway (Fig. 4-25B). From the genetic screen for dominant modifiers of *lqfR/tel2* hypomorphic eye phenotype, *Delta* and *neuralized* were identified as dominant enhancers (chapter 3). This suggests functional relationship between *lqfR/tel2* and the Notch signaling. Synergistic effects between the Wingless pathway and the Notch pathway for proliferation and cell survival has been recognized (Fre et al, 2009; Giraldez & Cohen, 2003). It has also been shown that Notch associates with

Armadillo and antagonizes the Armadillo transcriptional activity (Hayward et al, 2005). A recent report showed that Notch inhibits β-catenin accumulation by associating with β-catenin for lysosomal degradation in stem and progenitor cells (Kwon et al, 2011). Consistent with this, I observed that the level of Notch receptor increases at the plasma membrane near apical region in *lqfR/tel2* null cells (Fig. 4-23). The level difference is most significant near the morphogenetic furrow where Notch is normally upregulated. I further tested the Notch target gene expression in *lqfR/tel2* null clones and observed the expression level of *mβ-lacZ* increases. Ahead of the morphogenetic furrow, *mβ-lacZ* expression was limited at the D/V midline with the highest level at the center and weaker toward margins. In $lqfR^{\Delta 117}$ clones generated in eye discs, *mβ-lacZ* expression level was higher compared to wild type neighbor cells (Fig. 4-24). However, the gradient of the *mβ-lacZ* expression level was still maintained in $lqfR^{\Delta 117}$ clones and clones far away from where *mβ-lacZ* was expressed did not express it, either (Fig. 4-24). Further careful tests are required to understand the specific role of LqfR/Tel2 in the Notch signaling pathway. It would also be interesting to identify functional relationship between *lqfR/tel2* and its dominant enhancers *Delta* and *neuralized*.

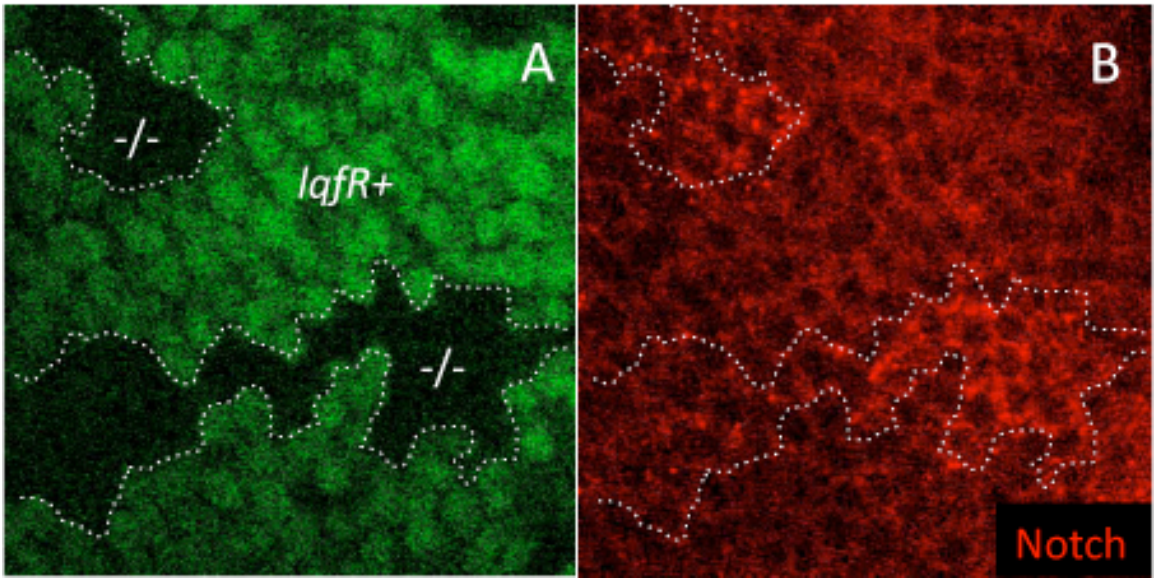

Figure 4-23. Increased Notch in *lqfR* null clones.

Confocal images of an apical plane in an eye disc with $lqfR^{\Delta 117}$ clones immunostained with anti-Notch intracellular domain antibody (red). $lqfR^{\Delta 117}$ clones are marked with the absence of GFP (A). Dotted lines in (A) and (B) denote a clone boundary. Genotype is: *ey-flp;;FRT82B* $lqfR^{\Delta 117}$*/FRT82B ubi-gfp*.

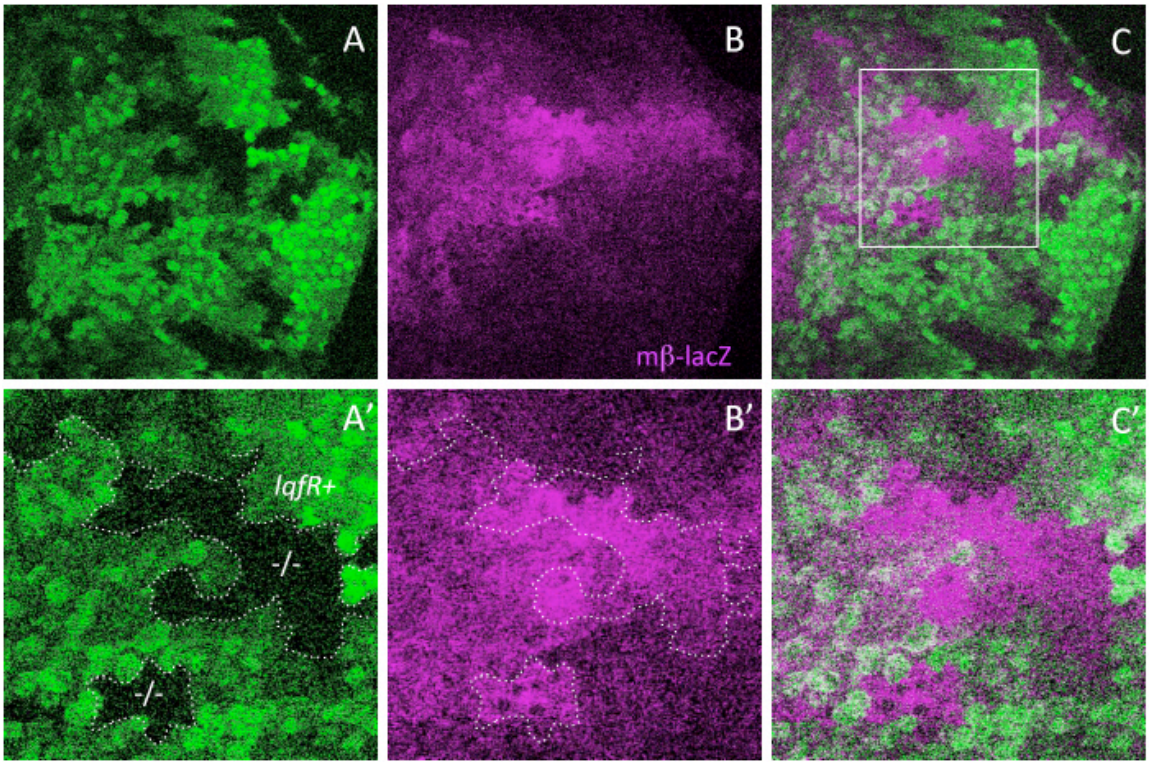

Figure 4-24. Increased *mβ-lacZ* expression in *lqfR* null clones.

Confocal images of an eye disc with Notch target gene expression marker *mβ-lacZ* and $lqfR^{\Delta 117}$ clones. *mβ-lacZ* expression level was visualized by immunostaining with anti-β-galactosidase shown in purple. $lqfR^{\Delta 117}$ clones are marked with the absence of GFP (A). Dotted line in (A') and (B') denote a clone boundary. White square in (C) denotes magnification of the area in (A', B', and C'). (C) and (C') are merged images of (A, B) and (A', B'), respectively. Genotype is: *ey-flp ; mβ-lacZ/+ ; FRT82B* $lqfR^{\Delta 117}$*/FRT82B ubi-gfp*.

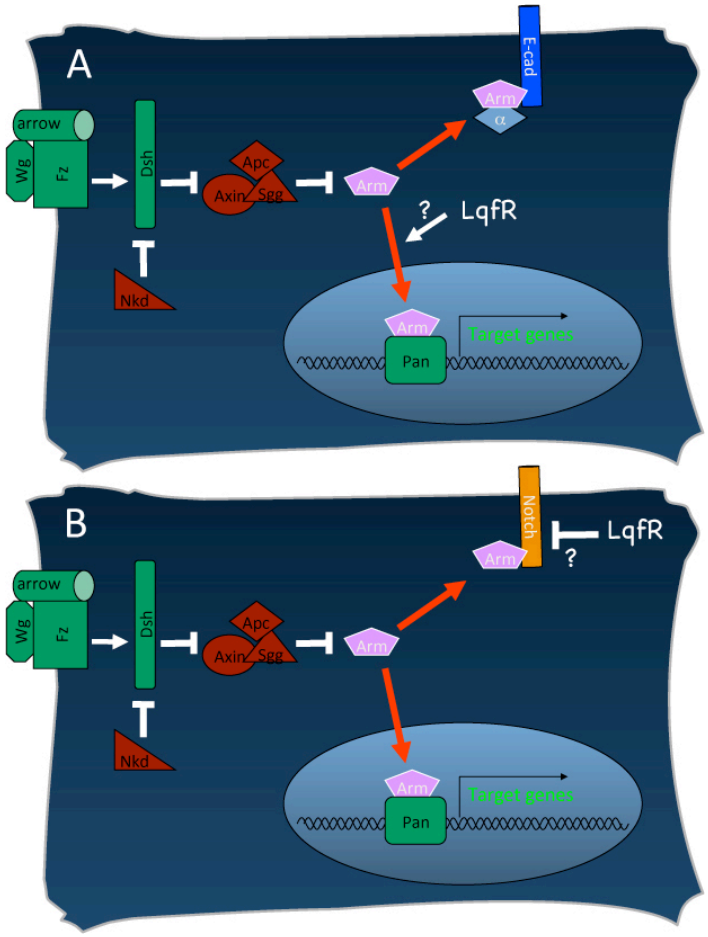

Figure 4-25. Two new models for the molecular function of LqfR.

Model (A) is based on the hypothesis that LqfR might be required for nuclear import or retainment of Armadillo. Increased E-cadherin level in *lqfR* null clones may be an indirect effect due to increased Armadillo at the cytoplasm. Model (B) is based on the observation that Notch antagonizes the Wingless signaling activity by binding to Armadillo and facilitating its lysosomal degradation (Hayward et al, 2005; Kwon et al, 2011).

Appendix. Materials and Methods

A.1 Materials and Methods in Chapter 2

Drosophila strains

Flies were grown on standard media at 25 °C unless indicated otherwise. Strains from our laboratory's collection, Bloomington Stock Center and individual stock collections:

OregonR

w^{1118}

yw

w; Sco/CyO; MKRS/TM6B

MKRS/TM2, ry

TM3, ry Sb Δ2-3/Df(3R)C7, ry

$lqfR^{P3685}$ *ry/TM3 (FBal0009480)*

$mirror^{P69Df7}$*/TM6B (FBal0083801; from D. Strutt)*

$l(3)SG62^{1}$*/TM6B (FBal0011236)*

InR^{339}*/TM3 (FBal0122080; from H. McNeill)*

W; Act5C-gal4/CyO (FBti0012293)

Df(3R)hh/TM3i (FBab0002795)

w; ro-gfp (on chr. 2) (Overstreet et al., 2004)

yw, hs-flp (FBti0015982)

w; FRT82B (FBti0002074)

w; FRT 82B Pw^+ (FBti0001288)

yw; FRT82B GMR-hid (FBti0012710) l(3)CL-R^l (FBal0098712)/TM6B

w; FRT82B arm-lacZ (FBti0023291)/TM6B

w; FRT82B ubi-gfp (FBti0012695)/TM6B

FRT40A (FBti0002071) ubi-gfp/CyO.

Strains generated for this work:

w; FRT82B $lqfR^{P3685}$/TM6B

w; FRT82B $lqfR^{\Delta 117}$/TM6B

yw, ey-flp; Sco/CyO; FRT82B GMR-hid l(3)CL-R^l/TM6B

w; $mirr^{P69Df7}$ FRT82B $lqfR^{\Delta 117}$/TM6B

yw, ey-flp; FRT82B arm-lacZ/TM6B

w; ro-gfp/CyO; FRT82B $lqfR^{\Delta 117}$/TM6B

yw, hs-flp; FRT82B arm-lacZ/TM6B

yw, ey-flp; Sco/CyO; FRT82B/TM6B

w; FRT82B InR^{339}/TM6B

w; FRT82B InR^{339} $lqfR^{\Delta 117}$/TM6B

w; $glqfR^+$/CyO; FRT82B $lqfR^{\Delta 117}$/TM6B

w; $glqfR^{\Delta ENTH}$/CyO; FRT82B $lqfR^{\Delta 117}$/TM6B

w; Act5C-gal4/CyO; FRT82B $lqfR^{\Delta 117}$/TM6B

w; UAS_t-lqfRa-gfp/CyO; FRT82B $lqfR^{\Delta 117}$/TM6B

w; UAS_t-$lqfRa^{\Delta ENTH}$-gfp/CyO; FRT82B $lqfR^{\Delta 117}$/TM6B

yw, ey-flp; Sco/CyO, gfp; FRT82B GMR-hid l(3)CL-R^l

w; Act5C-gal4, UAS_t-lqfRa-gfp/CyO; FRT82B $lqfR^{\Delta 117}$/TM6B.

Molecular biology

Standard procedures were used for molecular biology. PCR of genomic DNA was performed on DNA from single flies as described (Overstreet et al, 2003). Restriction enzymes and phosphatases were from New England BioLabs, Boehringer Mannheim, and Promega Biotech. Automated fluorimetric DNA sequencing was performed in the DNA analysis facility of the Institute for Cell and Molecular Biology (ICMB), at UT Austin.

Generation of *lqfR$^{\Delta 117}$* by P element mobilization

lqfR$^{\Delta 117}$ was generated by imprecise excision of the *Pry+* element in *lqfR^{P3685}* (Spradling et al, 1999). Approximately 200 crosses were set up where males of the genotype *lqfR^{P3685} ry/TM3, ry, Δ2–3* were crossed with *MKRS/TM2, ry* females. Male progeny in which the *Pry+* element had excised were identified as *ry*-flies, whose genotype was *Pry+$^{\Delta ry}$/TM2, ry* or *Pry+$^{\Delta ry}$/MKRS*. The *Pry+$^{\Delta ry}$* chromosome from a single male progeny from each cross was amplified and balanced by crossing the males individually to *MKRS/TM2, ry* females and stocks were generated from the *Pry+$^{\Delta ry}$/TM2, ry* progeny. Of the 200 *Pry+$^{\Delta ry}$* chromosomes, 9 were lethal in trans to *Df(3R)hh*. Molecular lesions in 3 of the 9 chromosomes were defined using a variety of PCR primers flanking the *Pry+* insertion site to amplify genomic DNA, and determining the DNA sequence of the PCR products whose sizes were smaller than that obtained from wild-type template DNA. *lqfR$^{\Delta 117}$* was chosen for further genetic analysis because its

molecular lesion suggested that it might be a null allele of *lqfR* that did not affect surrounding genes.

Transgene construction and transformation

P element transformation of *yw* flies was performed in our laboratory using standard techniques, or by Genetic Services (Sudbury, MA) or Genetivision (Houston, TX).

pglqfR+

This plasmid is Casper 4 (Thummel and Pirrotta, 1992) containing an ~ 11.5 kb fragment of *D. melanogaster* genomic DNA that includes a wild-type *lqfR* gene: sequences from – 663 to + 10,905 relative to the *lqfR* translation start site. BAC clone 30J14 (BacPac Resources) was restricted with *Bss HII* and the fragments ligated into containing an *Asc I* site *pBAscI* (Chen & Fischer, 2000) restricted with *Asc I*. As the *lqfR* gene should be contained in an ~ 12 kb *Bss HII* fragment, a plasmid with a 12 kb insert (*pGenBssHII*) was identified and DNA sequence determination of one end of the insert confirmed its identity. The fragment was modified in order to eliminate most of the upstream gene, *CG13850*, as follows. *pGenBssHII* was used a PCR template to amplify an ~ 1.1 kb fragment containing genomic DNA sequences from 663 bp 5′ to the insertion point of the P*ry*+ element in $lqfR^{P3685}$, to a downstream *Aat II* site. The PCR primers used were 5′-GCGGCCGCCCACACGCTGCAAGAGACCAC-3′ and 5′-AAACTTGGGGCGTGGG-3′. The amplified product was subcloned in *pGEMT* (Promega), its DNA sequence determined, and a plasmid with the correct sequence,

pGEM-5′gE2, was identified. An ~ 1.1 kb *Not I–Aat II* fragment of *pGEM-5′gE2* and an ~ 9 kb *Aat II–Hind III* fragment of *pGenBssHII* were ligated together into *pBSKSII* restricted with *Not I* and *Hind III*, to generate *pBSKSII-gE2*. An ~ 11.5 kb *Not I–Kpn I* fragment from this plasmid was ligated into *pCasper4* restricted with *Not I* and *Kpn I*.

pglqfR$^{\Delta ENTH}$

This plasmid is *pglqfR+* with a 461 bp deletion that includes exon 2, intron 2, and part of exon 3, and results in removal of 122 codons, corresponding to amino acids V^{32}–R^{153} (Tweedie et al., 2009). The deletion was introduced by generating two PCR amplification products using *pglqfR+* as a template, and then by using both products simultaneously as templates for PCR. The first amplification product (~ 420 bp) contains a restriction site unique to the *glqfR+* DNA fragment (*Avr II*) and the deletion: it began at the *Avr II* site in intron 1 and included all the rest of intron 1 and also exon 3 sequences corresponding to the deletion breakpoint. The 3′ PCR primer included the deletion, meaning that in addition to intron 1 sequences, it contained 25 bp of xon 3 sequence, corresponding to the deletion breakpoint. The two primers used were 5′-GTACACCTTTCCTAGGGCTTATCTCGAA-3′ (5′, contains *Avr II* site) and 5′-TTCGCCTTTTTGCTGCAAGTGGGAACGAAGTCATTG-3′ (3′ENTH1, contains deletion). The second amplification product (~ 1000 bp) contains a restriction site, *Sgr A1*, unique to the *lqfR+* genomic fragment: it began at the deletion breakpoint in exon 3 and included sequences up to the downstream *Sgr AI* site. The primers used were 5′-CCCACTTGCAGCAAAAAGGCGAAGAAGAACAAGGAC-3′ (5′ENTH2) and 5′-

AATCGTTCGCCGGCGTGG-3′ (3′ENTH2, includes *Sgr AI* site). Both amplification products were used together as the template for PCR amplification with the primers 5′ENTH1 and 3′ENTH2. As the two template DNAs have 23 bp of overlapping DNA, they will anneal and generate an ~ 1.5 kb *Avr II–Sgr AI* template fragment that includes the deletion. The amplified product was restricted with *Avr II* and *Sgr AI*, and the resulting fragment was ligated into *pglqfR*+ restricted with the same enzymes. The DNA sequence of the insertion was confirmed.

pUAS$_t$-lqfRa

Because we initially had difficulty obtaining a full-length *lqfRa* cDNA using RT-PCR, this plasmid was generated using cDNA for exons 1-5, and genomic DNA for exon 6. A DNA fragment containing exons 1–5 was generated using reverse transcribed (Superscript II and oligo-dT, Invitrogen) total embryo RNA (prepared with TriReagent, Ambion) as the template for PCR with primers 5′-GCAAAACAGTCAGAAAACGGCAC and 5′-AGCCTTGGAACGCCGCAAAG. The amplified product was cloned into *pGEMT* and its DNA sequence confirmed to generate *pGEM-epsinR-I*. Next, a 450 bp fragment containing 5′ sequences of *lqfR* cDNA with an Asc I just upstream of the ATG and an in-frame *Pml I* site just downstream, was generated by PCR using *pGEM-epsinR-I* as template, the mutagenic primer 5′-GGCGCGCCATGCACGTGGTGGATAAATTCATC, and a primer that includes the downstream *Bso BI* site. The amplified product was ligated into *pGEM* and its sequence confirmed, to generate *pGEM-E2Epml*. A 450 bp *Asc I–Bso BI* fragment of *pGEM-E2Epml* and a 900 bp *Bso BI–Eco RI* fragment were ligated together into *pBSKSII*

restricted with *Asc I* and *Eco RI* to generate *pBSKSII-D-epsinR-I*. Next, an in-frame *Sap I* site was introduced at the 3′ end of exon 5 (there is a *Sap I* site that spans the exon 5/6 splice junction) by using *pBSKSII-D-epsinR-I* as template for PCR with the primers 5′-TTGCTGAAGACTGCCACGC and 5′-CGAAGATGTGCCAATGAAAATGTATC. The 355 bp amplification product was ligated into *pGEM* and its sequence confirmed to generate *pGEM-e2Sap*. Using genomic DNA as template, 5′ sequences of exon 6 (1.85 kb) were amplified with the primers 5′-TTGCTGAAGACTGCCACGC and 5′-CGAAGATGTGCCAATGAAAATGTATC, and 3′ sequences of exon 6 (1.9 kb) were amplified with the primers 5′-CCTTTGTGGGAATCTTGTAATG and 5′-ATACCTGGAATACAATGGCTTC. Each amplified fragment was ligated into *pGEMT* and its sequence was confirmed, to generate *pGEM-exon6A* and *pGEM-exon6B*, respectively. A 350 bp *Eco RI–Sap I* fragment of *pGEM-e2Sap*, and a 900 bp *Sap I–Bam HI* fragment of *pGEM-exon6A*, were ligated together into *pBSKSII* restricted with *Eco RI* and *Bam HI* to generate *pBS-exon6RIBam*. A 400 bp *Bam HI–Bts I* fragment of *pGEM-exon6A* and a 1.35 kb *Bts I–Xho I* fragment of *pGEM-exon6B* were ligated together into *pBSKSII* restricted with *Bam HI* and *Xho I* to generate *pBS-exon6BamXho*. A 1.4 kb *Asc I–Eco RI* fragment of *pBS-D-epsinR-I*, a 1.25 kb *Eco RI–Bam HI* fragment of *pBS-exon6RIBAM*, and a 1.75 kb fragment of *pBS-exon6BamXho* were ligated together into *pBSKSII* restricted with *Asc I* and *Xho I* to generate *pBS-D-epsinRa*. A 4.4 kb *Bss HII* fragment of *pBS-D-epsinRa* was ligated into *pUAS$_t$-XA* (Huang and Fischer-Vize, 1996) restricted with *Asc I* to generate *pUAS$_t$-lqfRa*.

pUAS$_t$-lqfRa-gfp

A 3′ fragment of *lqfRa* cDNA extending from the *Sna BI* site to the final codon was amplified by PCR using *pUAS$_t$-lqfRa* as a template, and the primers 5′-TTTACGTAAAATACGAAAATATT-3′ and 5′-ACGCGTGGCAGCCTGTTCCATG-3′. An in-frame *Mlu I* site was inserted in place of the stop codon using a mutagenic primer. After ligation into *pGEMT*, the fragment sequence was verified, and then the subclone was restricted with *Sna BI* and *Not I* to generate a 450 bp fragment. A 3.7 kb *Asc I–Sna BI* fragment of *pUAS$_t$-lqfRa* was isolated, and ligated with the 450 bp *Sna BI–Not I* fragment into *pBSKSII* restricted with *Asc I* and *Not I*, to generate *pBS-lqfRaMlu*. *gfp* sequences were amplified as an *Mlu I–Asc I* fragment using *p8036* (Harris and Macdonald, 2001) as a template, and the primers 5′-ACGCGTAGTAAAGGAGAAG-3′ and 5′-GGCGCGCCTTATTTGTATAGTTCATCC-3′, which generated a stop codon prior to the *Asc I* site. The amplified product was ligated into *pGEM* and its sequence verified, to generate *pGEM-3'GFP*. A 750 bp *Mlu I–Not I* fragment containing *gfp* was isolated from *pGEM-3'GFP* and ligated into *pBS-lqfRaMlu* restricted with *Mlu I* and *Not I*, to generate *pBS-lqfRa-gfp*. A 5.0 kb *Bss HII* fragment of *pBS-lqfRa-gfp* was isolated and ligated into *pUAS$_t$-XA* restricted with *Asc I*, to generate *pUAS$_t$-lqfRa-gfp*.

pUAS$_t$-lqfRa$^{\Delta ENTH}$-gfp

A central fragment of *lqfRa*, extending from just 3′ of the ENTH domain to the downstream *Bgl II* site, was generated by PCR using *pUAS$_t$-lqfRa* as the template and primers 5′-CATATGAAGTACATCGGCATGAGCAG-3′ and 5′-

AGATCTGTAGCCGTTGTGGCTGC-3′. An in-frame *Nde I* site was inserted at the 5′-end of the fragment by the 5′-primer. The amplification product was ligated into *pGEMT*, and its sequence verified to generate *pGEM-4*. A 900 bp *Eco RI–Nhe I* fragment of *pGEM-4* and a 4.2 kb *Nhe I–Asc I* fragment of *pUAS$_t$-lqfRa-gfp* were ligated together into *pBSKSII* resticted with *Eco RI* and *Asc I* to generate *pBS-E2aΔENTH-gfp*. A 4.7 kb *Asc I* fragment of *pBS-E2aΔENTH-gfp* was ligated into *pUAS$_t$* restricted with *Asc I* to generate *pUAS$_t$-lqfRa$^{\Delta ENTH}$-gfp*.

Generation of anti-LqfR

The antigen used to generate anti-LqfR is present in both the a and b isoforms, and contains amino acids M^{1}-F^{396} (Tweedie et al., 2009), which includes the ENTH domain and some downstream amino acids (exons 1–4 and part of exon 5). The plasmid used to express the antigen in bacteria, *pET28a-comm*, was generated as follows. A 5′ *lqfRa* fragment extending from the start codon to the downstream *Eco RI* site was generated by PCR using *pBS-D-epsinRa* (see above) as the template and the primers 5′-CATATGGTGCATAAATTCATC-3′ and the T7 promoter primer (Promega). The 5′ primer inserted an *Nde I* site just upstream of the start codon. The amplification product was ligated into *pGEM*, and its sequence verified to generate *pGEM-comm*. A 1.3 kb *Nde I–Eco RI* fragment of *pGEM-comm* was ligated into *pET28a* restricted with *Nde I* and *Eco RI* to generate *pET28a-comm*. The LqfR protein was expressed in *E. coli* Codon-Plus RIL (Stratagene), and the purified using Chelating Sepharose Fast Flow (Pharmacia Biotech). The purified antigen was sent to Pocono Farms (Canadensis, Pa) where it was used to generate antisera in two guinea pigs.

Protein blots

Eye disc protein extracts were generated and analyzed on Western blots as described (Chen et al., 2002). The blots were probed with anti-LqfR diluted 1:1000 and mouse mAbE7 (anti-β-tubulin from DSHB) at 1:100. Secondary antibodies were HRP-anti-guinea pig (Jackson) at 1:20,000, and HRP-anti-mouse (Santa Cruz Biochemicals) at 1:500. The results were quantified using Adobe Photoshop CS3.

Analysis of mRNA by RT-PCR

The structure of *lqfRa* was demonstrated by the following experiment. Total RNA was purified from adult flies or third instar larval eye disc using TriReagent (Ambion), and reverse transcribed using Superscript II RT (Invitrogen), 5 μg RNA, 2 pmole primer (5′-GTCTTCTACCCAGTCG-3′; from exon 6). The RT reaction (2 μl) was used as a template for PCR using Platinum PCR Supermix (Invitrogen), and the following primers: 5′-GGAGGAGGCGGCGGTGGCAGC-3′(exon 3) and 5′-TTGATTCAGCAATGCGGCATACTC-3′(exon 6). After agarose gel electrophoresis, a band of the expected size for a *lqfRa* template was obtained (1146 bp) and its structure confirmed by DNA sequencing. A no-RT control reaction yielded a light band of the size expected for a genomic DNA template (1623 bp). The structure of *lqfRb* (that exon 5 is connected to exon 7) was demonstrated by a 3′-RACE experiment (Ambion 3′-RACE kit) and the primer 5′-TTCGCCATCGCCGTCTACTTCC-3′ (exon 5). The DNA sequence of the resulting 1.5 kb was determined and it contained *lqfRb* sequences from 1.3 kb downstream of the start codon through the 3′-UTR.

Analysis of eyes, wings, nota, and salivary glands

Plastic sectioning of adult eyes was as described (Tomlinson and Ready, 1987). Scanning electron microscopy of adult eyes was peformed on flies dehydrated in 70%, 100% ethanol, critical point dried in CO_2, and coated with Pt/Pd, using a Zeiss Supra 40VP FE-SEM. For immunostaining, eye discs were fixed in PEMS and antibody incubations and washes were in PBST (Fischer-Vize et al, 1992). Primary antibodies used were: guinea pig anti-LqfR (1:100), mouse monoclonal anti-p120 (1:200; Calbiochem), rabbit anti-Lava (1:2000; from John Sisson, UT Austin), rat monoclonal anti-Elav (1:9; Developmental Studies Hybridoma Center [DSHB]), mouse monoclonal anti-β-gal (1:50, DSHB). Secondary antibodies (1:500; Molecular Probes) were: Alexa^{633}-anti-mouse, Alexa^{568}-anti-mouse, Alexa^{633}-anti-rat, Alexa^{633}-anti-rabbit, Alexa^{488}-anti-mouse, Alexa^{488}-anti-guinea pig. TOPRO-3 (Molecular Probes) was used 1:1000. Salivary glands were dissected in PBS, fixed in 4% paraformaldehyde (45 min), incubated with Alexa^{568}-phalloidin (used 1:10 in PBST; Molecular Probes) and mounted in Vectashield (Vector). Wings were dehydrated in 70% ethanol and mounted in DPX (Fluka). Wing and eye sections were photographed with a Zeiss Axioplan equipped with an Axiocam HRc. Nota and eyes were photographed in whole flies using an Olympus SZX12 microscope equipped with a SPOT idea (Diagnostic Instruments) digital camera. Immunofluorescent tissues were photographed with a Leica TCSSP2 or SP2AOBS confocal microscope. Images were processed with Adobe Photoshop.

Calculation of rhabdomere size and box plots

In order to control for differential effects of sample preparation on rhabdomere size between samples, the relative sizes of wild-type and mutant rhabdomeres were assessed in individual mosaic facets. Using images of eye sections in Adobe Photoshop, the number of pixels in each mutant rhabdomere and each wild-type rhabdomere of R1–R6 was counted, and the average of each was calculated, and used to compute the ratio of mutant/wild-type size. This ratio represents each data point (n). Box plots were calculated using GraphPad Prism software (version 3.0).

Quantitation of Lqf$^{\Delta ENTH}$ protein produced by genomic transgene

The data for these experiments is in Fig. 2-13. In order to determine if the LqfR$^{\Delta ENTH}$ protein produced by the *glqfR$^{\Delta ENTH}$* transgene accumulates to similar levels as the endogenous LqfR protein, we first used anti-LqfR to visualize the proteins in blots of extracts from animals with one copy of the transgene and one copy of the endogenous gene. The signals from the endogenous LqfR proteins and the LqfR$^{\Delta ENTH}$ proteins were of similar strength. However, the polyclonal antibody was generated to amino acids 1–396 of LqfR, and the ENTH-less protein is missing 122 of those amino acids. The polyclonal antibody signal could rely heavily on antibodies that recognize epitopes missing in the ENTH-less protein. If so, the similar signal strength obtained for the LqfR and LqfR$^{\Delta ENTH}$ bands could indicate that LqfR$^{\Delta ENTH}$ is present at much higher levels that LqfR. In order to determine whether anti-LqfR gives similar signals for similar amounts of LqfR or LqfR$^{\Delta ENTH}$ proteins, we used anti-GFP to detect LqfRa-GFP and LqfRa$^{\Delta ENTH}$-GFP relative to tubulin, and then used anti-LqfR to detect the same proteins. We found that the signal strength for the full-length and ENTH-less proteins, relative to tubulin, was similar for

both anti-GFP and anti-LqfR. Thus, we conclude that in flies containing the *glqfR*$^{\Delta ENTH}$ transgene, LqfR$^{\Delta ENTH}$ is not grossly overexpressed relative to endogenous LqfR. Protein blots were performed as described above, with rabbit anti-GFP at 1:1000 (Cell Signaling Technologies), and HRP-conjugated anti-rabbit secondary at 1:10,000 (Amersham). The secondary for detecting tubulin was HRP-conjugated anti-mouse at 1:5000 (Sigma).

A.2 Materials and Methods in Chapter 3

Drosophila strains

Flies were grown on standard media at 25 °C unless indicated otherwise. Strains from our laboratory's collection, Bloomington Stock Center and individual stock collections:

lqf^{FDD9} *lqfR*^{P}*/TM6B*

lqf^{L71} *lqfR*^{P}*/TM6B*

hrs^{D28}*/CyO; lqfR*^{P}*/TM6B*

chico^{1}*/CyO; lqfR*^{P}*/TM6B*

Tor$^{\Delta P}$*/CyO; lqfR*^{P}*/TM6B*

aux^{e727} *lqfR*^{P}*/TM6B*

aux^{ed136} *lqfR*^{P}*/TM6B*

vn^{G115} *lqfR*^{P}*/TM6B*

vn^{11749} *lqfR*^{P}*/TM6B*

hh^{rJ413} *lqfR*^{P}*/TM6B*

hh^{AC} $lqfR^{P}$/TM6B

fng^{rG554} $lqfR^{P}$/TM6B

fng^{13} $lqfR^{P}$/TM6B

$syx5^{AR113}$/CyO; $lqfR^{P}$/TM6B

ras^{e1b} $lqfR^{P}$/TM6B

wg^{l-17}/CyO; $lqfR^{P}$/TM6B

dpp^{s-11}/CyO; $lqfR^{P}$/TM6B

InR^{05545} $lqfR^{P}$/TM6B

gig^{109} $lqfR^{P}$/TM6B

$syx1A_{s}^{229}$ $lqfR^{P}$/TM6B

$egfr^{1sla}$/CyO; $lqfR^{P}$/TM6B

w; fng^{rG554} $lqfR^{P}$/TM6B

w; fng^{13} $lqfR^{P}$/TM6B

w; FRT82B $lqfR^{P}$/TM6B

w; FRT82B $lqfR^{\Delta 117}$/TM6B

yw, ey-flp; FRT82B arm-lacZ/TM6B

yw, ey-flp; FRT82B ubi-gfp/TM6B

w; EGUF; FRT82B GMR-hid l(3)CL-R^{1}/TM6B

w; EGUF/CyO; FRT82B GMR-hid l(3)CL-R^{1}/TM6B

yw, ey-flp; Sco/CyO; FRT82B GMR-hid l(3)CL-R^{1}/TM6B

ru h th cu sr e/TM6B

ru h th cu sr e Pr/TM6B

al dp b c px/CyO

Strains from the dominant modifier screen:

w; FRT82B lqfR^{P} 356/TM6B

w; FRT82B lqfR^{P} 358/TM6B

w; FRT82B lqfR^{P} 3513/TM6B

w; FRT82B lqfR^{P} 3514/TM6B

w; FRT82B lqfR^{P} 3515/TM6B

w; FRT82B lqfR^{P} 3518/TM6B

w; FRT82B lqfR^{P} 362/TM6B

w; FRT82B lqfR^{P} 368/TM6B

w; FRT82B lqfR^{P} 3610/TM6B

w; FRT82B lqfR^{P} 372/TM6B

w; FRT82B lqfR^{P} 37102/TM6B

w; FRT82B lqfR^{P} 37104/TM6B

w; FRT82B lqfR^{P} 37105/TM6B

w; FRT82B lqfR^{P} 37106/TM6B

w; FRT82B lqfR^{P} 37107/TM6B

w; FRT82B lqfR^{P} 387/TM6B

w; FRT82B lqfR^{P} 388/TM6B

w; FRT82B lqfR^{P} 389/TM6B

w; FRT82B lqfR^{P} 3813/TM6B

w; FRT82B lqfR^{P} 386/TM6B

w; FRT82B lqfR^{P} 3223/TM6B

w; FRT82B lqfR^{P} 3234/TM6B

w; FRT82B lqfR^{P} D29/TM6B

w; FRT82B lqfR^{P} A56/TM6B

w; FRT82B lqfR^{P} C13/TM6B

w; FRT82B lqfR^{P} D110/TM6B

w; FRT82B lqfR^{P} D191/TM6B

w; FRT82B lqfR^{P} E85/TM6B

w; FRT82B lqfR^{P} E92/TM6B

w; FRT82B lqfR^{P} F2/TM6B

w; FRT82B lqfR^{P} F91/TM6B

w; FRT82B lqfR^{P} G2/TM6B

w; FRT82B lqfR^{P} G47/TM6B

w; FRT82B lqfR^{P} G54/TM6B

w; FRT82B lqfR^{P} G61/TM6B

w; FRT82B lqfR^{P} G115/TM6B

w; FRT82B lqfR^{P} G127/TM6B

w; FRT82B lqfR^{P} G136/TM6B

w; FRT82B lqfR^{P} G146/TM6B

w; FRT82B lqfR^{P} G156/TM6B

w; FRT82B lqfR^{P} G160/TM6B

w; FRT82B lqfR^{P} G161/TM6B

w; FRT82B lqfR^{P} G207/TM6B

w; FRT82B lqfR^{P} G215/TM6B

w; FRT82B lqfR^{P} H49/TM6B

w; FRT82B lqfR^{P} I28/TM6B

w; FRT82B lqfR^{P} I36/TM6B

w; FRT82B lqfR^{P} I63/TM6B

w; FRT82B lqfR^{P} I75/TM6B

w; FRT82B lqfR^{P} I81/TM6B

w; FRT82B lqfR^{P} J5/TM6B

w; FRT82B lqfR^{P} J8/TM6B

w; FRT82B lqfR^{P} J33/TM6B

w; FRT82B lqfR^{P} K31/TM6B

Deficiency lines for mapping the Chromosome 2 complementation group:

Df(2L)Exel6001 (BL#7488) : Complemented

Df(2L)Exel6002 (BL#7489) : Complemented

Df(2L)Exel6003 (BL#7490) : Did not complement

Df(2L)Exel6004 (BL#7491) : Did not complement

Df(2L)Exel6005 (BL#7492) : Complemented

Df(2L)Exel6007 (BL#7493) : Complemented

Df(2L)Exel6008 (BL#7494) : Complemented

Df(2L)Exel6009 (BL#7495) : Complemented

Df(2L)Exel6010 (BL#7496) : Complemented

Df(2L)Exel6011 (BL#7497) : Complemented

Df(2L)Exel6012 (BL#7498) : Complemented

Df(2L)Exel6013 (BL#7499) : Complemented

Df(2L)Exel6014 (BL#7450) : Complemented

Df(2L)Exel6015 (BL#7501) : Complemented

Df(2L)Exel6018 (BL#7504) : Complemented

Df(2L)Exel6021 (BL#7505) : Complemented

Df(2L)Exel6022 (BL#7506) : Complemented

Df(2L)Exel6024 (BL#7507) : Complemented

Df(2L)Exel6025 (BL#7508) : Complemented

Df(2L)Exel7005 (BL#7775) : Complemented

Df(2L)Exel7006 (BL#7776) : Complemented

Df(2L)Exel7007 (BL#7778) : Complemented

Df(2L)Exel8005 (BL#7779) : Complemented

Deficiency lines for mapping Group 1:

Df(3R)Dl-KX23 (BL#2411) : Did not complement

Df(3R)e-N19 (BL#2425) : Complemented

Df(3R)Cha7 (BL#3011) : Complemented

Df(3R)Dl-BX12 (BL#3012) : Did not complement

Df(3R)H-B79 (BL#4962) : Complemented

Df(3R)Cha1a (BL#5599) : Complemented

Df(3R)Cha9 (BL#5600) : Did not complement

Df(3R)LK19-1 (BL#6375) : Complemented

Df(3R)BSC43 (BL#7413) : Complemented

Df(3R)ED5815 (BL#9208) : Complemented

Df(3R)BSC141 (BL#9501) : Complemented

Deficiency lines for mapping Group 2:

Df(3R)Antp17 (BL#1842) : Complemented

Df(3R)Dsx48 (BL#1872) : Complemented

Df(3R)p-XT103 (BL#1962) : Complemented

Df(3R)Tpl10 (BL#1990) : Complemented

Df(3R)M-Kx1 (BL#3128) : Complemented

Df(3R)2-2 (BL#3688) : Complemented

Df(3R)BSC24 (BL#6756) : Did not complement

Df(3R)BSC38 (BL#7080) : Complemented

Df(3R)ED5156 (BL#8965) : Complemented

Df(3R)ED5147 (BL#8967) : Complemented

Df(3R)ED5331 (BL#9203) : Complemented

Df(3R)BSC464 (BL#24968) : Complemented

Df(3R)BSC506 (BL#25010) : Complemented

Deficiency lines for mapping Group 3:

Df(3R)Antp17 (BL#1842) : Complemented

Df(3R)Dsx48 (BL#1872) : Complemented

Df(3R)p-XT103 (BL#1962) : Did not complement

Df(3R)Tpl10 (BL#1990) : Complemented

Df(3R)M-Kx1 (BL#3128) : Complemented

Df(3R)2-2 (BL#3688) : Complemented

Df(3R)BSC24 (BL#6756) : Complemented

Df(3R)BSC38 (BL#7080) : Complemented

Df(3R)ED5156 (BL#8965) : Complemented

Df(3R)ED5147 (BL#8967) : Complemented

Df(3R)ED5331 (BL#9203) : Complemented

Df(3R)BSC464 (BL#24968) : Complemented

Df(3R)BSC506 (BL#25010) : Did not complement

Deficiency lines for mapping Group 4:

Df(3R)ED10838 (BL#9485) : Complemented

Df(3R)BSC677 (BL#26529) : Complemented

Df(3R)ED6085 (BL#8923) : Complemented

Df(3R)ED6096 (BL#8684) : Complemented

Df(3R)BSC619 (BL#25694) : Complemented

Df(3R)Exel6194 (BL#7673) : Complemented

Df(3R)Exel6195 (BL#7674) : Complemented

Df(3R)Exel9013 (BL#7991) : Complemented

Df(3R)Exel6196 (BL#7675) : Complemented

Df(3R)Exel6197 (BL#7676) : Complemented

Df(3R)ED6187 (BL#9347) : Complemented

Df(3R)ED6220 (BL#9211) : Did not complemented

Df(3R)BSC461 (BL#24965) : Complemented

Df(3R)Exel6202 (BL#7681) : Complemented

Df(3R)BSC522 (BL#25050) : Complemented

Df(3R)Exel6203 (BL#7682) : Complemented

Df(3R)BSC321 (BL#24909) : Complemented

Df(3R)BSC140 (BL#9500) : Complemented

Df(3R)BSC495 (BL#24999) : Complemented

Df(3R)BSC496 (BL#25000) : Complemented

Df(3R)ED6255 (BL#9210) : Complemented

Df(3R)BSC497 (BL#25001) : Complemented

Df(3R)BSC567 (BL#25390) : Complemented

Df(3R)Exel6210 (BL#7688) : Complemented

Df(3R)BSC806 (BL#27378) : Complemented

Df(3R)Exel6212 (BL#7690) : Did not complemented

Df(3R)ED6310 (BL#8961) : Did not complemented

Df(3R)BSC501 (BL#25005) : Did not complemented

Df(3R)BSC846 (BL#27919) : Did not complemented

Df(3R)ED6316 (BL#8925) : Did not complemented

Df(3R)BSC547 (BL#25075) : Complemented

Df(3R)BSC620 (BL#25695) : Complemented

Df(3R)BSC502 (BL#25006) : Complemented

Df(3R)Exel6214 (BL#7692) : Complemented

Df(3R)BSC503 (BL#25007) : Complemented

Df(3R)BSC504 (BL#25008) : Complemented

Df(3R)Exel8194 (BL#7918) : Complemented

Df(3R)ED6346 (BL#24142) : Complemented

Df(3R)BSC749 (BL#26847) : Complemented

Df(3R)BSC793 (BL#27365) : Complemented

Df(3R)ED6361 (BL#24143) : Complemented

Df(3R)ED50003 (BL#24516) : Complemented

Deficiency strains for mapping Group 6:

Df(3R)ED5577 (BL#8029) : Complemented

Df(3R)BSC486 (BL#24990) : Complemented

Df(3R)ED5612 (BL#9088) : Complemented

Df(3R)Exel6169 (BL#7648) : Complemented

Df(3R)ED5622 (BL#8959) : Complemented

Df(3R)BSC616 (BL#25691) : Complemented

Df(3R)ED5644 (BL#9090) : Complemented

Df(3R)ED10555 (BL#23714) : Complemented

Df(3R)BSC635 (BL#26505) : Complemented

Df(3R)BSC741 (BL#26839) : Complemented

Df(3R)BSC515 (BL#25019) : Complemented

Df(3R)BSC728 (BL#26580) : Complemented

Df(3R)Exel7328 (BL#7983) : Complemented

Df(3R)ED10639 (BL#9481) : Complemented

Df(3R)Exel6270 (BL#7737) : Complemented

Df(3R)BSC748 (BL#26846) : Complemented

Df(3R)ED5780 (BL#8104) : Did not complemented

Df(3R)BSC790 (BL#27362) : Did not complemented

Df(3R)BSC510 (BL#25014) : Complemented

Deficiency lines for mapping Group 7:

Df(3R)ED10838 (BL#9485) : Complemented

Df(3R)ED6052 (BL#9480) : Complemented

Df(3R)ED6058 (BL#24140) : Complemented

Df(3R)Exel6186 (BL#7665) : Complemented

Df(3R)BSC677 (BL#26529) : Did not complemented

Df(3R)BSC678 (BL#26530) : Did not complemented

Df(3R)ED6076 (BL#8962) : Did not complemented

Df(3R)BSC805 (BL#27377) : Did not complemented

Df(3R)ED6085 (BL#8923) : Complemented

Df(3R)ED6096 (BL#8684) : Complemented

Df(3R)BSC619 (BL#5694) : Complemented

Df(3R)Exel6194 (BL#7673) : Complemented

Df(3R)Exel6195 (BL#7674) : Complemented

Df(3R)Exel9013 (BL#7991) : Complemented

Df(3R)Exel9014 (BL#7992) : Complemented

Df(3R)Exel6196 (BL#7675) : Complemented

Df(3R)Exel6197 (BL#7676) : Complemented

Df(3R)ED6187 (BL#9347) : Complemented

Df(3R)ED6220 (BL#9211) : Complemented

Df(3R)BSC461 (BL#24965) : Complemented

Df(3R)Exel6202 (BL#7681) : Complemented

Df(3R)BSC522 (BL#25050) : Complemented

Df(3R)Exel6203 (BL#7682) : Complemented

Df(3R)BSC321 (BL#24909) : Complemented

Df(3R)BSC140 (BL#9500) : Complemented

Df(3R)BSC495 (BL#24999) : Complemented

Df(3R)BSC496 (BL#25000) : Complemented

Df(3R)ED6255 (BL#9210) : Complemented

Df(3R)BSC497 (BL#25001) : Complemented

Df(3R)BSC567 (BL#25390) : Complemented

Df(3R)Exel6210 (BL#7688) : Did not complement

Df(3R)BSC806 (BL#27378) : Complemented

Df(3R)BSC501 (BL#25005) : Complemented

Df(3R)BSC547 (BL#25075) : Complemented

Df(3R)BSC620 (BL#25695) : Complemented

Df(3R)BSC502 (BL#25006) : Complemented

Df(3R)Exel6214 (BL#7692) : Complemented

Df(3R)BSC503 (BL#25007) : Complemented

Df(3R)BSC504 (BL#25008) : Complemented

Df(3R)Exel8194 (BL#7918) : Complemented

Df(3R)ED6346 (BL#24142) : Complemented

Df(3R)BSC749 (BL#26847) : Complemented

Df(3R)BSC793 (BL#27365) : Complemented

Df(3R)ED6361 (BL#24143) : Complemented

Df(3R)ED50003 (BL#24516) : Complemented

Deficiency lines for mapping Group 8:

Df(3R)Antp17 (BL#1842) : Complemented

Df(3R)Dsx48 (BL#1872) : Complemented

Df(3R)p-XT103 (BL#1962) : Complemented

Df(3R)Tpl10 (BL#1990) : Complemented

Df(3R)M-Kx1 (BL#3128) : Complemented

Df(3R)2-2 (BL#3688) : Complemented

Df(3R)BSC24 (BL#6756) : Complemented

Df(3R)BSC38 (BL#7080) : Complemented

Df(3R)ED5156 (BL#8965) : Complemented

Df(3R)ED5147 (BL#8967) : Complemented

Df(3R)ED5331 (BL#9203) : Complemented

Df(3R)BSC464 (BL#24968) : Complemented

Df(3R)BSC506 (BL#25010) : Complemented

Df(3R)BSC507(BL#25011) : Complemented

Df(3R)BSC476 (BL#24980) : Complemented

Df(3R)ED5429 (BL#8919) : Complemented

Df(3R)by10 (BL#1931) : Complemented

Df(3R)ED5330 (BL#9077) : Complemented

Df(3R)BSC549 (BL#25077) : Complemented

Df(3R)ME15 (BL#1518) : Complemented

Df(3L)K-2 (BL#26260) : Complemented

Df(3L)ED5017 (BL#8102) : Complemented

Df(3L)BSC554 (BL#25669) : Complemented

Df(3L)ED230 (BL#8089) : Complemented

Df(3L)BSC451 (BL#24955) : Complemented

Df(3L)BSC223 (BL#9700) : Complemented

Df(3L)BSC284 (BL#23669) : Complemented

Df(3L)ED4978 (BL#8101) : Complemented

Df(3L)BSC418 (BL#24922) : Complemented

Df(3L)BSC419 (BL#24923) : Complemented

Df(3L)BSC553 (BL#25116) : Complemented

Df(3L)BSC449 (BL#24953) : Complemented

Df(3L)BSC797 (BL#27369) : Did not complement

Df(3L)BSC452 (BL#24956) : Complemented

Df(3L)BSC563 (BL#25721) : Complemented

Df(3L)BSC796 (BL#27368) : Complemented

Df(3L)Exel6136 (BL#7615) : Complemented

Df(3L)BSC734 (BL#26832) : Complemented

Df(3L)rdgC-co2 (BL#2052) : Complemented

Df(3L)BSC830 (BL#27912) : Complemented

Df(3L)BSC445 (BL#24949) : Complemented

Df(3L)alpha1S1 (BL#25396) : Complemented

Df(3L)Exel6135 (BL#7614) : Complemented

Df(3L)XS705 (BL#5584) : Complemented

Df(3L)Exel9007 (BL#7942) : Complemented

Df(3L)ED228 (BL#8086) : Complemented

Df(3L)BSC220 (BL#9697) : Complemented

Df(3L)BSC775 (BL#27347) : Complemented

Df(3L)ED4710 (BL#8100) : Complemented

Df(3L)ED4685 (BL#8099) : Complemented

Df(3L)ED4674 (BL#8098) : Complemented

Df(3L)BSC561 (BL#25123) : Complemented

Df(3L)BSC555 (BL#25117) : Complemented

Df(3L)ED4606 (BL#8078) : Complemented

Loss-of-function mutant alleles used for gene identification:

Group 1: Dl^{9P}/*TM3*, Dl^{B2}/*TM6C*

Group 2: $neur^{1}$/*TM3*, $neur^{11}$/*TM6B*

Group 3: pyd^{1} (BL#562), $pyd^{1\,4}$/*TM2* (BL#8850)

Group 4: stg^{4}/*TM3* (BL#2500)

Group 6: $Mps1^{1}$/*TM3* (Christian Lehner)

Group 7: $lsn^{5F8\text{-}3}$/*TM6B* (Andreas Bergmann)

Complementation test

For the complementation group on chromosome 2, mutant chromosomes were balanced with CyO and third chromosomes *FRT82B* $lqfR^{P}$/*TM6B* were replaced with the wild-type chromosome. 5 males and 5 females from each member of the group were crossed. For third chromosome complementation test, all stocks were crossed to have the genotype of: *glqfR+* ; *FRT82B* $lqfR^{P}$ *Enhancer-/TM6B*. 5 males and females from each stock were crossed and incubated at 25^{O}C.

Validation assay

For the validation of dominant modification of the $lqfR^{P}$ eye phenotype, 5 males and females were crossed in a fresh vial and incubated at 23^{O}C for a day. The next day,

adults were removed from the original vial to a new fresh vial. Both the old vial with only embryos and the new vial with adults were incubated at 23^{O}C. I kept doing this until I have 5 vials each was given to adult flies to lay eggs for a day. Adult progeny from each vial were counted.

Meiotic mapping

Meiotic mapping has been performed as explained in Fig. 3-6.

Clonal analysis using larval eye discs

Eye discs were dissected from late third instar larvae in PBS and fixed in 4% paraformaldehyde for 45 minutes. After that eye discs were incubated in PBS + 0.1% Triton X-100 (PBT) for 15 minutes. This step was repeated twice more. Primary antibody diluted in PBT was incubated overnight at 4^{O}C. After 2 washes in PBT for 10 minutes each, secondary antibody was incubated for 3 hours at 4^{O}C. After 2 washes in PBT for 10 minutes, eye discs were mounted in Vectashield. The slides were examined under a confocal microscope. Rat anti-CyclinE antibody (from Helena Richardson) was diluted to 1:250 in PBT + 5% non-fat dry milk. For clone marker, *ubi-gfp* or *arm-lacZ* was used. When *arm-lacZ* was used, mouse anti-β-galactosidase (DSHB, 40-1a) was diluted to 1:50 in PBT. Rabbit anti-activated caspase 3 (Cell signaling, #9661) was diluted to 1:20. Secondary antibodies with fluorescence tags were diluted to 1:200.

A.3 MATERIALS AND METHODS IN CHAPTER 4

Drosophila strains

Flies were grown on standard media at 25 °C unless indicated otherwise. Strains from our laboratory's collection, Bloomington Stock Center and individual stock collections:

w;; FRT82B lqfR$^{\Delta 117}$/TM6B

ey-flp;; FRT82B ubi-gfp/TM6B

shotgun-lacZ/CyO; FRT82B lqfR$^{\Delta 117}$/TM6B

wg^{l-17}/CyO-gfp; FRT82B lqfR^{P}/TM6B

wg^{l-8}/CyO-gfp; FRT82B lqfR^{P}/TM6B

arm^{3}/FM7;; FRT82B lqfR$^{\Delta 117}$/TM6B

arm^{8}/FM7;; FRT82B lqfR$^{\Delta 117}$/TM6B

dachsous-lacZ/CyO; FRT82B lqfR$^{\Delta 117}$/TM6B

w; ds^{38K}/CyO-gfp; FRT82B lqfR$^{\Delta 117}$/TM6B

Act5C-gal4 UASt-lqfRa-gfp/CyO; MKRS/TM6B

Act5C-gal4 UASt-lqfR^{ENTH}-gfp/CyO; MKRS/TM6B

EGUF; FRT82B GMR-hid cl

UAS-6xMyc-lqfRa (12)/CyO; FRT82B lqfR$^{\Delta 117}$/TM6B

UAS-6xMyc-lqfRa (59)/CyO; FRT82B lqfR$^{\Delta 117}$/TM6B

UAS-6xMyc-lqfRa$^{\Delta ENTH}$ (32)/CyO; FRT82B lqfR$^{\Delta 117}$/TM6B

UAS-6xMyc-lqfRa$^{\Delta ENTH}$ (72)/CyO; FRT82B lqfR$^{\Delta 117}$/TM6B

UAS-6xMyc-lqfRa exon 6 (8)/CyO; FRT82B lqfR$^{\Delta 117}$/TM6B

UAS-6xMyc-lqfRa exon 6 (17)/CyO; FRT82B lqfR$^{\Delta 117}$/TM6B

UAS-6xMyc-lqfRb (36)/CyO; FRT82B lqfR$^{\Delta 117}$/TM6B

UAS-6xMyc-lqfRb (57)/CyO; FRT82B lqfR$^{\Delta 117}$/TM6B

UAS-6xMyc-lqfR exons 1-5 (43)/CyO; FRT82B lqfR$^{\Delta 117}$/TM6B

UAS-6xMyc-lqfR exons 1-5 (53)/CyO; FRT82B lqfR$^{\Delta 117}$/TM6B

UAS-6xMyc-lqfR^{ENTH} (8)/CyO; FRT82B lqfR$^{\Delta 117}$/TM6B

UAS-6xMyc-lqfR^{ENTH} (40)/CyO; FRT82B lqfR$^{\Delta 117}$/TM6B

UAS-6xMyc-lqfRa exon 6Δ1/CyO; FRT82B lqfR$^{\Delta 117}$/TM6B

UAS-6xMyc-lqfRa exon 6Δ2/CyO; FRT82B lqfR$^{\Delta 117}$/TM6B

UAS-6xMyc-lqfRa exon 6Δ3/CyO; FRT82B lqfR$^{\Delta 117}$/TM6B

UAS-6xMyc-lqfRa exon 6Δ4/CyO; FRT82B lqfR$^{\Delta 117}$/TM6B

UAS-6xMyc-lqfRa exon 6Δ5/CyO; FRT82B lqfR$^{\Delta 117}$/TM6B

hs-flp; FRT42D ubi-gfp/TM6B

FRT42D vps35^{E42}/TM6B

mβ-lacZ/CyO; FRT82B lqfR$^{\Delta 117}$/TM6B

EGUF; FRT82B GMR-hid/TM6B

Act5C-gal4/CyO; FRT82B lqfR$^{\Delta 117}$/TM6B

Clonal analysis

The *lqfR*$^{\Delta 117}$ clones in the eye discs were generated, stained, and observed as explained in Appendix A-2.

Co-immuno precipitation assay

Fly stocks overexpressing either *lqfRa-gfp* or *lqfR*^{ENTH}*-gfp* were prepared. The genotypes were:

w; Actin5C-gal4 UAS-lqfRa-gfp/CyO; MKRS/TM6B

w; Actin5C-gal4 UAS- lqfR^{ENTH}*-gfp/CyO; MKRS/TM6B*

Each of the stock was grown in large cages to collect embryos. 500 GFP+ embryos were selected from both stocks and homogenized in 100 ul of lysis buffer (1% NP40, 0.5% deoxycholate, 1 mM DTT, 150 mM NaCl, 50 mM Tris pH 8.0 with protease inhibitor cocktail (Roche, Complete-Mini, EDTA-free) and 2 mM PMSF). After homogenization, 300 ul of lysis buffer was added and centrifuged at 12000 rpm at 4°C. 310 ul of the supernatant was removed. Out of the 310 ul, 300 ul was mixed with 20 ul of 50% slurry of GFP-trap_A (Chromotek), and 10 ul was mixed with 2x SDS loading buffer for loading control. After incubating 2 hours at 4°C with mild shaking, the 300 ul of the lysate with GFP-trap_A was centrifuged. The GFP-trap_A pellet was washed for 5 minutes with shaking in 1 ml of lysis buffer. The pellet was washed again for 10 minutes with shaking in 1 ml of 500 mM NaCl solution. The pellet was washed 4 more times in 1 ml of 500 mM NaCl solution without shaking incubation. The pellet was mixed with 20 ul of 2x SDS lysis buffer. Each sample was boiled for 5 minutes. After centrifugation, all supernatant was loaded in 7.5% SDS-polyacrylamide gel. SDS-PAGE and Western blot

were performed. Primary antibodies against endogenous E-cadherin, Armadillo, or α-catenin were used with the dilution shown below.

Primary antibodies

Anti-E-cadherin:

Obtained from: DSHB (DCAD2, concentrated)

Host species: Rat

Antigen species: *Drosophila*

Dilutions: 1:100 (IHC), 1:1000 (WB)

Anti-Armadillo:

Obtained from: DSHB (N2 7A1, concentrated)

Host species: mouse

Antigen species: *Drosophila*

Dilutions: 1:100 (IHC), 1:500 (WB)

Anti-α-catenin:

Obtained from: DSHB (DCAT-1, concentrated)

Host species: rat

Antigen species: *Drosophila*

Dilution: 1:100 (WB)

Anti-β-galactosidase:

Obtained from: DSHB (40-1a)

Host species: mouse

Dilution: 1:50 (IHC)

Anti-β-tubulin:

Obtained from: DSHB (E7)

Host species: mouse

Antigen species: *E. coli*

Dilution: 1:100 (IHC)

Anti-LqfR (Chapter 2):

Dilution: 1:100 (IHC)

Anti-Myc:

Obtained from: Santa Cruz Biotechnology (sc-40)

Host species: mouse

Epitope: 9E10 (monoclonal)

Dilutions: 1:20 (IHC), 1:500 (WB)

Anti-Wingless:

Obtained from: DSHB (4D4)

Host species: mouse

Antigen species: *Drosophila*

Dilution: 1:100 (IHC)

Anti-Notch, intracellular domain:

Obtained from: DSHB (C17.9C6)

Host species: mouse

Antigen species: *Drosophila*

Dilution: 1:10 (IHC)

Secondary antibodies

Goat anti-rat-HRP:

Obtained from: Santa Cruz (sc-2006)

Dilution: 1:5000

Goat anti-mouse-HRP:

Obtained from: Santa Cruz (sc-2005)

Dilution: 1:5000

Secondary antibodies for immunostaining were used as explained in Appendix A.1.

Genetic interaction tests

The fly crosses for genetic interaction test were incubated at 23°C. Non-*TM6B* pupae from the cross were carefully removed to a new fresh vial and further incubated at 23°C until they eclose. Pictures were taken from eclosed adults or dead pharates.

Transgene construction and transformation

lqfR deletion constructs were generated by cloning PCR products into *pENTR/D-TOPO* vector (Invitrogen). The template for PCR was *pUASt-lqfRa-gfp* generated by Erin Overstreet. PCR primers for each construct were:

lqfRa (full length):

(forward) 5'- CACCGTGGATAAATTCATCAGCATGTGGAAAG

(reverse) 5'- TTAGGCAGCCTGTTCCATGGCG

lqfRb:

(forward) 5'- CACCATGCACGTGGTGGATAAATTCATCAG

(reverse) 5'- TTATCATTGAAACAAGTCGAATGCCG

lqfRa$^{\Delta ENTH}$:

(forward) 5'- CACCGTGGATAAATTCATCAGCATGTGGAAAG

(reverse) 5'- TTAGGCAGCCTGTTCCATGGCG

lqfRa^{ENTH}:

(forward) 5'- CACCGTGGATAAATTCATCAGCATGTGGAAAG

(reverse) 5'- TTAGTCCTTGTTCTTCTTCGCCTTTTTGC

lqfRa exon 6:

(forward) 5'- CACCGCTGTTGAAGAGCAGTTGGCATCC

(reverse) 5'- TTAGGCAGCCTGTTCCATGGCG

lqfRa exon 6Δ1:

(forward) 5'- CACCGCTGTTGAAGAGCAGTTGGCATCC

(reverse) 5'- TTACACCTGGGCATCCAGCTCCTC

lqfRa exon 6Δ2:

(forward) 5'- CACCGCTGTTGAAGAGCAGTTGGCATCC

(reverse) 5'- TTACGGGCTTTCAAACTGGCCAAG

lqfRa exon 6Δ3:

(forward) 5'- CACCGCTGTTGAAGAGCAGTTGGCATCC

(reverse) 5'- TTACTTCTCCATTTGATCTCCAGCTTTTGG

lqfRa exon 6Δ4:

(forward) 5'- CACCAAAGCGTTCTTTCAATTGCTAATCAGTCTG

(reverse) 5'- TTAGGCAGCCTGTTCCATGGCG

lqfRa exon 6Δ5:

(forward) 5'- CACCAGCAAAACTAAGCTAGATGAGAAGCCTTGTG

(reverse) 5'- TTAGGCAGCCTGTTCCATGGCG

lqfRa exon 6Δ6:

(forward) 5'- CACCGCCAATCCATTTCACCCCGTTG

(reverse) 5'- TTAGGCAGCCTGTTCCATGGCG

pENTR-lqfR exons 1-5 were generated by modifying *pENTR-lqfRa*. *pENTR-lqfRa* was digested with *StuI* and *SnaBI,* both of which make blunt end. After the *StuI-SnaBI* fragment was removed, the vector was re-ligated. The *StuI-SnaBI* fragment includes 38 bp from 3' side of exon 5 and most of exon 6, except 402 bp at the 3' side.

lqfR inserts in *pENTR-lqfR* vectors were transferred to the *pTMW* vector (Drosophila Genomics Resourse Center, #1107) by using site-specific recombination as explained in: http://emb.carnegiescience.edu/labs/murphy/Gateway%20vectors.html. The sequences of each *pTMW-lqfR* vector were verified. P element transformation of *yw* flies was performed by Genetivision (Houston, TX).

References

Aguilar RC, Longhi SA, Shaw JD, Yeh LY, Kim S, Schon A, Freire E, Hsu A, McCormick WK, Watson HA, Wendland B (2006) Epsin N-terminal homology domains perform an essential function regulating Cdc42 through binding Cdc42 GTPase-activating proteins. *Proc Natl Acad Sci U S A* **103:** 4116-4121

Aguilar RC, Wendland B (2005) Endocytosis of membrane receptors: two pathways are better than one. *Proc Natl Acad Sci U S A* **102:** 2679-2680

Ahmed S, Alpi A, Hengartner MO, Gartner A (2001) C. elegans RAD-5/CLK-2 defines a new DNA damage checkpoint protein. *Curr Biol* **11:** 1934-1944

Anderson CM, Blackburn EH (2008) Mec1 function in the DNA damage response does not require its interaction with Tel2. *Cell Cycle* **7:** 3695-3698

Anderson CM, Korkin D, Smith DL, Makovets S, Seidel JJ, Sali A, Blackburn EH (2008) Tel2 mediates activation and localization of ATM/Tel1 kinase to a double-strand break. *Genes Dev* **22:** 854-859

Andrade MA, Petosa C, O'Donoghue SI, Muller CW, Bork P (2001) Comparison of ARM and HEAT protein repeats. *J Mol Biol* **309:** 1-18

Baker NE (2007) Patterning signals and proliferation in Drosophila imaginal discs. *Curr Opin Genet Dev* **17:** 287-293

Banks SM, Cho B, Eun SH, Lee JH, Windler SL, Xie X, Bilder D, Fischer JA (2011) The functions of auxilin and Rab11 in Drosophila suggest that the fundamental role of ligand endocytosis in notch signaling cells is not recycling. *PLoS One* **6:** e18259

Banziger C, Soldini D, Schutt C, Zipperlen P, Hausmann G, Basler K (2006) Wntless, a conserved membrane protein dedicated to the secretion of Wnt proteins from signaling cells. *Cell* **125:** 509-522

Barlowe C, Orci L, Yeung T, Hosobuchi M, Hamamoto S, Salama N, Rexach MF, Ravazzola M, Amherdt M, Schekman R (1994) COPII: a membrane coat formed by Sec proteins that drive vesicle budding from the endoplasmic reticulum. *Cell* **77:** 895-907

Barriere H, Nemes C, Lechardeur D, Khan-Mohammad M, Fruh K, Lukacs GL (2006) Molecular basis of oligoubiquitin-dependent internalization of membrane proteins in Mammalian cells. *Traffic* **7:** 282-297

Bartscherer K, Pelte N, Ingelfinger D, Boutros M (2006) Secretion of Wnt ligands requires Evi, a conserved transmembrane protein. *Cell* **125:** 523-533

Becker HJ (1957) [Roentgen mosaic spots & defective mutations at the eye of Drosophila & the evolutive physiology of the eye]. *Z Indukt Abstamm Vererbungsl* **88:** 333-373

Beckett K, Franch-Marro X, Vincent JP (2008) Glypican-mediated endocytosis of Hedgehog has opposite effects in flies and mice. *Trends Cell Biol* **18:** 360-363

Bejsovec A, Wieschaus E (1995) Signaling activities of the Drosophila wingless gene are separately mutable and appear to be transduced at the cell surface. *Genetics* **139:** 309-320

Belenkaya TY, Wu Y, Tang X, Zhou B, Cheng L, Sharma YV, Yan D, Selva EM, Lin X (2008) The retromer complex influences Wnt secretion by recycling wntless from endosomes to the trans-Golgi network. *Dev Cell* **14:** 120-131

Benard C, McCright B, Zhang Y, Felkai S, Lakowski B, Hekimi S (2001) The C. elegans maternal-effect gene clk-2 is essential for embryonic development, encodes a protein homologous to yeast Tel2p and affects telomere length. *Development* **128:** 4045-4055

Benchabane H, Hughes EG, Takacs CM, Baird JR, Ahmed Y (2008) Adenomatous polyposis coli is present near the minimal level required for accurate graded responses to the Wingless morphogen. *Development* **135:** 963-971

Bischoff M, Schnabel R (2006) Global cell sorting is mediated by local cell-cell interactions in the C. elegans embryo. *Dev Biol* **294:** 432-444

Brand AH, Perrimon N (1993) Targeted gene expression as a means of altering cell fates and generating dominant phenotypes. *Development* **118:** 401-415

Brauchle M, Baumer K, Gonczy P (2003) Differential activation of the DNA replication checkpoint contributes to asynchrony of cell division in C. elegans embryos. *Curr Biol* **13:** 819-827

Brittle AL, Repiso A, Casal J, Lawrence PA, Strutt D (2010) Four-jointed modulates growth and planar polarity by reducing the affinity of dachsous for fat. *Curr Biol* **20:** 803-810

Brodsky MH, Steller H (1996) Positional information along the dorsal-ventral axis of the Drosophila eye: graded expression of the four-jointed gene. *Dev Biol* **173:** 428-446

Brogiolo W, Stocker H, Ikeya T, Rintelen F, Fernandez R, Hafen E (2001) An evolutionarily conserved function of the Drosophila insulin receptor and insulin-like peptides in growth control. *Curr Biol* **11:** 213-221

Brown KE, Baonza A, Freeman M (2006) Epithelial cell adhesion in the developing Drosophila retina is regulated by Atonal and the EGF receptor pathway. *Dev Biol* **300:** 710-721

Brunner E, Peter O, Schweizer L, Basler K (1997) pangolin encodes a Lef-1 homologue that acts downstream of Armadillo to transduce the Wingless signal in Drosophila. *Nature* **385:** 829-833

Cadavid AL, Ginzel A, Fischer JA (2000) The function of the Drosophila fat facets deubiquitinating enzyme in limiting photoreceptor cell number is intimately associated with endocytosis. *Development* **127:** 1727-1736

Cadigan KM, Nusse R (1997) Wnt signaling: a common theme in animal development. *Genes Dev* **11:** 3286-3305

Carthew RW (2007) Pattern formation in the Drosophila eye. *Curr Opin Genet Dev* **17:** 309-313

Chanut F, Luk A, Heberlein U (2000) A screen for dominant modifiers of ro(Dom), a mutation that disrupts morphogenetic furrow progression in Drosophila, identifies groucho and hairless as regulators of atonal expression. *Genetics* **156:** 1203-1217

Chen C, Jack J, Garofalo RS (1996) The Drosophila insulin receptor is required for normal growth. *Endocrinology* **137:** 846-856

Chen H, Fre S, Slepnev VI, Capua MR, Takei K, Butler MH, Di Fiore PP, De Camilli P (1998) Epsin is an EH-domain-binding protein implicated in clathrin-mediated endocytosis. *Nature* **394:** 793-797

Chen H, Ko G, Zatti A, Di Giacomo G, Liu L, Raiteri E, Perucco E, Collesi C, Min W, Zeiss C, De Camilli P, Cremona O (2009) Embryonic arrest at midgestation and disruption of Notch signaling produced by the absence of both epsin 1 and epsin 2 in mice. *Proc Natl Acad Sci U S A* **106:** 13838-13843

Chen X, Fischer JA (2000) In vivo Structure/Function analysis of the Drosophila fat facets deubiquitinating enzyme gene. *Genetics* **156:** 1829-1836

Chen YT, Stewart DB, Nelson WJ (1999) Coupling assembly of the E-cadherin/beta-catenin complex to efficient endoplasmic reticulum exit and basal-lateral membrane targeting of E-cadherin in polarized MDCK cells. *J Cell Biol* **144:** 687-699

Chidambaram S, Mullers N, Wiederhold K, Haucke V, von Mollard GF (2004) Specific interaction between SNAREs and epsin N-terminal homology (ENTH) domains of epsin-related proteins in trans-Golgi network to endosome transport. *J Biol Chem* **279:** 4175-4179

Chidambaram S, Zimmermann J, von Mollard GF (2008) ENTH domain proteins are cargo adaptors for multiple SNARE proteins at the TGN endosome. *J Cell Sci* **121:** 329-338

Chien AJ, Conrad WH, Moon RT (2009) A Wnt survival guide: from flies to human disease. *J Invest Dermatol* **129:** 1614-1627

Cho KO, Chern J, Izaddoost S, Choi KW (2000) Novel signaling from the peripodial membrane is essential for eye disc patterning in Drosophila. *Cell* **103:** 331-342

Cho KO, Choi KW (1998) Fringe is essential for mirror symmetry and morphogenesis in the Drosophila eye. *Nature* **396:** 272-276

Clifford RJ, Schupbach T (1989) Coordinately and differentially mutable activities of torpedo, the Drosophila melanogaster homolog of the vertebrate EGF receptor gene. *Genetics* **123:** 771-787

Copic A, Starr TL, Schekman R (2007) Ent3p and Ent5p exhibit cargo-specific functions in trafficking proteins between the trans-Golgi network and the endosomes in yeast. *Mol Biol Cell* **18:** 1803-1815

Costaguta G, Duncan MC, Fernandez GE, Huang GH, Payne GS (2006) Distinct roles for TGN/endosome epsin-like adaptors Ent3p and Ent5p. *Mol Biol Cell* **17:** 3907-3920

Cox RT, Pai LM, Miller JR, Orsulic S, Stein J, McCormick CA, Audeh Y, Wang W, Moon RT, Peifer M (1999) Membrane-tethered Drosophila Armadillo cannot transduce Wingless signal on its own. *Development* **126:** 1327-1335

Crowther RA, Pearse BM (1981) Assembly and packing of clathrin into coats. *J Cell Biol* **91:** 790-797

Dell'Angelica EC, Klumperman J, Stoorvogel W, Bonifacino JS (1998) Association of the AP-3 adaptor complex with clathrin. *Science* **280:** 431-434

Derheimer FA, Kastan MB (2010) Multiple roles of ATM in monitoring and maintaining DNA integrity. *FEBS Lett* **584:** 3675-3681

Dodd ME, Hatzold J, Mathias JR, Walters KB, Bennin DA, Rhodes J, Kanki JP, Look AT, Hammerschmidt M, Huttenlocher A (2009) The ENTH domain protein Clint1 is required for epidermal homeostasis in zebrafish. *Development* **136:** 2591-2600

Dominguez M, de Celis JF (1998) A dorsal/ventral boundary established by Notch controls growth and polarity in the Drosophila eye. *Nature* **396:** 276-278

Dominguez M, Hafen E (1997) Hedgehog directly controls initiation and propagation of retinal differentiation in the Drosophila eye. *Genes Dev* **11:** 3254-3264

Duncan MC, Costaguta G, Payne GS (2003) Yeast epsin-related proteins required for Golgi-endosome traffic define a gamma-adaptin ear-binding motif. *Nat Cell Biol* **5:** 77-81

Duncan MC, Payne GS (2003) ENTH/ANTH domains expand to the Golgi. *Trends Cell Biol* **13:** 211-215

Edgar BA, O'Farrell PH (1990) The three postblastoderm cell cycles of Drosophila embryogenesis are regulated in G2 by string. *Cell* **62:** 469-480

Eugster A, Pecheur EI, Michel F, Winsor B, Letourneur F, Friant S (2004) Ent5p is required with Ent3p and Vps27p for ubiquitin-dependent protein sorting into the multivesicular body. *Mol Biol Cell* **15:** 3031-3041

Eun SH, Banks SM, Fischer JA (2008) Auxilin is essential for Delta signaling. *Development* **135:** 1089-1095

Eun SH, Lea K, Overstreet E, Stevens S, Lee JH, Fischer JA (2007) Identification of genes that interact with Drosophila liquid facets. *Genetics* **175:** 1163-1174

Fagotto F, Gluck U, Gumbiner BM (1998) Nuclear localization signal-independent and importin/karyopherin-independent nuclear import of beta-catenin. *Curr Biol* **8:** 181-190

Fanning AS, Jameson BJ, Jesaitis LA, Anderson JM (1998) The tight junction protein ZO-1 establishes a link between the transmembrane protein occludin and the actin cytoskeleton. *J Biol Chem* **273:** 29745-29753

Feger G, Vaessin H, Su TT, Wolff E, Jan LY, Jan YN (1995) dpa, a member of the MCM family, is required for mitotic DNA replication but not endoreplication in Drosophila. *Embo J* **14:** 5387-5398

Fischer JA, Eun SH, Doolan BT (2006) Endocytosis, endosome trafficking, and the regulation of Drosophila development. *Annu Rev Cell Dev Biol* **22:** 181-206

Fischer JA, Giniger E, Maniatis T, Ptashne M (1988) GAL4 activates transcription in Drosophila. *Nature* **332:** 853-856

Fischer MG, Heeger S, Hacker U, Lehner CF (2004) The mitotic arrest in response to hypoxia and of polar bodies during early embryogenesis requires Drosophila Mps1. *Curr Biol* **14:** 2019-2024

Fischer-Vize JA, Rubin GM, Lehmann R (1992) The fat facets gene is required for Drosophila eye and embryo development. *Development* **116:** 985-1000

Ford MG, Mills IG, Peter BJ, Vallis Y, Praefcke GJ, Evans PR, McMahon HT (2002) Curvature of clathrin-coated pits driven by epsin. *Nature* **419:** 361-366

Franch-Marro X, Wendler F, Guidato S, Griffith J, Baena-Lopez A, Itasaki N, Maurice MM, Vincent JP (2008) Wingless secretion requires endosome-to-Golgi retrieval of Wntless/Evi/Sprinter by the retromer complex. *Nat Cell Biol* **10:** 170-177

Fre S, Pallavi SK, Huyghe M, Lae M, Janssen KP, Robine S, Artavanis-Tsakonas S, Louvard D (2009) Notch and Wnt signals cooperatively control cell proliferation and tumorigenesis in the intestine. *Proc Natl Acad Sci U S A* **106:** 6309-6314

Friant S, Pecheur EI, Eugster A, Michel F, Lefkir Y, Nourrisson D, Letourneur F (2003) Ent3p Is a PtdIns(3,5)P2 effector required for protein sorting to the multivesicular body. *Dev Cell* **5:** 499-511

Funke L, Dakoji S, Bredt DS (2005) Membrane-associated guanylate kinases regulate adhesion and plasticity at cell junctions. *Annu Rev Biochem* **74:** 219-245

Gallet A, Staccini-Lavenant L, Therond PP (2008) Cellular trafficking of the glypican Dally-like is required for full-strength Hedgehog signaling and wingless transcytosis. *Dev Cell* **14:** 712-725

Garcia-Bellido A, Merriam JR (1969) Cell lineage of the imaginal discs in Drosophila gynandromorphs. *J Exp Zool* **170:** 61-75

Gatti M, Baker BS (1989) Genes controlling essential cell-cycle functions in Drosophila melanogaster. *Genes Dev* **3:** 438-453

Gibson MC, Schubiger G (2001) Drosophila peripodial cells, more than meets the eye? *Bioessays* **23:** 691-697

Giraldez AJ, Cohen SM (2003) Wingless and Notch signaling provide cell survival cues and control cell proliferation during wing development. *Development* **130:** 6533-6543

Golic KG, Lindquist S (1989) The FLP recombinase of yeast catalyzes site-specific recombination in the Drosophila genome. *Cell* **59:** 499-509

Goodman RM, Thombre S, Firtina Z, Gray D, Betts D, Roebuck J, Spana EP, Selva EM (2006) Sprinter: a novel transmembrane protein required for Wg secretion and signaling. *Development* **133:** 4901-4911

Gottardi CJ, Wong E, Gumbiner BM (2001) E-cadherin suppresses cellular transformation by inhibiting beta-catenin signaling in an adhesion-independent manner. *J Cell Biol* **153:** 1049-1060

Grammont M, Irvine KD (2001) fringe and Notch specify polar cell fate during Drosophila oogenesis. *Development* **128:** 2243-2253

Hardwick KG, Weiss E, Luca FC, Winey M, Murray AW (1996) Activation of the budding yeast spindle assembly checkpoint without mitotic spindle disruption. *Science* **273:** 953-956

Hartman PS, Herman RK (1982) Somatic damage to the X chromosome of the nematode Caenorhabditis elegans induced by gamma radiation. *Mol Gen Genet* **187:** 116-119

Hayashi T, Hatanaka M, Nagao K, Nakaseko Y, Kanoh J, Kokubu A, Ebe M, Yanagida M (2007) Rapamycin sensitivity of the Schizosaccharomyces pombe tor2 mutant and organization of two highly phosphorylated TOR complexes by specific and common subunits. *Genes Cells* **12:** 1357-1370

Hayward P, Brennan K, Sanders P, Balayo T, DasGupta R, Perrimon N, Martinez Arias A (2005) Notch modulates Wnt signalling by associating with Armadillo/beta-catenin and regulating its transcriptional activity. *Development* **132:** 1819-1830

Herz HM, Woodfield SE, Chen Z, Bolduc C, Bergmann A (2009) Common and distinct genetic properties of ESCRT-II components in Drosophila. *PLoS One* **4:** e4165

Heuberger J, Birchmeier W (2010) Interplay of cadherin-mediated cell adhesion and canonical Wnt signaling. *Cold Spring Harb Perspect Biol* **2:** a002915

Hirst J, L DB, Francisco GC, Sahlender DA, Seaman MN, Dacks JB, Robinson MS (2011) The fifth adaptor protein complex. *PLoS Biol* **9:** e1001170

Hirst J, Miller SE, Taylor MJ, von Mollard GF, Robinson MS (2004) EpsinR is an adaptor for the SNARE protein Vti1b. *Mol Biol Cell* **15:** 5593-5602

Hirst J, Motley A, Harasaki K, Peak Chew SY, Robinson MS (2003) EpsinR: an ENTH domain-containing protein that interacts with AP-1. *Mol Biol Cell* **14:** 625-641

Huber AH, Stewart DB, Laurents DV, Nelson WJ, Weis WI (2001) The cadherin cytoplasmic domain is unstructured in the absence of beta-catenin. A possible mechanism for regulating cadherin turnover. *J Biol Chem* **276:** 12301-12309

Hurov KE, Cotta-Ramusino C, Elledge SJ (2010) A genetic screen identifies the Triple T complex required for DNA damage signaling and ATM and ATR stability. *Genes Dev* **24:** 1939-1950

Irvine KD, Wieschaus E (1994) fringe, a Boundary-specific signaling molecule, mediates interactions between dorsal and ventral cells during Drosophila wing development. *Cell* **79:** 595-606

Itoh M, Nagafuchi A, Moroi S, Tsukita S (1997) Involvement of ZO-1 in cadherin-based cell adhesion through its direct binding to alpha catenin and actin filaments. *J Cell Biol* **138:** 181-192

Itoh T, Koshiba S, Kigawa T, Kikuchi A, Yokoyama S, Takenawa T (2001) Role of the ENTH domain in phosphatidylinositol-4,5-bisphosphate binding and endocytosis. *Science* **291:** 1047-1051

Kalderon D (2005) The mechanism of hedgehog signal transduction. *Biochem Soc Trans* **33:** 1509-1512

Kalthoff C, Groos S, Kohl R, Mahrhold S, Ungewickell EJ (2002) Clint: a novel clathrin-binding ENTH-domain protein at the Golgi. *Mol Biol Cell* **13:** 4060-4073

Kay BK, Yamabhai M, Wendland B, Emr SD (1999) Identification of a novel domain shared by putative components of the endocytic and cytoskeletal machinery. *Protein Sci* **8:** 435-438

Kemler R (1992) Classical cadherins. *Semin Cell Biol* **3:** 149-155

Khalsa O, Yoon JW, Torres-Schumann S, Wharton KA (1998) TGF-beta/BMP superfamily members, Gbb-60A and Dpp, cooperate to provide pattern information and establish cell identity in the Drosophila wing. *Development* **125:** 2723-2734

Kirchhausen T (1999) Adaptors for clathrin-mediated traffic. *Annu Rev Cell Dev Biol* **15:** 705-732

Kohn AD, Moon RT (2005) Wnt and calcium signaling: beta-catenin-independent pathways. *Cell Calcium* **38:** 439-446

Kwon C, Cheng P, King IN, Andersen P, Shenje L, Nigam V, Srivastava D (2011) Notch post-translationally regulates beta-catenin protein in stem and progenitor cells. *Nat Cell Biol* **13:** 1244-1251

Lakowski B, Hekimi S (1996) Determination of life-span in Caenorhabditis elegans by four clock genes. *Science* **272:** 1010-1013

Landis G, Kelley R, Spradling AC, Tower J (1997) The k43 gene, required for chorion gene amplification and diploid cell chromosome replication, encodes the Drosophila homolog of yeast origin recognition complex subunit 2. *Proc Natl Acad Sci U S A* **94:** 3888-3892

Le Roy C, Wrana JL (2005) Clathrin- and non-clathrin-mediated endocytic regulation of cell signalling. *Nat Rev Mol Cell Biol* **6:** 112-126

Lee JH, Overstreet E, Fitch E, Fleenor S, Fischer JA (2009) Drosophila liquid facets-Related encodes Golgi epsin and is an essential gene required for cell proliferation, growth, and patterning. *Dev Biol* **331:** 1-13

Legendre-Guillemin V, Wasiak S, Hussain NK, Angers A, McPherson PS (2004) ENTH/ANTH proteins and clathrin-mediated membrane budding. *J Cell Sci* **117:** 9-18

Legent K, Treisman JE (2008) Wingless signaling in Drosophila eye development. *Methods Mol Biol* **469:** 141-161

Lloyd TE, Verstreken P, Ostrin EJ, Phillippi A, Lichtarge O, Bellen HJ (2000) A genome-wide search for synaptic vesicle cycle proteins in Drosophila. *Neuron* **26:** 45-50

Lustig AJ, Petes TD (1986) Identification of yeast mutants with altered telomere structure. *Proc Natl Acad Sci U S A* **83:** 1398-1402

Maurel-Zaffran C, Treisman JE (2000) pannier acts upstream of wingless to direct dorsal eye disc development in Drosophila. *Development* **127:** 1007-1016

Miele AE, Watson PJ, Evans PR, Traub LM, Owen DJ (2004) Two distinct interaction motifs in amphiphysin bind two independent sites on the clathrin terminal domain beta-propeller. *Nat Struct Mol Biol* **11:** 242-248

Milan M, Cohen SM (2000) Temporal regulation of apterous activity during development of the Drosophila wing. *Development* **127:** 3069-3078

Millar JB, McGowan CH, Lenaers G, Jones R, Russell P (1991) p80cdc25 mitotic inducer is the tyrosine phosphatase that activates p34cdc2 kinase in fission yeast. *Embo J* **10:** 4301-4309

Miller SE, Collins BM, McCoy AJ, Robinson MS, Owen DJ (2007) A SNARE-adaptor interaction is a new mode of cargo recognition in clathrin-coated vesicles. *Nature* **450:** 570-574

Mills IG, Praefcke GJ, Vallis Y, Peter BJ, Olesen LE, Gallop JL, Butler PJ, Evans PR, McMahon HT (2003) EpsinR: an AP1/clathrin interacting protein involved in vesicle trafficking. *J Cell Biol* **160:** 213-222

Moon RT, Bowerman B, Boutros M, Perrimon N (2002) The promise and perils of Wnt signaling through beta-catenin. *Science* **296:** 1644-1646

Morgan JR, Prasad K, Hao W, Augustine GJ, Lafer EM (2000) A conserved clathrin assembly motif essential for synaptic vesicle endocytosis. *J Neurosci* **20:** 8667-8676

Morgan TH (1910) Sex Limited Inheritance in Drosophila. *Science* **32:** 120-122

Moser SC, von Elsner S, Bussing I, Alpi A, Schnabel R, Gartner A (2009) Functional dissection of Caenorhabditis elegans CLK-2/TEL2 cell cycle defects during embryogenesis and germline development. *PLoS Genet* **5:** e1000451

Neufeld TP, de la Cruz AF, Johnston LA, Edgar BA (1998) Coordination of growth and cell division in the Drosophila wing. *Cell* **93:** 1183-1193

Nishida Y, Hata M, Ayaki T, Ryo H, Yamagata M, Shimizu K, Nishizuka Y (1988) Proliferation of both somatic and germ cells is affected in the Drosophila mutants of raf proto-oncogene. *Embo J* **7:** 775-781

Oldham S, Hafen E (2003) Insulin/IGF and target of rapamycin signaling: a TOR de force in growth control. *Trends Cell Biol* **13:** 79-85

Overstreet E, Chen X, Wendland B, Fischer JA (2003) Either part of a Drosophila epsin protein, divided after the ENTH domain, functions in endocytosis of delta in the developing eye. *Curr Biol* **13:** 854-860

Overstreet E, Fitch E, Fischer JA (2004) Fat facets and Liquid facets promote Delta endocytosis and Delta signaling in the signaling cells. *Development* **131:** 5355-5366

Owen DJ, Collins BM, Evans PR (2004) Adaptors for clathrin coats: structure and function. *Annu Rev Cell Dev Biol* **20:** 153-191

Pearse BM (1976) Clathrin: a unique protein associated with intracellular transfer of membrane by coated vesicles. *Proc Natl Acad Sci U S A* **73:** 1255-1259

Peifer M, Pai LM, Casey M (1994) Phosphorylation of the Drosophila adherens junction protein Armadillo: roles for wingless signal and zeste-white 3 kinase. *Dev Biol* **166:** 543-556

Peifer M, Rauskolb C, Williams M, Riggleman B, Wieschaus E (1991) The segment polarity gene armadillo interacts with the wingless signaling pathway in both embryonic and adult pattern formation. *Development* **111:** 1029-1043

Piddini E, Vincent JP (2003) Modulation of developmental signals by endocytosis: different means and many ends. *Curr Opin Cell Biol* **15:** 474-481

Pimm J, McQuillin A, Thirumalai S, Lawrence J, Quested D, Bass N, Lamb G, Moorey H, Datta SR, Kalsi G, Badacsonyi A, Kelly K, Morgan J, Punukollu B, Curtis D, Gurling H (2005) The Epsin 4 gene on chromosome 5q, which encodes the clathrin-associated protein enthoprotin, is involved in the genetic susceptibility to schizophrenia. *Am J Hum Genet* **76:** 902-907

Popoff V, Mardones GA, Tenza D, Rojas R, Lamaze C, Bonifacino JS, Raposo G, Johannes L (2007) The retromer complex and clathrin define an early endosomal retrograde exit site. *J Cell Sci* **120:** 2022-2031

Port F, Kuster M, Herr P, Furger E, Banziger C, Hausmann G, Basler K (2008) Wingless secretion promotes and requires retromer-dependent cycling of Wntless. *Nat Cell Biol* **10:** 178-185

Raftery LA, Twombly V, Wharton K, Gelbart WM (1995) Genetic screens to identify elements of the decapentaplegic signaling pathway in Drosophila. *Genetics* **139:** 241-254

Rijsewijk F, Schuermann M, Wagenaar E, Parren P, Weigel D, Nusse R (1987) The Drosophila homolog of the mouse mammary oncogene int-1 is identical to the segment polarity gene wingless. *Cell* **50:** 649-657

Robinow S, White K (1991) Characterization and spatial distribution of the ELAV protein during Drosophila melanogaster development. *J Neurobiol* **22:** 443-461

Rohatgi R, Scott MP (2007) Patching the gaps in Hedgehog signalling. *Nat Cell Biol* **9:** 1005-1009

Roignant JY, Treisman JE (2009) Pattern formation in the Drosophila eye disc. *Int J Dev Biol* **53:** 795-804

Rosenthal JA, Chen H, Slepnev VI, Pellegrini L, Salcini AE, Di Fiore PP, De Camilli P (1999) The epsins define a family of proteins that interact with components of the clathrin coat and contain a new protein module. *J Biol Chem* **274:** 33959-33965

Rosin-Arbesfeld R, Townsley F, Bienz M (2000) The APC tumour suppressor has a nuclear export function. *Nature* **406:** 1009-1012

Russell P, Nurse P (1986) cdc25+ functions as an inducer in the mitotic control of fission yeast. *Cell* **45:** 145-153

Saint-Pol A, Yelamos B, Amessou M, Mills IG, Dugast M, Tenza D, Schu P, Antony C, McMahon HT, Lamaze C, Johannes L (2004) Clathrin adaptor epsinR is required for retrograde sorting on early endosomal membranes. *Dev Cell* **6:** 525-538

Sanson B, White P, Vincent JP (1996) Uncoupling cadherin-based adhesion from wingless signalling in Drosophila. *Nature* **383:** 627-630

Seaman MN, McCaffery JM, Emr SD (1998) A membrane coat complex essential for endosome-to-Golgi retrograde transport in yeast. *J Cell Biol* **142:** 665-681

Secombe J, Pispa J, Saint R, Richardson H (1998) Analysis of a Drosophila cyclin E hypomorphic mutation suggests a novel role for cyclin E in cell proliferation control during eye imaginal disc development. *Genetics* **149:** 1867-1882

Sekelsky JJ, Newfeld SJ, Raftery LA, Chartoff EH, Gelbart WM (1995) Genetic characterization and cloning of mothers against dpp, a gene required for decapentaplegic function in Drosophila melanogaster. *Genetics* **139:** 1347-1358

Seppa MJ, Johnson RI, Bao S, Cagan RL (2008) Polychaetoid controls patterning by modulating adhesion in the Drosophila pupal retina. *Dev Biol* **318:** 1-16

Shearn A, Garen A (1974) Genetic control of imaginal disc development in Drosophila. *Proc Natl Acad Sci U S A* **71:** 1393-1397

Shearn A, Rice T, Garen A, Gehring W (1971) Imaginal disc abnormalities in lethal mutants of Drosophila. *Proc Natl Acad Sci U S A* **68:** 2594-2598

Shevchenko A, Roguev A, Schaft D, Buchanan L, Habermann B, Sakalar C, Thomas H, Krogan NJ, Stewart AF (2008) Chromatin Central: towards the comparative proteome by accurate mapping of the yeast proteomic environment. *Genome Biol* **9:** R167

Sigismund S, Woelk T, Puri C, Maspero E, Tacchetti C, Transidico P, Di Fiore PP, Polo S (2005) Clathrin-independent endocytosis of ubiquitinated cargos. *Proc Natl Acad Sci U S A* **102:** 2760-2765

Silva E, Tsatskis Y, Gardano L, Tapon N, McNeill H (2006) The tumor-suppressor gene fat controls tissue growth upstream of expanded in the hippo signaling pathway. *Curr Biol* **16:** 2081-2089

Simon MA (2004) Planar cell polarity in the Drosophila eye is directed by graded Four-jointed and Dachsous expression. *Development* **131:** 6175-6184

Sisson JC, Field C, Ventura R, Royou A, Sullivan W (2000) Lava lamp, a novel peripheral golgi protein, is required for Drosophila melanogaster cellularization. *J Cell Biol* **151:** 905-918

Speicher SA, Thomas U, Hinz U, Knust E (1994) The Serrate locus of Drosophila and its role in morphogenesis of the wing imaginal discs: control of cell proliferation. *Development* **120:** 535-544

Spradling AC, Stern D, Beaton A, Rhem EJ, Laverty T, Mozden N, Misra S, Rubin GM (1999) The Berkeley Drosophila Genome Project gene disruption project: Single P-element insertions mutating 25% of vital Drosophila genes. *Genetics* **153:** 135-177

Stanley H, Botas J, Malhotra V (1997) The mechanism of Golgi segregation during mitosis is cell type-specific. *Proc Natl Acad Sci U S A* **94:** 14467-14470

Stirling PC, Bloom MS, Solanki-Patil T, Smith S, Sipahimalani P, Li Z, Kofoed M, Ben-Aroya S, Myung K, Hieter P (2011) The complete spectrum of yeast chromosome instability genes identifies candidate CIN cancer genes and functional roles for ASTRA complex components. *PLoS Genet* **7:** e1002057

Stowers RS, Schwarz TL (1999) A genetic method for generating Drosophila eyes composed exclusively of mitotic clones of a single genotype. *Genetics* **152:** 1631-1639

Takai H, Wang RC, Takai KK, Yang H, de Lange T (2007) Tel2 regulates the stability of PI3K-related protein kinases. *Cell* **131:** 1248-1259

Takai H, Xie Y, de Lange T, Pavletich NP (2010) Tel2 structure and function in the Hsp90-dependent maturation of mTOR and ATR complexes. *Genes Dev* **24:** 2019-2030

ter Haar E, Musacchio A, Harrison SC, Kirchhausen T (1998) Atomic structure of clathrin: a beta propeller terminal domain joins an alpha zigzag linker. *Cell* **95:** 563-573

Thomas C, Ingham PW (2003) Hedgehog signaling in the Drosophila eye and head: an analysis of the effects of different patched trans-heterozygotes. *Genetics* **165:** 1915-1928

Tian X, Hansen D, Schedl T, Skeath JB (2004) Epsin potentiates Notch pathway activity in Drosophila and C. elegans. *Development* **131:** 5807-5815

Tolwinski NS, Wieschaus E (2001) Armadillo nuclear import is regulated by cytoplasmic anchor Axin and nuclear anchor dTCF/Pan. *Development* **128:** 2107-2117

Tomlinson A (2003) Patterning the peripheral retina of the fly: decoding a gradient. *Dev Cell* **5:** 799-809

Treisman JE, Follette PJ, O'Farrell PH, Rubin GM (1995) Cell proliferation and DNA replication defects in a Drosophila MCM2 mutant. *Genes Dev* **9:** 1709-1715

Tweedie S, Ashburner M, Falls K, Leyland P, McQuilton P, Marygold S, Millburn G, Osumi-Sutherland D, Schroeder A, Seal R, Zhang H (2009) FlyBase: enhancing Drosophila Gene Ontology annotations. *Nucleic Acids Res* **37:** D555-559

Walston T, Tuskey C, Edgar L, Hawkins N, Ellis G, Bowerman B, Wood W, Hardin J (2004) Multiple Wnt signaling pathways converge to orient the mitotic spindle in early C. elegans embryos. *Dev Cell* **7:** 831-841

Walworth NC (2001) DNA damage: Chk1 and Cdc25, more than meets the eye. *Curr Opin Genet Dev* **11:** 78-82

Wang CW, Hamamoto S, Orci L, Schekman R (2006a) Exomer: A coat complex for transport of select membrane proteins from the trans-Golgi network to the plasma membrane in yeast. *J Cell Biol* **174:** 973-983

Wang H, Traub LM, Weixel KM, Hawryluk MJ, Shah N, Edinger RS, Perry CJ, Kester L, Butterworth MB, Peters KW, Kleyman TR, Frizzell RA, Johnson JP (2006b) Clathrin-mediated endocytosis of the epithelial sodium channel. Role of epsin. *J Biol Chem* **281:** 14129-14135

Wang J, Gossing M, Fang P, Zimmermann J, Li X, von Mollard GF, Niu L, Teng M (2011) Epsin N-terminal homology domains bind on opposite sides of two SNAREs. *Proc Natl Acad Sci U S A* **108:** 12277-12282

Wang W, Struhl G (2004) Drosophila Epsin mediates a select endocytic pathway that DSL ligands must enter to activate Notch. *Development* **131:** 5367-5380

Wang W, Struhl G (2005) Distinct roles for Mind bomb, Neuralized and Epsin in mediating DSL endocytosis and signaling in Drosophila. *Development* **132:** 2883-2894

Wang YJ, Wang J, Sun HQ, Martinez M, Sun YX, Macia E, Kirchhausen T, Albanesi JP, Roth MG, Yin HL (2003) Phosphatidylinositol 4 phosphate regulates targeting of clathrin adaptor AP-1 complexes to the Golgi. *Cell* **114:** 299-310

Wasiak S, Legendre-Guillemin V, Puertollano R, Blondeau F, Girard M, de Heuvel E, Boismenu D, Bell AW, Bonifacino JS, McPherson PS (2002) Enthoprotin: a novel clathrin-associated protein identified through subcellular proteomics. *J Cell Biol* **158:** 855-862

Weinmaster G, Fischer JA (2011) Notch ligand ubiquitylation: what is it good for? *Dev Cell* **21:** 134-144

Wendland B (2002) Epsins: adaptors in endocytosis? *Nat Rev Mol Cell Biol* **3:** 971-977

Wendland B, Steece KE, Emr SD (1999) Yeast epsins contain an essential N-terminal ENTH domain, bind clathrin and are required for endocytosis. *Embo J* **18:** 4383-4393

Wieschaus E, Gehring W (1976) Clonal analysis of primordial disc cells in the early embryo of Drosophila melanogaster. *Dev Biol* **50:** 249-263

Wieschaus E, Riggleman R (1987) Autonomous requirements for the segment polarity gene armadillo during Drosophila embryogenesis. *Cell* **49:** 177-184

Wilbur JD, Hwang PK, Ybe JA, Lane M, Sellers BD, Jacobson MP, Fletterick RJ, Brodsky FM (2010) Conformation switching of clathrin light chain regulates clathrin lattice assembly. *Dev Cell* **18:** 841-848

Willecke M, Hamaratoglu F, Sansores-Garcia L, Tao C, Halder G (2008) Boundaries of Dachsous Cadherin activity modulate the Hippo signaling pathway to induce cell proliferation. *Proc Natl Acad Sci U S A* **105:** 14897-14902

Yanagawa S, Lee JS, Haruna T, Oda H, Uemura T, Takeichi M, Ishimoto A (1997) Accumulation of Armadillo induced by Wingless, Dishevelled, and dominant-negative Zeste-White 3 leads to elevated DE-cadherin in Drosophila clone 8 wing disc cells. *J Biol Chem* **272:** 25243-25251

Yang CH, Axelrod JD, Simon MA (2002) Regulation of Frizzled by fat-like cadherins during planar polarity signaling in the Drosophila compound eye. *Cell* **108:** 675-688

Zhao Y, Tong C, Jiang J (2007) Hedgehog regulates smoothened activity by inducing a conformational switch. *Nature* **450:** 252-258